2016

SYNTHESIS AND CHARACTERIZATION OF ANTIOXIDANT CONJUGATED POLY(BETA-AMINO ESTER) MICRO/NANOGELS FOR THE SUPPRESSION OF OXIDATIVE STRESS

Prachi Gupta
University of Kentucky, guptprachi@gmail.com
Digital Object Identifier: http://dx.doi.org/10.13023/ETD.2016.035

STUDENT AGREEMENT:

I represent that my thesis or dissertation and abstract are my original work. Proper attribution has been given to all outside sources. I understand that I am solely responsible for obtaining any needed copyright permissions. I have obtained needed written permission statement(s) from the owner(s) of each third-party copyrighted matter to be included in my work, allowing electronic distribution (if such use is not permitted by the fair use doctrine) which will be submitted to UKnowledge as Additional File.

I hereby grant to The University of Kentucky and its agents the irrevocable, non-exclusive, and royalty-free license to archive and make accessible my work in whole or in part in all forms of media, now or hereafter known. I agree that the document mentioned above may be made available immediately for worldwide access unless an embargo applies.

I retain all other ownership rights to the copyright of my work. I also retain the right to use in future works (such as articles or books) all or part of my work. I understand that I am free to register the copyright to my work.

REVIEW, APPROVAL AND ACCEPTANCE

The document mentioned above has been reviewed and accepted by the student's advisor, on behalf of the advisory committee, and by the Director of Graduate Studies (DGS), on behalf of the program; we verify that this is the final, approved version of the student's thesis including all changes required by the advisory committee. The undersigned agree to abide by the statements above.

Prachi Gupta, Student

Dr. Thomas D. Dziubla, Major Professor

Dr. Thomas D. Dziubla, Director of Graduate Studies

SYNTHESIS AND CHARACTERIZATION OF ANTIOXIDANT CONJUGATED POLY(BETA-AMINO ESTER) MICRO/NANOGELS FOR THE SUPPRESSION OF OXIDATIVE STRESS

DISSERTATION

A dissertation submitted in partial fulfillment of
the requirements for the degree of Doctor of
Philosophy in the College of Engineering at the
University of Kentucky

By

Prachi Gupta

Lexington, Kentucky

Director: Dr. Thomas Dziubla, Associate Professor of Chemical and Materials Engineering

Co-director: Dr. J. Zach Hilt, Professor of Chemical and Materials Engineering

Lexington, Kentucky

ABSTRACT FOR DISSERTATION

SYNTHESIS AND CHARACTERIZATION OF ANTIOXIDANT CONJUGATED POLY(BETA-AMINO ESTER) MICRO/NANOGELS FOR THE SUPPRESSION OF OXIDATIVE STRESS

Oxidative stress is a pathophysiological condition defined by an increased production of reactive oxygen species (ROS), which can result in the growth arrest of cells followed by cell disintegration or necrosis. A number of small molecule antioxidants (e.g. curcumin, quercetin and resveratrol) are capable of directly scavenging ROS, thereby short-circuiting the self-propagating oxidative stress state. However, poor solubility and rapid 1st pass metabolism results in overall low bioavailability and acts as a barrier for its use as a drug to suppress oxidative stress efficiently.

To overcome this limitation, these small molecule antioxidants were covalently conjugated into poly(β-amino ester) (PβAE) cross-linked networks to formulate prodrug gel microparticles and nanoparticles (nanogels). Being hydrolytically degradable in nature, these PβAE crosslinked systems released antioxidants in their original structural form in a sustained controlled fashion.

Both quercetin and curcumin-PβAE nanogels showed prolonged suppression of cellular oxidative stress induced by H_2O_2. Curcumin PβAE nanogels also demonstrated protection against mitochondrial oxidative stress induced by H_2O_2 and polychlorinated biphenyls.

Curcumin-PβAE gel microparticles were also developed as a platform to treat oral mucositis through a local antioxidant delivery route. The same synthesis chemistry was transferred to formulate resveratrol PβAE gel microparticles for topical applications, to treat UV radiation induced oxidative stress. Both formulations showed suppression of induced oxidative stress. An *in vivo* trial with curcumin-PβAE microparticles further showed relatively reduced the severity of induced oral mucositis (OM) in hamster check pouch as compared to placebo.

Keywords: Poly(β amino esters), antioxidants, oxidative stress, nanogels, microparticles

Prachi Gupta

3/11/16

SYNTHESIS AND CHARACTERIZATION OF ANTIOXIDANT CONJUGATED POLY(BETA-AMINO ESTER) MICRO/NANOGELS FOR THE SUPPRESSION OF OXIDATIVE STRESS

By

Prachi Gupta

Dr. Thomas Dziubla
(Director of Dissertation)

Dr. J. Zach Hilt
(Co-director of Dissertation)

Dr. Thomas Dziubla
(Director of Graduate Studies)

3/17/16
(Date)

ACKNOWLEDGEMENT

This dissertation is coming to its existence as a result of positive forces that have always surrounded me; motivating parents, encouraging mentors, supportive friends and continuous blessings from an unseen force we call God.

I am sincerely grateful to Dr. Thomas Dziubla, who has been my advisor, a counselor, and a boss, who constantly kept my doctoral journey interesting and challenging. Accompanying him, I would like to thank Dr. J. Zach Hilt, my co-advisor who has taken care of me and my research track with great effort and spirit. I would like to thank both of them for instilling in me the skills of an independent and innovative researcher with a very positive attitude that no result is negative. This theory surely applies in every phase of our day to day life and has transformed me into a better person over the past years.

I would like to convey my gratitude to my committee members, Dr. Stephen Rankin and Dr. Bernard Hennig for giving resourceful insights into my research. I would like to further acknowledge Dr. Robert Yokel, my external examiner for taking his time to look into my dissertation and pass on valuable suggestions.

I would like to thank all my research companions Paritosh, Dave, Sundar, Andrew, Nihar, Vinod, Mark, Irfan and Carolyn for maintaining a versatile, healthy and supportive work environment with a great team spirit. I also thank my undergraduate researchers, Erin, Manali, Donavyn, Caroline and John whom I got the opportunity to mentor in their research, giving me a wonderful experience throughout.

I am blessed with great friends, and I would like to acknowledge them for their love, support and memorable time gifted to me. I am grateful to have immense support from Sakshi (Chinki), Abhinav, Rishali, Chetna, Ashwini, Bhakti, Maulik, Mitesh, Prathemesh, Manali and Hersh for countless years.

My special acknowledgement goes to people who became my extended family away from home (popularly known as gazette janta) consisting of Shristi, Sonam, Suvid, Rutooj, Saket, Anwesha, Pratik Sogani, Amit, Suraj, Ishan, Ashish,, Abhishek, Priyesh, Shreya Patel, Raghav, Sumesh, Abhijit, Mini, Russel, Ravinder, and Pratik Rane. Thanks for making each and every day full of fun, adventure and innovation in this beautiful town, Lexington.

I would like to acknowledge the blessings of my parents (Mrs. Manju Gupta and Prof. T. C. Gupta), and dedicate my dissertation to them. This achievement came to fruition due to their support and never ending patience. Their encouraging attitude to explore with creative freedom meanwhile instilling values into me, kept me inclined towards science from childhood. I am also grateful to my brother (Sudhanshu) and sister-in-law (Liza), who always made sure that I cross all the hurdles with confidence and guided me with practical advice during challenging times.

TABLE OF CONTENTS

LIST OF TABLES

LIST OF FIGURES

1. INTRODUCTION

Oxidative stress (OS) is a pathophysiological state, which is defined by the imbalance of oxidants and antioxidants present in the body. This imbalance can be initiated by increasing reactive oxygen species (ROS) and reactive nitrogen species (RNS) production in a variety of scenarios, including exposure to environmental toxicants such as polychlorinated biphenyls (PCBs), intake of cancer treatment drugs like doxorubicin for chemotherapy, and radiation therapies. The lack of antioxidant capacity to balance out this preliminary excess ROS production leads to the cascading ROS production cycle involving processes such as ischemia reperfusion and lipid peroxidation. This excess production, in turn, leads to the oxidation of cell components, such as cell membranes, DNA, lipids etc., ultimately resulting in cell death. Common examples of ROS include singlet oxygen ($^1O_2$), transition metal ions, superoxide radicals ($O_2^{\cdot -}$), hydrogen peroxide, hydroxyl radicals and peroxynitrite ($ONOO^-$). Mitochondrial oxidative stress has been shown to play a vital role in development of several neurodegenerative diseases like Alzheimer's and Parkinson's disease [1].

Administration of antioxidants as therapeutics is a potential solution to alleviate the steady-state oxidative stress and help metabolism cope beyond its natural antioxidant capacity against oxidants/ROS/RNS. Plants and fruit derived dietary small molecule antioxidant scavengers, such as curcumin, quercetin, and vitamin E, have gained critical interest in the area concerning mitigation of OS. In spite of their excellent self-sacrificial property to neutralize free radicals, these bioactive compounds have failed to substantiate themselves as potential drugs for suppression of OS. Some of the key underlying explanations behind this poor performance is due to their limited aqueous solubility, structural instability in the physiological environment and hence overall low

bioavailability [2]. Taken together, these properties greatly limit bioavailability, preventing systemic drug concentrations from reaching the therapeutic window. While, these are some interpretations derived from several *in vivo* and clinical trials, *in vitro* studies shows evidence of suppressing oxidative stress [3]. The extent of this protection is again limited due to their very low viable concentrations at the cellular level or demonstration of pro-oxidant effects at high administered doses [4]. Thus, high levels of antioxidants could be seen as a solution to inhibit cancerous cell growth but not a fix for OS in healthy cells.

As a result, though highly potent, maintaining an effective drug concentration without being toxic is a challenge with antioxidants. Further, preserving them in their active form after administration is another barrier to effective drug delivery. An antioxidant prodrug system with controlled drug release could be a possible solution to this challenge and direct polymerization of antioxidants into a poly(β amino ester) (PβAE) style polymer could be a possible way to achieve this approach. Synthesized via Michael addition reaction of an acrylate with a primary or secondary amine, PβAEs are hydrolytically biodegradable systems through their ester linkages. They can be formulated into crosslinked networks via reaction of a multiacrylate compound with a multifunctional amine [5]. Further utilizing the synthesis chemistry covalently conjugating antioxidants into the crosslinked networks would protect the bioactive functional groups from getting deactivated until released [6]. Upon hydrolytic degradation, these PβAE crosslinked networks would release conjugated antioxidants in their original structural form in a controlled manner.

Owing to these benefits of the synthesis chemistry, formulating the antioxidant PβAE systems into microgels or nanogel networks would open up the options to various

delivery routes including local, intravenous, inhalation and other injectable approaches. Control over drug release kinetics and particle size would further make the system more adaptable in drug delivery systems.

Therefore, development of robust and functionally active antioxidant-PβAE particles in the nano to micro size range was pursued for local and systemic therapy applications.

A single step synthesis chemistry to conjugate polyphenolic antioxidant into PβAE crosslinked systems, previously designed in the Dziubla lab, was adopted involving the reaction of acrylate functionalized antioxidants with multifunctional amines [6]. While the PβAE synthesis processes were modified according to the type of particle system desired, different anti-inflammatory polyphenolic antioxidant drug molecules (quercetin, curcumin and resveratrol) were also explored to analyze the pliability of the formulation processes. Figure 1.1 summarizes the overall idea of the research goals and is also discussed below.

Quercetin-PβAE nanogels (CHAPTER 4) were synthesized using a novel single step reaction-precipitation method utilizing the Michael addition chemistry. Allowing control over the nanogel diameter as a function of monomer concentration, the synthesis process was also amenable to the formulation of curcumin-PβAE nanogels (CHAPTER 5 and 6). Curcumin-PβAE crosslinked systems were further explored to synthesize antioxidant-PβAE gel microparticles systems (10-20 μm) via gel cryomilling method (CHAPTER 7). The gel microparticle synthesis process was also successfully employed in the formulation of resveratrol-PβAE gel microparticles (CHAPTER 8). Being able to synthesize these prodrug systems in different particle sizes and with different compounds demonstrated the flexible nature of the synthesis processes in drug delivery applications.

The hydrolytic degradation rate of these crosslinked systems was studied to analyze the antioxidant release rates. Both nano and microsystems showed a uniform and extended release of the structurally active antioxidants with no burst release effects, which is a critical requirement in most drug delivery applications. Further, tunable antioxidant release properties of curcumin and resveratrol microparticle systems were observed due to the incorporation of poly(ethylene glycol)diacrylate (PEGDA) as a co-monomer during PβAE gel synthesis.

With control over the above mentioned physicochemical properties of these antioxidant conjugated PβAEs, *in vitro* response of endothelial and dermal fibroblasts showed prolonged protection against H_2O_2 induced cellular oxidative stress. The uniform release profile of curcumin-PβAE nanogels with no burst release, in fact, resulted in a reduced cytotoxicity of curcumin at higher concentrations, thereby increasing the safety limit of the antioxidant. This characteristic allowed the antioxidant to be administered at therapeutic levels and work against mitochondrial and cellular OS in endothelial cells. The protective effect of these nanogels was also seen at mitochondrial levels with cells exposed to PCBs, which are considered environmentally persistent toxicants and are known to induce cellular disorders via OS route (CHAPTER 6).

While nanocarriers are the desired choices for systemic applications through various injectable or inhalation routes, use of larger particles i.e. microparticle drug carrier systems is not often favored for local drug delivery. Therefore, extending the application of antioxidant-PβAE systems, curcumin-PβAE microparticles were analyzed as a treatment therapy for oral mucositis through local delivery. Hence, a preliminary *in vivo* study employing the hamster pouch model under induced oral mucositis conditions was carried out. Locally delivering suspended curcumin-PβAE

microparticles during the developmental stage of oral mucositis showed decreased levels of oxidative stress markers and a reduced intensity in epithelial layer damage as compared to the placebo. Similarly, resveratrol-PβAE microparticles were also tested for their protective application towards UV radiation-induced OS. Although this project is currently at a partially completed stage, the system has shown promising results towards cellular OS suppression but needs optimization in synthesis processes and cleaner demonstration of the intended application.

Apart from the direct antioxidant conjugation method, another novel route through transesterification was identified to chemically conjugate –OH group containing drug molecules (detailed discussion in the Appendix). With the concept that an alcohol can be substituted into an ester bond to form a new ester, different alcohols were substituted into the already existing crosslinked PβAE gel matrix synthesized using PEGDA and 4, 7, 10-trioxatridecane-1, 13-diamine (TTD). Transesterification rate varied depending upon various ambient parameters and showed faster degradation with increasing polarity of gel matrix due to amine catalyzing effect. The effect was further enhanced by using alcohols of different chemical nature. This approach was applied towards conjugation of riboflavin into PEGDA-TTD gels and the rate of conjugation depended upon the polar nature of the synthesized gels.

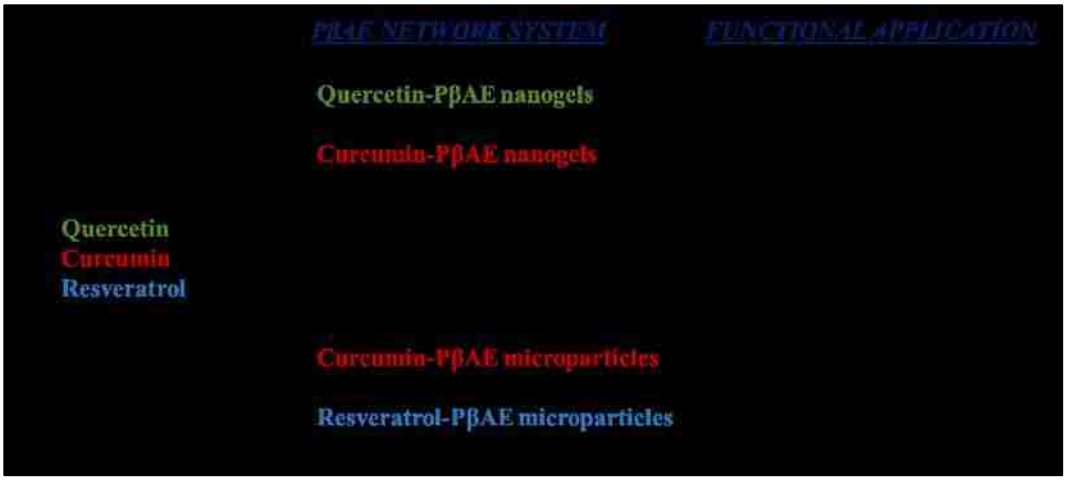

Figure 1.1 **Figure 1.1 PβAE crosslinked prodrug network systems**

2 BACKGROUND: A FREE RADICAL PRIMER

Based on the book chapter to be published:

Prachi Gupta, Andrew Lakes, Thomas Dziubla, Free Radical Chemistry Primer; To appear in 'Oxidative Stress and Biomaterials: The Science, Challenges and Opportunities' (Elsevier)

2.1 Free radical biology – importance

Free radicals, represented with a superscript 'dot' ($A^{\bullet}$), are defined as any atom or molecule containing an unpaired electron which has a strong tendency to gain another electron to achieve a non-radical state [7]. These molecules are considered to be highly reactive, are capable of reacting with a non-radical molecule in their quest for self-stabilization. Radical species can be found through a variety of mechanisms, one of which is an abstraction of an electron from an atom or a molecule. Radicals can also be generated by the splitting of a molecule at a very high-energy state. A classic example would be radiation induced homolysis of a water molecule into a hydroxyl radical and a hydrogen atom [8](eq 1)

$$\boldsymbol{H_2O + eV \rightarrow H^+ + OH^-} \qquad (1)$$

As these radical ions exist in a high and unstable potential energy state, they can react in a variety of ways. For example, two radica species can react with each other to form a non-radical molecule or one radical can donate an electron to another yielding two stable compounds [9].

As oxygen serves as the primary player in most biological free radical reactions, free radicals are also commonly known as reactive oxygen species (ROS). In a similar way, nitrogen base free radicals are called reactive nitrogen species (RNS). **Table 2.1** lists some of the most common free radicals/oxidants/ROS important in biology. Most of the essential cellular matrix components (protein, cellular membrane, DNA, lipids, polyunsaturated fatty acids etc.) in physiological systems are stable non-radical entities and perform their regular function of energy production in the form of ATP and maintain the cellular redox balance. But, the presence of more than the basal level of free radical molecules/ROS can lead to reactions of ROS with alternative cellular components in a quest to stabilizing themselves, damaging the chemical integrity of cellular biomolecules [10, 11]. One well-known example is lipid membrane damage via lipid peroxidation, where highly reactive hydroxyl radical react with polyunsaturated fatty acids (PUFAs) of the cellular membrane by extracting an electron yielding a lipid free radical. If this reaction phenomenon is not controlled in a timely manner, it can initiate a chain reaction of free radical molecules with intact lipids resulting in overall cellular membrane damage [12].

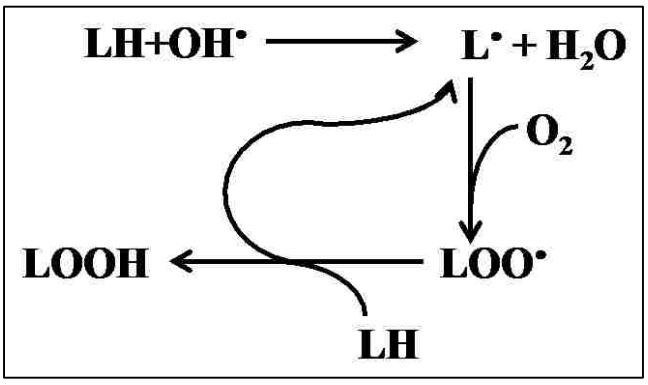

Figure 2.1 Lipid peroxidation cycle in presence of hydroxyl radical (OH•)

Although most of the research concerning the role of ROS/RNS has been done towards the potential cellular damage and subsequent pathological events, they do serve as a beneficiary to the body under certain conditions. When present in optimum concentrations, they help maintain the redox homeostasis in the cellular environment. This helps in regulation of cell functioning, cell signaling and appropriate response to endogenous and exogenous stimuli [13]. Under normal physiological conditions, a balance between generation and elimination of ROS/RNS via endogenous antioxidant enzymes/molecules helps the redox-sensitive signaling proteins to function properly [14]. Endogenous ROS enzymes like myeloperoxidase, and NADPH oxidase (NOX), also known as phagocyte oxidase, actually help the neutrophils perform their phagocytic function against microbial intrusion in an event known as respiratory burst. To briefly explain, NADPH oxidase catalyzed superoxide production forms hydrogen peroxide with the help of superoxide dismutase (SOD), which in turn converts to hypochlorous acid (HOCl) having bactericidal properties (eq 2) [15, 16].

Reaction:

$$NADPH + O_2 \xrightarrow{NADPH\ oxidase} O_2^{-\bullet} \xrightarrow{SOD} H_2O_2 \xrightarrow{Myloperoxidase} HOCl \quad (2)$$

Table 2.1 Potential free radical species

ROS/RNS	Symbol	ROS/RNS	Symbol
Superoxide	O_2^-	Hydroxyl	$OH^\bullet$
Hydroperoxyl	$HOO^\bullet$	Peroxyl	$ROO^\bullet$
Nitric oxide	$NO^\bullet$	Nitrogen oxide	$NO_2^\bullet$
Peroxynitrite	$ONOO^-$	Singlet oxygen	$^1O_2$
Hypochlorous acid	HOCl		

2.2 RED/Ox Chemistry

2.2.1 Oxidation/reduction reactions and voltage potentials

Originally, the term ‘oxidation’ was described as a process of any element, primarily metals, to combine with oxygen to form metal oxides and ‘reduction’ was defined as a process that will convert the metal oxide back to pure metal again. For example, conversion of magnesium (Mg) to magnesium oxide is oxidation and back to magnesium at high temperature in the presence of carbon is a reduction. Later, the discovery of electrons changed the definition of oxidation-reduction to a phenomenon of encountering any transfer of electrons from one species to another. As per the law of conservation of mass applied to electrons, oxidation and reduction are always linked to one another. Meaning, if one species is oxidized, the counter reactant species will be reduced [17, 18].

(3)

(4)

By definition, oxidation of any given element or molecule will involve a loss of an electron and the element/molecule will be known as a reducing agent while the reduction of any molecule will be a gain of electron and that molecule will be known as an oxidizing agent [19]. In reference to free radicals or ROS as such, they are commonly known to be strong oxidizing agents or have a tendency to get reduced [20,

21]. This is because most radicals have one unpaired electron, and the addition of another electron (or getting reduced) with opposite electron spin would help in stabilizing the electron pair taking them to a more inert state. However, this is not always true. The oxidizing tendency of any free radical will depend on its affinity to gain an electron or its own reduction potential against the affinity or potential of the co-reactant. It is possible that free radical 'A' gets reduced in presence of 'B' but might get oxidized itself by losing another electron in presence of 'C' because the reduction potential or electron gaining affinity of 'C' is greater than 'A'.

2.1.1.1 Types of redox reactions

Corrosion and rusting:

Iron has served as a common example of corrosion, which is the electrochemical oxidation of metals in the presence of oxygen to form respective oxides. In reference to iron, it is specifically termed as the formation of 'rust' (eq 5) [22].

$$4Fe + 3O_2 \rightarrow 2Fe_2O_3 \quad \text{……..Oxidation of Fe to } Fe^{+3} \qquad (5)$$

In presence of an acid, iron (II) is oxidized to iron (III) by reaction with hydrogen peroxide, which acts as an oxidizing agent [23], although iron (III) can be reduced back to iron (II) in presence of stronger reducing agents or free radicals such as superoxide anion [24]. This oxidation-reduction chemistry of iron, popularly known in terms of the Fenton or Haber-Weiss reaction mechanism, is very critical in maintaining the redox state of the cell.

$$2Fe^{+2} + H_2O_2 + 2H^+ \rightarrow 2Fe^{+3}\,(oxidized) +$$

$$2H_2O(reduced)$$ ……Oxidation of Fe^{+2} to Fe^{+3} (6)

Nitrification and Denitrification:

Nitrification often occurs naturally and is a biologically oxidative process where ammonia is oxidized to nitrite followed by formation of nitrate by nitrifying bacteria. On the other hand, reduction of nitrate to nitrogen in the presence of an acid is termed as denitrification and is often used as water purification process [25]. These nitrates have the ability to diffuse through the cellular membrane and play a significant role in the production of RNS in a cellular environment.

Nitrification:

$$NH_3 + O_2 \rightarrow NO_2^-(oxidized) + 3H^+ + 2e^-$$ (Ammonia to nitrite) (6)

$$NO_2^- + H_2O \rightarrow NO_3^-(oxidized) + 2H^+ + 2e^-$$ (Nitrite to nitrate) (7)

Denitrification: $2NO_3^- + 10e^- + 12\mathrm{H}^+ \rightarrow \mathrm{N}_2$ (reduced) + $6\mathrm{H}_2\mathrm{O}$ (Oxidized) (8)

Dismutation reaction:

Dismutation or disproportionation is a specific kind of redox reaction where both oxidized and reduced forms of a chemical species are produced. For example, superoxide free radicals produced in mitochondria dismutate to hydrogen peroxide and oxygen (equation 9) [26] or ascorbyl radical to ascorbate (vitamin C) and

dehydroascorbate (DHA) (eq 10) in order to maintain intracellular nutrient requirements for the cells [27, 28].

$$2O_2^- + 2H^+ \rightarrow H_2O_2(reduced) + O_2(oxidized) \quad (9)$$

$$2ascorbyl^\bullet + H^+ \rightarrow ascorbate\ (oxidized) + DHA\ (reduced) \quad (10)$$

Cellular respiration:

Oxidation of glucose to carbon dioxide with simultaneous reduction of oxygen to water is another kind of natural oxidation-reduction reaction required for energy production in living organisms. [29].

$$C_6H_{12}O_6 + 6O_2 \rightarrow 6CO_2 + 6H_2O \quad (11)$$

All the reactions (equation 5-11) showed their tendency to either undergo oxidation or reductions is controlled by their reduction potential. Reduction potential (E^o) is defined as a tendency of a chemical species to be reduced by gaining an electron and is defined with electrochemical reference of hydrogen, which is globally given the reduction potential of zero [30]. As this is an electric potential, it is measured in volts and each chemical species has its own intrinsic reduction potential. Numerically, the more positive the potential, the stronger is the affinity of the species to acquire an electron and get reduced.

2.1.1.2 Redox potential:

A normal redox reaction example could be as given below (eq 12):

$$Fe^{+3} + Cu^+ \rightarrow Fe^{+2} + Cu^{+2} \quad (12)$$

And this can be broken down into two parts:

$$Fe^{+3} + e^{-} \rightarrow Fe^{+2} \text{ .....reduction} \quad (13)$$

$$Cu^{+} \rightarrow Cu^{+2} + e^{-} \text{.....oxidation} \quad (14)$$

For a combined redox reaction, the overall redox potential is estimated by:

$$\Delta E = E^{o}_{acceptor} - E^{o}_{donor} \quad (15)$$

The electrochemical potential or reduction potential stated above is directly related to the Gibbs free energy (ΔG) of the reaction:

$$(\Delta G) = -nF\Delta E \quad (16)$$

where

n: number of electrons associated with the reaction

F: Faraday's constant

For a reaction to proceed total Gibb's free energy (ΔG) must be negative or ΔE should be positive. In equation 14, Cu is the electron donor with redox potential of Cu^{+2} to Cu^{+} is +0.16 V and that of Fe^{+3} to Fe^{+2} is 0.77 V. Therefore overall redox potential becomes +0.61 V.

To state this simply, for a system to undergo a redox reaction, the redox potential of a species to be reduced should be higher than the species to be oxidized. Table 2 lists some of the common redox potentials of certain half-cell redox couples and of some biomolecules important to physiological redox environment.

Table 2.2. Half-cell reduction potentials of biologically significant molecules

Redox couple	E^o (v)
$O_2 + 4H^+ + 4e^- \rightarrow 2H_2O$	+0.816
$NO_2 + e^- \rightarrow NO_2^-$	+ 1.04
$NO_3^- + 4H^+ + 3e^- \rightarrow NO + H_2O$	+ 0.96
$H_2O_2 + 2H^+ + 2e^- \rightarrow 2H_2O$	+ 0.82
$Fe^{+3} + e^- \rightarrow Fe^{+2}$	+ 0.77
$O_2 + 2H^+ + 2e^- \rightarrow H_2O_2$	+ 0.68
$2I_2 + 2e^- \rightarrow 2I^-$	+ 0.54
$2H_2O + O_2 + 4e^- \rightarrow 4OH^-$	+ 0.40
$2Cu^{+2} + 2e^- \rightarrow Cu$	+ 0.34
$2Cytochorme\ c^{+3} + 2e^- \rightarrow 2\ cytochorme\ c^{+2}$	+0.254
$2Cytochorme\ b^{+3} + 2e^- \rightarrow 2\ cytochorme\ b^{+2}$	+0.070
$Fumarate + 2H^+ + 2e^- \rightarrow succinate$	+0.031
$2H^+ + 2e^- \rightarrow H_2$	0.00
$FAD^+ + 2H^+ + 2e^- \rightarrow FADH_2$ (free coenzyme)	-0.22
$Oxaloacetate + 2H^+ + 2e^- \rightarrow malate$	-0.166
$Pyruvate + 2H^+ + 2e^- \rightarrow lactate$	-0.185
$NAD^+ + 2H^+ + 2e^- \rightarrow NADH + H^+$	-0.320
$NADP^+ + 2H^+ + 2e^- \rightarrow NADPH^+ + H^+$	-0.324
$O_2 + e^- \rightarrow O_2^-$	-0.33
$Succinate + CO_2 + 2H^+ + 2e^- \rightarrow \alpha - ketoglutarate + H_2O$	-0.324
$Na^+ + e^- \rightarrow Na$	-2.71

2.2.2 Thermodynamic treatment (Ellingham diagram)

A voltage potential is not the only way to determine the direction of the reaction. As stated earlier, for a reaction to proceed, ΔG should be negative which requires ΔE to be positive, but ΔG is also a function of temperature (Equation 17). An alternative to

determine the direction of a reaction can be obtained by a thermodynamic analysis of the reaction equilibrium.

$$\Delta G = \Delta H - T\Delta S \quad (17)$$

Where

T: reaction temperature

ΔS: Entropy change

ΔH: Enthalpy change

The temperature dependence of a reaction using equation (17) above is also utilized in redox chemistry to drive the direction of reactions of metal oxides and sulfides to pure metal. This phenomenon is usually illustrated in the form of an Ellingham's diagram, which represents the stability of a metal oxide as a function of temperature in reference to ΔG (Figure 2.2). Each line for a particular metal shows the free energy values for its metal oxide formation where slope depicts the ΔS values while the y-intercept gives ΔH. The position of the line of a metal with reference to another helps in depicting the metal oxide reduction ability in presence of another metal. To illustrate, the lower the position of metal ($Mg + O \rightarrow MgO$) is on Elligham's diagram, the more stable its oxide is at a particular temperature than the one that lies above it ($\frac{4}{3}Al + O_2 \rightarrow \frac{2}{3}Al_2O_3$). Therefore, magnesium can reduce aluminum oxide to metallic aluminum. Looking at the diagram, all the metal oxide formations have a positive slope while carbon oxidation to carbon monoxide has a negative slope and it cuts across many of the metals at particular temperatures. Therefore, carbon becomes very useful as a reducing agent for metal oxides at higher temperature. For example, carbon can reduce manganese oxide

(MnO) to its metallic form Mn once the reaction temperature goes above 1400°C while it will be able to reduce TiO_2 to Ti above 1600°C [31-33].

Therefore, with an analogous theory, the way reduction potential of two reacting molecules decide their possibility to get reduced or oxidized, in a similar way, ΔG of metal oxides of two interacting metal decides the fate of one getting reduced in presence of another.

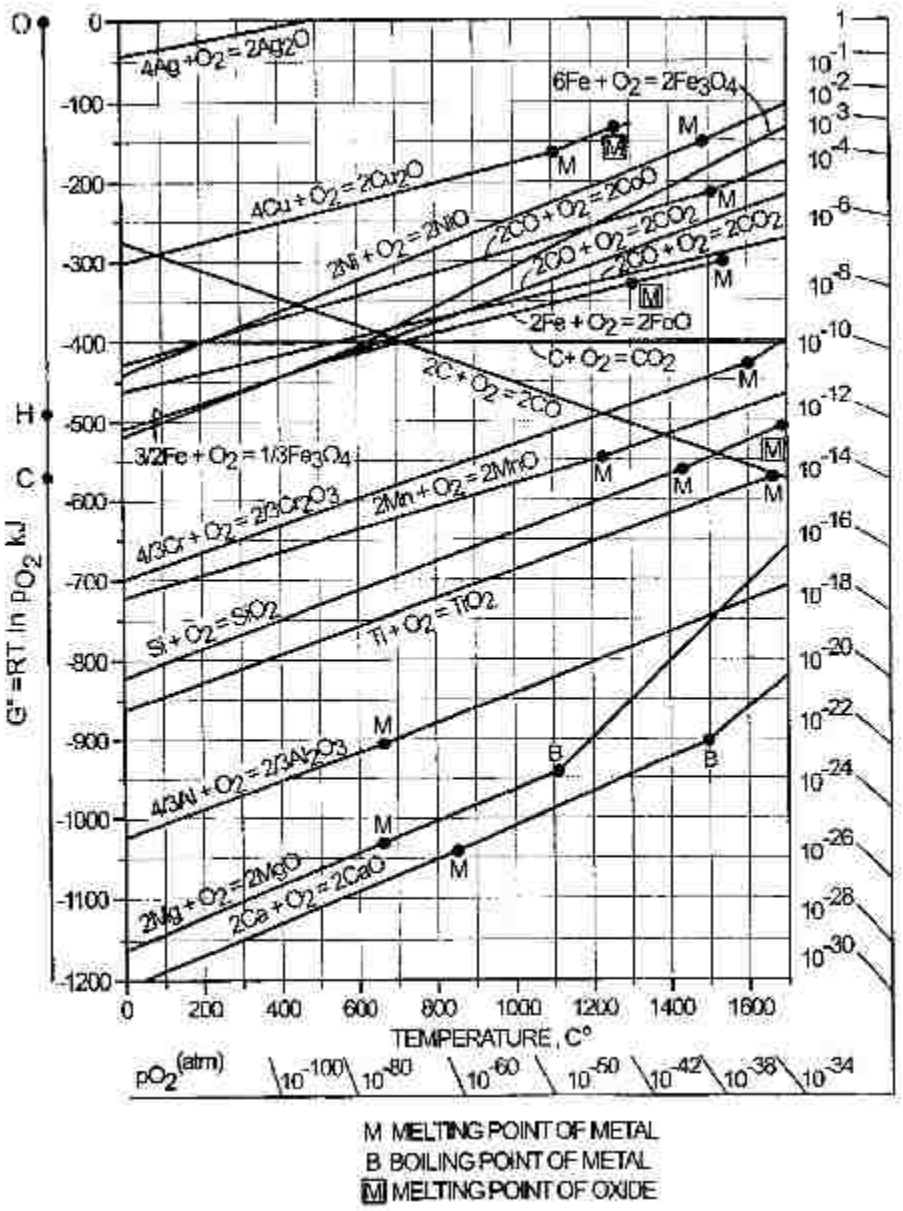

Figure 2.2 Ellingham's diagram [34]

2.2.3 Combustion sequences and/or metal oxides

Combustion is a classic example of free radical reactions and generation. It is a high temperature exothermic process involving multiple redox reactions of a fuel (hydrocarbons) with an oxidant, mostly oxygen, resulting in oxidized products primarily carbon dioxide and water, to generate heat and light. The overall combustion process of oils is described by the reaction below:

$$C_nH_{2(n+1)} + (4n + \frac{n+1}{2})O_2 \rightarrow nCO_2 + (n+1)H_2O \qquad (18)$$

While this equation is simple and describes the process in a general fashion, the exact chemistry of combustion is highly complex, multifaceted and not easy to describe.

As such molecular oxygen in its ground state is a very stable molecule and unreactive to hydrocarbons until a catalyst is introduced but at elevated temperature as high as 2200^{o}C, oxygen converts into highly reactive singlet oxygen (O_2^1) [35] and is known to have high oxidizing power. Singlet oxygen can react with and break carbon-carbon or carbon-hydrogen bonds of large hydrocarbons into smaller molecules and, subsequently, hydrogen and water. In the process, it is also capable of initiating numerous radical chain reactions via reaction with molecular hydrogen (H_2) resulting in the hydroxyl radical ($OH^{\bullet}$) and a proton (H^+). The combination of many such reactions results in the generation and simultaneous consumption of hydroperoxyl ($HCOO^{\bullet}$), formyl ($HCO^{\bullet}$) radicals, carbon monoxide [36, 37]. As for hydrocarbon pyrolysis, the process involves generation of various aliphatic and aromatic radicals.

Below are some of the common series of radical reactions that can occur during combustion process:

$$O_2 + H^+ \rightarrow O^{\cdot -} + OH^\bullet \quad (19)$$

$$O_2^1 + H_2 \rightarrow H^+ + OH^\bullet \quad (20)$$

$$C_3H_8 + M \rightarrow C_2H_5^\bullet + CH_3^\bullet + M \quad (21)$$

$$C_2H_5^\bullet + M \rightarrow C_2H_4 + H^+ + M \quad (22)$$

$$C_3H_8 + OH^\bullet \rightarrow C_3H_7^\bullet + H_2O \quad (23)$$

$$C_3H_8 + H^+ \rightarrow C_3H_7^\bullet + H_2 \quad (24)$$

$$C_3H_8 + O^{\bullet -} \rightarrow C_3H_7^\bullet + OH^\bullet \quad (25)$$

$$C_3H_7^\bullet \rightarrow C_3H_6 + H^+ \quad (26)$$

Decay to unsaturated hydrocarbons

These radical react with oxygen radical to produce formyl radical and formaldehyde and $CH_3^\bullet$, CH_2, H_2CO finally oxidize to CO_2 and H_2O.

$$C_3H_6 + O^{\bullet -} \rightarrow C_2H_5 + HCO \quad (27)$$

$$C_2H_4 + O_2 \rightarrow 2CO + H_2 \quad (28)$$

$$CO + 1/2O_2 \rightarrow CO_2 \quad (29)$$

Production of oxygen radicals also result in nitrogen oxide species production via reaction with atmospheric nitrogen as shown below:

$$O^{\bullet -} + N_2 \rightarrow NO + N \quad (30)$$

$$N + O_2 \rightarrow NO + O \quad (31)$$

$$N + OH^\bullet \rightarrow NO + H^+ \quad (32)$$

Therefore, looking at all the reactions above that are involved in the process of producing heat energy via oxidation of long/short chain hydrocarbon fuels it is clear, a milieu of free radicals are generated. Analogously, a host of free radicals are produced in the process of carbohydrate, glucose, or fructose metabolism to generate cellular energy in the form ATP. These free radicals play a critical part in maintaining cell function depending on their local and overall concentrations.

To explain this combustion further, a spatial relationship can also be generated described by the 'zone theory'. This concept divides the combustion process into four distinct zones: zone 1-free flame zone (fuel zone), zone 2-high temperature flame zone (>1200^{o} C), zone 3-post flame thermal zone (600-1200^{o} C) and zone 4-gas quench cool and surface catalysis zone (<600^{o} C) [38]. Usually radical formation and consumption takes place during zone 3 and zone 4 combustion. As the process reaches the lower temperature in the cool down zone (150 to 400^{o} C), free radicals, mostly phenoxyl and semiquinone exists. These aromatic compounds have resonating electrons and hence tend to stabilize via surface-mediated reactions with any surrounding transition metal ions. They tend to form a metal oxide complex and are known as persistent free radicals. These radicals are sometimes very stable in ambient conditions and can become environmentally persistent free radicals (EPFRs) [39]. These aromatic compounds generated during combustion also known as organic aerosols, mostly come from biomass ignition processes. The fact that EPFRs are stabilized due to interaction with metal oxides, their half-lives consistently depend upon the kind of metal oxide they interact with. As per the studies, EPFRs associated with zinc oxide (ZnO) were found to have the longest half-lives ranging from 3 to 73 days depending on the adsorbate [39].

The combination of radicals/oxidants generated during cellular metabolism and subsequent reaction combinations with transition metal ions also plays a similar role in accelerating the production of more radicals just like EPFRs. Figure 2.3 illustrates an analog of combustion zone theory with cellular respiration/metabolism at various stages, where oxidative phosphorylation process can be compared with the flame zone as the energy production step, heat energy for combustion and ATP for cellular respiration. Following that, just like the post flame zone defines incomplete combustion and initial production of radicals, partial oxygen reduction or proton leak during phosphorylation processes results in superoxide generation, which subsequently lead to H_2O_2 formation. In both cases, the role of radicals produced at this stage are boosted by the presence of a transition metal ion. With combustion, transition metal ion combination with radicals makes more environmentally stable EPFRs and are reactive to other biological species. During cellular metabolism, transition metal ions act as a catalyst towards production of more reactive and damaging oxidants namely hydroxyl radical ($OH^{\bullet}$).

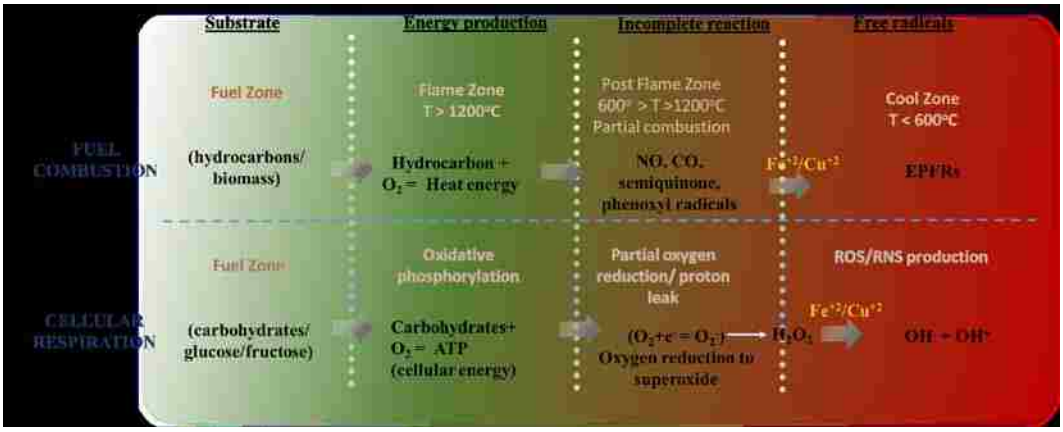

Figure 2.3 Analogous comparison of various stages of combustion zone theory with cellular respiration during energy production along with free radical generation [3]

2.2.4 Fenton/Haber-Weiss chemistry

Both the Fenton and Haber-Weiss reactions are associated with iron and the production of hydroxyl radicals. The Fenton reaction describes the formation of hydroxide (OH^-) and hydroxyl ($OH^\bullet$) radical by reaction between of Iron (II) (Fe^{+2}) with hydrogen peroxide (H_2O_2) [40], Haber-Weiss reaction is where hydroxyl and hydroxide ions are generated from the reaction of H_2O_2 and superoxide ion ($O_2^{\bullet-}$) catalyzed by iron [41].

$$Fe^{+2} + H_2O_2 \rightarrow Fe^{+3} + OH^- + OH^\bullet \text{.....Fenton reaction} \quad (33)$$

$$O_2^{\bullet-} + H_2O_2 \rightarrow OH^- + OH^\bullet + O_2 \text{.....Haber-Weiss reaction} \quad (34)$$

The Haber-Weiss cycle is actually a two-step reaction, where the ferric ion reduces to ferrous ion via reaction with superoxide, which, in turn, reacts with H_2O_2 to form OH^- and $OH^\bullet$ ions, converting ferrous back to ferric ion.

$$O_2^{\bullet-} + Fe^{+3} \rightarrow Fe^{+2} + O_2 \quad (35)$$

$$Fe^{+2} + H_2O_2 \rightarrow Fe^{+3} + OH^- + OH^\bullet \quad (36)$$

Though these reactions are named after these three scientists, there is a lot of history associated with the naming, discovery, and progression of this concept of iron redox reaction involvement in radical production. Henry J. H. Fenton reported for the 1st time the oxidation power of H_2O_2 and Fe^{+2} towards tartaric acid in 1876 but never mentioned the existence of the hydroxyl radical intermediate in the oxidation process although the reaction was named after him [42]. The existence of $OH^\bullet$ was 1st proposed by two German chemists, Fritz Haber and Joseph Joshua Weiss in 1934 via reaction of

hydrogen peroxide and superoxide in presence of iron as a catalyst [43]. Formation of this hydroxyl radical via transition metal catalyzed reaction has gained plenty of attention over the years and is considered to be one of the key processes for the production of the highly reactive $OH^{\bullet}$ in the cellular redox chemistry.

Not only hydroxyl radicals, but Fenton/Haber-Weiss chemistry involving redox coupling between iron and hydrogen peroxide gives rise to several other oxidizing intermediates including hydro peroxides ($HOO^{\bullet}$), superoxide (O_2^-) etc during various chain initiation and propagation reactions shown in equations 38-46. $OH^{\bullet}$ act as the chain carrier with the ability to react with Fe^{+2}, H_2O_2 or any other organic species to propagate the reaction. But in some instances chain termination also comes into effect via combination of two radicals ($OH^{\bullet}/OH^{\bullet}$ or $OOH^{\bullet}/OH^{\bullet}$) producing just hydrogen peroxide, water and oxygen as shown in equation 45 and 46 [44]. The existence and propagation of any of these reactions highly depends on the density of iron in its required oxidation state as well as the rate constant. An important condition for iron induced reduction of hydrogen peroxide is the low pH requirement between 3 and 6.

$$Fe^{+2} + H_2O_2 \rightarrow Fe^{+3} + OH^- + OH^{\bullet} \qquad K=5.7\text{x}10^2\ M^{-1}s^{-1} \qquad (37)$$

$$Fe^{+3} + H_2O_2 \rightarrow Fe^{+2} + H^+ + OOH^{\bullet}/O_2^- \qquad K=2.6\text{x}10^{-3}\ M^{-1}s^{-1} \qquad (38)$$

$$OH^{\bullet} + H_2O_2 \rightarrow OOH^{\bullet}/O_2^- + H_2O \qquad K=3.3\text{x}10^7\ M^{-1}s^{-1} \qquad (39)$$

$$Fe^{+3} + OOH^{\bullet}/O_2^- \rightarrow Fe^{+2} + O_2 + H^+ \qquad K=3.1\text{x}10^5\ M^{-1}s^{-1} \qquad (40)$$

$$Fe^{+2} + OH^{\bullet} \rightarrow Fe^{+3} + OH^- \qquad K=3.2\text{x}10^8\ M^{-1}s^{-1} \qquad (41)$$

$$Fe^{+2} + OOH^{\bullet}/O_2^- \rightarrow Fe^{+3} + H_2O_2 \qquad K=6.6\text{x}10^6\ M^{-1}s^{-1} \qquad (42)$$

$$OOH^{\bullet}/O_2^- + OOH^{\bullet}/O_2^- \rightarrow H_2O_2 \qquad K=2.3x10^6\ M^{-1}s^{-1} \qquad (43)$$

$$OOH^{\bullet}/O_2^- + OH^{\bullet} \rightarrow H_2O + O_2 \qquad K=8.9x10^9\ M^{-1}s^{-1} \qquad (44)$$

$$OH^{\bullet} + OH^{\bullet} \rightarrow H_2O_2 \qquad K=5.2x10^9\ M^{-1}s^{-1} \qquad (45)$$

Chain propagation and termination reactions associated with iron and hydrogen peroxide with rate constant measured at pH=5 [45-47].

Fenton chemistry is utilized commercially to treat water pollution, contaminated soils, sludge etc by oxidizing the pollutants like benzene, formaldehyde, rubber chemicals, pesticides etc. The rate constant for the initial reaction between Fe^{+2} and H_2O_2 is generally observed to be around 10^2 $M^{-1}s^{-1}$ but in biological systems, this rate of reaction with free Fe^{+2} is not enough for the oxidation to occur. However, when bound to ADP, ATP or citrate as a backbone, the oxidation rate goes up by at least two orders of magnitude giving a significant rate of reaction for the iron-catalyzed redox process to occur [48].

2.2.5 Thiol Chemistry (-SH -SS-)

Thiol-disulfide reactions are one of the most important redox reactions. In biology, oxidation/reductions govern the metabolic redox state of a cell. Thiol-disulfide interchange/exchange reaction is significant in itself where a thiol (RSH) reacts with a disulfide molecule (R'SSR'') to give a new oxidized disulfide (R'SSR) and the corresponding reduced thiol (R''SH) [49]. The reaction is base catalyzed and is proposed to proceed through S_N2, 2 step reactions as follows [50, 51]:

$$RSH \rightleftarrows RS^- + H^+ \qquad (46)$$

$$RS^- + R'SSR'' \rightleftarrows R'SSR + R''S^- \quad (47)$$

$$H^+ + R''S^- \rightleftarrows R''SH \quad (48)$$

$$\frac{d[R''S^-]}{dt} = k_{RS-}[RS^-][R'SSR''] \quad (49)$$

$$\frac{d[R''S^-]}{dt} = k_{obs}[RSH]_{total}[R'SSR'] \quad (50)$$

$$k_{RS-} = k_{obs}(1 + 10^{pKa-pH}) \quad (51)$$

R: Attacking group, R': central group, R'': leaving group

k_{RS-} *: calculated rate constant dependent on thiolate concentration but independent of pH*

$k_{obs:}$ *: observed rate constant dependent on total thiol concentration and pH*

In the reaction mechanism, thiolate anion (RS^-) acts as the active nucleophile or reactive species to propagate the reaction. Concerning the cellular environment, glutathione plays a key role in the thiol redox chemistry as it is the most abundant small molecule cellular antioxidant (see section 2.3.2 for an in-depth discussion on glutathione redox reactions). One of the important factors that contribute towards the occurrence of this thiol exchange reaction is the pKa of the corresponding thiol and the pH of the reaction environment [52]. For example, a thiol with pKa value of 10, 0.1% of the total thiol will form thiolate at pH 7 while at pH 8, 10 times higher thiolate ions would be present in comparison [50]. In other words, we can say that thiol-disulfide interchange is most favorable at pHs near to the pKa values of the thiol. For example, oxidation of glutathione (GSH) (pKa=9.33) to its oxidized form (GSSG) is faster at a higher pH of 9.43 with a rate constant k=45 L/mol.s as compared to at pH of 8.46 with k=9.1 L/mol.s

[53]. As pKa is a function of the structure of the thiol molecule, chemical properties of thiol molecules involved in the reaction will dictate the extent of reaction and their existence in reduced or oxidized form. For instance, reaction of 2-mercaptoethanol (pKa=10.14) with Ellman's disulfide (5-(3-Carboxy-4-nitrophenyl)disulfanyl-2-nitrobenzoic acid) (pKa=4.5) is faster than mercaptoethanol with oxidized glutathione (GSSG) (pKa=9.33) by the order of 10^4 in water [54, 55]. Also, the exchange reaction is faster when the pKa of a nucleophilic thiol (RSH) is as high as possible and that of the corresponding disulfide molecule ((R'SH/R''SH) is as low as possible. Stearic interference is another factor that would affect the rate constants of the thiol-disulfide exchange reactions. It is most pronounced when there is any carbon substitution at the α-position to sulfur. For instance, reaction of bis (t-butyl) disulfide with 1-butylthiolate ($k=0.26\ M^{-1}s^{-1}$) is 10^6 times faster than that with t-butyl thiolate ($k=10^{-7}\ M^{-1}s^{-1}$). Similarly, charge on the thiolate anion also affects the rate constants [56]. The effect is higher when the charged entity is near to the sulfur group [57].

The rate of reaction is often correlated with the Bronsted plot, which display the relationship between pKa of the reacting thiols/disulfide and the rate constant. The slope of the plot is defined by the bronsted coefficient (β), which normally lies between 0.4-0.5 for different thiol-disulfide exchange reaction. Equation 53 is generally recommended for calculating k_{RS^-} values for the thiolate content [58] and figure 2.4 shows the graphical association between pKa of thiol v/s log (k_{RS^-}) at pH 7 for a thiol-disulfide exchange reaction. Figure 2.4 also shows the degree of dissociation (θ) of the thiol and observed rate constant for the thiol/disulfide exchange reaction be predicted by equation 54. Therefore, the highest observed rate constant for exchange reaction is observed at pKa^{RSH} equivalent to pH of the solution, pH=7 in the figure.

$$\log(k_{RS-}) = 6.3 + 0.59pKa^{RSH} - 0.40pKa^{R'SH} - 0.59pKa^{R''SH} \quad (52)$$

$$k_{obs} = \theta k_{RS-} \quad (53)$$

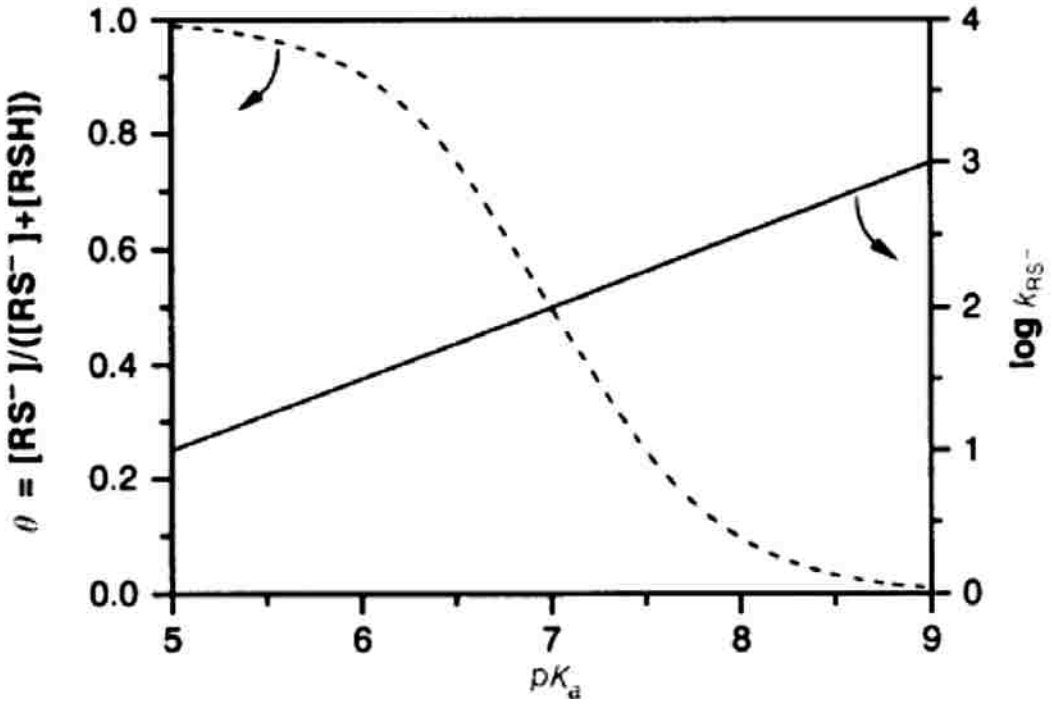

Figure 2.4 Correlation between pKa of reacting thiol and rate constant (k_{RS-+})/degree of dissociation (θ) where k_{RS-} was calculated using the equation (53), considering pKa of R'SH and R''SH group as 8.5 [50]

2.3 Biological oxidation events

2.3.1 Oxygen and nitrogen currency

Oxygen and nitrogen are the most abundant diatomic gaseous molecules in the atmosphere and play a significant role in regulating both, human and plant metabolism. Nitrogen is known to be highly inert and even oxygen (O_2) in its ground state is a stable molecule. But O_2 at a higher energy state form, such as singlet oxygen (O_2^1) [59] or in the reduced form of superoxide ($O_2^{\bullet -}$), it can become an active source of free radical generation leading to disruption of the cellular redox state [60], while oxide forms of nitrogen (NO, NO_2) generally produced during combustion process can diffuse and lead

to the formation of intracellular free radicals or RNS. The age old Superoxide Theory of Oxygen Toxicity stated that the partially reduced form of oxygen i.e. superoxide via enzyme, auto-oxidation, mitochondrial electron transport chain, heme proteins etc is a primary cause of cellular toxicity [61]. Oxygen upon its one electron reduction to superoxide can further yield hydrogen peroxide via the dismutation process [62]. Hydrogen peroxide can reduce to the hydroxyl radical in the presence of transition metal ions like Fe^{+2}/ Cu^{+2}, a highly reactive radical in cellular biology capable of reacting with DNA, lipid membranes, proteins etc.[7]. Reactivity and reduction potential at various stages of oxygen radical production chains are different is shown in figure 2.5 and these reactions are often enzyme catalyzed. For example, dismutation of superoxide to hydrogen peroxide mainly occurs via superoxide dismutase (SOD) catalyzed reaction [63, 64], but a part of hydrogen peroxide production also takes place via a 2-step route of oxygen conversion to peroxyl radical followed by further reduction to H_2O_2. In an oxygen derived free radical production chain, H_2O_2 is although not a very reactive molecule species but serves as an intermediate to the production of hydroxyl radical ($OH^{\bullet}$) [65] via the Fenton reaction, which is highly reactive towards all cellular components and can lead to complete cell damage. Similarly, superoxide ion by itself is not very reactive towards non radical species but it can react very quickly with $NO^{\bullet}$ or phenoxyl radicals [66]. This radical has a unique selectivity towards its oxidizing properties. For example, it is not very reactive towards oxidation of NADH/ NAD^{+} but can readily oxidize enzyme-bound (lactate degydrogenase) NADH to NAD+ [67]. Apart from being an oxidizing agent (oxidation of ascorbate to ascorbyl radical), superoxide can also act as a reducing agent where it can reduce cytochrome c or Fe^{+3} to Fe^{+2} which is one of the steps in cellular redox cycling discussed later in section 2.3.3 [68, 69].

In reference to biological free radical production, oxygen nucleated free radicals are produced from all the oxygen that is inhaled or consumed by organisms and mitochondrion is considered to be the main source of superoxide radical production due to oxygen leakage in electron transport chain during ATP production and is reported to be produced by complex I and III [70-72]. Reported *in vitro* studies show that about 4% of the oxygen consumed gets converted into superoxide, though *in vivo* analysis have reported about 10-fold lower production i.e. about 0.4% of the total consumed which is still a significant amount of production leading to about 10 µM of intracellular concentration [73]. This charged radical readily diffuses through the mitochondrial membrane to react with other biological entities like proteins, PUFAs or produce other reactive species (H_2O_2, $OH^{\bullet}$).

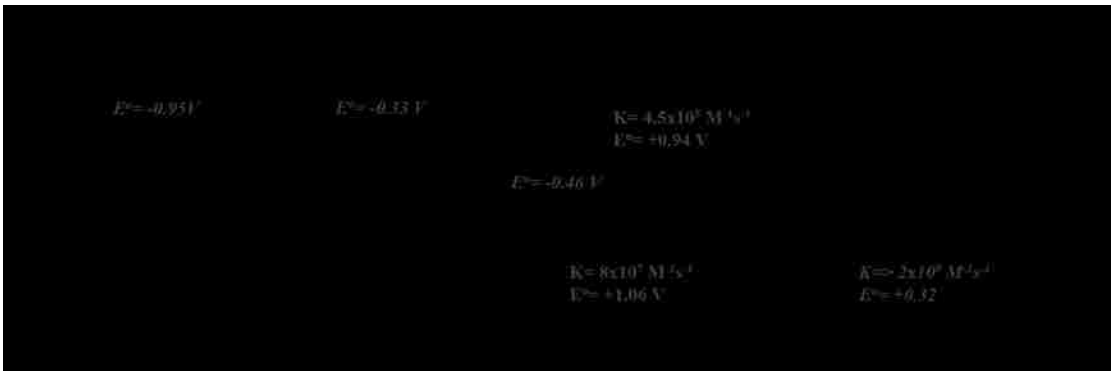

Figure 2.5 Free radical production/reactive oxygen species with oxygen as a precursor [7]

Although nitrogen is a stable and inert molecule by itself but its oxide form such as nitric oxide (NO), act as precursor to a variety of free radicals collectively known as reactive nitrogen species (RNS), which are equally capable of carrying out cell damage if produced in excess. Nitric oxide ($NO^{\bullet}$), due to its lipophilic property readily diffuses through cell membranes from the atmosphere where it is a byproduct of various combustion processes [74] (figure 2.6). In cellular metabolism, it is also a product of

the reaction of L-arginine and oxygen with NADPH in the presence of nitric oxide synthase (NOS) to give nitric oxide, L-citrulline and $NADP^+$ [75]. Nitric oxide by itself, is not very reactive towards non-radical species similar to superoxide anion, but can generate highly reactive free radicals such as, nitrogen dioxide ($NO_2^{\bullet}$) via slow reaction with oxygen (O_2) [76]. $NO_2^{\bullet}$ with the E^o value of 1.04 V is a potent oxidant in metabolic redox system and in RNS chains, it further reacts with $NO^{\bullet}$ leading to the production of N_2O_3, which eventually decomposes to give another reactive nitrite (NO_2^-) free radical [77]. In the presence of superoxide, $NO^{\bullet}$ reacts to form peroxynitrite ($ONOO^-$), which in itself is also a powerful oxidizing molecule [78, 79]. It is present in the form of acidified peroxynitrous acid (ONOOH) or its activated form ($^{\bullet}NO_2\ldots OH^{\bullet}$), both forms are capable of oxidizing most biological molecules such as DNA, proteins and lipids. $NO^{\bullet}$ also takes part in the modification of some biological molecules with thiols or amine groups during the process called nitrosation via direct reaction with thiols or via metal bound $NO^{\bullet}$ reaction with thiols/amines resulting in formation of nitrosothiols (RSNO) or nitrosamine (RN_2O) which are also regarded as non-radical RNS [80, 81].

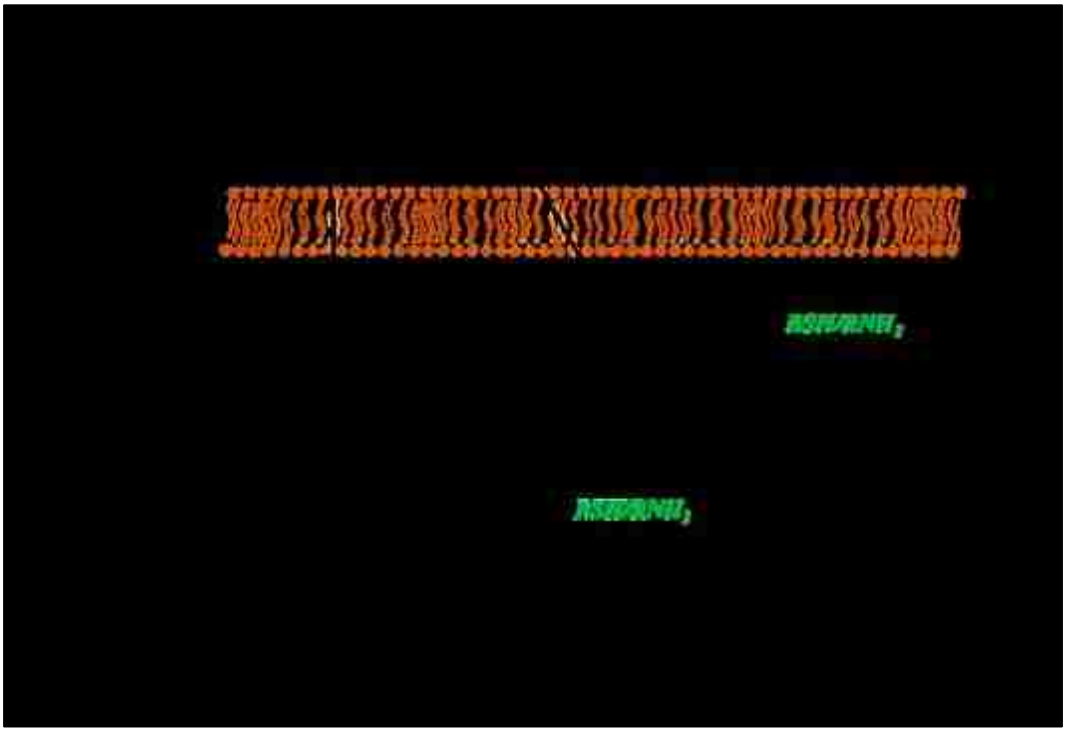

Figure 2.6 Reactive nitrogen species production

2.3.2 Cellular redox chemistry

Within the cellular environment, there exists an equilibrium between oxidants and antioxidants. Major players of these processes are defined in Figure 2.7. Of particular note is the small molecule antioxidant, glutathione (GSH), which contains an antioxidant thiol group and is the most abundant small molecule in eukaryotic cells, roughly found intracellularly from 1-10 mM and about 1-10 µM extracellular. [82-85] Synthesized within the cell from the three amino acids, glutamate, glycine, and cysteine, GSH production is rate limited by cysteine content, a semi-essential amino acid in biology. Cysteine is transported from extracellular space in the disulfide form, cystine. [86] Reaction of cysteine with glutamic acid in the presence of glutamate-cysteine-ligase (GCL) followed by reaction with glycine via glutathione synthetase (GSS) results in GSH production. [86] GSH may act in several mechanisms as an antioxidant, whether directly through electron donation to reactive oxygen or nitrogen

species in the intracellular or extracellular space, or via enzymatic routes such as with glutathione S-transferase (GST) to irreversibly reduce toxic species like lipid peroxides and protein carbonyls. [87] In addition to direct chemical reaction with oxidative species, GSH participates in several mechanisms to regenerate other important antioxidant enzymes such as glutathione peroxidase (GPx), glutaredoxin (GRX), and peroxiredoxins non-specifically. Oxidized glutathione (GSSG) may be reduced back to GSH via glutathione reductase (GR), which is driven by NADPH and the glucose-6-phosphate dehydrogenase (G6PD) cycle via oxidation of NADPH to $NADP^+$. There are also other thiol-based oxidoreductases such as thioredoxin, which utilizes cysteine thiol-disulfide exchange (instead of GSH), and is regenerated with thioredoxin reductase, similarly utilizing NADPH for regeneration akin to GSSG with GR.

Depending on the cellular compartment, redox equilibrium may vary. For instance, the cytosol (GSH:GSSG 100:1) and nucleus (GSH:GSSG >100:1) maintain a reducing environment [83, 88], whereas there are high concentrations of oxidants in the endoplasmic reticulum (GSH:GSSG of 1-3:1 [89], where disulfide bonds fortify the protein structures), mitochondria (GSH: GSSG of 20-40:1 [88]), secretory pathways, and extracellular space (GSH:GSSG 20:1 [85]). It is important to note that extracellularly while the GSH:GSSG ratio is around 10-20:1, cysteine and cystine are in greater concentration by about an order of magnitude, and maintain the oxidative environment around cysteine:cystine of 0.2:1 [85]. In a similar manner, NADPH is a reducing coenzyme involved in processes like fatty acid synthesis and is required to drive various redox reactions in the metabolic pathway. Therefore, NADPH:$NADP^+$ (200:1) ratios are found to be in same order of magnitude as for GSH/GSSG redox equilibrium to drive the reaction forward. On the other hand, another coenzyme NADH plays an essential part in both reduction and oxidation in general, hence a significant

concentration of both oxidized and reduced form is maintained in the cell with NAD^+ at higher concentrations. Cytoplasmic NADH which is produced by oxidation of cytoplasmic NAD^+ acts as an electron donor and is transported to the mitochondrion to reduce mitochondrial NAD^+ to NADH, which in turn is oxidized again during oxidative phosphorylation processes to generate ATP. It is postulated via several experimental studies that the NAD^+/NADH ratio in the cytoplasm is around 700:1 though the overall cellular ratio varies between 0.5:1 to 4:1. This ratio is involved in regulation of several metabolic enzymes such as glyceraldehyde 3-phosphate dehydrogenase, and pyruvate dehydrogenase used in the conversion of pyruvate to acetyl-CoA.

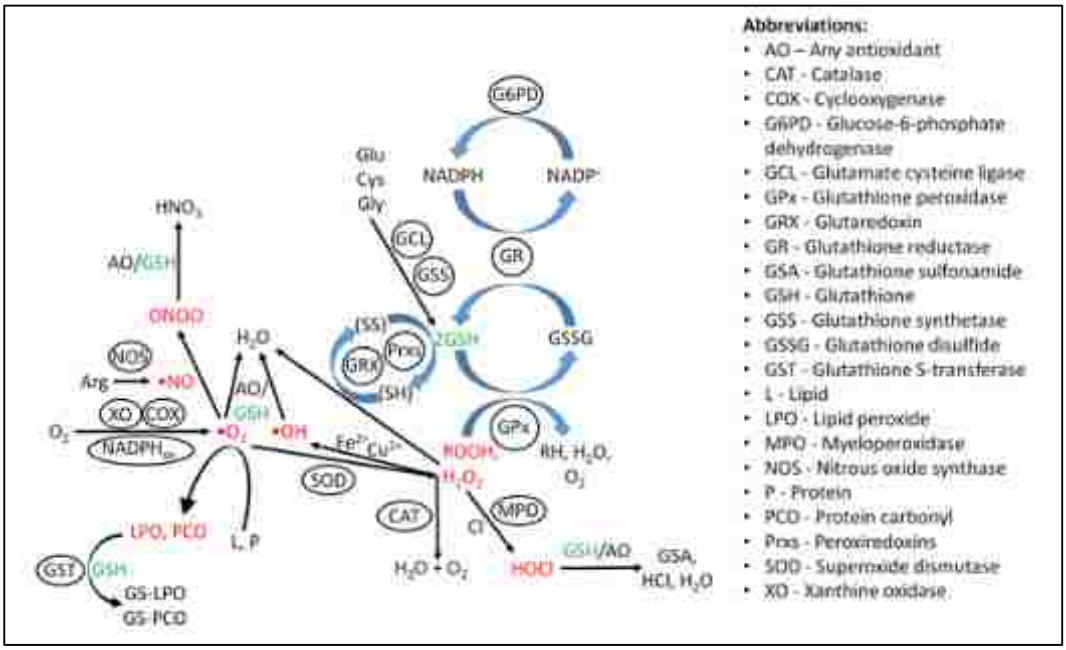

Figure 2.7 Significant cellular redox molecule interactions. Green: glutathione processes. Red: oxidant species reduced by glutathione processes.

2.3.3 Radical generation in metabolism and role of enzymes in redox cycle

ROS/RNS production takes place in a cellular environment via multiple metabolic pathways with the aid of specific enzymes at various sites in a cellular matrix and its organelles. In that, mitochondria are one of the most important cellular components

with the highest potential to produce free radicals ranging from hydroxyl to peroxynitrite to hypochlorite radicals. Figure 2.8 depicts the role of mitochondrion in the redox of cycle of a cell. Mitochondria are known to be the energy producer or ATP production center of the cell which takes place via tetravalent reduction of oxygen (O_2) in the presence of mitochondrial cytochrome c oxidase (COX) also called complex IV [90]. About 2-4% of this oxygen taken by mitochondria undergoes univalent reduction to superoxide ion ($O_2^{\bullet-}$) via the complex I enzyme (NADH-ubiquinone oxidoreductase) to a concentration of about 10 μM [73, 91]. Oxidation of NADPH to $NADP^+$ by O_2 in the presence NADPH oxidase is another source of $O_2^{\bullet-}$ which occurs as an important inflammatory response in phagocytes against bacterial infection and this process is often termed as oxidative burst [92-94]. NADPH oxidase also facilitates $O_2^{\bullet-}$ production in non-phagocytic systems like fibroblasts, endothelial cells, smooth muscle cells, although the rate of $O_2^{\bullet-}$ production here is $1/3^{rd}$ than that in neutrophils [13, 95, 96]. This superoxide anion is further converted to hydrogen peroxide by mitochondrial manganese superoxide dismutase (MnSOD) [97, 98]. Apart from controlling the $O_2^{\bullet-}$ concentrations inside the mitochondrion, cytosolic CuZn-SOD also catalyzes the superoxide dismutation to H_2O_2, 10^4 times faster than an uncatalyzed reaction ($k=2x10^9$ $M^{-1}s^{-1}$) [99]. Hydrogen peroxide is also known to be formed by two electron reduction of O_2 by cytochrome P-450 or acetyl coenzyme A oxidase [100-102].

Hydrogen peroxide is relatively stable and a membrane permeable non radical ROS, which either decomposes to water and oxygen with the help of catalase, glutathione peroxidase (GPx) etc [103, 104] or can further reduce to a highly reactive hydroxyl radical under transition metal ion catalytic conditions (oxidation of Fe^{+2} or Cu^{+2} to Fe^{+2} or Cu^{+3}) (Figure 2.9) [105]. In this pathway, oxidized iron or copper (Fe/Cu^{+3}) is reduced back to ferrous or cuprous ions (Fe^{+2}/Cu^{+2}) by superoxide ions present in the

vicinity, which in turn produce more hydroxyl radicals. The concentrations of superoxide anion, and transition metal ions significantly define the free radical production rates [106, 107]. Other active route of $OH^{\bullet}$ production is through disproportionation of peroxynitrous acid intermediate ($HO\ldots NO_2$) to hydroxyl and nitrous oxide (NO_2) radicals [108]. Due to the extremely high reactivity of the hydroxyl radical, it is very difficult to monitor its real-time concentration *in vivo.*

Peroxynitrite is a product of reaction of superoxide with endogenously generated nitric oxide ($NO^{\bullet}$) radical [109],[110]. NO is also generated in the cellular matrix via reduction of L-arginine in presence of nitric oxide synthase (NOS). As such NOS has three isoforms namely: (i) NOS1 (NOS I) found in neural tissues, (ii) NOS II or iNOS, inducible NOS, which is found in various cell types stimulated upon inflammatory response and (iii) eNOS found in endothelium [111]. Mitochondrial NOS (mtNOS) is another isoform, which facilitates the formation of $NO^{\bullet}$ inside the mitochondria. This NO formation plays an important role in regulating mitochondrial respiration and has the potential to reversibly inhibit cytochrome oxidase activity, which is responsible for superoxide production [112]. Reaction of superoxide with nitric oxide under physiological conditions to produce peroxynitrite is found to be 3 times faster than hydrogen peroxide production and again is also a highly reactive RNS [113]. Hydrogen peroxide also contributes to the production of hypochlorite radical upon reaction with chloride ion (Cl^-) in activated leukocytes by the action of myeloperoxidase (neutrophils and monocytes) and eosinophil peroxidase (eosinophils) [114, 115]. Their ideal function is to act as antimicrobial agents, but excess or unregulated production can result in fragmentation and aggregation of proteins [115, 116]. As for the production of singlet oxygen, it is known to be generated at the catalytic sites of multiple enzymes in the cellular matrix or via dismutation of unstable oxidation products like superoxide

both spontaneous and enzyme catalyzed. It is also known to be produced as a byproduct of peroxyl radical reaction between hydrogen peroxide and hypochlorite via the Russell Mechanism, found to occur in stimulated neutrophils mostly during the respiratory burst phenomena (anti-microbial cell lyses process) [117, 118].

Table 2.3 Role of enzymes in carrying out various redox reaction and maintaining cell homeostasis

Enzyme	Function	Ref
SOD (CuZn-SOD, Mn-SOD, Fe-SOD)	Catalyzes dismutation of superoxide to hydrogen peroxide	[119, 120]
NOS (eNOS, iNOS, NOSI)	Oxidation of L-arginine with production of nitric oxide (NO)	[75, 121]
NADPH oxidase	Superoxide production from dioxygen molecule	[75, 122]
GPx	Reduction of GSH to GSSG with simultaneous conversion of hydrogen peroxide to water	[123, 124]
Myeloperoxidase (abundant in neutrophils)	Produces HOCl from H_2O_2 and Cl^- ion, oxidation of tyrosine to tyrosyl radical in presence of H_2O_2	[125]
Catalase (in peroxisomes)	Decomposition of hydrogen peroxide to water and oxygen	[126, 127]
5-lipoxygenase	Inducible source of ROS production in lymphocytes	[128, 129]
Cyclooxygenease	ROS generation in TNF-α stimulated cells	[130, 131]
Xanthine oxidase	Source of ROS in diabetes mellitus, catalyzes oxidation of hypoxanthine to xanthine with simultaneous production of H_2O_2, xanthine further catalyzes to uric acid and H_2O_2, sometimes can also produce superoxide radical	[33]
monoamine oxidase (outer mitochondrial membrane)	Catalyzes oxidative deamination of biogenic amines, large source of H_2O_2 and $OH^\bullet$ radical as well.	[132]

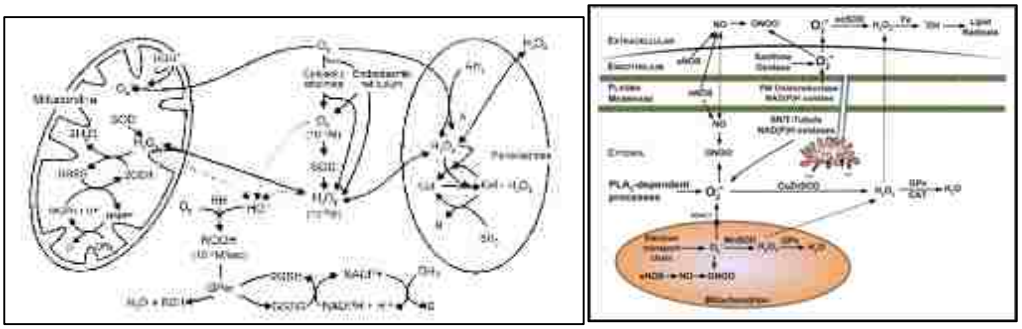

Figure 2.8 Examples of various routes of metabolic free radical production and detoxification pathways [113, 133]

Figure 2.9 Concept of redox cycle in maintaining the healthy redox state of a cell.

2.4 Known targets and elements of concern

Proteins, polyunsaturated fatty acids (PUFAs) and carbohydrates are very common targets to ROS. These molecules constitute very important cell organelles including lipid membranes, mitochondria, DNA and other nucleic acids. Reaction with these biological components starts with the excess production of ROS and insufficient endogenous antioxidants available to stabilize them, resulting in disruption of the cellular redox balance. Extent or affinity of ROS/RNS to react with the cellular components varies with the type of ROS depending on its reduction potential. For instance, hydroxyl and peroxynitrite radicals discussed in section 2.3.1 have relatively

higher reduction potential amongst other oxidants (Table 2.2) and are considered to be the most reactive towards lipids, DNA etc. It is difficult to detect or measure their quantity *in vivo* as their rate constants are in the range of 10^7 to 10^{10} $M^{-1}s^{-1}$, which almost matches their diffusion rates [133, 134]. In theory, oxidation of proteins, peptides, and amino acids by these free radicals can take place via several routes including hydrogen abstraction (favorable with aliphatic amino acids), electron transfer, dimerization, disproportionation, rearrangement and many more [135, 136]. Protein and amino acids have multiple sites of attack on their backbone and their reactivity depends on the stability of the resulting radical and degree of carbon hydrogenation [37]. Aromatic amino acids have a tendency to undergo an addition reaction with free radicals rather than hydrogen abstraction due to their stabilizing resonance property forming hydroxylated/ quinone molecules after reaction with hydroxyl radical [137, 138].

One of the most prone target sites to free radicals are mitochondria and their DNA components (mtDNA) [139, 140]. This is because, mitochondrion is the key production site of ROS/RNS where superoxide anion concentration is found to be 5-10 times higher than in the cytosol, with mtDNA to the closest proximity in comparison to nuclear DNA to the cytosolic ROS [141, 142]. There are numerous studies demonstrating that mitochondrial dysfunction due to excess ROS/RNS production is a kick-off event towards the final stage of cell apoptosis or necrosis [133]. The mitochondrial dysfunction is thought to start via mtDNA damage and protein deactivation. This leads to the incapability of the mitochondrion to maintain its membrane potential, resulting in the net loss of ATP production, de-structuring of the mito-membrane (inner and outer both), resulting in release of excess calcium ion (Ca^{+2}), cytochrome c and lysosomes.

These apoptogenic proteins/enzymes finally activate the apoptotic pathway leading to cell death [143].

Another potential target of ROS like singlet oxygen, peroxynitrite or hydroxyl radical is the cellular lipid membrane, which is made of unsaturated fatty acids. It is thought that the central carbon of the unsaturated fatty acids (L) is attacked by ROS/RNS to produce lipid free radical ($L^{\bullet}$), which oxidizes further to its alkoxyl ($LO^{\bullet}$) and peroxyl ($LOO^{\bullet}$) radical form [144]. These radicals, considered to be important intermediates in the lipid oxidation process, again reacts with another fatty acid chain (L) to produce more $L^{\bullet}$ radical and the chain reaction continues. In this propagation event, radicals like $NO^{\bullet}$ can act as an antioxidant towards termination of the chain by forming stable alkyl nitrites ($LONO_2$) or as pro-oxidant to form more $LO^{\bullet}$ and NO_2 through the peroxynitrite pathway (eq 54, 55 and 56) [145]. Due to this process, lipid fatty acid chains are often considered as secondary free radicals as they form reactive intermediates that propagate the lipid peroxidation chain reaction resulting in membrane degeneration and membrane protein dysfunction [113]. This degeneration leads to loss of membrane integrity making membrane bound protein even more susceptible to free radical attack. Alkyl peroxyl radicals (another form of secondary radicals) generated by decomposition of alkyl hydroperoxide in the presence of transition metal ion also contributes in the propagation of lipid peroxidation [146-149].

$$LOO^{\bullet} + NO^{\bullet} \rightarrow LOONO \quad (54)$$

$$LOONO \rightarrow LO^{\bullet} + NO_2 \ldots\ldots \text{ Chain propagation (14\%)} \quad (55)$$

$$\text{Or } LOONO \rightarrow LONO_2 \ldots\ldots \text{chain termination (86\%)} \quad (56)$$

3 RESEARCH OUTLINE

3.1 Overall hypothesis:

Antioxidant conjugated PβAE crosslinked micro/nanoparticles can be synthesized using the Michael addition chemistry of acrylates with amines, which exhibit tunable degradation properties, capable of releasing active polyphenolic antioxidants as well as increase the apparent solubility of these antioxidants. With controlled drug release through these systems, the apparent safe concentrations of the antioxidants can be increased, thereby opening the routes for prolonged suppression of cellular oxidative stress (OS) at therapeutic levels.

3.1 Specific aim 1. Synthesis and characterization of quercetin conjugated PβAE nanogels (Chapter 4)

a. Formulate quercetin-PβAE nanogels via single step reaction-precipitation Michael addition under dilute conditions.
b. Evaluate the impact of synthesis parameters (e.g. feed reactant concentrations, acrylate to amine ratio) on nanogel diameter and effect of PEG conjugation as a second step towards their aqueous stability and protein binding properties.
c. Study quercetin release profile during hydrolytic degradation of nanogels and the antioxidant activity of the degradation products.
d. Evaluate dose dependent cytotoxicity of nanogels and their ability to suppress externally induced OS.

Hypothesis:

a. The hydrodynamic diameter of Quercetin-PβAE nanogels increases with increasing feed reactant concentration and PEG conjugation helps in the

aqueous stabilization of these hydrophobic systems as well as decreases opsonization effects.

b. *Hydrolytic degradation of quercetin-PβAE nanogels at the ester linkage releases active quercetin in a steady state manner with bulk erosion kinetics. Extended release kinetics allows the system to suppress induced cellular OS for a prolonged period of time.*

3.2 Specific aim 2. Synthesis and characterization of curcumin conjugated PβAE nanogels (Chapter 5)

a. Formulate curcumin-PβAE nanogels using a reaction-precipitation method under dilute conditions and study the curcumin release kinetics via hydrolytic degradation.
b. Evaluate dose dependent cytotoxicity of curcumin-PβAE nanogels and compare them with free curcumin at similar equivalent concentrations with endothelial cells.
c. Evaluate their ability to prevent cellular oxidative stress and protection against mitochondrial OS using a H_2O_2 injury model by monitoring real-time mitochondrial bioenergetics.

Hypothesis:

a. *Uniform and steady release kinetics of curcumin with no burst release effect increases the in vitro viable concentration and hence widens the safety window of curcumin towards endothelial cells*
b. *Non-toxic nature at higher concentrations via administration of curcumin via curcumin-*PβAE *nanogels allows the OS injury to be treated at therapeutic levels and suppresses the mitochondrial oxidative damage for at least 24 hours.*

3.3 Specific aim 3. Curcumin P*β*AE nanogels for the protection against polychlorinated biphenyls (PCBs) induced toxicity (Chapter 6)

a. Study the dose dependent effect post PCB 126 and 153 treatment on overall cell toxicity and mitochondrial bioenergetics.
b. Analyze the protection against PCB-induced mitochondrial OS with the help of curcumin-PβAE nanogels by analyzing both overall cell viability and mitochondrial bioenergetics at variable nanogels pretreatment conditions.

Hypothesis:

a. Mitochondrial bioenergetics are more sensitive towards PCB exposure compared to overall cell viability and immediate toxic effects can be better analyzed at mitochondrial level than overall cellular response.

b. Curcumin-PβAE nanogel pre-treatment helps prevent mitochondrial dysfunction of PCB-exposed endothelial cells. Longer the nanogel pretreatment, better the suppression of OS during PCB exposure.

3.4 Specific aim 4. Synthesis and characterization of curcumin-P*β*AE gel microparticles to treat oral mucositis (Chapter 7)

a. Formulate curcumin-P*β*AE gel microparticles of different compositions using PEGDA as co-monomer to formulate tunable degradation systems.
b. Study the degradation kinetics of the curcumin-P*β*AE microparticles as a function of co-monomer compositions and antioxidant activity of the degradation products containing released curcumin.

c. Evaluate dose dependent cytotoxicity of the released products *in vitro* and the extent of protection against induced oxidative stress using Normal Human Dermal Fibroblasts as the model cell line.

d. Test the treatment/protection efficacy of microparticles *in vivo* on hamsters with induced oral mucositis injury using 5FU/scratch experimental model.

Hypothesis:

a. Increasing the content of PEGDA in curcumin-PβAE gel microparticles accelerates the degradation rate due to increased hydrophilic content in the gels.

b. Released products are active as free radical scavengers and microparticles with similar curcumin loading show relatively less cellular toxicity when compared with free curcumin.

c. Microparticles with high yet safe curcumin loading shows prolonged protection against induced OS in vitro and reduces the extent of oral mucositis injury in vivo with lesser dosage frequency.

3.5 Specific aim 5. Synthesis and characterization of resveratrol conjugated PβAE gel microparticles (Chapter 8)

a. Synthesize resveratrol conjugated PβAE gel films with PEGDA as a co-monomer (R-PβAE microparticles) and optimize antioxidant release kinetics based on polymer composition.

b. Analyze dose dependent toxicity of the microparticles and anti-inflammatory capacity to suppress H_2O_2 induced oxidative stress with normal human dermal fibroblasts.

Hypothesis:

a. *Increasing resveratrol content intensifies the hydrophobic nature of the crosslinked system leading to slower degradation kinetic and hence slow resveratrol release.*

4 SYNTHESIS AND CHARACTERIZATION OF QUERCETIN CONJUGATED POLY (β-AMINO ESTERS) NANOGELS

Based on the research articles published in:

Prachi Gupta, J. Zach Hilt, Thomas D. Dziubla, 'Quercetin conjugated Poly (β-Amino Esters) Nanogels for the Treatment of Cellular Oxidative Stress', (Acta Biomaterialia), 2015, 27, 194-204

Abstract

PβAE polymers have emerged as highly promising candidates for biomedical and drug delivery applications owing to their tunable, degradable and pH sensitive properties. These polymeric systems can serve as prodrug carriers for the delivery of bioactive compounds, which suffer from poor aqueous solubility, low bioavailability and are biologically unstable, such as the antioxidant, quercetin. Using acrylate functionalized quercetin, it is possible to incorporate the polyphenol into the backbone of the polymer matrix, permitting slow release of the intact molecule which is perfectly timed with the polymer degradation. While formulating the quercetin conjugated PβAE matrix into nanocarriers would allow for multiple delivery routes (oral, intravenous, inhalation etc.), well-known oil-water nano-emulsion formulation methods are not amenable to crosslinked hydrolytically sensitive nanoparticles/nanogels. In this work, a single-phase reaction–precipitation method was developed to formulate quercetin conjugated PβAE nanogels (QNG) via reaction of acrylated quercetin (4–5 acrylate groups) with a secondary diamine under dilute conditions using acetonitrile as the reaction medium, resulting in a self-stabilized suspension. The proposed approach permits the post synthesis modification of the spherical nanogels with a PEGylated

coating, enhancing their aqueous stability and stealth characteristics. Nanogel size was controlled by varying feed reactant concentrations, achieving drug loadings of 25–38 wt%. Uniform release of quercetin over 45–48 hours was observed upon PβAE ester hydrolysis under physiological conditions with its retained antioxidant activity over the extended times.

4.1 Introduction

Oxidative stress is a pathophysiological condition when endogenous antioxidants are unable to counteract the production of oxidants, leading to cellular dysfunction. The origins for this overproduction of the reactive oxygen and nitrogen species (ROS/RNS) (e.g., hydroxyl radicals, singlet oxygen, hydrogen peroxide, peroxyl radicals) can be caused by both endogenous sources and exogenous sources. Examples of endogenous routes include ROS-generating enzymes such as nitric oxide synthase, xanthine oxidase, amplified mitochondrial metabolism especially in aging cells resulting in mitochondrial dysfunction, damaged membrane and hence leakage of ROS into the intracellular environment [150-153]. Some of the exogenous sources include exposure to ozone, UV, ϒ-irradiation, air pollutants penetrating through the skin or via inhalation, intake of various drugs, xenobiotic and many more [153-158]. At a systemic level, oxidative stress has been shown to play a role in the development and acceleration of many diseases, including diabetes, cardiovascular diseases, Alzheimer's and Parkinson's disease, acute renal failure, acute lung injury, radiation injury, etc. [159, 160].

Rationally, one would expect that the supplementation of dietary antioxidants would be sufficient to reduce the excess ROS into non-reactive stable molecules, resolving the oxidative stress and thereby mitigating many diseases. In fact, this beneficial property of antioxidants, including polyphenol flavonoids, has been successfully demonstrated

in vitro several times using different assays [161, 162]. But despite these *in vitro* demonstrations, nearly all clinical trials with antioxidants have failed to demonstrate substantial benefit [3, 163]. As a result of these outcomes, it was inferred that the major limitation of dietary antioxidants was their inability to impact the oxidative stress levels in the patients. Given the highly unstable nature of these antioxidants, their typically poor aqueous solubility and lack of natural accumulation in tissues of interest, it is unsurprising that these molecules were unable to perform their intended function. For instance, quercetin has been shown in multiple *in vitro* and *in vivo* studies to possess anti-inflammatory [34], anti-hypertensive [164], anti-allergic [165] properties and an ability to control metabolic syndrome [166]. Yet, it has not been used therapeutically for pharmaceutical applications due to its low bioavailability, which is likely due to its poor aqueous solubility, structural instability and extensive first pass metabolism [167, 168]. It has been reported that the oral bioavailability of quercetin is 17% in rats and merely 1% in humans [168, 169]. Moreover, upon intravenous injection, a 100 mg of dose resulted in 12 µM plasma concentration after 5 minutes and 1 µM after 3 hours, demonstrating the relatively short half-life of the compound [170].

In order to overcome this difficulty of low systemic bioavailability, one potential solution is to deliver quercetin through encapsulation into nanoparticles, which can be administered via a number of routes (e.g., intravenous, subcutaneous, inhalation, etc.) with an objective of extended drug release and control the rate of first-pass metabolism [171]. Several studies have demonstrated the ability to encapsulate quercetin into nanoparticles composed of poly (lactic acid) (PLA), poly (lactic-co-glycolic acid) PLGA, solid lipid nanoparticles (SLN). However, these approaches, while potentially useful, possessed significant burst drug release and low overall drug loading, ranging from only 0.05 to 2 wt% of the total particle weight [172, 173]. Incorporating

antioxidants into the backbone of a polymer system could be an alternative towards the effective antioxidant delivery as demonstrated by Wattamwar et. al. in his work on enzymatically biodegradable poly(trolox) nanoparticle system to deliver trolox, a water soluble analog of vitamin E [174].

Building upon this prior work, it may be possible to overcome drug stability, solubility and drug release limitations by conjugating the drug into the backbone of a hydrolytically biodegradable polymer, such as poly(β-amino esters) (PβAEs), to form prodrug nanoparticles/nanogels [175, 176]. Our lab has shown previously that antioxidants like curcumin and quercetin can be loaded into crosslinked PβAEs and subsequently released into their original structural form upon hydrolysis [177]. But due to the fast reaction kinetics and hydrolyzing property of PβAE, the bulk crosslinking approach is not amendable towards typical nanoparticles synthesis approaches (e.g., o/w emulsion polymerization). To overcome this problem, we have synthesized quercetin conjugated PβAE gel nanoparticles/nanogels using a novel approach of single phase reaction-precipitation method in an organic solvent under dilute conditions giving a stable suspension of uniformly sized particles. Covalently reacting terminal amine groups with poly (ethylene glycol) monomethacrylate resulted in a coating that minimizes post purification instability, is expected to reduce the rate of first-pass metabolism and serves as an alternative to conventional surfactant based stabilization of nanoparticles. Uniform degradation of these nanogels over 48 hours successfully demonstrated release of active quercetin with negligible burst release. Particle sizes were easy to control with resulting quercetin loading capacities of 25-38 wt%, which possessed biocompatibility equivalent to pure quercetin and were able to suppress cellular oxidative stress over 48 hours.

4.2 Materials and methods

4.2.1 Reagents

Quercetin was purchased from Cayman Chemicals, Michigan, USA. Acryloyl chloride, potassium carbonate**,** N, N'-dimethyl 1-3-propanediamine, polyethylene glycol methyl ether methacrylate (Mn=4000) (PEGMEMA4000), potassium persulfate, 2, 2'-azo-bis (3-ethylbenzothiazoline-6-sulphonic acid), and hydrogen peroxide were purchased from Sigma-Aldrich. IgG antibody was purchased from Jackson Immuno Research Laboratory Inc. For cell culture studies, EBM basal medium (phenol red free), EGM-2 growth factors, and Human Umbilical Vein Endothelial Cells were purchased from Lonza. Calcein-AM red-orange and 2', 7 dichlorodihydrofluorescein diacetate (H_2DCFDA) were purchased from Life Technologies. Iodogen® iodination reagent (1, 3, 4, 6-tetrachloro-3α-6α-diphenylglycouril) was bought from Thermo Scientific, Rockford, IL.

4.2.2 Quercetin functionalization to quercetin multiacrylate monomer

Quercetin multiacrylate (4-5 acrylate groups per molecule) (QMA) was prepared in accordance with the protocol described by Wattamwar et. al. [178] with a slight change of using potassium carbonates as the acid capturing agent instead of triethylamine. Briefly, the reaction between quercetin (20 gms in 200 ml of Tetrahydrofuran (THF)) and acryloyl chloride was carried out in anhydrous THF. Potassium carbonate was added to the reaction system to capture the hydrogen chloride forming its salt as the reaction byproduct. The system was purged with nitrogen for 30 minutes initially and then was further allowed to react overnight at room temperature to functionalize quercetin phenolic groups into acrylate. Acryloyl chloride and potassium carbonate, were added in the molar ratio of 1:1.2 with respect to the phenolic groups present in quercetin. Quercetin has four phenolic groups, which can be actively functionalized.

Therefore, for every mole of quercetin, five moles of acryloyl chloride and potassium carbonate were added to the reaction medium. Acrylated quercetin solubilizes in THF as the reaction proceeds. After the reaction, solubilized product was separated from the precipitated salts via filtration. Subsequently, filtrated was vacuum dried to remove all the THF and was re-dissolved in dichloromethane (DCM) in order to carry out an aqueous-organic solvent extraction process to remove any unreacted acryloyl chloride/acrylic acid and quercetin. A basic solution of 0.1 M potassium carbonate in DI water was used as the extraction medium for acrylic acid and quercetin both. After extraction, magnesium sulfate was added to the product solubilized in DCM to remove any remains of water. Finally, the pure QMA was obtained as a dry product after evaporation of DCM overnight. Characterization of the functionalized quercetin was completed using ^{1}H-NMR and mass spectroscopy to identify the number of acrylate groups per molecule of quercetin.

4.2.3 Quercetin PβAE nanogel (QNG) synthesis

Quercetin PβAE nanogels were prepared using a single-pot dilute synthesis approach. QMA was dissolved in anhydrous acetonitrile to specified concentrations of 0.75, 1.25, 2.5, 5 and 10 mg/ml. A stock solution of N, N'dimethyl-1-3 propane diamine (NNDA, a secondary diamine) (100 mg/ml) was prepared in acetonitrile. Calculated volume of NNDA stock: 3.67, 6.12, 12.25, 24.5, and 49 µl was added to the reaction solutions with QMA concentrations: 0.75, 1.25, 2.5, 5 and 10 mg/ml respectively to achieve the required reaction concentration, maintaining a stoichiometric ratio of acrylate to reactive amine at 1:1.1. QMA-NNDA reaction in these diluted conditions resulted in precipitation into nanogel form. These quercetin-PβAE nanogels will be further referred as QNG (0.75), QNG (1.25), QNG (2.5), QNG (5), and QNG (10) for different systems with feed QMA concentrations of 0.75, 1.25, 2.5, 5 and 10 mg/ml respectively.

The reaction time of the nanogel synthesis was determined by analyzing the reaction supernatant at different time point to observe the decrease in QMA absorbance peak. After about 45 minutes of reaction, peak intensity does not change. Therefore with a buffer of 15 minutes, the reaction was carried out for one hour, resulting in precipitated nanogels. The hydrodynamic radius of the synthesized nanogels in acetonitrile was determined using dynamic light scattering (DLS) (Malvern Zetasizer (ZS 90)). Appropriate dilution using fresh acetonitrile were used in order to get the count rate between 200 to 300 cps. Hydrodynamic diameter was reported as z-average. All the parameters were set for acetonitrile medium at 25^{o} C.

After completion of the reaction, 63 µl (32 mg) of a concentrated solution (500 mg/ml) of polyethylene glycol methyl ether methacrylate 4000 (PEGMEMA4000) in acetonitrile was added to 1 ml of the nanogel suspension along with gentle mixing for few seconds to get 3% wt/vol PEGMEMA4000 in suspension. This system was allowed to react for one hour, followed by centrifugation at 6700 rpm for 10 minutes (Figure 4.1). The pellets were re-suspended in fresh acetonitrile by sonication for 3-5 minutes. Particles were then centrifuged and nanogels pellets were freeze-dried and stored at -80^{o} C for further analysis.

Nanogels were also synthesized at variable acrylate to reactive amine hydrogen stoichiometric ratios ranging from 0 to 10, in order to study the effect of reactant molar ratio. For this system, QMA feed concentration was kept constant at 2.5mg/ml and amine content was varied. Nanogel suspension obtained from each ratio was diluted with DMSO, in order to dissolve any precipitated quercetin due to the excess amine. The size of the nanogels in suspension was measured using DLS after adjusting the instrument parameters according to the suspension medium.

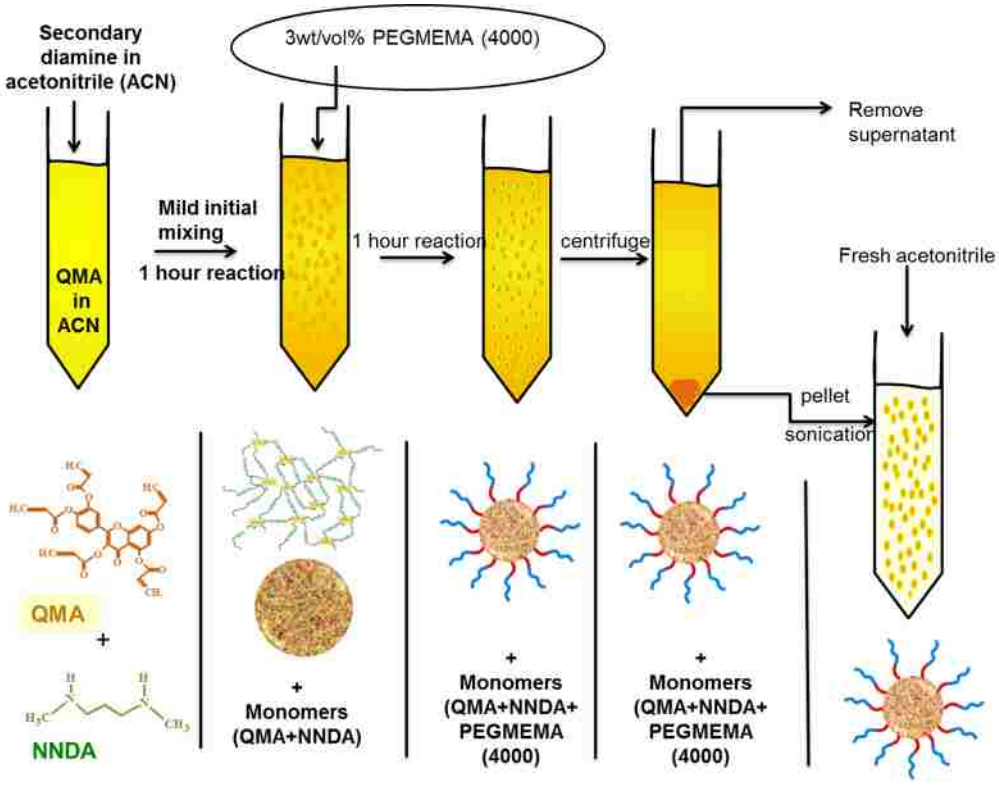

Figure 4.1 Schematic of Q-PBAE nanogel synthesis

4.2.4 Size and yield of nanogel synthesis reaction

In order to determine reaction yield, concentration of unreacted QMA in the supernatant obtained after first centrifugation was measured, via UV-VIS spectroscopy. The sample was prepared by diluting 100 µl of supernatant with 1 ml of acetonitrile. The absorbance of the diluted solution was measured at 350 nm using UV-VIS spectrophotometer (Varian Cary 50 Bio UV-Vis spectrophotometer). The amount of unreacted QMA was calculated using standard calibration curve of pure QMA dissolved in acetonitrile and percent QMA reacted or yield was back calculated subsequently. The size of the nanogels was measured using DLS at different stages of synthesis.

4.2.5 SEM imaging

In order to determine particle morphology, scanning electron microscopy was performed on the synthesized nanogels. 50 µL of PEG coated nanogel suspension in

acetonitrile (synthesized using 2.5 mg/ml feed QMA concentration) was diluted to 1 ml with acetonitrile and probe sonicated 8-10 times at 2-6 watts. A drop of the solution was dried on gold plated surface overnight in the bio-hood and covered with Kim wipes as an added precaution to prevent dust settling. Next day the dried sample on a gold surface was sputter coated with gold-palladium alloy and images were taken at various magnifications using S-4300 Hitachi Scanning Electron Microscope.

4.2.6 Analysis of enhanced stability of nanogels after the reaction with PEGMEMA4000

To determine the impact of PEGMEMA4000 treatment on nanogel stability, particle size was analyzed at two stages, first before the PEGMEMA4000 reaction and second after the PEGMEMA4000 reaction. To prepare the samples, 50 µL of nanogel suspension was added to 1 ml of PBS (pH=7.4) to form a suspension. Size measurement of the suspended nanogels in PBS was carried out using DLS without any further agitation at an interval of 10 minutes for a total time of 50 minutes and recorded to analyze the effect of PEGylation. The size measurement was done for nanogels obtained at both the stages described above. Nanogels were also treated with only polyethylene glycol methyl ether Mn=5000 (PEGME5000) for 1 hour and analyzed for the size afterwards in order to determine the kind of linkage of PEG to nanogel surface.

4.2.7 PEG content analysis after nanogel formulation

Analysis of PEG content in nanogels was performed using the barium-iodide assay [179]. To carry out the assay, two solutions were prepared. A) 60 mg/ml barium chloride in 1.2 N HCl (HCl stock diluted in DI water), B) potassium iodide and iodine in DI water with a final concentration of 20 and 12.5 mg/ml respectively. Separately, 1 mg of nanogels was rapidly hydrolyzed in 500 µL of 5 N NaOH for 4 hours at 80^{o} C. Hydrolyzed nanogels were neutralized by addition of 500 µL of 5 N HCL.

PEGMEMA4000 dissolved in DI water was used for standard calibration within the range of 0-10 µg per well in a 96 well plate. 20 µL of the hydrolyzed nanogel solution was added to the wells. Sample and the calibration volumes were diluted to 170 µL with DI water. 40 µL of solution A was then added to each well followed by mixing. 40 µL of solution B after doing 1/5th dilution was added subsequently to all the wells and mixed. The reaction was allowed to develop for 10 minutes after which absorbance was recorded at 550 nm using Varian Cary 50 Bio UV-Vis spectrophotometer. Calibration curve of pure PEG was used to calculate the PEG content in the nanogels.

4.2.8 Antibody Binding studies of Q-PBAE nanogels using IgG using radiolabeling

^{125}I-IgG stock preparation: IgG was radiolabeled with ^{125}I to serve as a tracer to protein bound to the nanogels. Briefly, 200 µL of 2 mg/ml Iodogen® iodination reagent (1, 3, 4, 6-tetrachloro-3α-6α-diphenylglycouril) in chloroform was dried in a glass tube using dry nitrogen gas to form a thin layer on the glass wall. 100 µL of 1 mg/ml Mouse IgG was added to iodogen coated tube and radioactive iodine ($Na^{125}I$) was added and incubated for 5 minutes. Free iodide was removed from the protein using a Thermo Scientific protein desalting spin column according to manufacturing instructions. Any free iodine remaining in the spun down solution was determined using trichloroacetic acid (TCA) precipitation. Gamma counts of both the precipitate and supernatant were analyzed using a Perkin Elmer 2470 automatic gamma counter. The amount of free iodine in hot IgG was found to be 5.6%.

IgG binding to quercetin nanogels: Three different formulations of QNG were used: QNG (0.75), QNG (1.25), and QNG (2.5). IgG having 2 wt% *^{125}I-IgG* was added to the nanogels (with and without PEG coating) suspended in PBS. Final concentrations of IgG and nanogels in the buffer were maintained at 1.17 and 0.4 mg/ml respectively.

After 3 hours of incubation, the suspension was then centrifuged at 6700 g for 20 minutes to collect the pellet at the bottom and supernatant from the top. Both pellet and the supernatants of all the nanogel formulation were analyzed for the total gamma counts using gamma counter.

4.2.9 Quercetin release profile of Q-PBAE nanogels in PBS

QNGs were suspended in PBS buffer (pH=7.4) using probe sonication to a concentration of 1 mg/ml. As quercetin has very limited aqueous solubility, degradation buffer was prepared using 2 vol% DMSO in order to solubilize any released quercetin during hydrolytic degradation. This suspension was incubated at 37^{o} C in a shaker bath at 70 RPM. Every 2 hours, nanogel suspensions were centrifuged at 6700 RCF for 10 minutes and the supernatant was collected and stored at -20^{o} C for further analysis. The centrifuged pellet was re-suspended in the fresh buffer to continue degradation. Absorbance of the supernatant was measured at 370 nm using Varian Cary 50 Bio UV-Vis spectrophotometer to determine the amount of quercetin released. Degradation was carried out for 50 hours and quercetin concentration in supernatants were analyzed after each collection.

4.2.10 *In vitro* antioxidant activity capacity of the degradation products of nanogels

Antioxidant activity of released quercetin and degradation products was evaluated using the Trolox Equivalent Antioxidant Capacity (TEAC) assay, which is based on scavenging of 2, 2'-azinobis-(3- ethylbenzothiazoline-6-sulfonate) radical anions ($ABTS^{\cdot}$-). Briefly, 7 mM ABTS radical cation stock solution was prepared by mixing 1 ml of 8 mg/ml of ABTS solution with 1 ml of 1.32 mg/ml of potassium persulfate solution, both prepared in DI water. This solution was allowed to react overnight to form ABTS radical cation stock solution. After 24 hours, ABTS radical cation working

solution was prepared by diluting the stock solution in PBS to an absorbance of 0.4 at 734 nm. For calibration purposes, a standard solution of trolox of known concentrations (0 to 0.27 mM) in PBS were prepared and used for the assay. To carry out the TEAC assay, 10 µL of the test sample (degradation supernatants/trolox standards) was added in a 96-well plate. Subsequently, 200 µL of the ABTS radical cation working solution was added to all the wells. After 5 minutes absorbance of all the samples was measured at 734 nm. Trolox standard curve with respect to the obtained absorbance was prepared and equivalent trolox concentration in the samples was calculated using the trolox calibration curve. The equivalent quercetin concentrations were calculated by obtaining the TEAC value of pure quercetin using the same assay.

4.2.11 Cell toxicity study of QNGs on Human Umbilical Vein Endothelial Cells (HUVECs)

HUVECs were cultured in EBM basal medium (phenol red free) with EBM-2 growth factors to an 80% confluence in a 48-well plate overnight. A range of concentrations (from 1 to 70 µg/ml of equivalent quercetin content) of nanogels in media were prepared and added to the well plate (n=4). After 24 hours, treated and non-treated control cells were washed with fresh media followed by incubation in 1 mM Calcein AM red-orange live cell tracer. After 1 hour, cells were washed again with fresh media once, followed by addition of fresh media. Fluorescence was recorded at excitation/emission of 540/590 nm using BioTek Synergy Mx, Gen5 2.0, Winooski, VT to analyze the cell viability.

4.2.12 Cellular oxidative stress suppression

HUVECs were cultured in 48 well plate in EBM basal medium with EBM-2 growth factors. In order to determine the ability of Q-PBAE nanogels to block oxidative stress injury, HUVECs exposed to hydrogen peroxide (0.5 mM) were treated with free

quercetin and nanogels (QNG (1.25)) with equivalent quercetin concentrations of 5 and 10 µg/ml. DCF-DA to a final concentration of 10 µM was added at the time of treatment and DCF fluorescence was used as a measure of oxidative stress levels in the cells. Three similar 48 well plates were prepared. DCF fluorescence at 490/525 nm and cell viability was measured at 24 and 48 hours using BioTek Synergy Mx, Gen5 2.0, Winooski, VT.

4.3 Results

4.3.1 Hydrodynamic radius and yield of reaction of Q-PBAE nanogels

The hydrodynamic diameter of the nanogels was determined using DLS before and after PEGylation. The extent of reaction was evaluated by UV-Vis spectrophotometer. As the concentration of reactants increased, nanogels size increased from 273 ± 6 to 642 ±21 nm, and reaction yields increased from 81.4 ± 2.6 % to 97.8 ± 0.54 % (Figure 4.2). A slight increase in nanogel diameter (approximately 50 nm), for smaller diameter particles was observed after the reaction with 3 wt/vol% of PEGMEMA4000 (Figure 4.3). This increase can be likely be attributed to the attachment of PEG chains at the surface of nanogels as shown in figure 4.1.

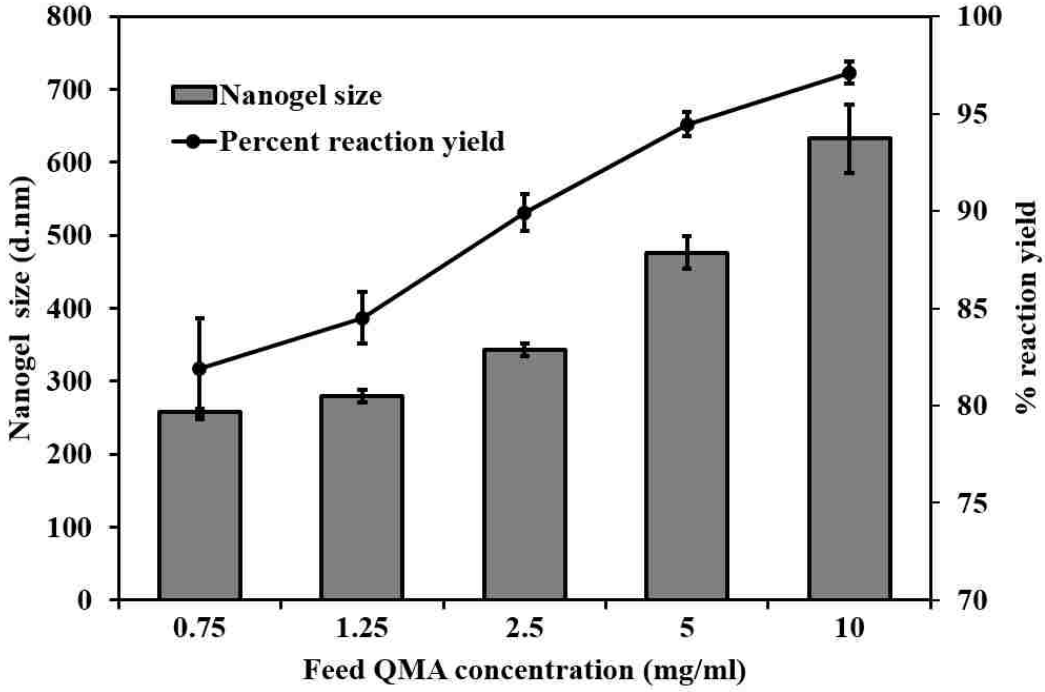

Figure 4.2 Percent reaction yields and size variation of QNGs with respect to variable reactant QMA concentration. All samples were analyzed with n=3.

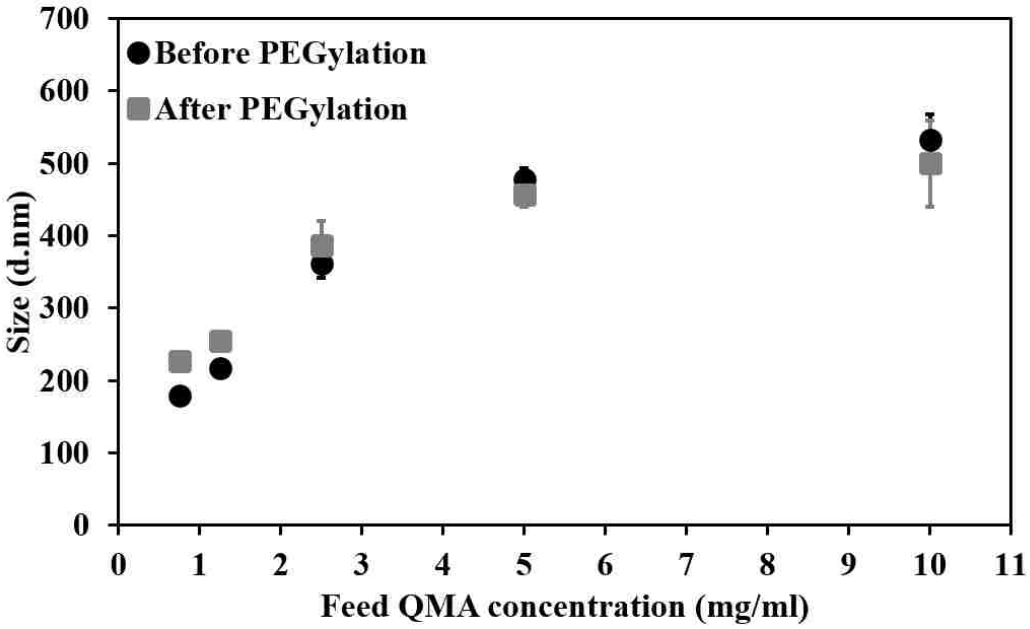

Figure 4.3 QNGs size variation before and after PEGylatio with PEGMEMA4000. *Black circles: Nanogel diameter before reaction with PEGMEMA4000. Grey squares: Nanogel diameter after reaction with PEGMEMA4000 followed by centrifugation and re-suspension in fresh acetonitrile. N=3, error bars: std. dev.*

4.3.2 Analysis of shape and size of nanogels

Nanogels prepared using 2.5 mg/ml feed QMA concentration were imaged in SEM to examine shape and size. Nanogels with diameter ranging from 100-250 nm with an average of 197 ± 57 nm as analyzed using Image J software were observed (Figure 4.4 a, b). The nanogels' spherical morphology was confirmed by imaging at an angled view at 38^{o} (Figure 4.4, c and d). There was an observed phenomenon of fusion at nanogel surface as they are soft polymeric particles, which might be undergoing interfacial attraction forces during solvent evaporation on the gold substrate.

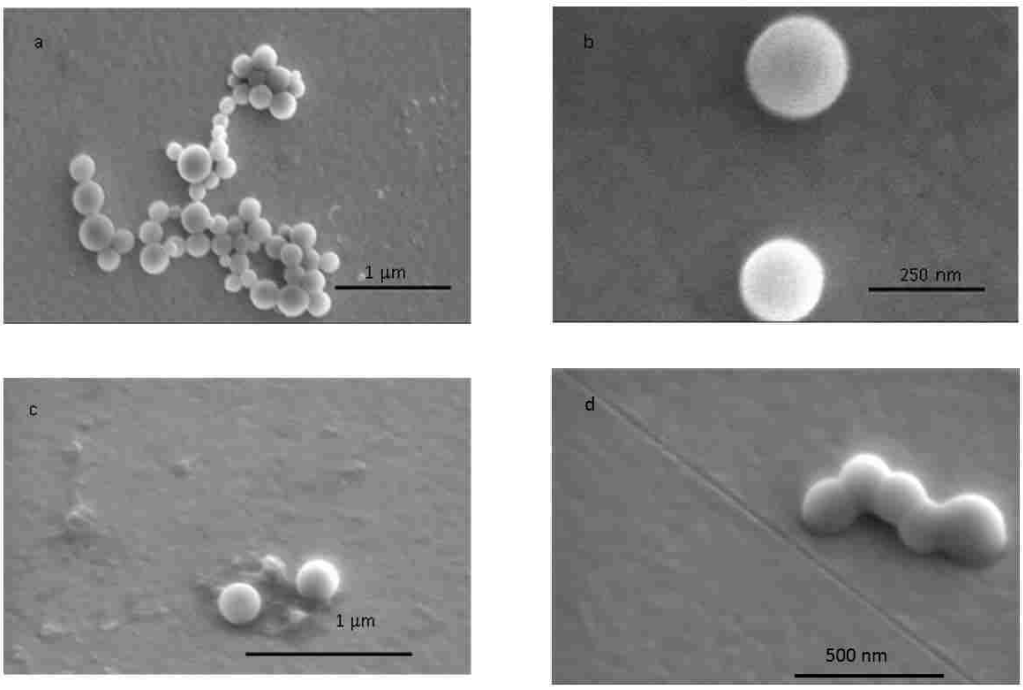

Figure 4.4 Scanning electron microscopy of the QNGs synthesized with reactant QMA concentration of 2.5 mg/ml. a, b: plain view (Top view); c, d: angled view, 38^{o}.

4.3.3 Effect of the acrylate to amine ratio on nanogel size (stoichiometric feed ratio)

Different acrylate to amine ratios during the synthesis were investigated to study the effect of stoichiometric ratios on nanogel diameter and reaction yield. Because of the possibility that a higher amount of amine can result in hydrolysis of QMA and precipitation of quercetin, 200 μL of DMSO was added to each 1 ml suspension of nanogels to dissolve any precipitated quercetin but not crosslinked nanogels. The dissolution of precipitated quercetin was verified by conducting a control experiment. In the control experiment, highest possible amount of quercetin that could get precipitated for the QNG (2.5) was suspended in acetonitrile, followed by addition of 200 μL of DMSO resulting in dissolution of suspended quercetin. It was observed (as shown in figure 4.5), the highest hydrodynamic diameter (311 nm) was obtained with an acrylate to reactive amine hydrogen ratio of 1:1.1 while higher or lower ratio resulted in smaller sizes with either incomplete reaction of QMA or precipitation of nascent quercetin. This ratio also gave highest yield of the reaction (89%) not shown in the figure. For all further studies, QNGs were synthesized with feed ratio of 1:1.1, which results in slightly excess of amine, which permits conjugation of the PEGMEMA4000 system

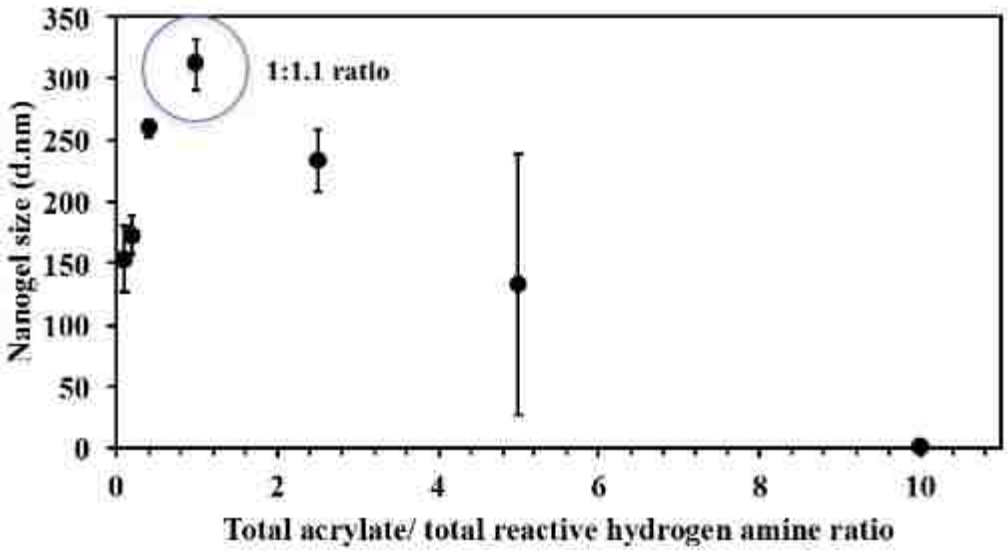

Figure 4.5 Effect of total acrylate to total reactive amine hydrogen on QNGs size. *Variable acrylate to amine ratio ranging from 0.1 to 10 was taken and size was measured after 1 hour of reaction with 2.5 mg/ml of reactant QMA concentration constant for all formulation changing the amount of amine added. (n=3). Nanogel diameter at acrylate to amine ratio of 1.1 was found to be the highest with respect to other stoichiometric ratios mostly due to the maximum extent of reaction. Hence, this ratio was used for all the formulations with variable feed reactant concentrations. N=3, error bars: std. dev.*

4.3.4 Analysis of enhanced stability of nanogels after the reaction with PEGMEMA4000

PEGylation of nanogels with PEGMEMA4000 resulted in the physical stability of nanogel suspension in aqueous media (PBS. pH=7.4). As shown in figure 4.6, PEGMEMA4000 treated retained their size from 373 ± 5.8 at t=0 to 364 ± 68 after 50 minutes of suspension. This could be due to the stearic hindrance of the PEG groups that leads to the formation of stable suspensions in contrast to non-PEGylated nanogels that aggregated with time in PBS giving the size of over 1 micron within 20 minutes. Incubation of nanogels with PEGME5000 did not result in their stability in PBS either but in aggregation of nanogels over time with an observed diameter of 2.5 µM within 50 minutes of suspension, confirming that the stability of nanogels after PEGylation is due to the covalent bonding of PEG to its surface due to the reaction of mono acrylate

from PEG with unreacted terminal amine hydrogen of the nanogels. The size of the nanogels treated with PEGMEMA4000 after 30, 40 and 50 minutes of suspension was significantly lower than the other two groups with $p < 0.005$, while did not show any significant increase in size when compared at different time points of suspension.

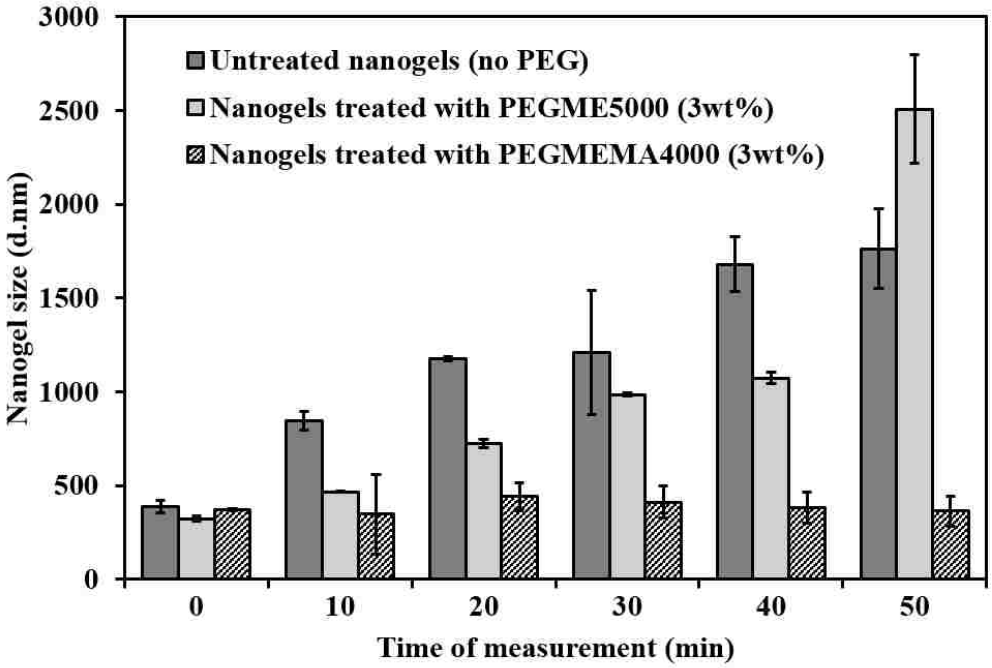

Figure 4.6 Stability analysis of QNGs before and after reaction with PEGMEMA4000 and PEGME5000 in PBS.
Size measurements were taken at various time intervals after suspension of nanogels in PBS. Nanogels after PEGMEMA4000 coating were more stable than non-coated nanogels. Nanogels were prepared with 2.5 mg/ml reactant QMA concentration and reacted with 3 wt/vol% PEGMEMA4000. N=3, error bars: std. dev. Nanogel PEGylation and protein binding

4.3.5 PEG content analysis after nanogel formulation

PEG content in the nanogels has been represented as PEG weight percent in the total nanogel mass shown in figure 4.7. It was observed that nanogels synthesized from lower QMA feed concentrations of 0.75 and 1.25 mg/ml had 40.7 and 30.4 wt% PEG respectively, while the higher concentration systems, 2.5, 5, and 10 mg/ml, had lower

PEG content at 7.6, 1.23 and 3.1 wt% respectively. The influence of this variable PEG content was seen in the IgG binding capacity as discussed below.

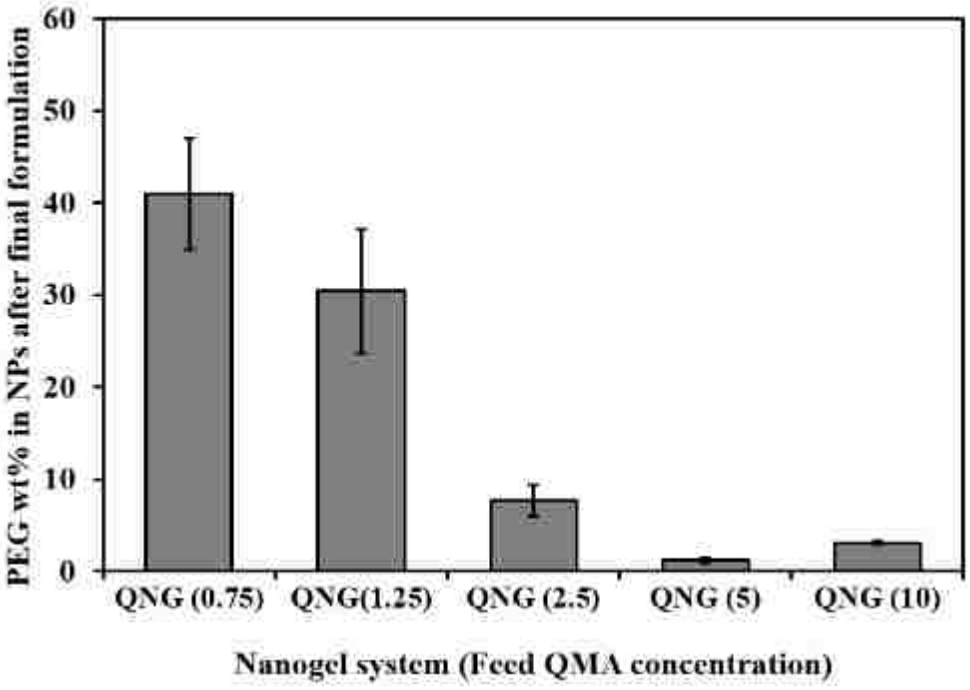

Figure 4.7 PEG weight percent in QNGs after reaction with 3 wt/vol %.
Barium Iodide assay for PEG content determination was used with n=3 for each formulation.

4.3.6 Decrease in QNG-antibody binding by using radiolabeled IgG

Nanogels without PEG coated system showed high IgG binding, 59.8 ± 1.6, 73.84 ± 2.1 and 71.25 ± 1.2 % surface coverage for QNG (0.75), QNG (1.25) and QNG (2.5), respectively. PEG coated nanogels with the same formulations showed a substantial decrease in IgG binding, 18.4 ± 4.8, 37.3 ± 7.4 and 50.6 ± 5.4 % surface coverage for QNG (0.75), QNG (1.25) and QNG (2.5), respectively (Figure 4.8, bar chart). Additionally, as the PEG weight percent decreased, the percent IgG bound increased, indicating the presence of a PEG coating of the nanogels (Figure 4.8, line graph).

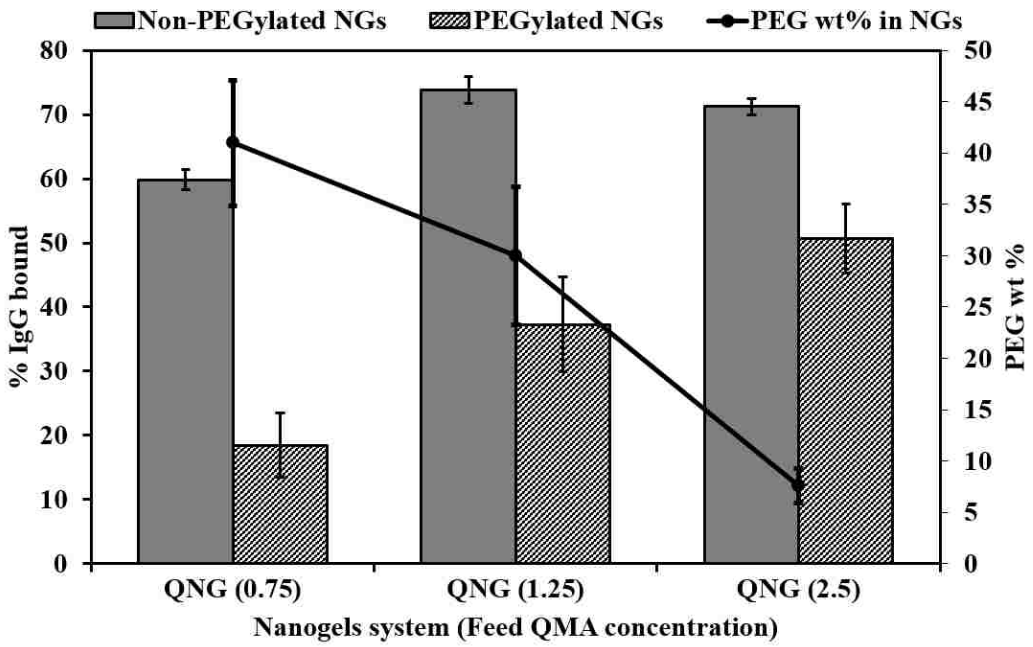

Figure 4.8 Extent of IgG binding to non-PEG coated and PEG coated QNGs compared in three different nanogel systems having different PEG wt% in them.

4.3.7 Quercetin release profile and antioxidant activity

Figure 4.9 a,b shows the released products and degradation profile of the nanogels in PBS at 37° C. Supernatants containing the degradation products were analyzed using UV-Vis spectroscopy. Quercetin release was linear for the first 36 hours, followed by a plateauing profile, with approximately 95% total release in 35-40 hours. These nanogels had initial burst release of 11.93 ± 1.5, 4.43 ± 0.4, 6.8 ± 0.27, 9.3 ± 1.6, 9.9 ± 0.97 % for QNG (10), QNG (5), QNG (2.5), QNG (1.25) and QNG (0.75), respectively. This low level is likely due to unconjugated quercetin in the gel matrix. Taking into account the first 60% of the total release, profiles were fit to the Korsmeyer-Peppas model ($M_t/M_{inf} = Kt^n$) for the *in vitro* release model fit [180, 181]. To identify between the diffusion, anomalous and erosion controlled release regimes, exponent 'n' values were identified. For a spherical system, n=0.43 implies pure diffusion, n=0.85 suggests erosion and $0.43<n<0.85$ implies anomalous transport or a combination of diffusion and erosion. The 'n' values of 0.55, 0.85, 0.69, 0.58 and 0.58 for QNG (10), QNG (5),

QNG (2.5), QNG (1.25) and QNG (0.75) respectively, indicate the anomalous diffusion release mechanism of nanogel degradation according to the model definition. R^2-values were within the range of 0.97-0.99. Since similar release profiles were seen for all formulations irrespective of the different nanogels formulations, which gave varied nanogel diameter and given the swellable nature of PβAE polymer, bulk erosion phenomenon is likely to happen via hydrolysis instead of surface erosion for these systems. This study was conducted in three different batches and was found to be reproducible, although figure 4.9 shows data from only one batch. Figure 4.9 (a) represents the HPLC chromatograms of quercetin, quercetin multiacrylate and degradation products of Q-PβAE bulk gel system and nanogel systems. HPLC Analysis of degradation products of Q-PβAE bulk gels (#3) in the Figure 4.9 (a) identified release of both quercetin and the monoacrylate form. However, degradation products of the synthesized Q-PβAE nanogels (#4)) resulted in the release of pure quercetin, with no detectable trace of mono or higher acrylate products, confirming the retrieval of the original drug. Meanwhile, TEAC studies of the degraded product indicated that the released compounds possessed antioxidant activity against free radicals for 36-40 hours (Figure 4.9 (c)) and possessed a similar release profile as obtained from degradation product UV-Vis analysis. Equivalent active quercetin was also calculated for each time point taking 4.2 as the TEAC value of quercetin. It was observed that equivalent active quercetin either complied with the released quercetin or was higher than that implying no loss of quercetin activity during degradation and release. Higher values of equivalent active quercetin is likely from oligomers released during hydrolysis and degradation products of quercetin, which also have some inherent antioxidant activity. Taken together, quercetin was successfully kept intact within the polymer matrix for an extended period of time without loss of activity. This result is in contrast to the usual

behavior of quercetin, where structural stability and antioxidant activity is lost within 2 hours of incubation in aqueous media.

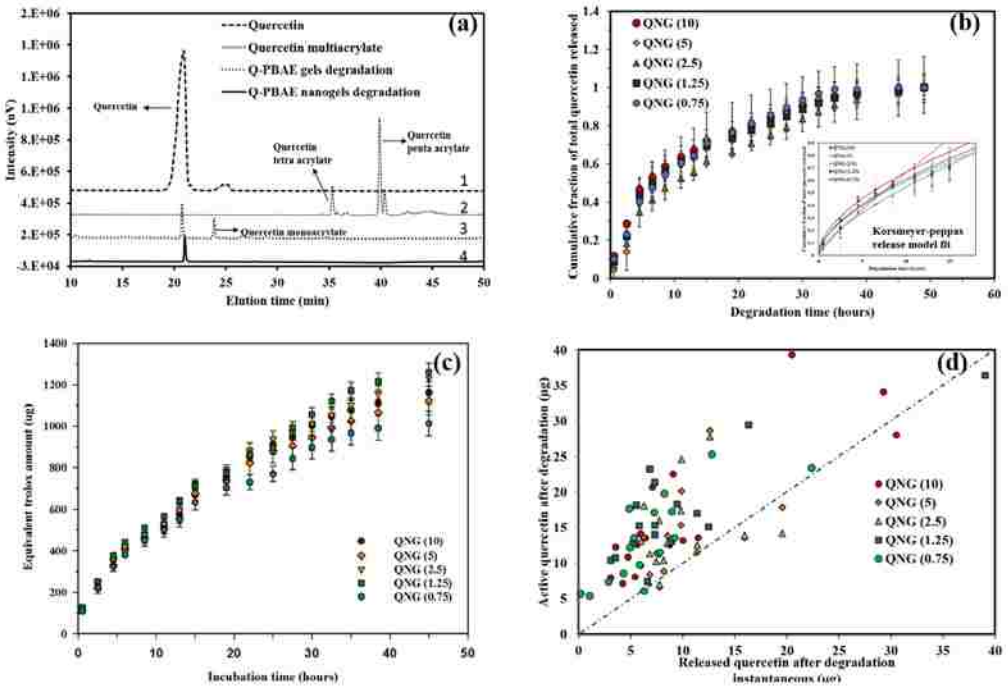

Figure 4.9 Degradation of QNGs at physiological conditions and subsequent analysis.
(a) HPLC analysis of QNG degradation products to confirm the recovery of pure quercetin and not any other mono or higher quercetin acrylates. This was confirmed by comparing the nanogel degradation products with quercetin, QMA (monomer) and degradation products of bulk Q-PBAE gels, which results in quercetin and quercetin monoacrylate release, (b) Degradation/quercetin release profile from QNGs in PBS (pH 7.4 with 2vol% DMSO). 90% of the quercetin was released within 35 hours of incubation. N=3 and the profile fits Korsmeyer-Peppas release kinetic model $\boldsymbol{M_t/M_{inf} = Kt^n}$ *with n values within 0.45-0.85 showing anomalous release. R-square ranged from 0.9737 to 0.9923, (c) Antioxidant activity profile of the degraded products of QNGs. The study was done using the trolox equivalent antioxidant capacity assay (TEAC), and the activity is expressed in terms of equivalent amount of trolox. n=3, (d) Instantaneous active quercetin values calculated from TEAC values compared with instantaneous quercetin released values obtained after each degradation time interval.*

4.3.8 Effect of QNGs on human umbilical vein endothelial cells

4.2.1.1 Dose dependent cell toxicity

Cytotoxicity of quercetin-based nanogels in the biological environment was analyzed by exposing HUVEC monolayers to quercetin nanogels. The cells were exposed to

equivalent quercetin concentrations ranging from 1 to 70 µg/ml of nanogels for 24 hours followed by treatment with Calcein AM red-orange (fluorescent cell tracer), as a measure of cell viability. Calcein AM red-orange was used as it does not interfere with the fluorescence of quercetin itself, being in the different fluorescence wavelength region. As shown in figure 4.10, cell viability starts to decrease to about 50% at 70 µg/ml of equivalent quercetin concentrations. All nanogel formulations showed similar viability trends when compared within themselves as well as when compared with pure quercetin for both 24-hour exposure time. This was confirmed after conducting two-way ANOVA test considering nanogel composition and treatment concentrations as two groups. The two-factor analysis of variance showed no significant effect of composition towards cell viability but dose dependent cytotoxic effect was statistically different after 24-hour treatment. This demonstrates that presence of PβAE nanogels or its degradation products apart from quercetin did not contribute to cell cytotoxicity.

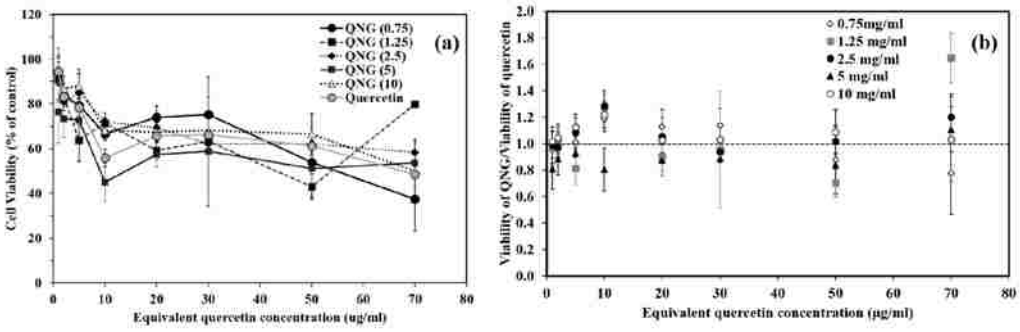

Figure 4.10 Dose dependent toxicity of QNGs on HUVECS
(a) Cell viability after exposure of HUVECs with QNGs and pure quercetin for 24 hours. Calcein AM red-orange was used as a live cell tracer. (n=4), (b) Specific viability of QNGs with respect to quercetin. A two-way ANOVA test was conducted taking nanogel compositions and treatment concentrations as two variables. No significant difference in viability was observed due to different compositions and pure quercetin while treatment concentrations showed statistically significant difference in cell viability.

4.2.1.1 Effect of nanogels on H_2O_2 treated HUVECs for 24 hours

HUVECs at 80% confluence were treated with two different concentrations of QNG-1.25 (5 and 10 µg/ml equivalent quercetin concentration) and 0.5 mM H_2O_2 as an inducer of cellular injury and oxidative stress. 10 µM DCFDA was added to each well. Cell viability and DCF fluorescence were measured at 24 and 48 hours and compared with the no particle treatment and no H_2O_2 controls. Cell viability was maintained on a concentration basis for only quercetin/QNG treatment after 48 hours. A slight increase in viability was seen after 48 hours with the antioxidant treatments (Figure 4.11 (a) and 4.11 (b)). When looking at DCF fluorescence for the same treatment system, antioxidant treatment suppressed the background oxidative stress to a significant level at both 24 and 48 hours when compared with no treatment controls (Figure 4.12 (a)). External oxidative stress induced using H_2O_2, as shown in figure 4.12(b), resulted in cell viability dropping down to 10% after 24-hour exposure and 20% after 48-hour exposure. H_2O_2 exposed groups treated with free quercetin or QNG showed different responses after 24 and 48-hour exposure. For 24 -hour, all the treatments with either free quercetin or QNGs, showed same protection from H_2O_2 with cell a viability of approximately 50%. With 48-hour exposure study, though we saw equivalent protection from both free quercetin and QNG with 5 µg/ml, QNGs at 10 µg/ml showed improved performance than just quercetin despite having same inherent toxicity at that concentration. Suppression of DCF fluorescence at both 24 and 48 hours for 10 µg/ml QNG system was superior to pure quercetin.

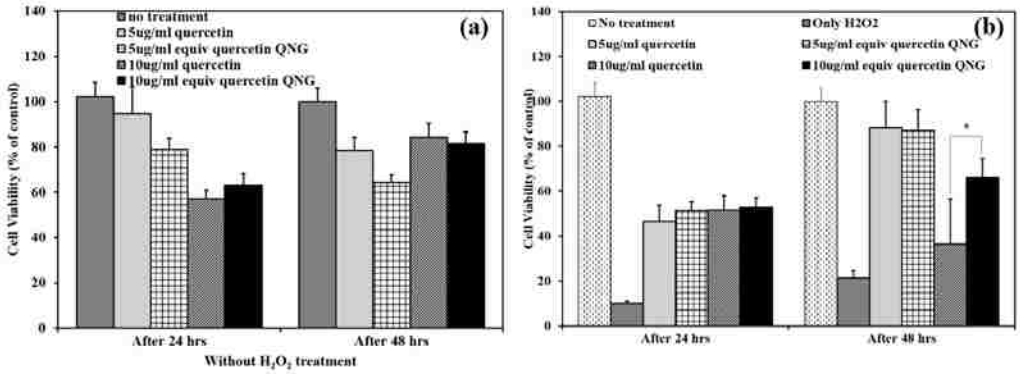

Figure 4.11 Cell viability of HUVECs treated with two different concentrations of QNG (1.25): 5 and 10 µg/ml and/or 0.5mM H_2O_2.
*Cell death analyzed after 24 and 48 hours of treatment. (a) Treatment with only QNG/quercetin. (b) Treatment with QNG/quercetin and H_2O_2. * $p<0.05$*

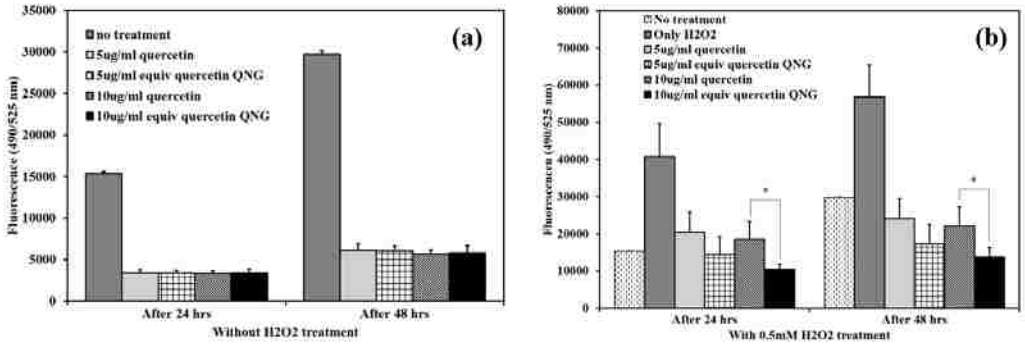

Figure 4.12 Oxidative stress suppression analysis using 10 µM DCF-DA as an oxidative stress marker.
*Two different of QNG/quercetin, 5 and 10 µg/ml were used. Fluorescence was measured after 24 and 48 hours of treatment. (a) Treatment with QNG/quercetin. (b) Treatment with QNG/quercetin and 0.5 mM H_2O_2. * $p<0.05$*

4.4 Discussion

Numerous trials have been conducted over the years evaluating the continuous administration of antioxidants and their effect on chronic diseases like atherosclerosis or diabetes. Yet, results have been inconclusive and debatable towards their beneficial effects [182]. However, as the use of antioxidants in sub-acute inflammatory diseases (e.g., N-acetyl cysteine in acetaminophen toxicity) have shown clinical acceptance,

there must be something more to this observed discrepancy [183]. One explanation for the better in vivo performance of N-acetyl cysteine in this setting is the improved natural accumulation in the intended site of action (e.g., the liver) and more favorable circulation times over that of other antioxidants, which has a half-life of 6 hours compared to minutes for many polyphenolic antioxidants [184, 185]. However the use of N-acetyl cysteine is also complicated with side effects common of sulfur containing compounds, including nausea, vomiting and risk factors of asthma, drug allergy etc. [186]. As such, it may be possible to rescue small antioxidant therapy for short-term oxidative stress disorders through changing their inherent pharmacokinetics.

The objective of this work was to design a biocompatible polymeric nanocarrier capable of systemically delivering highly active though labile antioxidant, quercetin, over an extended period of time to fight acute oxidative stress conditions. We have incorporated PβAE gel synthesis chemistry in making quercetin conjugated PβAEs nanogels. Our lab group and other researchers have previously reported successful synthesis of PβAE bulk hydrogels using different co-monomers including polyphenolic antioxidants along with PEGDA and DEGDA [178, 187, 188]. By taking advantage of its polyphenolic structure, quercetin can be acrylated, which when reacted with an amine can form a crosslinked gel via a Michael addition mechanism. However, due to rapid kinetics and multifunctional nature of the monomer, translation from bulk gel to nanogel is a technically challenging hurdle. Owing to the hydrolytically degradable property of PβAEs, standard two-phase (oil-water or oil-oil) emulsion techniques are not feasible. However, formulating quercetin-PβAE nanogels (QNG) via a single-phase reaction-precipitation method in acetonitrile under dilute conditions resulted in a nanogel suspension as the reaction proceeded to completion, the spherical nature of which was confirmed by SEM imaging (Figure 4.4). The presence of excess available terminal

amines permitted the covalent linkage of PEG monoacrylate grafts to the nanogel resulting in a stable coating. As PEG grafts are able to stearically stabilize nanoparticles, PEGylation of the nanogels enhanced their post-purification stability and improved their stealth characteristics. The single-phase reaction systems/ one-pot synthesis simplified the synthesis process, eliminating the requirement of any stabilizer and removal of the excess stabilizer added during purification. A very simple purification step of centrifugation was used, after which nanogels restored their original size without any aggregation (figure 4.1 and 4.3). PEGylation improved the stability in organic-aqueous solutions. This is in contrast to QNGs incubated with PEGME5000 (MW in the range similar to PEGMEMA4000). The lack of the acrylate group prevented covalent addition to the particles and was, therefore, unable to prevent particle aggregation (Figure 4.6). This confirms the presence of covalent linkage between PEG acrylate group and NNDA unreacted terminal hydrogen amines, which eventually results in QNG physical stability.

Precise control of nanogel size was made possible by varying the feed reactant concentration while keeping the stoichiometric ratio constant, with increasing concentration increasing particle size (Figure 4.3). Interestingly, as the ratio of acrylate to amine decreased, the excess amine catalyzes the hydrolysis of the acrylate groups. To minimize the occurrence, the stoichiometric ratio of acrylate to reactive hydrogen amine was limited to 1:1.1 which still offered maximum reaction yield, diameter and provides the opportunity to covalently bind PEGMEMA4000 to terminal amines (Figure 4.4). It was observed that after using the same concentration of PEGMEMA4000 for all formulations, the smaller nanogels had a higher amount of PEG attached (30-40% wt/wt) while the larger diameter nanogels had PEGylation of only 3-5 wt% (Figure 4.7). This could be due to the presence of more amine reactive

sites on smaller particles due to the overall higher surface area for the same quantity. The PEG presence was further substantiated by performing a radiolabeled-IgG binding studies where reduced amount of IgG binding was observed for PEGylated nanogels as opposed to non-PEGylated nanogels (Figure 4.8). Also, as wt% of PEG decreased with different nanogel formulations, percent IgG bound increased clearly implying that presence of PEG was altering the antibody binding effect in a positive fashion.

These hydrophobic polymeric quercetin-PBAE systems are hypothesized to degrade in PBS via hydrolysis of ester bond to release quercetin. This was confirmed by injecting degradation products through HPLC where we saw the most significant elution peak coinciding with pure quercetin peak with no oligomer or other forms of quercetin acrylate present (Figure 4.9 (a)) confirming the presence of original quercetin molecule in the degradation product. Nanogels showed uniform degradation over 48 hours with about 5-10% of the total quercetin released in first 30 minutes as analyzed by UV-Vis (Figure 4.9 (b)). While the Korsmeyer-Peppas (K-P) release profile model for spherical systems with $0.43<n<0.85$ suggests the contribution of diffusion, as well as erosion based degradation, similar release profile of all the formulations (QNG (0.75)-QNG (10)) with variable diameter, confirms the bulk erosion instead of surface erosion degradation mechanism, (Figure 4.9 (b)). An important fact to notice in the release profile is that the value of 'n' obtained using the K-P model closely correlates with the percent burst release considering it to occur at 1st sampling time point of 30 minutes. The system with highest burst release of 11.93% (QNG (10)) fits with the 'n' value of 0.55 (near diffusion boundary) while QNG (5) with lowest burst release of 4.43% amongst all the systems gives the 'n' value of 0.85 (pure erosion mechanism). This trend of higher burst release with lower 'n' value clearly implies that the diffusion contribution in the release model is largely coming due to the unconjugated quercetin

being diffused through the spherical gel matrix at early time points while the quercetin released due to the ester hydrolysis is derived by erosion based mechanism. Analyzing the antioxidant activity of the released products using TEAC assay confirmed that the products released at 24 hours or 48 hours still possess antioxidant activity and quercetin conjugated to PBAE backbone was structurally intact even after being incubated in aqueous media for several hours (Figure 4.9 (c)). Comparing the equivalent quercetin amount obtained from TEAC assay and actual quercetin release in figure 4.9 (c), it is clear that the nanogel degradation products are showing higher activity than would be estimated through pure quercetin release (Figure 4.9 (d)). One possible explanation for the persistent excess activity throughout the degradation process could be due to the auto-oxidation or molecular degradation of the released quercetin in the aqueous environment resulting in metabolized fragments such as phloroglucinol, protocatechuic acid etc [189]. These small fragmented molecules though not quantifiable at the same wavelength as quercetin have some potential towards free radical scavenging which could be contributing towards ABTS radical consumption in the TEAC assay [190]. Hence, even the fragmented degradation products contributed to the total antioxidant potential of the system over time.

As a pharmaceutically active compound, quercetin like any other therapeutic compound has a window of safety with TC50 value of 0.23 mM or ~ 70 μg/ml (Fig 4.10 (a)). When loaded into a drug carrier system, it is important to investigate the potential toxicity of the carrier system along with the loaded drug. As literature for PβAE systems indicates low relative toxicity in vitro and in vivo, it is expected that quercetin PβAE nanogels would have a similar safety window as for pure quercetin with no added effect due to the polymer backbone. This was confirmed with the dose dependent cytotoxicity study of all the QNG systems and when compared with quercetin, QNGs toxicity patterns the

cytotoxic profile of quercetin directly confirming once again the viable nature of PβAE nanogel by itself (Figure 4.10 (a) and (b)). These nanogels were further evaluated for their ability to suppress oxidative stress due to external injury induced using 0.5 mM H_2O_2 exposure. They not only showed ROS scavenging capacity against H_2O_2 induced injury as good as pure quercetin at equivalent quercetin loading of 5 µg/ml, but the treatments done with QNGs having 10 µg/ml of equivalent quercetin loading showed enhanced protection against oxidative stress as compared to nascent quercetin after 48 hours probably due to prolonged supply of active quercetin during nanogel degradation. This was verified by both viability and DCF fluorescence studies showing superior properties of QNGs than pure quercetin even though present in same quantities (Figure 4.11 and 4.12). Therefore, with the ability to suppress oxidative stress in vitro, slow uniform release, and longer circulation efficacy; these nanogels can serve as an effective delivery system a therapeutically potential yet fragile antioxidant, quercetin, which shows very low bioavailability in vivo otherwise.

4.5 Conclusions

Nanogels were synthesized using a novel but simple single-phase reaction-precipitation system with control over the size through varying feed reactant concentrations. These nanogels were able to be PEGylated post-synthesis through a secondary Michael addition reaction with available amines on the nanogel surface, resulting in decreased opsonization. The PBAE chemistry to chemically conjugate quercetin protects quercetin from losing antioxidant activity until the polymer degrades and releases the quercetin. To the best of our knowledge, these nanogel systems when compared with other nanocarriers have the highest reported quercetin drug loading. The uniform, prolonged release of quercetin from QNGs due to hydrolytic cleavage showing

equivalent antioxidant activity as pure quercetin potentially shows protection against induced oxidative stress for as long as 48 hours.

5 CURCUMIN CONJUGATED POLY (B- AMINO ESTERS) NANOGELS AND SUSTAINED SUPPRESSION OF MITOCHONDRIAL OXIDATIVE STRESS

Based on the research to be published in:

Prachi Gupta, Mihail Mitov, J. Zach Hilt, Thomas D. Dziubla. Sustained Suppression of Mitochondrial Oxidative Stress using Curcumin conjugated Poly (β-Amino Esters) Nanogels (s*ubmitted)*

Abstract

Mitochondria are considered to be the “power plant” of the cell, but can also initiate and execute cell death, stimulated by oxidative stress (OS). OS induced mitochondrial dysfunction is characterized by a loss in oxygen consumption and reduced ATP production. Curcumin, with potential therapeutics and interventions, has been explored as a potential candidate for mitochondrial OS suppression, but rapid metabolism and aqueous insolubility prevent it from being an effective therapeutic. Further, effective delivery of curcumin via incorporation into nanocarrier formulation has again been limited due to low drug loading capacities and/or significant burst release effects resulting in cytotoxicity. Hence, to increase therapeutic opportunities and ease toxic effects of curcumin, self-precipitated curcumin conjugated poly(β-amino ester) nanogels (CNGs) were synthesized using the Michael addition chemistry. With easy control over the nanogel size, CNGs showed a uniform release of active curcumin over 48 hours with no burst release. This uniformly releasing system significantly increased the safety limit for curcumin as a treatment drug (10xfree curcumin). Further, real-time mitochondrial response analysis with Seahorse XF96 showed effective and prolonged suppression of H2O2 induced mitochondrial oxidative stress upon pre-treating

endothelial cells with CNGs and this potential of nanogels was studied at different pre-treatment times prior to H2O2 exposure.

5.1 Introduction

Given its ubiquity in a number of disease states, oxidative stress (OS) and its consequent effects are extensively researched topics in biological and pharmaceutical disciplines. Its cascading effects are seen in diabetes, cancers, neurological disorders, cardiac disorders and many more [191-193]. OS occurs when the natural balance of oxidants and antioxidants is disturbed, leading to excess production of free radicals such as reactive oxygen species (ROS) and reactive nitrogen species (RNS). Higher levels of ROS and RNS lead to cellular damage by lipid peroxidation, protein carbonylation, DNA damage, etc. [194, 195]. Mitochondrion, the central system for energy production pathways and metabolism in most cells, is also a key organelle for ROS generation [196, 197]. Interestingly, mitochondria are not just a key generating source of free radicals but also a sensitive target to ROS and RNS damage [198]. Mitochondrion is believed to be specifically affected by lipid peroxidation, leading to the generation of hydrogen peroxide and superoxide radicals and hence resulting in additional ROS production [199]. This cycle cascades in a feed forward fashion leading to cell necrosis and apoptosis [199, 200]. Therefore, it is believed that when a cell is exposed to any free radical or ROS, the mitochondria are the first one of the cellular organelles to be targeted by ROS. This leads to mitochondrial dysfunction, disturbing the normal respiration mechanism and loss in ATP production before finally losing a major energy pathway of the cells. Mitochondrial protein, lipids and DNA (mtDNA) are considered the primary target of ROS. As a result, mitochondrial oxidative stress (Mito OS) becomes the indirect cause of many diseases, primarily neurogenerative disorders such as Alzheimer's and Parkinson's disease, numerous metabolic disturbances,

cardiomyopathies and metabolic complexities in patients suffering from diabetes mellitus [1, 201-205].

Because mitochondrion becomes the generation source of more ROS, it is important to control the damage to mitochondrial structure and function when the cells encounter increased ROS/RNS. One potential solution to prevent mito OS is to reduce excess ROS production in mitochondria by effectively supplementing with antioxidants. Most attempts to accomplish this have failed *in vivo* due to the non-specific delivery of antioxidants to mitochondria below therapeutic limits as well as *in vivo* molecular instability issues with most of the antioxidants. Among the molecules/compounds studied, curcumin has shown protective effects, including a cytoprotective effect against aluminum induced neurogenerative disorders [206], maleate induced oxidative stress [207], and preventing mitochondrial OS in high fat diet induced obese mice [208]. Despite these promising findings in animal models, most clinical studies performed with high and frequent oral doses up to 4 g/day for 48 weeks, specifically for Alzheimer's, have failed to show clinically significant improvement in reducing symptoms for the disease [209]. Among limitations for curcumin, poor aqueous solubility, and extremely low bioavailability are most significant because pure curcumin has shown to be below detectable serum concentrations within a few minutes of administration [210]. Attempts have been made to incorporate curcumin into any viable polymeric or similar nanocarriers with the aim for higher curcumin loading, sustained release characteristics and ability to perform its antioxidant function with no cytotoxic effect. Unfortunately, curcumin drug loading capacities of most nanocarriers have not exceeded more than 4 wt%, resulting in the higher amount of carrier material but minimal doses of the functional drug [211]. Furthermore, little work has been pursued using curcumin as a treatment targeted towards stressed endothelial cells for

cancer and tumor treatment. In our approach to fight OS (specifically mito OS) with C-PβAE nanogels, curcumin is chemically conjugated to the polymer backbone, which upon hydrolytic degradation of the ester bonds releases pure curcumin. Theoretically, chemical conjugation into the PβAE matrix gives curcumin a structural stability and prevents deactivation prior to hydrolysis. Uniform drug release over 36-40 hours resulted in protected functionality of curcumin for a longer period. A higher IC_{50} value of more than 100 µg/ml of loaded curcumin in contrast to free curcumin (IC_{50}=5.3 µg/ml) increased the safety window of this potential drug. An increased safety window gives higher flexibility to work in therapeutic dosage amounts and reach adequate curcumin levels to treat and or prevent OS. In contrast, free curcumin administered at therapeutic levels will kill endothelial cells. A mitochondrial stress assay using Seahorse XF96 analyzer with the ability to monitor real-time mitochondrial bioenergetics was employed to analyze mitochondrial bioenergetics post induced oxidative stress and protective effect of C- PβAE nanogels (CNGs) versus free curcumin. CNGs with higher, yet viable, treatment concentrations (5 µg/ml) were able to shield against dropping ATP production or basal respiration rates due to hydrogen peroxide induced mito OS. On the other hand, free curcumin proved to be fatal at these high treatment concentrations and showed no protection at safe concentrations of 1 µg/ml against mito OS.

5.2 Methods and materials

5.2.1 Reagents

Curcumin was purchased from Chem-impex Int'l 'Inc, (Wood Dale, IL). 4,7,10 Trioxatridecane-1,13-diamine (TTD), acryloyl chloride, 2,2′-azinobis-(3-ethylbenzothiazoline-6-sulfonic acid) (ABTS), triethylamine (TEA) and potassium carbonate were bought from Sigma-Aldrich (St. Louis, MO). Sodium chloride,

potassium phosphate, sodium phosphate and sodium dodecyl sulfate (SDS) were purchased from Fisher Scientific (Fair Lawn, NJ). Human Umbilical Vein Endothelial Cell line (HUVECs), EBM-2 basal medium and its growth factors were purchased from Lonza, (Walkersville, MD). All solvents were purchased from Pharmco-aaper (Shelbyville, KY). All media kit and cell culture plates for XF96 Seahorse experiments were purchased from Seahorse Bioscience (Massachusetts, USA). Calcein AM red-orange tracer was bought from Invitrogen (Grand Island, NY).

5.2.2 Curcumin acrylate (CA) synthesis

Acrylation of the curcumin phenolic group was carried out via reaction of curcumin with acryloyl chloride in the molar ratio of 1:3 with anhydrous THF as the reaction medium. Triethylamine (TEA) was added in the same molar ratio as acryloyl chloride to capture byproduct hydrogen chloride by forming a chloride salt with the progression of the reaction. The reaction was carried out for 15 hours at room temperature in dark (aluminum foiled). The acrylated product was filtered from the salts formed during the reaction. The product was further purified via a solvent extraction process to remove any unreacted monomers then vacuum dried to obtain dry curcumin acrylate product. Obtained curcumin acrylate was analyzed using HPLC to verify product quality.

5.2.3 Synthesis of curcumin PβAE nanogels (CNGs)

CA solubilized in acetonitrile at known concentrations was reacted with TTD keeping acrylate to reactive hydrogen amine ratio of 1:1. Curcumin has two phenolic groups and upon acrylate functionalization should react to form curcumin diacrylate. TTD has four reactive hydrogen amines. Therefore, for each mole of TTD (molecular weight 220.31 g/mol), two moles of CA (molecular weight~ 476 g/mol) are reacted to get the required acrylate to reactive hydrogen amine ratio of 1:1. To formulate 1 ml of curcumin conjugated PβAE nanogels with the starting CA feed concentration of 10

mg/ml, 2.3 mg of TTD was added and allowed to react for 24 hours. Feed reaction concentrations of CA were varied from 0.75 to 10 mg/ml, hence the amount of TTD added to the reaction system was changed accordingly to keep the stoichiometric ratio constant. After 24 hours and self-precipitation of CA and TTD into C- PβAE nanogels (CNGs), the suspension was diluted in anhydrous THF with BHT as inhibitor, in a 1:4 ratio v/v (1 ml CNG suspension with 4 ml THF) as a purification step. An hour later, the system was centrifuged at 6.7 RCF for 20 minutes. The supernatant was removed and another wash with THF was given to remove any remaining unreacted monomers. After the second purification step, the centrifuged pellet was re-suspended in 1 ml acetonitrile via sonication and then freeze-dried overnight to get dry C- PβAE nanogels (CNGs).

5.2.4 Yield of reaction, nanogel size and morphology characterization

Yield: Yield of the C-PβAE nanoparticle reaction synthesis was determined by calculating the unreacted CA concentration in the supernatant after nanoparticle centrifugation. The unreacted CA concentration was determined by analyzing the degradation supernatants using a Varian Cary 50 UV-Vis spectrophotometer and quantifying the absorbance at the curcumin characteristic wavelength of 420 nm. The yield was determined by subtracting the amount of unreacted CA from the starting amount added. An assumption that CA and TTD reacted in the same ratio was taken into account while calculating the yield.

Size and morphology**:** Hydrodynamic radii of the different CNGs formulations were measured using dynamic light scattering (DLS) after suspending dried nanoparticles in acetonitrile and setting the measurement parameters according to the solvent used. CNGs were scanned with electron microscopy to determine their shape and morphology. To prepare the samples, synthesized nanoparticles were first suspended in

acetonitrile at a concentration of 100 µg/ml using probe sonication. A drop of 10 µl of this suspension was put on ODT treated gold substrate and allowed to dry for 2 hours. The sample was then sputter coated using gold-palladium alloy and images were taken at various magnifications using S-4300 Hitachi Scanning Electron Microscope.

5.2.5 Hydrolytic degradation of C-PβAE nanogels and the subsequent curcumin release profile

In order to test the degradation of these nanogels with subsequent release of pure curcumin upon ester hydrolysis, nanoparticles synthesized with 5 mg/ml as the CA feed concentration were suspended in PBS buffer containing 0.1% SDS wt/vol (pH 7.4). SDS was added to the buffer to enhance the solubility of released curcumin or its oligomeric products for further quantification. The nanogels were suspended in the buffer at a concentration of 100 µg/ml. At time points 0, 2, 4, 6, 8, 12, 24, 30, 36, 52 and 71 hours, the suspension was centrifuged at 6.7 RCF for 20 minutes and the supernatant was collected and stored at -20^{o} C for further analysis. The centrifuged pellet was re-suspended in fresh buffer maintaining appropriate sink condition. A degradation study was carried out over 72 hours under sink conditions at 37°C. To determine the release rate of curcumin during hydrolytic degradation of CNGs, UV-Vis spectrophotometry was used to analyze the curcumin concentration in the collected supernatants. The absorbance of the supernatants was measured at 420 nm using Varian Cary 50 Bio UV-Vis spectrophotometer followed by quantification of the amount of curcumin released using a standard calibration curve.

5.2.6 Antioxidant activity of released curcumin

It was important to assess that the released curcumin from CNGs was still active with its antioxidant potential intact as its phenolic groups were chemically altered during the

nanoparticle synthesis. Therefore, a trolox equivalent antioxidant capacity (TEAC) assay was performed in order to verify the antioxidant potential or radical scavenging property of released degradation products. TEAC is a colorimetric assay based on scavenging of 2, 2'-azinobis-(3- ethylbenzothiazoline-6-sulfonate) radical anions (ABTS.-) in the presence of an antioxidant. Briefly, 7 mM ABTS radical cation stock solution was prepared by mixing 1 ml of 8 mg/ml of ABTS solution with 1 ml of 1.32 mg/ml of potassium persulfate solution in DI water overnight. This concentrated ABTS radical stock solution was diluted in PBS to an absorbance of 0.4 AU at 734 nm to prepare a working solution after baseline correction. Trolox, with known concentrations ranging from 0 to 0.27 mM, was used for calibration. The assay was carried out in a 96-well plate and 10 µl of the sample was added to each well, followed by 200 µl of ABTS radical working solution. Five minutes later, absorbance was read at 734 nm using a Varian Cary 50 Bio UV-Vis spectrophotometer. A trolox calibration curve was used to determine equivalent trolox concentrations in the supernatant degradation products.

5.2.7 Dose dependent cytotoxicity of C-PβAE nanogels (CNGs) towards HUVECs

HUVECs were cultured in EBM basal medium (phenol red free) with EBM-2 growth factors to an 80% confluence in a 96-well plate overnight. Curcumin and CNGs (CA feed concentration = 5 mg/ml) suspension in media with equivalent curcumin concentrations ranging from 0 to 70 µg/ml were prepared. Wells containing HUVECs received and were treated with antioxidant/CNG solution for 24 hours (n=5). After 24 hours, media with antioxidant was removed from the wells, then incubated in 1 mM calcein AM red-orange live cell tracer. After 1 hour, cells were washed and fresh media was added to each well. The well-plate was subjected to fluorescence measurement with 540/590 nm as excitation and emission wavelength, respectively, using BioTek

Synergy Mx, Gen5 2.0, Winooski, VT to measure dose dependent toxicity of C-PBAE nanoparticles.

5.2.8 Effect of CNGs exposure on H2O2 induced cellular OS: cell viability analysis

HUVECs cultured in EBM-2 basal medium were seeded in a 96-well plate and incubated overnight to achieve 80% confluency with respect to well area. CNGs (CA feed concentration = 5 mg/ml) at a concentration of 7.5 μg/ml (5 μg/ml equivalent curcumin loading) were suspended uniformly in EBM-2 basal medium with the aid of bath sonication. The media from the cells was removed and 200 μl of the CNG suspension was added to the well of interest. 10 μl of 10 mM H_2O_2 stock solution prepared in EBM media was added simultaneously to the CNGs containing to get final exposure concentration of 0.5mM. A control group of only CNGs and only H_2O_2 exposed cells was also prepared. To all the wells, 10 μl of DCF-DA prepared in EBM-2 media was added to get a final cell exposure concentration of 10 μM. 24 hours later, DCF fluorescence was read at 490/525 nm as excitation/emission wavelength using BioTek Synergy Mx, Gen5 2.0, Winooski, VT spectrophotometer. Post fluorescence measurement, CNGs ± H_2O_2 solutions were removed and wells were washed with fresh media, followed by addition of 1 mM Calcein AM red-orange live cell tracer. Cell viability was measured by following the similar protocol as given in section 2.7

5.2.9 Measurement of mitochondrial OS changes after treatment with C-PβAE nanogels (CNGs) using XF-96 extracellular flux analyzer.

A Seahorse XF-96 Flux Analyzer (Seahorse Bioscience, North Billerica, MA) was used to analyze the effect of CNGs on cellular bioenergetics. HUVECs were seeded in a Seahorse 96-well tissue culture plate at a seeding density of approximately 35,000

cells/well. Cells were then allowed to adhere and grow for 24 hours. Prior to assay, the cell growth media was replaced with 175 µL of FX media (FX Assay Modified DMEM from Seahorse Bioscience with 5.5 mM glucose, 1 mM pyruvate, and 2 mM glutamix). Wells and cells were washed once, media exchange was completed and then cells were equilibrated for 60 minutes at 37˚ C in a non-CO_2 incubator. The 96-well plate was then subjected to Mitochondrial stress assay to analyze mitochondrial energetics and cellular metabolic profile. The mitochondrial stress assay consisted of subsequent injections of three mitochondrial inhibitor drugs: oligomycin A (1 µM), which act as ATP synthase inhibitor; FCCP (1 µM), an uncoupling agent; and a mixture of 1 µM rotenone and 1 µM antimycin A, each used as inhibitors for mitochondrial respiratory chain complex I and III to shut down the mitochondrial oxygen consumption. Oxygen consumption rates (OCR) and extracellular acidification rates (ECAR) were measured using measurement periods of 3 minutes minimum and 3 minutes maximum with drug injection series. Once OCR/ECAR measurements were completed, the FX media was carefully removed from all individual wells and replaced with 25uL of cell lysis buffer containing 0.32 mM Sucrose, 2 mM EDTA, 2 mM EGTA, 20 mM HEPES, pH 7.4, containing protease inhibitors 4 µg/mL leupeptin, 4 µg/mL pepstatin, 5 µg/mL aprotinin, and 0.2 mM PMSF. The plates then put in -20° C freezer overnight to disrupt cells membranes. The next day, plates were taken out to room temperature and put on an orbital shaker for an hour. Unknown protein levels (samples) of the wells were measured using the modified BCA protein assay (Thermo Scientific, Rockford IL). Known amounts of protein standards (2.5 µg, 5.0 µg, 10 µg etc.) were added in the background wells of the plate to construct an optical density standard curve. Protein levels were determined after the optical densities were measured on iMark plate reader (Bio-Rad, Hercules, CA).

The OCR pmol/min were normalized to protein levels of pmol/min/µg or calculated as percent change (%OCR) from the third basal measurement for each group.

To analyze the mitochondrial response towards free curcumin and CNGs, a 96-well plate seeded with 35,000 cells/well was treated with curcumin/CNG (synthesized with 5 mg/ml as feed reactant concentration) at equivalent curcumin concentrations of 1 and 5 µg/ml. After 24 hours of treatment, media was replaced with XF media for 1 hour at 37˚ C. The plate was then subjected to the mitochondrial stress assay to analyze mitochondrial energetics and metabolic profile. Metabolic respiration rates were measured and quantified as OCR (pmol/min) at this step. After analyzing different concentrations of curcumin and CNGs having the same equivalent curcumin concentrations for mitochondrial respiration rates, viable concentrations of curcumin (1 µg/ml) and CNGs (5 µg/ml) were used for further analysis of protective effect against OS. HUVECs in 96-well plates were first pre-treated with curcumin/CNGs at specified concentrations (1 and 5 µg/ml) for 0, 12 and 24 hours, then followed by the introduction of 0.25 mM H_2O_2 for 2 hours. Next, cells were washed and replaced with un-buffered DMEM media and kept at 37˚ C for 1 hour, followed by mitochondrial stress assay.

5.2.10 Statistical Analysis

Data for figures 5.1 (A), (B), 6.2 (A) and (C) is presented as mean ± St. Dev., while for figures 5.3 (A), (C), 6.4 (A), (B), (C) and 6.5 (A), (B) and (C) is presented as mean ± SEM. The statistically significant differences between the mean values were calculated using one-way ANOVA test followed by Bon-ferroni post hoc test with the help of SigmaPlot software. A p value of <0.050 was considered to be representative of the significant difference between the means under comparison.

5.3 Results

5.3.1 Curcumin nanogel size, yield and morphology

CA with 2 to 3 acrylate groups was set to react with TTD in acetonitrile under dilute conditions. Varying the feed concentration of CA and maintaining the total acrylate to total reactive hydrogen amine ratio resulted in self-precipitated nanogels with variable hydrodynamic diameter. Upon UV-Vis analysis of the supernatants obtained after centrifugation, reaction yield was calculated to be 62.7%. Increasing the reactant concentration resulted in an increase in diameter. As shown in figure 5.1 A, hydrodynamic diameters of 64 ± 8, 87 ± 3, 131 ± 5, 221 ± 4, 416 ± 31 nm were obtained for CA feed reactant concentrations of 0.75, 1.25, 2.5, 5, 10 mg/ml respectively. These will be abbreviated as CNG (0.75), CNG (1.25), CNG (2.5), CNG (5) and CNG (10) throughout this text.

After the washing and purification step in anhydrous THF, CNG (5) was again analyzed on DLS giving the hydrodynamic diameter of 210 ± 20, similar to the pre-wash diameter of the nanogels (Figure 5.1 B). This suggests little to no aggregation and no morphological change of nanogels post purification steps. The spherical morphology of the nanogel system was further confirmed after electron microscopy imaging (Figure 5.1 A inset) and an average diameter of 176 ± 26 nm was calculated using Image-J software.

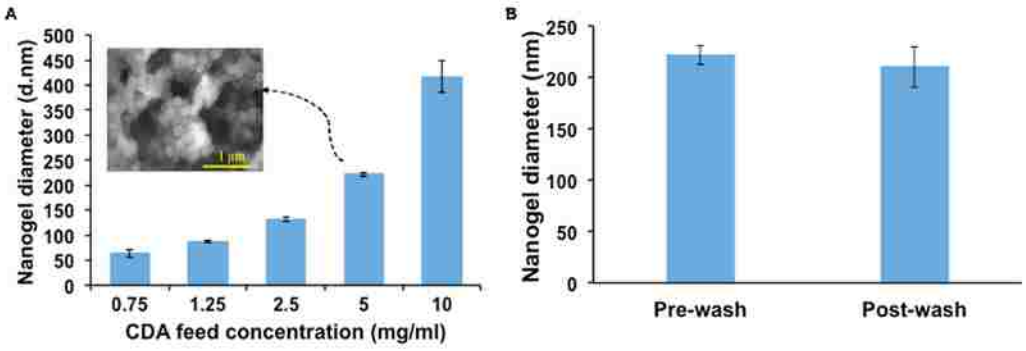

Figure 5.1 Hydrodynamic diameter and SEM of precipitated CNGs after 24-hour reaction of CDA with TTD in acetonitrile

(A) Different CDA feed reactant concentrations. Acrylate to reactive hydrogen amine ratio was kept constant at 1:1 for all the formulations Inset: SEM image of nanogels corresponding to 5 mg/ml feed concentration. (B) Hydrodynamic diameter of nanogels (5 mg/ml feed concentration) pre- and post-wash with THF as a purification step showing no significant difference at both the stages. N=3, error bars: std. dev.

5.3.2 Degradation, curcumin release and its anti-oxidant activity

Curcumin nanogels (CNG (5)) were suspended in 0.1% SDS-PBS buffer at a concentration of 100 µg/ml. To dissolve released curcumin, 0.1% SDS wt/vol was added. Released curcumin in the supernatant was quantified using a UV-Vis analytical method by recording the absorbance at 420 nm to determine sample concentration and cumulatively adding the obtained concentrations of each sample with increasing degradation time to obtain the degradation profile of CNGs. As shown in figure 5.2 A, 90% of the total curcumin release was uniformly distributed over 36 hours, and the remaining 10% release was spread throughout the next 30 hours. Meanwhile, taking into account 62.7% wt/wt as the theoretical loading of curcumin to nanogels, 55.58±3% of the total curcumin loaded was recovered during degradation. This lag in recovered curcumin could be due to release of oligomeric/monoacrylated products and may be underestimated in quantification during UV-Vis analysis. HPLC analysis of the degradation products at characteristic wavelength of 420 nm showed elution of pure curcumin (peak at 7.9 minutes) as the major product, but also constituted a minute amount of other products (peaks at 2.9 and 11 minutes) also absorbing at 420 nm

(Figure 5.2 B). These small peaks could count towards added value to curcumin estimation but are not fully accurate due to peak shift artifacts commonly observed in UV-Vis. Carrying out the TEAC assay on the released products supernatants gave an estimate of releasing curcumin's antioxidant capacity over 70 hours. All the instantaneously collected samples were assayed for antioxidant activity and quantified as mM of equivalent trolox because known concentrations of trolox were used as the standards. Finally, equivalent trolox amount were cumulatively added with respect to the degradation time to obtain a uniform increase in the antioxidant activity profile with time from 0.031 mM at t = 0 to 0.502 mM trolox after 70 hours of incubation. This implies that at each time point of hydrolytic ester cleavage, released curcumin was active to scavenge free radicals.

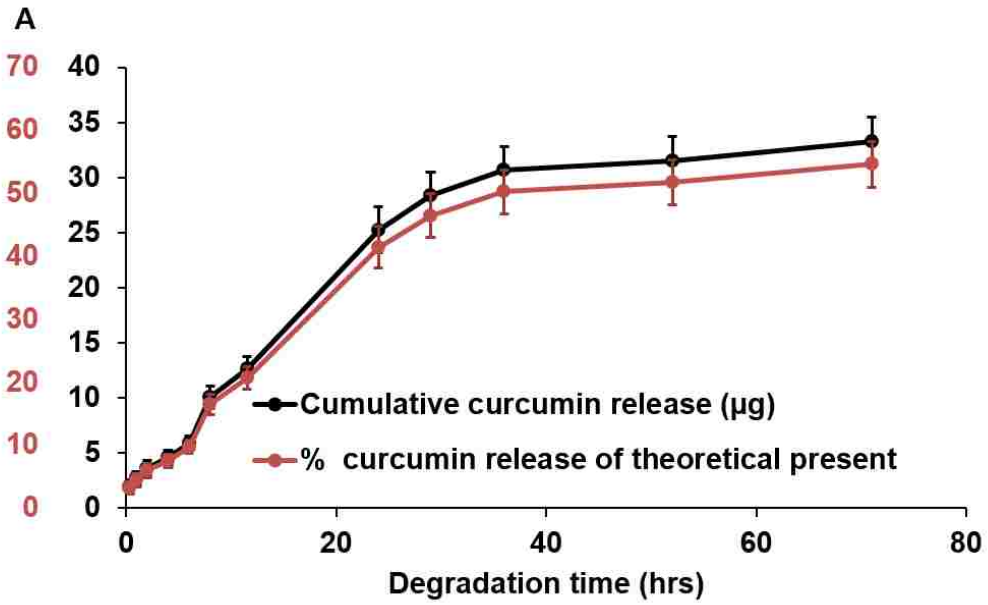

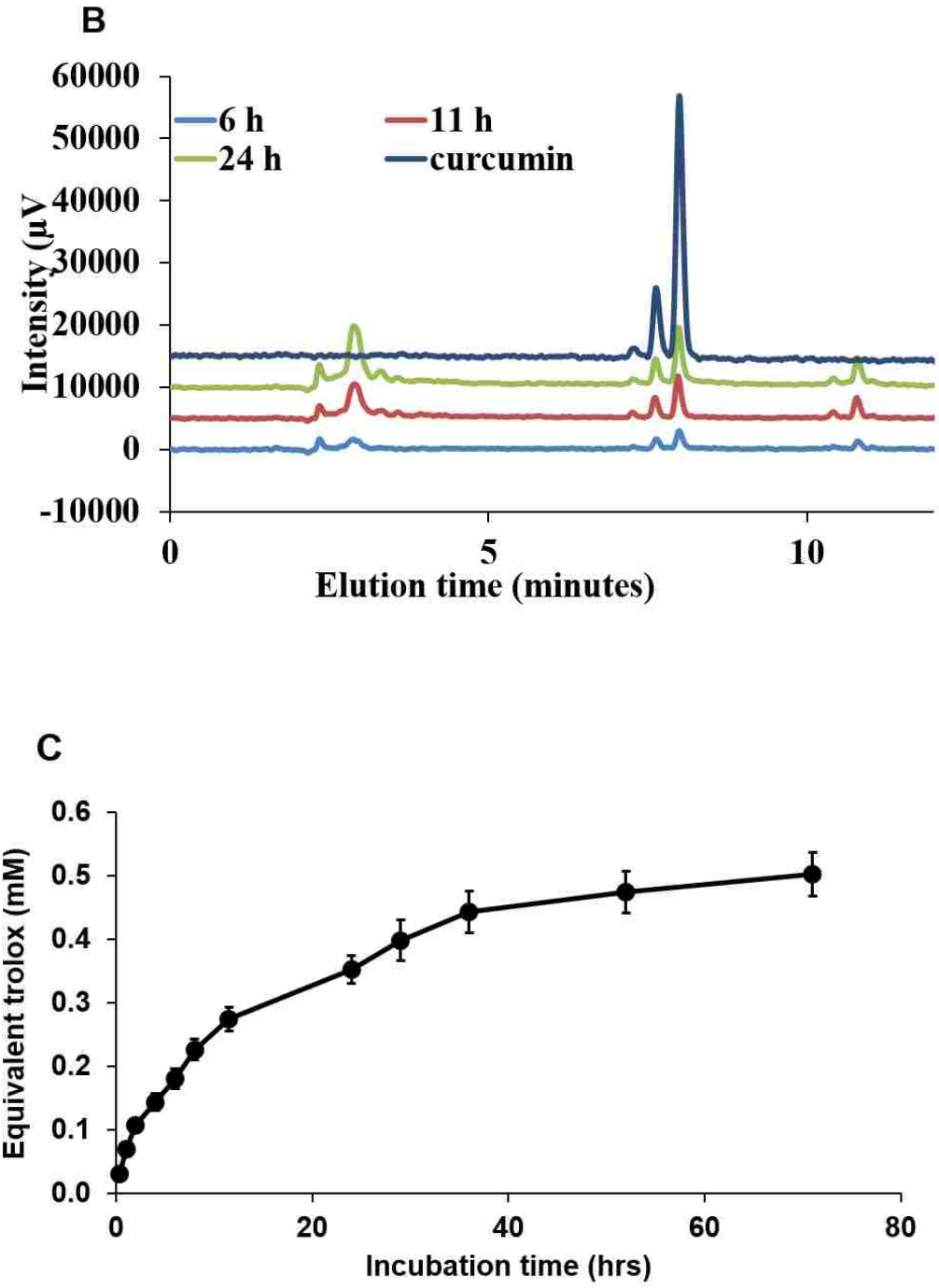

Figure 5.2 Degradation of CNGs in PBS buffer with 0.1% SDS (pH=7.4) at 37˚C in a shaker bath.

(A) Curcumin release profile during hydrolytic degradation (B) HPLC chromatogram of nanogel released products recorded at 420 nm showing elution of pure curcumin with minor amount of monoacrylate. (C) Equivalent trolox amount of the released products representing the antioxidant activity analyzed using TEAC assay. N=3, error bars: std. dev.

5.3.3 Dose dependent toxicity of CNGs on HUVECs and protection from oxidative stress

HUVECs were treated with variable concentrations of CNG (5) with equivalent curcumin concentrations ranging from 0.5 to 70 µg/ml. HUVECs were simultaneously, yet separately, treated with pure curcumin as a control. After 24 hours treatment, pure curcumin started showing toxicity towards HUVECs at 5 µg/ml (IC_{50} = 5.3 µg/ml) while CNGs were non-toxic up to 20 µg/ml of equivalent curcumin and cells were still 60% viable at a concentration of 70 µg/ml (Figure 5.3 A).

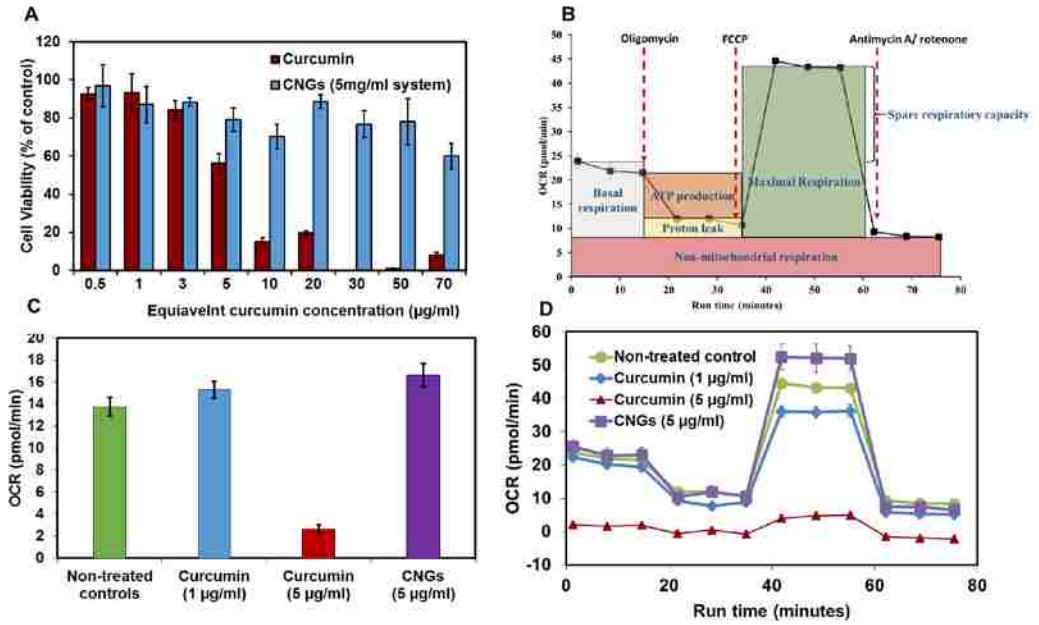

Figure 5.3 Dose dependent cytotoxicity of CNGs towards HUVECs after 24 hours of treatment and comparison with free curcumin.
(A) Cell viability calculated after carrying out the Calcein AM red-orange live cell tracer assay (B) Mitochondrial oxygen consumption rate profile of a typical mitochondrial stress assay conducted using the Seahorse XF96 instrument. (C) Basal respiration rates of curcumin and CNG (5) represented at pmol/min after the calculations as depicted in figure 5.3 B. (D) OCR (profile) of the controls and curcumin/CNG at different curcumin concentrations in response to mitochondrial stress assay reagents added in a series at selected time points. N=5, error bars: std. err.

5.3.4 Protection from cellular oxidative stress

Cell viability for each treatment group was measured keeping non-treated control group as reference of 100% viability. Only H_2O_2 treated groups after 24-hour exposure resulted in 53 ± 3 % viability, while only CNG treated groups showed no significant change with respect to the control with percent viability of 108 ± 4 (Figure 5.4). With simultaneous treatment of CNGs with 0.5 mM H_2O_2 exposure for 24 hours, 71 ± 4 % viability which is significantly higher than only H_2O_2 treated groups. In order to get an estimate of oxidative stress, amount of free radical generation was measured with DCF fluorescence. Only H_2O_2 treated groups gave a measured DCF fluorescence of 12250 ± 1220, which is significantly higher than non-treated control group with fluorescence measurement of 8620 ± 1198. Only CNGs treated group did not result in major difference w.r.t controls with DCF fluorescence of 7913 ± 980. Fluorescence measurement of CNGs+H_2O_2 group demonstrated suppression in oxidative stress due to H_2O_2 with lower values of DCF values of 8358 ± 1350 as compared to only H_2O_2 group.

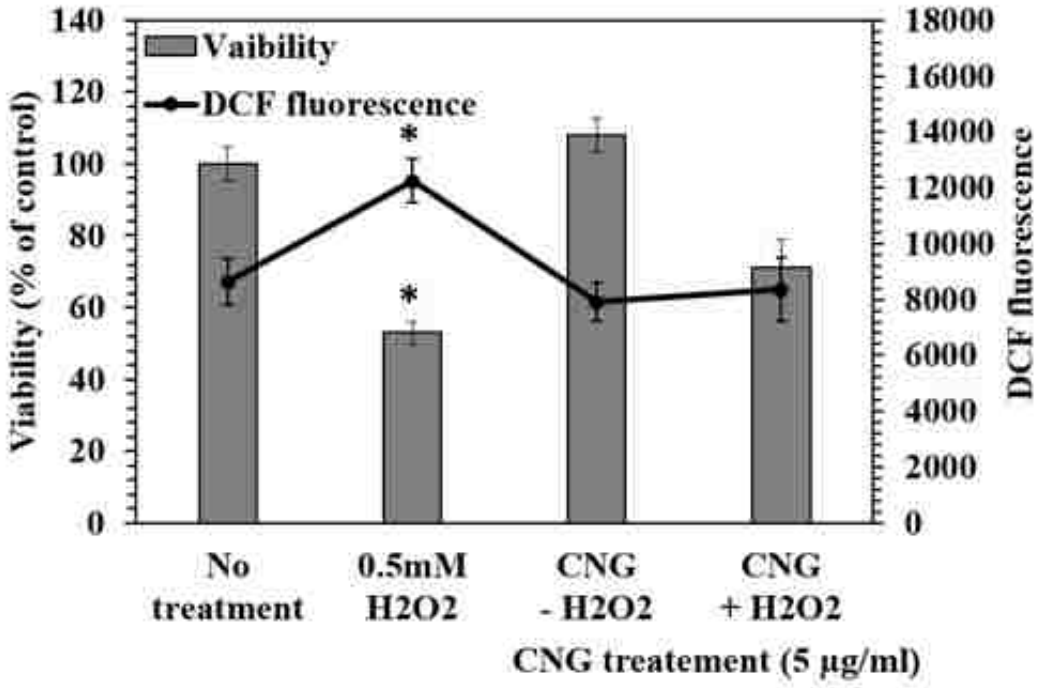

Figure 5.4 HUVECs cell viability and suppression in DCF fluorescence due to CNGs (5 mg/ml feed concentration system) with simultaneous treatment of 0.5 mM H_2O_2. *DCF fluorescence and viability both were measures after 24 hours treatment with CNGs and H_2O_2. CNGs with equivalent concentration of 5 µg/ml of loaded curcumin were administered to the cells. '*' significantly different from rest of the groups, $p<0.05$.*

5.3.5 Protection from mitochondrial oxidative stress

To assess the potential of CNGs toward mitochondrial OS protection and its comparison with pure curcumin, HUVECs were incubated with both CNGs and curcumin at two different concentrations for 24 hours. This incubation was followed by basal respiration rate measurements and a mitochondrial stress test. Basal respiration rates, ATP-linked respiration, proton leak, maximum respiration and spare respiratory capacity were calculated from the mitochondrial stress test drug-response OCR values according to the calculation scheme shown in figure 5.3 B. The curcumin treatment at 1 µg/ml showed nominal OCR of 15.29 ± 0.73 pmol/min which is comparable to the non-treated controls: 13.7 ± 0.9 but at 5 µg/ml of curcumin exposure, OCR values dropped down drastically to 2.68 ± 0.35 (Figure 5.3 C). This clearly implies the mitochondrial dysfunction at curcumin concentrations of 5 µg/ml.

On the other hand, HUVECs treatment with CNG at 7.97 µg/ml having equivalent curcumin concentration of 5 µg/ml retained its OCR at 16.6 ± 1.0 pmol/min and showed no signs of mitochondrial dysfunction or damage to the cells. The overall response of the curcumin/CNG treated cells in the mitochondrial stress assay can be seen in figure 5.3 D, where a healthy response similar to non-treated controls was seen for 1 µg/ml curcumin and CNG (5µg/ml equivalent curcumin loading). Curcumin with 5 µg/ml possessed no positive response towards the mitochondrial stress assay due to mitochondrial damage at that concentration.

Therefore, all additional studies of mitochondrial oxidative stress protection, viable concentration i.e. 1 µg/ml for free curcumin and 5 µg/ml of equivalent curcumin for CNGs were used. To assess and test the prolonged protection of CNGs against mitochondrial oxidative stress, two standards were set for the design of the experiment: 1) antioxidant treatment concentrations as stated above; and 2) concentration and exposure time to cells of oxidative stress inducer, H_2O_2 which is 0.25mM and 2 hours. This parameter was set so only mitochondrial bioenergetics were disturbed due to exposure but not the onset of cell necrosis/apoptosis which could result in added artifacts during OCR recordings. Mitochondrial respiration rate was measured as OCR (pmol/min) and the bioenergetics parameters are represented as basic OCR (pmol/min) as well as % OCR (after baseline normalization) to eliminate the effect of any variation in starting cell density as shown in figures 5.5 and 5.6. Two hours H_2O_2 exposure by itself led to a drop in basal respiration, ATP-linked and maximal respiration respectively to 34.5 ± 3.0%, 21.6 ± 3.6% and 34.8 ± 11.3% OCR from 76.1 ± 6.0%, 60.7 ± 5.7% and 149.6 ± 20.0% of the non-treated controls as shown in Figure 5.6 A, B and C. Curcumin treatments at 0, 12 and 24 hours prior to H_2O_2 addition did not aid in recovery of the OCR, basal respiration or maximal respiration, which were observed

to be 19.8 ± 10.2%, 25.0 ± 5.7% and 37.0 ± 26.7% respectively. In other words, viable concentrations of curcumin did not show any effective protection against mitochondrial OS. On the other hand, CNG (5) showed an enhanced OCR post H_2O_2 treatment at all exposure times giving basal OCR: 47.17 ± 3.93, 60.0 ± 2.0, 94.3 ± 10.0 as %OCR, ATP-linked OCR: 31.2 ± 7.5, 40.0 ± 14, 52.8 ± 5.2 and maximum respiration rates of 336.5 ± 12.5, 198.6 ± 37.3 and 161.7 ± 11.7 respectively for 0, 12 and 24 hours of prior nanogel treatment.

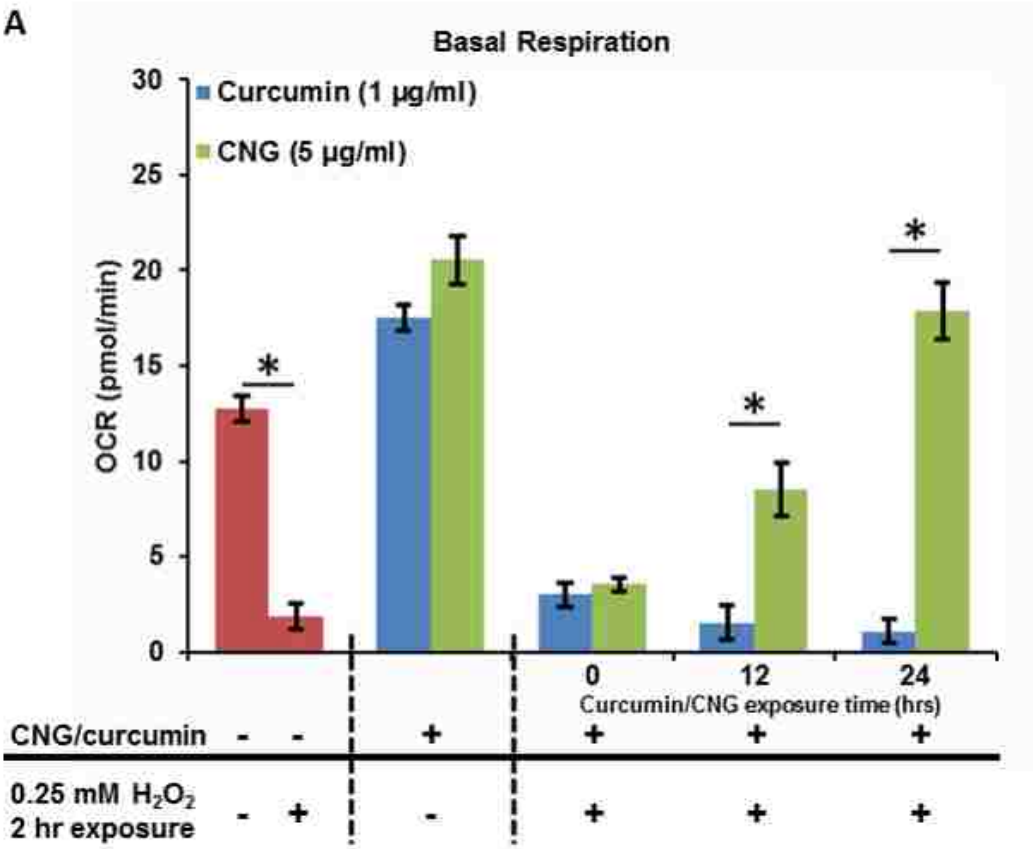
A
Basal Respiration
Curcumin (1 µg/ml)
CNG (5 µg/ml)
OCR (pmol/min)
30
25
20
15
10
5
0
*
*
*
0
12
24
Curcumin/CNG exposure time (hrs)
CNG/curcumin - - + + + +
0.25 mM H2O2
2 hr exposure - + - + + +

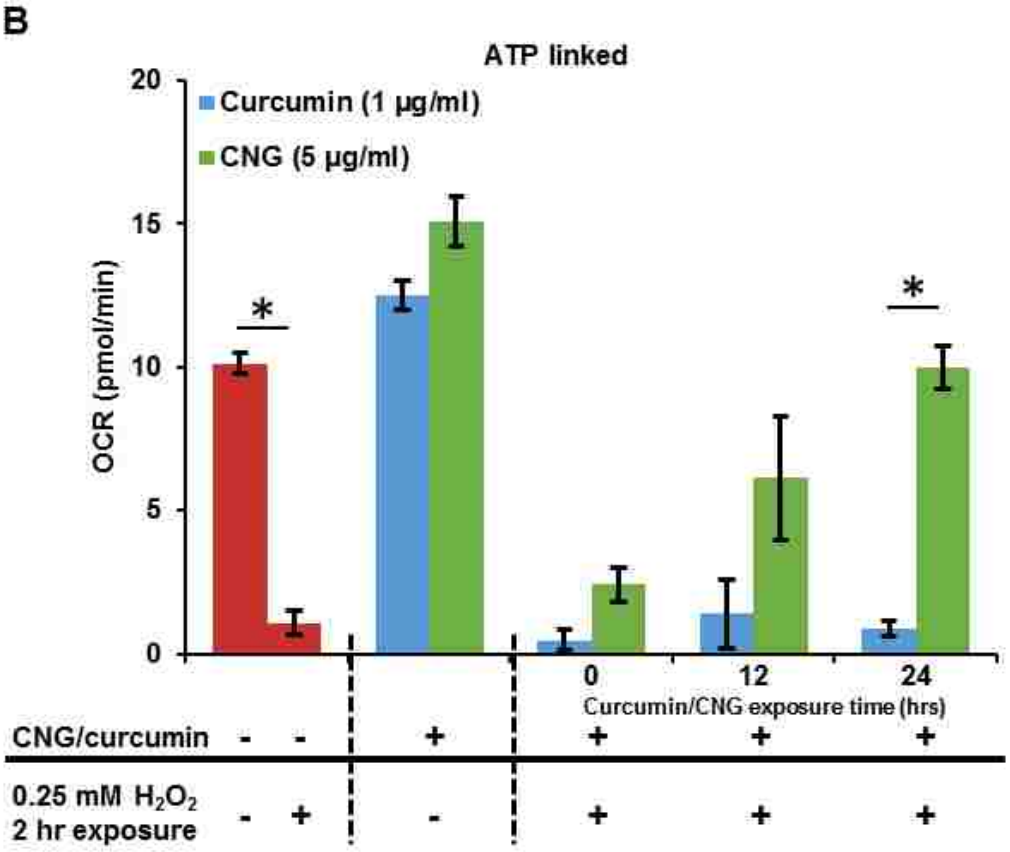
B
ATP linked
Curcumin (1 µg/ml)
CNG (5 µg/ml)
OCR (pmol/min)
20
15
10
5
0
*
*
0
12
24
Curcumin/CNG exposure time (hrs)
CNG/curcumin - - + + + +
0.25 mM H2O2
2 hr exposure - + - + + +

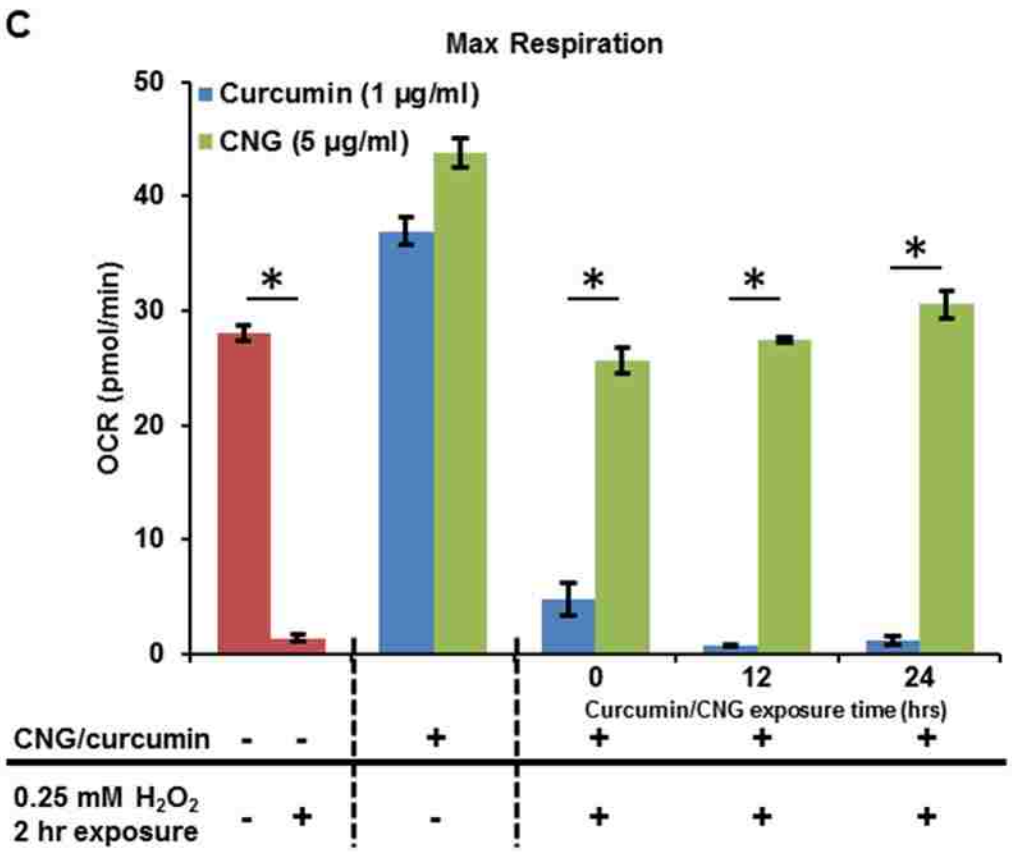

Figure 5.5 Mitochondrial function parameters after pre-treatment of curcumin/CNG for 0, 12 and 24 hours followed by 2-hour exposure of 0.25 mM H_2O_2.
Cells were subjected to mito stress assay with real-time OCR measurements using Seahorse XF96 instrument. (A) Basal respiration. (B) ATP-linked to mitochondria. (C) Maximum respiration. All OCR values are displayed as pmol/min. N=5, error bars: std. err.

5.3 Discussion

Significant efforts have been made to improve the delivery of mitochondria OS targeting drugs (e.g., MitoQ) with the help of nanocarriers, for the purpose of suppressing mitochondrial OS and reducing mitochondrial dysfunction [212, 213]. MitoQ is an ubiquinol moiety linked to a lipophilic triphhenylphosphonium (TPP) by a ten-carbon alkyl chain. A part of the TPP chain helps in the rapid cellular uptake of the drug loaded carrier across the cell membrane and further accumulation in mitochondria [214]. *In vivo*, MitoQ and its analogs (MitoVitE, MitoPBN) have shown positive results against Mito OS by inhibiting lipid peroxidation, ROS/RNS generation etc. [215]. TPP

based targeted antioxidant delivery approaches are most effective in rapid accumulation of antioxidants within the mitochondria, where the toxicity of the hydrophobic moiety (TPP) can result in nonspecific mitochondrial dysfunction, resulting in disruption of membrane integrity, respiration, and ATP production rate. This nonspecificity further depends on the amount of compound internalized. Therefore, the constraint is the amount of drug that can be delivered with TTP based nanocarrier so as to reach therapeutic levels before reaching disruptive concentrations [202, 216, 217]. Also, the ubiquinol based approaches may increase protection against peroxynitrite and superoxide radicals, but their efficacy has been reported to be small to negligible for one of the most significant oxidants (hydrogen peroxide H_2O_2) in cellular physiology [218].

As an alternative, a number of studies have demonstrated the protective effect of curcumin towards mitochondrial dysfunction and mitochondrial OS [219, 220]. Most research has concentrated on neurodegenerative diseases and finding new therapeutics for Alzheimer's [221, 222]. Curcumin has been shown to inhibit the depolarization of mitochondrial membrane potential as well as decreasing the levels of the pathological marker for the Alzheimer's disease amyloid-β [223, 224]. Similar results were observed in aluminum induced mitochondrial dysfunction studies, malate induced OS commonly known as nephropathy etc. [206] [225]. These positive results and outcomes from such approaches are reported only from *in vitro* models, but there is very little evidence of positive results *in vivo*. Faster *in vivo* metabolism and the inability of curcumin to reach therapeutic concentration in the targeted micro-locations may be the cause of success *in vivo* rather than *in vitro*.

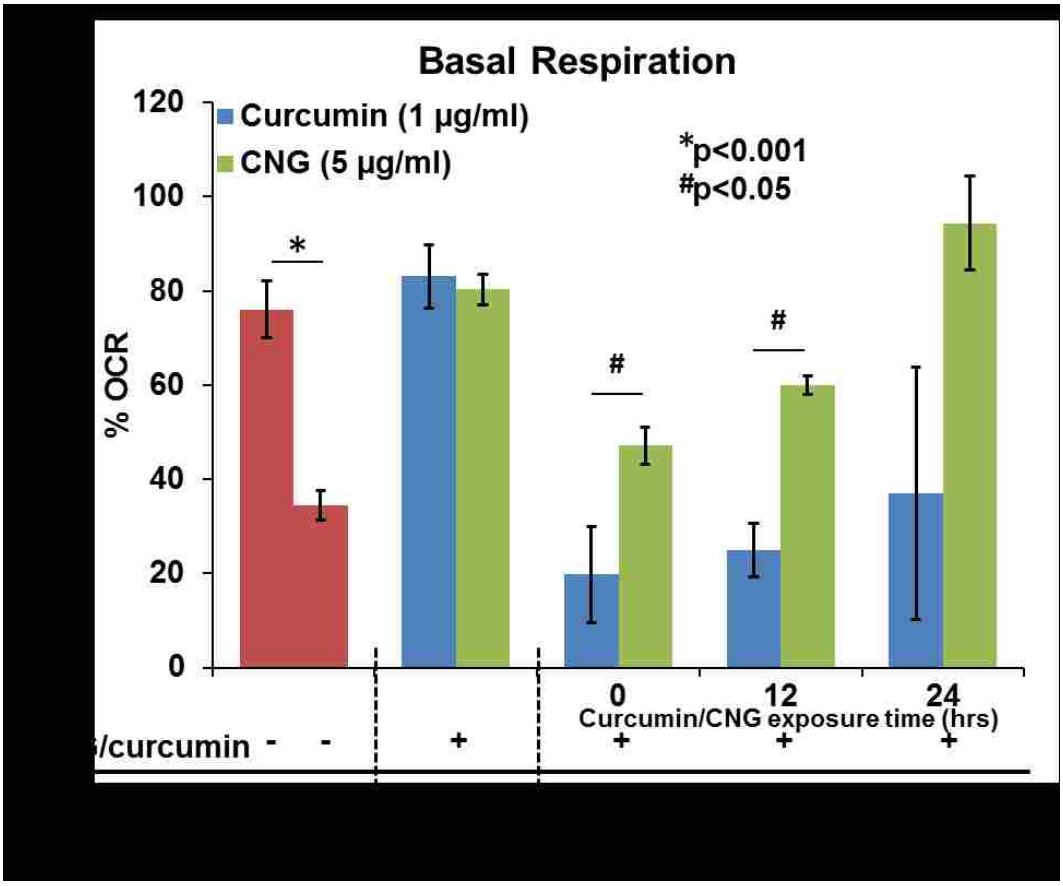
Basal Respiration
Curcumin (1 µg/ml)
CNG (5 µg/ml)
*p<0.001
#p<0.05
% OCR
120
100
80
60
40
20
0
*
#
#
0
12
24
Curcumin/CNG exposure time (hrs)
/curcumin - - + + + +

B

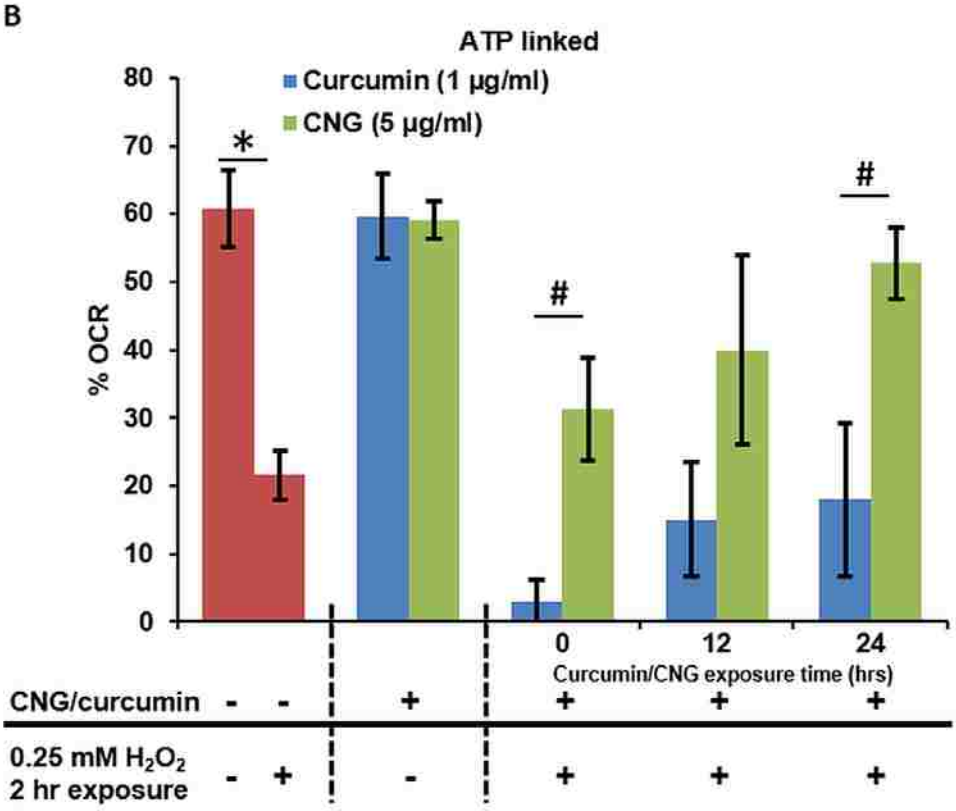
ATP linked
Curcumin (1 µg/ml)
CNG (5 µg/ml)
% OCR
80
70
60
50
40
30
20
10
0
*
#
#
0
12
24
Curcumin/CNG exposure time (hrs)
CNG/curcumin - - + + + +
0.25 mM H2O2
2 hr exposure - + - + + +

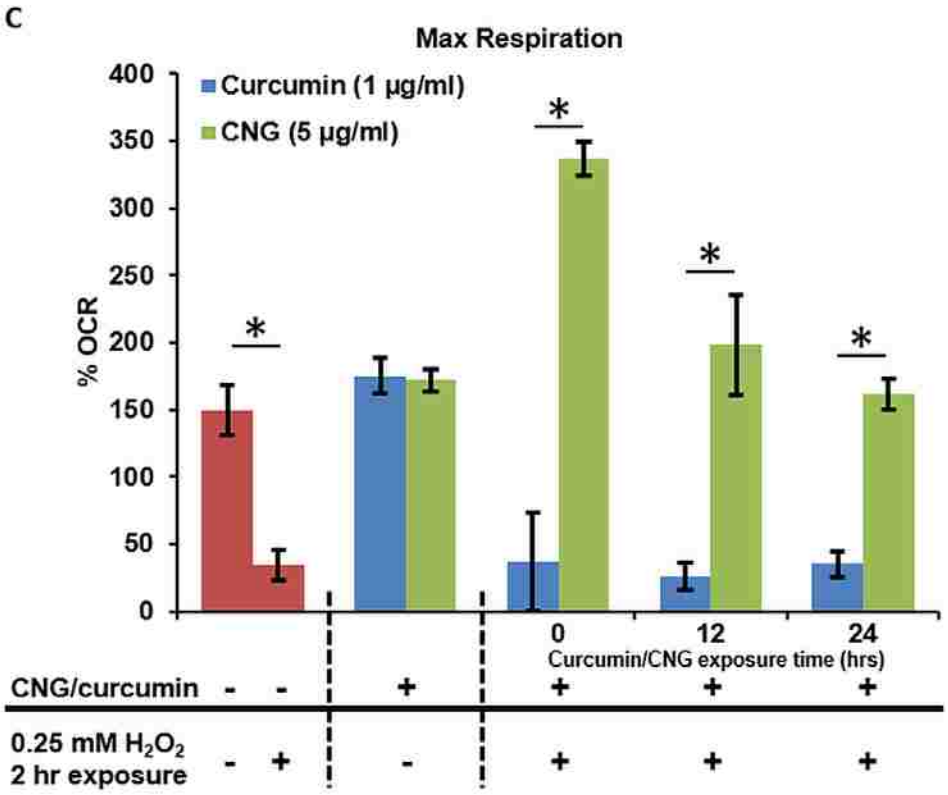

Figure 5.6 Mitochondrial function parameters presented as % OCR post total protein content normalization.

Pre-treatment of curcumin/CNG (5) for 0, 12 and 24 hours followed by 2-hour exposure of 0.25mM H_2O_2, subsequently subjected to mitochondrial stress assay with real-time OCR measurements using Seahorse CF96 instrument. (A) Basal respiration. (B) ATP-linked to mitochondria. (C) Maximum respiration. All OCR values are calculated as pmol/min. N=5, error bar: std. err.

Using synthesized PβAE conjugated curcumin nanogels, our aim was to improve the delivery of curcumin in its active and stable form at therapeutic, yet non-toxic concentration, with enough time to treat the site of action before being metabolized. With a mere change in monomer concentrations keeping the molar ratio constant, the nanogel diameter could be varied from 50 to 250 nm, and the spherical nature was confirmed by scanning electron microscopy (Figure 5.1 A). As no other competing monomer in front of curcumin acrylate was present to react with the tetra-functional amine (TTD), we expect the theoretical starting monomer composition of nanogel

reaction to be the final composition of synthesized nanogel, which when calculated gives 62.8% curcumin loading by mass. To our knowledge, this was the highest curcumin loading ever reported in nanocarriers.

These nanogels were synthesized by functionalizing the alcoholic group of curcumin into an acrylate conjugated into cross-linked PβAEs. At this point, hydrolysis released curcumin in its original structural form (Figure 5.2 B). This functionalization and conjugation step permits the structural stability of curcumin and prevents it from metabolized until released, potentially solving one of the *in vivo* limitations. Adding to the stability advantage, slow and uniform degradation of CNGs avoids the occurrence of any burst release, even at initial time points as shown in Figure 5.2 A (15% of the total released in first 10 hours or 28% release in first 20 hours). This is an important point to consider because burst release from drug carriers or high bolus doses of free curcumin start a pro-oxidant effect and, rather than act as a treatment drug, can be toxic *in vitro* to healthy tissues/endothelial cells. The uniform release profile of curcumin during degradation also helped increase the safety limit for curcumin treatment, giving IC_{50} values of more than 100 µg/ml as compared to free curcumin with IC_{50} values of 5.3 µg/ml, observed after 24 hours of treatment with HUVECs (Figure 5.3 A). This would provide an option to treat an injury at higher and more effective dosage levels.

Antioxidant potential of these nanogels with respect to time during degradation was initially analyzed by carrying out the TEAC antioxidant activity assay on all degradation samples. The cumulative increase in equivalent trolox content over time confirmed the protection of curcumin from losing its antioxidant activity in aqueous media until hydrolyzed from the polymer matrix (Figure 5.2 C). In other words, the functionality of the drug was kept intact until released.

Mitochondrial functional levels confirmed lower dose dependent cytotoxicity compared to free curcumin and prolonged active antioxidant release of CNGs. Seahorse XF96 analyzer recorded real time mitochondrial OCR in response to the treatments and/or mitochondrial stress assays specifically developed to determine basal respiration rates, ATP production, spare respiratory capacity, and maximal respiration. The dose dependent response post 24-hour treatment with 1 and 5 µg/ml of equivalent curcumin in CNGs showed no negative impact on OCR levels at either concentration. However, mitochondrial function/OCR was completely shut down with free curcumin at 5 µg/ml while 1 µg/ml was observed to be a safe concentration for mitochondria (Figure 5.3 C and Figure 5.3 D). These results comply with the cell viability assay (50% cell death at 5 µg/ml) but show a more acute response, thus providing an opportunity to analyze our material at more sensitive levels. With this understanding, non-fatal curcumin and curcumin nanogel concentrations, 1 and 5 µg/ml respectively (Figure 5.3 C and 5.4 D), were used to specifically observe any change in mitochondrial function upon induced OS injury without causing cell death.

We used H_2O_2 for mitochondrial OS insult because H_2O_2 is believed to induce mitochondrial dysfunction via sudden increase of ROS inside the mitochondria. This activity results in OS initiating cell necrosis and apoptotic processes. For the Seahorse XF96 studies, concentration and exposure time of H_2O_2 were selected to affect mitochondrial function without reaching the cells' necrotic or apoptotic state. This allowed mitochondrial respiration and energy production potential to be monitored with no cell death effects. H_2O_2 concentration of 0.25 mM with 2-hour exposure was enough to show a decrease in ATP production (% OCR) from 60.8 ± 5.7 to 21.6 ± 3.6, drop down of mitochondrial respiration from 76.0 ± 6.0 to 34.5 ± 3.0 (Figure 5.6 A and B). Oligomycin, FCCP and antimycinA/rotenone were used as the titrant substrates

(mitochondrial stress test assay) to analyze the functional state of the mitochondria post H_2O_2 ± CNG/curcumin treatment. Interestingly, upon pre-treating the cells with CNGs (5 μg/ml) or curcumin (1 μg/ml) for 0, 12, 24 hours before the 2-hour exposure to 0.25 mM H_2O_2, curcumin nanogels were able to retain and maintain the basal respiration rates, leveling to non-treated controls. Also, ATP-linked and maximum respiration analyzed after running stress assays for all treatment time scales was also higher than the H_2O_2 injury control group. In contrast, groups with 0, 12 and 24 hours of curcumin pre-treatment did not help the mitochondrion maintain basal respiration, ATP-linked production rates or maximum respiration rates, but were similarly low compared to H_2O_2 treated groups at those treatment times. As seen in Figures 5.4 and 5.5 A, B and C, mitochondrial bioenergetics worsened in curcumin groups simultaneously treated with H_2O_2 (t = 0), relapsing to H_2O_2 levels pretreatment time increased. A synergistic effect of curcumin and H_2O_2, where the pro-oxidant effect might have increased in the presence of another oxidant, may explain this. At t=0, when curcumin is at 20% concentration of its IC_{50} concentration i.e., 1 μg/ml along with H_2O_2 starts showing the pro-oxidant effect which decreases as curcumin active content starts reducing down with time due to curcumin molecular degradation and by 24 hour, cells would encounter the instant effect of H_2O_2 only. All this suggests that CNGs are benign to both the mitochondrion as a PβAE polymer matrix by itself and at a higher equivalent curcumin loading. This is due to the slow, steady curcumin release property of CNGs. Prolonged protection from Mito OS for at least 24 hours confirms the release of active curcumin when compared to no therapeutic effects shown by free curcumin. Therefore, a continuous supply of active antioxidant at therapeutically effective yet non-fatal concentrations would be capable of scavenging excess free radicals and suppressing mitochondrial oxidative stress and cell apoptosis.

5.4 Conclusion

Curcumin conjugated PβAE nanogels (CNGs) were synthesized, resulting in a slow and steady release of active curcumin molecule and an increased limit for the safe concentration of the drug. This work demonstrates the importance of delivery and controlled release upon the functional impact of biologically unstable compounds such as polyphenolic antioxidants. These spherical nanogels effectively suppressed mitochondrial OS over a 24 hour period, which was confirmed by real-time mitochondrial respiration state using Seahorse XF96 analyzer.

6 PROTECTION FROM COPLANAR AND NON-PLANAR PCBS INDUCED TOXICITY USING CURCUMIN CONJUGATED PβAE NANOGELS

Abstract

Curcumin-PβAE nanogels (CNGs) were analyzed for their therapeutic potential against PCB induced toxicity/oxidative stress. Extensive studies conducted by the Environmental Protection Agency (EPA) with these chlorinated aromatic compounds have shown clear evidence of their carcinogenic and toxic effects on the immune system, reproductive and also nervous system to count a few. As such PCBs falls into two categories, coplanar and non-coplanar congeners and induce immunotoxicity through activation of different cellular receptors. The protective effect of slow curcumin releasing CNGs was analyzed against both coplanar (PCB 126) and non-coplanar PCBs (PCB 153). Since, mitochondria are a more sensitive marker to such environmental toxicant exposure, real time mitochondrial bioenergetics were analyzed in response to PCB ± CNGs exposure. A dose dependent effect of both PCB 126 and 153 was observed after 24-hour exposure with compromised mitochondrial function as well as overall cellular toxicity in endothelial cells. It was also observed that PCB 153 induced higher toxicity to endothelial cells than PCB 126. As a potential treatment strategy, prior treatment with curcumin-PβAE nanogels before PCB exposure resulted in the restoration of mitochondrial bioenergetics and cell viability. This protective response with curcumin-PβAE nanogels was seen with both PCB 126 and PCB153. These results indicate that in spite of having different mechanisms for inducing toxicity, oxidative stress plays an important role in both manifestations and progression of the adverse effects. The fact that slow curcumin releasing CNGs protected cellular and mitochondrial function from PCB induced oxidative stress makes them a more versatile approach for PCB remediation.

6.1 Introduction

Concern about environmentally persistent polychlorinated biphenyls (PCBs) mediated chronic health effects is continuously increasing over the years [226]. A number of case studies have shown that prolonged exposure to these chlorinated aromatic compounds can result in the development of symptoms related to cancer and neurotoxicity [227-229]. Owing to these discoveries, PCB usage in industries was banned since 1976. But significant quantities of these compounds persist in soil, water, sea animals and in the human population as well [230, 231]. One of the underlying mechanisms for the PCB induced metabolic toxicity is thought to be oxidative stress, which is increased production of reactive oxygen species (ROS) than required for normal metabolic activity [232]. The continuous increased production of ROS can lead to cellular and mitochondrial membrane dysfunction, DNA damage, and disruption of membrane potentials leading to uncontrolled transfer of cytosolic nutrients and other components, resulting in total cell disruption, apoptosis and unwanted mutations [233]. Coplanar PCBs such as PCB 126 are thought to exert cellular toxicity via activation of aryl hydrocarbon receptor (AhR) followed by uncoupling of cytochrome P450 1A1 (CYP1A1), a potential reason for increased ROS production [234, 235]. On the other hand, exposure to non-coplanar PCBs activates the nuclear receptor proteins: PXR and CAR. Continuous activation of these proteins can lead to cellular toxicity and other adverse effects leading to unwanted mutations [236]. Studies have also shown evidence of increase in mitochondrial superoxide ($O_2^{\cdot-}$) in MCF-10A and RWPE-1 epithelial cells post PCB 153 exposure. This again proves the increased ROS production and also mitochondrial dysfunction during the exposure time [237]. PCB 77, 126 and even 153 post 6-hour exposure also induced oxidative stress in endothelial cells specifically, human umbilical vein endothelial cells (HUVECs). Because of the oxidative stress

involvement with PCB induced toxicity, antioxidants like resveratrol, quercetin, N-acetyl cysteine, catalase, and epigallocatechin-3-gallate (EGCG) have shown potential to suppress oxidative stress and hence PCB induced inflammation when cells were pre-exposed to these antioxidants before PCB administration [238-240]. An *in vivo* study performed with continuous supplements of green tea extract to mice during PCB 126 exposure showed a significant decrease in oxidative stress markers after 12 weeks of exposure as compared to non-green tea extract control [241]. These findings suggest that metabolic PCB toxicity includes the incidence of oxidative stress significantly where increased mitochondrial ROS or mitochondrial oxidative stress (mito OS) plays an important part and that antioxidant supplementation can serve as a remedy treatment to the exposed subjects by suppressing oxidative stress. To further explore this PCB response in HUVECs, we studied the effect of coplanar PCB 126 and non-coplanar 153 on overall cellular viability post 24-hour exposure to both kinds of PCBs and more importantly real time mitochondrial bioenergetics such as ATP production, maximal respiration rate. Response of human umbilical vein endothelial cells (HUVECs) was analyzed. Both of these studies showed a dose dependent decrease in viability and mitochondrial bioenergetics upon PCB administration. Also, pre-exposure of slow curcumin releasing curcumin-PβAE nanogels (CNGs) showed significant recovery in cell viability as well as mitochondrial respiration upon 12 and 24-hour prior treatment, demonstrating the anti-inflammatory properties against PCBs (both coplanar and non-coplanar) for a long period of time.

6.2 Materials and methods

6.2.1 Reagents

Curcumin was purchased from Chem-impex Int'l 'Inc, (Wood Dale, IL). 4, 7, 10-Trioxatridecane-1, 13-diamine (TTD), acryloyl chloride, triethylamine (TEA) and

potassium carbonate were bought from Sigma-Aldrich (St. Louis, MO). Sodium chloride, potassium phosphate, sodium phosphate and sodium dodecyl sulfate (SDS) were purchased from Fisher Scientific (Fair Lawn, NJ). Human Umbilical Vein Endothelial Cell line (HUVECs), EBM-2 basal medium and its growth factors were purchased from Lona, (Walkersville, MD). All solvents were purchased from Pharmco-aaper (Shelbyville, KY) and were used as received unless specified. All media kit and cell culture plates for XF96 Seahorse experiments were purchased from Seahorse Bioscience (Massachusetts, USA). Calcein AM red-orange tracer was bought from Invitrogen (Grand Island, NY). PCB 126 and PCB 153 were bought from Accustandard.

6.2.2 CA monomer and curcumin PβAE nanogels synthesis

Curcumin acrylate monomer was synthesized by reaction of curcumin with acryloyl chloride at room temperature for 15 hours in the dark. The protocol for the reaction and purification was adopted as described in section 5.2.2 To synthesize curcumin PβAE nanogels, dried monomer product (CA) was dissolved in anhydrous acetonitrile at a concentration of 5 mg/ml. A stock solution of TTD in acetonitrile at a concentration of 1 g/ml was prepared and 11.5 µl (11.5 µg TTD), was added to 10 ml of CA solution. The system was allowed to react and precipitate into self-stabilized nanogels for 15-16 hours in the dark. The nanogel suspension in acetonitrile was purified by diluting the suspension in anhydrous THF in the ratio of 1:4. After 2 washes, nanogels were suspended again in acetonitrile, centrifuged and the pellet was freeze-dried overnight to obtain dried nanogels.

6.2.3 In vitro PCB toxicity

In vitro cytotoxicity of PCB 126 and 153 on HUVECs was analyzed at three different concentrations after 24-hour exposure. HUVECs were seeded in a 96-well plate to about 80% confluency before the PCB administration. A 10 mM stock solution of both

the congeners (PCB 126 and PCB 153) was prepared in DMSO followed by dilution in EBM-2 media to a concentration of 15, 30 and 50 µM. Cells in each defined group were treated with 200 µl of PCB 126 and 153 solutions at the given concentration for 24 hours. After the treatment, incubation media was removed and all the wells were washed with fresh media followed by addition of 200 µl of 1 µM Calcein AM red-orange live cell tracer. After 1 hour of incubation with live cell tracer, media was removed from each well and fresh media was added. Fluorescence for the plate was read with excitation/emission wavelengths of 540/590 nm using BioTek Synergy Mx, Gen5 2.0, Winooski, VT fluorescence spectrophotometer to determine the viability of the cells post PCB exposure.

6.2.4 Effect of CNG treatment on PCB induced toxicity

Protection from PCB induced toxicity or cell death with the help of CNG was also analyzed after different antioxidant pre-exposure times. HUVECs were pre-treated with 10 µg/ml of CNGs for 0, 12 and 24 hour followed by 24-hour exposure to 50 µM PCB 126 or 153. Cells were subjected to Calcein AM red-orange fluorescence assay post exposure to analyze the cell death due to PCB ± CNG after different pre-treatment times.

6.2.5 Measurement of real-time mitochondrial bioenergetics due to PCB exposure, with and without CNG

Seahorse XF-96 Flux Analyzer (Seahorse Bioscience, North Billerica, MA) was used to monitor real-time respiration rates of mitochondrion after PCB 126 and 153 exposure for 24 hours and also any protective effect due to CNG treatment. By measuring oxygen consumption rates (OCR) and extracellular acidification rates (ECAR) with time, various mitochondrion respiratory parameters of treated cells were analyzed including

basal respiration, ATP production rate, maximum respiration rates and spare respiratory capacity using mitochondrial stress assay.

To carry out the experiment, HUVECs were 1st seeded in a Seahorse 96-well tissue culture plate at a seeding density of 35000 cells/well. Cells were allowed to adhere overnight, after which different combinations of PCB ± CNGs treatment were given.

6.2.5.1 Effect of PCB exposure on HUVECs

As a first step, HUVECs were treated with 15, 30 and 50 μM of PCB 126 or 153 for 24 hours, after which cells were subjected to the mitochondrial stress assay. Prior to the assay, cells were washed and the medium was replaced with 175 μL of FX media (FX Assay Modified DMEM from Seahorse Bioscience with 5.5 mM Glucose, 1 mM Pyruvate, and 2 mM Glutamix). Cells were incubated at 37° C in CO_2 free incubator after which the cells were subjected to the stress assay. The mitochondrial stress assay consists of series of injections of inhibitor drugs: (A) Oligomycin A (1 μM), which act as ATP synthase inhibitor; (B) FCCP (1 μM), an uncoupling agent; and (C) a mixture of 1 μM Rotenone and 1 μM Antimycin A, each used as inhibitors for mitochondrial respiratory chain complex I and III to shut down the mitochondrial oxygen consumption. OCR and ECAR were measured for 3 minutes with 3 minutes interval cycles. The inhibitor drugs were injected in series of A, B and C after the 3rd cycle of the previous one.

After the measurement was completed, the protein content in each sample was determined using BCA assay (Thermo Scientific, Rockford IL). Therefore, post stress assay, media was removed from all the wells and replaced with 25 μL of cell lysis buffer containing 0.32 mM Sucrose, 2 mM EDTA, 2 mM EGTA, 20 mM HEPES, pH 7.4, containing protease inhibitors 4 μg/mL leupeptin, 4 μg/mL pepstatin, 5 μg/mL

aprotinin, and 0.2 mM PMSF and plates were stored in -20^{o} C overnight to lyse the cell membrane.

Plates were taken out the next day and thawed to room temperature and put on an orbital shaker for an hour. Known amounts of protein standards (2.5 μg, 5.0 μg, 10 μg etc.) were added in the background wells of the plate to construct an optical density standard curve. Unknown protein levels of the samples were determined by measuring optical density using an iMark plate reader (Bio-Rad, Hercules, CA). Finally, the obtained OCR values as pmol/min were normalized to protein levels as pmol/min/μg and finally calculated as percent change (%OCR) from the third basal measurement for each group.

6.2.5.2 Analysis of protective effect of CNGs against PCB induced mitochondrial toxicity

To analyze the protective effect of CNGs against PCB-induced cytotoxicity or cellular oxidative stress, HUVECs seeded at a density of 35000 cells/well were first pre-incubated with 5 μg/ml of CNGs suspended in EBM-2 media for 12 and 24 hours. Media from the well plates was removed and a solution of PCB 126 or PCB 153 prepared in EBM-2 media at a concentration of 30 μM was added to the pre-treated cells for 24 hours. Cells were then subjected to the mitochondrial stress assay. The same protocol for mito stress assay was followed as discussed in section 6.3.4.1 for just PCB exposure. Basal respiration, ATP production, maximum respiration and spare respiratory capacity for each treatment groups were again calculated in terms of percent OCR after protein normalization. 5 μg/ml concentration of CNG was used after verifying it to be a viable concentration for mitochondrial bioenergetics, while 30 μM of PCBs was used in order to disturb the mitochondrial bioenergetics but not shut down down the cellular metabolism completely.

6.3 Results

6.3.1 Measurement of cell toxicity after 24 hour PCB 126 and 153 exposure

6.3.1.1 Cell viability

After 24-hour exposure of PCB 126 or 153 to HUVECs, dose dependent toxicity was observed for both PCB congeners. Cell viability of PCB 126 exposure at 15, 30 and 50 μM was calculated to be 93 ± 4.7, 89 ± 2.5 and 79.8 ± 5 % of non-treated controls respectively (Figure 6.1). On the other hand, PCB 153 was found to show higher toxicity than PCB 126 at the same concentrations and cell viability post exposure was found to be 97.9 ± 2.5, 74.4 ± 0.6 and 45.6 ± 4.5 % of non-treated controls for 15, 30 and 50 μM respectively (Figure 6.1).

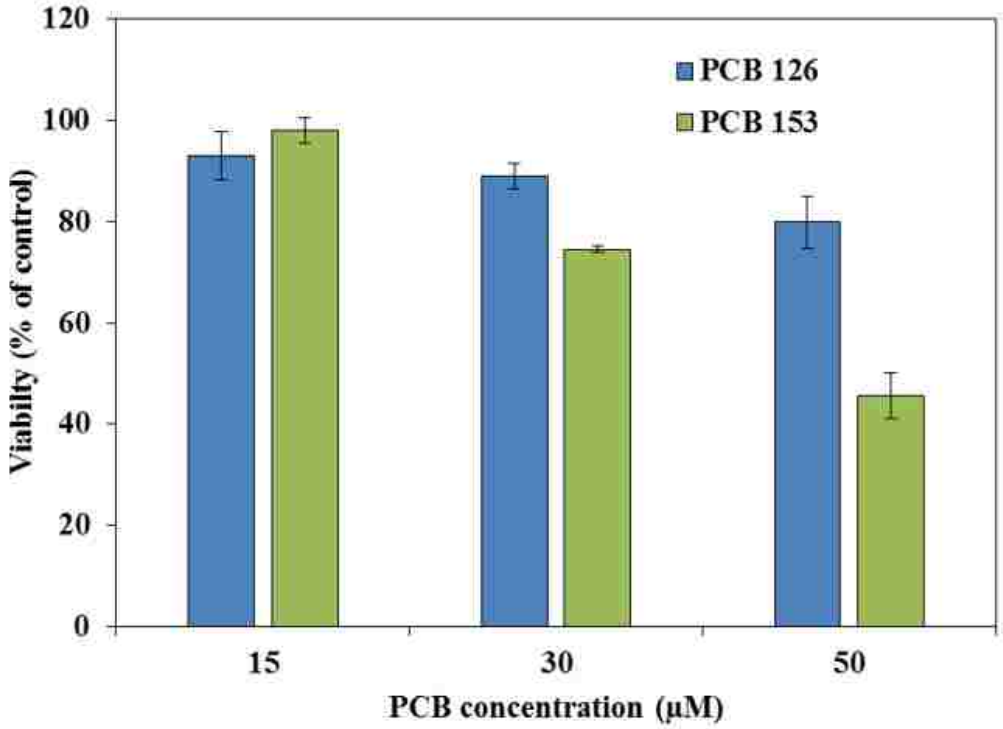

Figure 6.1 HUVECs viability after 24-hour PCB 126 and 153 exposures.
Cell Viability was determined using Calcein AM red-orange live cell tracer. Dose dependent exposure showed a decrease in viability with an increase in PCB concentrations. N=5, error bars: std. dev.

6.3.1.2 Mitochondrial bioenergetics

A more acute response on mitochondrial bioenergetics was observed at 30 and 50 μM after 24-hour exposure with basal respiration, ATP production rates, maximum respiration and spare respiratory capacity as well, when compared with cell viability at similar exposure concentrations. Here also, PCB 153 showed more acute response than PCB 126 at same concentrations (Figure 6.3). While basal respiration rates for PCB 126 as percent OCR were 76 ± 5, 53 ± 6 and 60 ± 5 after 24-hour exposure of 15, 30 and 50 μM respectively, PCB 153 exposure under similar conditions resulted in an intense response of 74 ± 3, 49 ± 7 and 0 % OCR at given increasing concentrations (Figure 6.3). These OCR values for 30 and 50 μM were found to be significantly lower than the non-treatment control with basal respiration of 78 ± 5. In the case of ATP-linked with mitochondrial respiration, % OCR of 47 ± 7, 40 ± 3 and 28 ± 3 for PCB 126; for PCB 153, 59 ± 4, 15 ± 12 and 0 was calculated after 15, 30 and 50 μM exposure respectively (Figure 6.3). Calculating maximum respiration gave the value of 183 ± 6, 145 ± 6 and 161 ± 3 for PCB 126; 179 ± 10, 82 ± 38 and 0 for PCB 153 with increasing concentrations mentioned above (Figure 6.3). Spare respiratory capacity was also calculated as % OCR 116 ± 10, 77 ± 12 and 78 ± 6 for PCB126; 104 ± 10, 53 ± 21 and 0 for PCB153 at increasing concentrations of 15, 30 and 50 μM respectively (Figure 6.3).

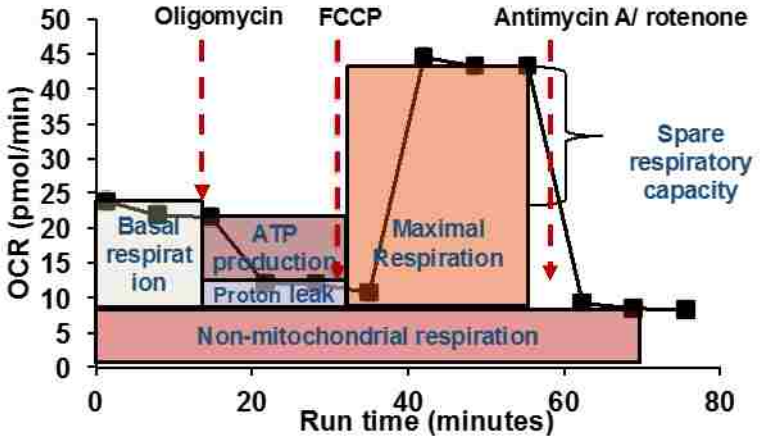

Figure 6.2 Mitochondrial oxygen consumption rate profile observed during mitochondrial stress assay.
All the bioenergetics shown in figure 6.3 and 6.5 were calculated according to the schematic shown in this figure.

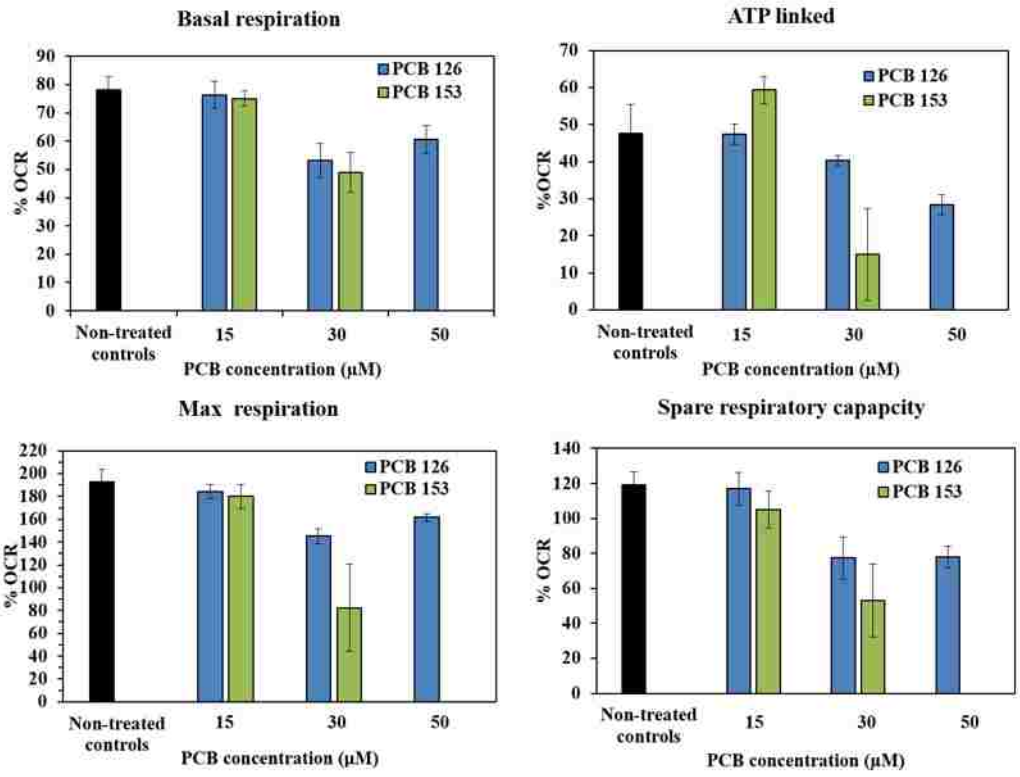

Figure 6.3 Mitochondrial bioenergetics parameters of HUVECs after 24-hour exposure to variable concentrations of PCB 126 or PCB 153.
The cells were subjected to the mito stress assay measuring real-time OCR values using Seahorse XF96 instrument. All the parameters after the assay were calculated in accordance with figure 6.2. N=5, error bars: std. err.

6.3.2 Protection from PCB 126 and 153 induced toxicity using CNG

6.3.2.2 Cell viability

A higher concentration of PCBs (i.e. 50 μM) was used in an *in vitro* cell viability assay in order to get a significant difference in response with respect to non-treated controls. As seen in figure 6.4, PCB 126 after 24-hour exposure resulted in 50% cell death while PCB 153 showed 98% cell death. Increasing cellular viability was observed with increase in CNG pre-exposure time and with 24-hour pre-exposure, cell viability was increased to 83 ± 6% for PCB 126 exposed cells and 11 ± 2 for PCB 153 exposed cells.

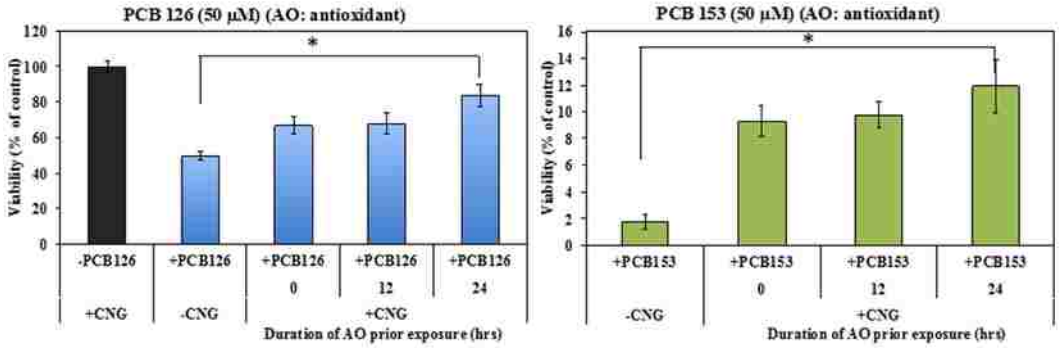

Figure 6.4 HUVECs viability analyzed after 0, 12 and 24-hour exposure to CNGs followed by 24-hour exposure to 50 μM PCB 126 or PCB 153.
Viability was determined using Calcein AM red-orange live cell tracer. 24-hour CNGs pre-exposure significantly increased % live cells post PCB 126 or 153 exposures showing effective protection against PCB induced toxicity. N = 5, error bars: std. dev.

6.3.2.3 Mitochondrial bioenergetics

To analyze the protective effect of CNG on mitochondrial function due to PCB 126 and 153 exposures, HUVECs were exposed to 5 μM (equivalent curcumin loading) CNGs for 12 and 24 hours, post which cells were washed and incubated with 30 μM of PCB for another 24-hour (Figure 6.5). CNGs after both 12 and 24-hour pre-exposure showed partial restoration of healthy mitochondrial functions for all its bioenergetics properties. Table 6.1shows the % OCR values for basal respiration, ATP-linked to the

mitochondrion, maximum respiration rates and spare respiratory capacity for the treated samples.

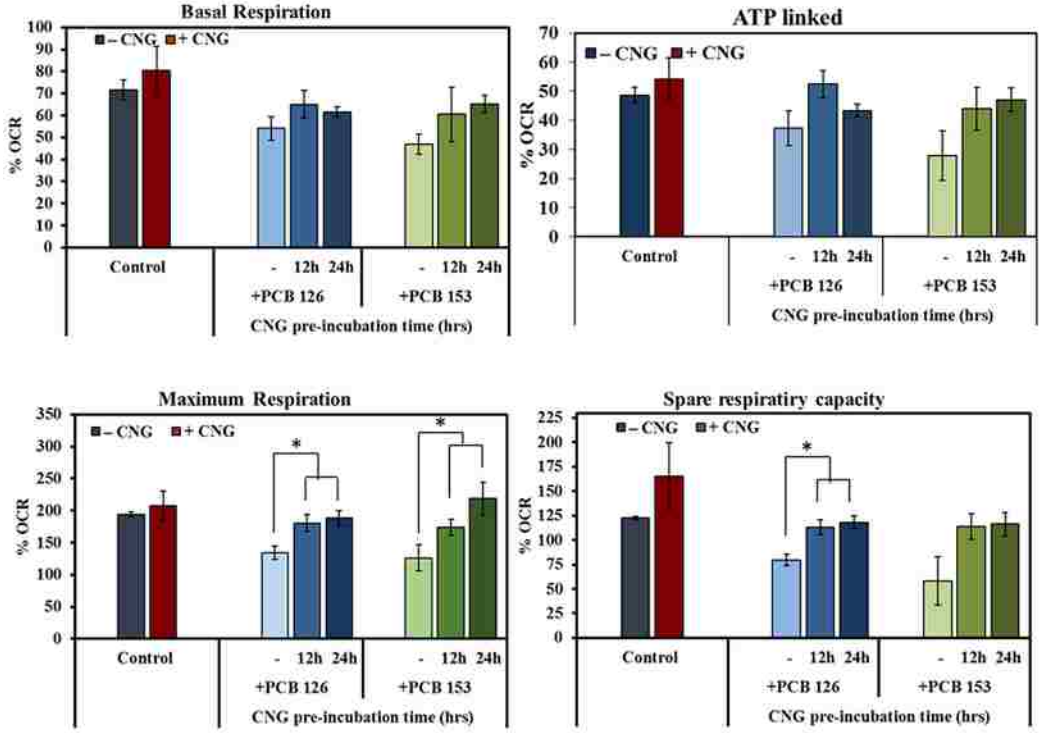

Figure 6.5 Mitochondrial bioenergetics of HUVECs after 12 and 24-hour exposure of CNGs followed by 24-hour exposure to 30 µM PCB 126 or 153.
CNG were washed off the wells prior to PCB incubation. The cells were subjected to mito stress assay measuring real-time OCR values using Seahorse XF96 instrument. All the parameters after the assay were calculated in accordance with figure 7.2. N = 5, error bars: std. err.

Table 6.1 Mitochondrial bioenergetics after PCB ± CNGs exposure to HUVECs as % OCR after protein normalization.
CNGs pre-exposure for 12 and 24 hours resulted in partial restoration of healthy mitochondrion function showing the protective effect of CNGs on PCB induced toxicity. N = 5, error bars: std. err.

		- CNGs	**+ CNGs**	
	CNG pre-exposure time		**12 h**	**24 h**
Basal respiration	Control	71 ± 5	-	80 ± 10
	PCB 126	54 ± 5	65 ± 6	62 ± 2
	PCB 153	47 ± 4	60 ± 12	65 ± 4
ATP linked	Control	49 ± 3	-	54 ± 7
	PCB 126	37 ± 6	52 ± 5	43 ± 3
	PCB 153	28 ± 8	44 ± 7	47 ± 11
Maximum respiration	Control	194 ± 4	-	207 ± 23
	PCB 126	134 ± 10	180 ± 13	188 ± 11
	PCB 153	126 ± 21	174 ± 12	218 ± 26
Spare respiratory capacity	Control	122 ± 2	-	166 ± 34
	PCB 126	80 ± 6	113 ± 7	118 ± 6
	PCB 153	58 ± 24	114 ± 13	116 ± 12

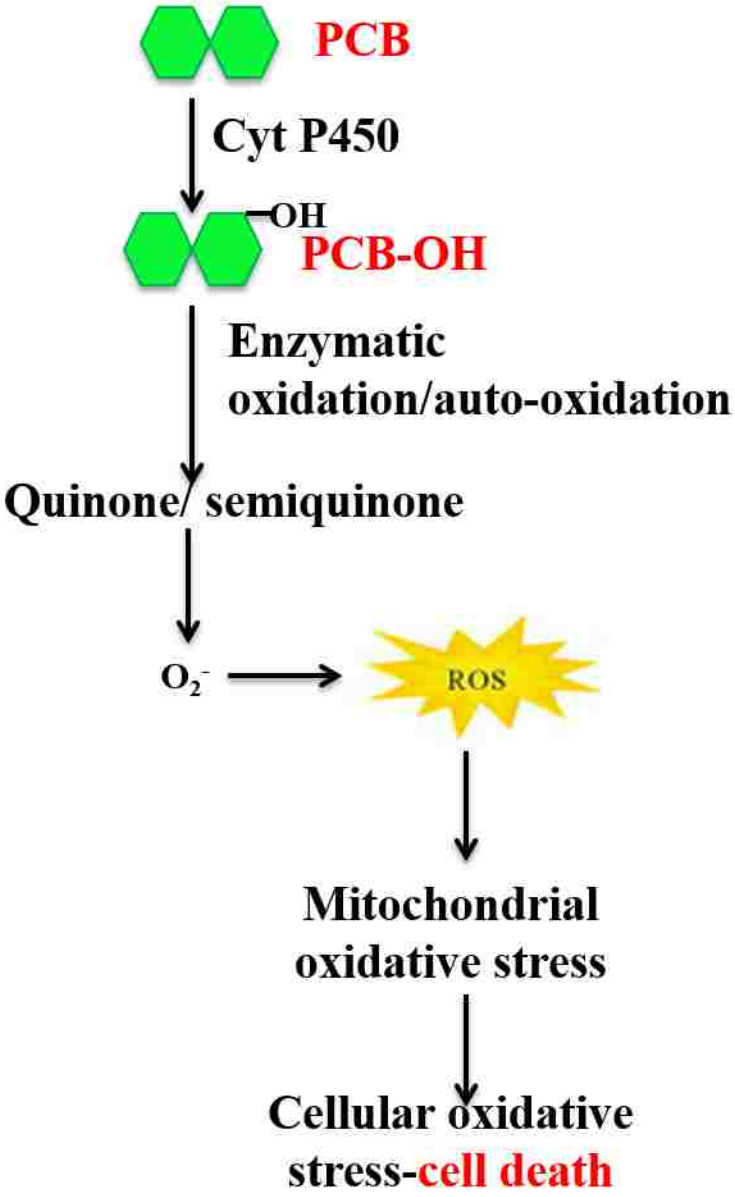

Figure 6.6 Mechanism of free radical production due to intracellular PCB metabolism for coplanar PCBs resulting in mitochondrial oxidative stress and finally cell death.

6.4 Discussion

PCB induced toxicity is not an immediate or acute effect but a long term event of slow cellular dysfunction that aggravates over time and leads to major metabolic disorder eventually. This is because it is found at very low concentrations in soil, water, air and sea animals. The underlying cause for this chronic response is due to development of

an oxidative stress (OS) condition via different activation pathways. OS is an imbalanced metabolic redox state in the body with increased oxidants or free radical species/reactive oxygen species (ROS) concentrations. A simple mechanism is depicted in figure 6.6, where superoxide anion produced due to enzymatic action 1st results in mitochondrion OS (most prone sight for increased free radical production), dysfunction of which ultimately leads to cell death.

To analyze the oxidative damage due to PCB exposure, HUVECs were subjected to PCB 126 and 153 exposure for 24-hour at variable concentrations, which resulted in increased toxicity with increasing concentrations (Figure 6.1). A more acute response was observed at a mitochondrial level as compared to overall cellular function (Figure 6.3). This is because, oxidative stressed induced mitochondrial dysfunction occurs prior to overall cellular toxicity. Therefore, monitoring mitochondrial bioenergetics served as a sensitive marker to study the acute response due to these chemical pollutants. Use of Seahorse Bioscience XF96 further aided the analysis because of its ability to monitor mitochondrial respiration in real time, a novel and non-invasive strategy for the *in vitro* systems.

Further, the loss in mitochondrial function was more severe with PCB 153 (non-coplanar) as compared to PCB 126 (coplanar), where at 50 μM, cells completely lost its mitochondrion function shutting down the metabolic activities. This is opposite to few studies in the literature showing more acute toxic effects due to coplanar PCBs (PCB 77, 126 etc) than non-coplanar ones. A possible explanation to these observations could be because most studies concentrated on analyzing the response by quantification of AhR activation, which is well known and induction path for coplanar PCBs but not for non-coplanar [242] [243]. But there have been other evidence showing toxic nature

of PCB 153 via nuclear receptor proteins, chronic activation of which can result in various disease syndrome and has been associated with breast cancer etc [227, 244].

As both the toxicity induction routes involve excess production of ROS, administration of curcumin through conjugated prodrug PβAE nanogels (CNGs) system served as a potential solution to prevent oxidative damage. These nanogel formulations are hydrolytically degradation systems with steady and prolonged drug release kinetics. Therefore, treating HUVECs with CNGs prior to PCB exposure showed reduced toxicity as compared to only PCB treated controls (Figure 6.4). The effect was more pronounced at the mitochondrial level, where partial to full recovery of mitochondrial bioenergetics (basal respiration, ATP-linked, maximum respiration, spare respiratory capacity) was seen with CNGs pre-treated groups (Figure 6.5). Also the fact that CNG administration was able to inhibit mitochondrial as well as cellular toxicity due to both coplanar and non-coplanar PCBs indicates the presence of oxidative stress in the injury path, irrespective of the different receptors being activated. Hence, administration of curcumin via CNGs becomes an adaptable approach to remediate cellular toxicity due to all kinds of PCBs.

Another possible pathway behind inhibition of PCB induced toxicity would be direct capturing of PCBs by polyphenolic curcumin via pi-pi bond interactions. This will inhibit the interaction of chlorinated compounds with cellular components, thereby reducing the possibility of fatal metabolic response.

6.5 Conclusion

PCB 126 and PCB 153 both showed toxic effects towards HUVECs, compromising mitochondrial function after 24-hour exposure at variable concentrations. PCB 153 showed more acute response than PCB 126 which complies with a few studies in the

literature while opposes most of the other studies with toxicity comparisons of coplanar and non-coplanar. Irrespective of this difference, curcumin conjugated PβAE nanogels (CNGs) with the slow and steady curcumin release property were able to suppress both mitochondrial as well as overall cell toxicity. This response is thought to be through either or a combination of two mechanisms, which includes suppression of oxidative stress due to antioxidants and capturing of PCBs by curcumin through physical pi-pi interactions.

7 SYNTHESIS AND CHARACTERIZATION OF CURCUMIN PβAE GEL MICROPARTICLES TO TREAT ORAL MUCOSITIS

Based on the research article to be submitted:

Prachi Gupta, Sandeep Ramineni, J. Zach Hilt, Thomas Dziubla, Joseph Wyse, Nihar Shah, Curcumin conjugated Poly (β-Amino Esters) gel microparticles to treat oral mucositis (Biomaterials) *(to be submitted)*

Note: The information in this chapter is the intellectual property of Bluegrass Advanced Materials LLC., not be disclosed in public.

Abstract

Oral mucositis (OM) is a very common and serious side effect of anti-cancer radiation and chemotherapies that manifests as deep and painful mouth ulcers. Oxidative stress (OS) is one of the key underlying mechanism in the development of OM. Therefore, curcumin (an antioxidant) has been extensively studied as an antioxidant and anti-inflammatory agent towards OS treatment. In the case of OM, it has shown positive signs towards delaying the onset and also reducing the severity of OM. However, it requires about 4-5 rinses per day, a total dosage ranging from 1-3 g per day, to stay in the therapeutic window for treatment. This is because of a combination of fast metabolism, rapid degradation and poor aqueous solubility of the hydrophobic antioxidant. In order to improve the bioavailability of this drug in buccal tissues and improve patient compliance, curcumin was converted into biodegradable curcumin-poly(beta-amino ester) (PβAE) polymer (poly(curcumin)) microparticles. These poly(curcumin) microparticles provide slow sustained release of the original active curcumin. Synthesized via Michael addition, acrylate functionalized curcumin (curcumin acrylate (CA)), PEGDA (co-monomer), and TTD (primary diamine

crosslinker) were reacted together into a PβAE polymer film and cryogenically milled into microparticles in the range of 20-25 μm. Poly(curcumin) formulations were prepared with different co-monomer molar ratios (CA v/s PEGDA) showed variable release profiles of active curcumin. Poly(curcumin) microparticles with a molar ratio of 70:30 CA:PEGDA and RTAAP of 1.0 showed the best combination of drug release profile and adhesion to buccal tissues. This selected formulation further showed prolonged protection against H_2O_2 induced oxidative stress *in vitro* with normal human dermal fibroblasts. A preliminary *in vivo* study in Syrian hamsters induced with OM in their cheek pouches showed that treatment with poly(curcumin) microparticles reduced the severity of induced OM, protein carbonyl content, and epithelial layer damage.

7.3 Introduction

Oral mucositis is a pathological condition in patients undergoing cancer treatments resulting in inflammation of oral mucosa, which manifests as oral ulceration, erythema, and severe pain. The discomfortness is a long-term and persistent response to patients undergoing chemo- and/or radiation therapies as anti-cancer treatments [245]. This response usually occurs after 7-10 days of undergoing anti-cancer treatment, peaks at about 7-9 weeks after beginning of the therapy and persists for up to 2-10 weeks after the end of the treatment depending on the patient's physical conditions and type of therapy [245, 246]. Though a side effect, this oral pain impacts the food intake of the patient, leads to oral infections, dehydration, weight loss, sometimes requiring extended hospitalization and even forcibly stalling the cancer treatment in between. On an average about 5-15% of the patients undergoing any kind of anti-cancer therapy suffer from OM. More acutely, 40% of the subjects getting treated with 5-fluorouracil and about 50% with radiotherapy tend to get OM [247]. The severity increases with patients suffering from head and neck cancer where 100% of the patients receiving cancer

treatment suffer from this condition of OM [248]. Therefore, there has been a continuous need for treatment and prevention of OM. Though the standard care procedures include the use of palliatives including intravenous narcotic analgesics, lubrication and analgesic mouth rinses (lidocaine), these have shown poor efficacy and low patient compliance [249-251]. Palifermin has been the only drug approved by FDA to be administered to the patients undergoing anti-cancer therapy [252]. Palifermin, which is keratinocyte growth factor-1 (KGF-1), is thought to inhibit epithelial cell damage, down-regulating pro-inflammatory cytokines as well as enhancing the growth rate of epithelial cells during the infectious state [253, 254]. Besides being selectively effective in patients suffering from hematological malignancies, Palifermin is an expensive drug with an average cost of about 8000 euros per treatment for a 70 kg patient over 6 days [255]. Other palliative treatments are also provided to patients, like Mugard and NeutraSal in the form of oral rinse or gels. These can temporarily soothe the oral discomfort conditions and provide primarily pain management solutions but not treatment or curing solutions [256-258]. Practically no single preventive or curative measure without side effects or limitations yet effective for the diverse population has been found and approved towards oral mucositis while research still continues to find the basic cause and solution to the problem.

Studies have shown that the long duration curve of this disease shows some lasting effects or morphological changes in the tissues apart from the acute toxicity resulting in instant cell death. The longer effect of OM is thought to be arising via a complex trajectory of biomolecular, cellular changes leading to epithelial layer damage and sub-epithelial cells damage associated with upregulation of nuclear factor kappa beta (NFkB) and interleuken-1 [259, 260]. These phenomena can be considered as a sensor to oxidative stress (OS) where the physiological environment or the cellular matrix

encounters an increased production of free radicals or ROS. The increased ROS production is a cyclic cascading event resulting in an imbalanced redox state of the cell. This leads to DNA, cellular membrane damage and finally cell apoptosis and necrosis, inhibiting epithelial layer proliferation ultimately resulting in ulceration [261]. Hence, OS is one of the base causes of the initiation and propagation of the OM until the body comes into its state of fighting OS naturally or by providing enough antioxidants to restore the redox balance [262].

A few studies have shown that certain drugs/molecules with antioxidant properties like hyaluronic acid (HA), vitamin E, curcumin and green tea extracts like epicatechin can control the symptoms of OM. For example, a human trial with *Gelclair* (0.2% HA containing gel) showed occurrence of fewer ulcers after day 5 of treatment as compared to placebo. The underlying mechanism for this response is thought be due to the anti-inflammatory nature of HA which upon rinsing coats the oral mucosa, enhances tissue hydration and helps in decreasing inflammation [263]. Similarly, curcumin, extracted from the spice turmeric has also been investigated for its antioxidant effect towards treatment and prevention of OM. In a recent pre-clinical trial with beta-radiated rats, administration of curcumin via oral gavage showed reduced incidence and severity of OM due to inhibition of the activation of NF-kB factor [264, 265]. Similarly a recent human clinical trial with subjects given turmeric mouth rinses showed delayed as well as reduced intensity of radiation-induced OM at all times during the treatments as compared to the placebo controls due to the presence of curcuminoid elements in turmeric. But this treatment required multiple dosage regimes of oral rinsed 4 times a day every 4 hours to see the effective treatment against OM [266-268]. Curcumin as a polyphenolic molecule undergoes rapid metabolization and shows low bioavailability once administered into the physiological environment [269-272]. This quick loss of

drug upon administration force the patient to go for multiple dosing frequency in order to stay in the therapeutic window. This becomes a cumbersome treatment process for patients already undergoing cancer therapy and can sometimes become a barrier during chemo or radiation treatments. Therefore, as a proposed solution, in this work we have aimed at formulating a mucoadhesive system with hydrolytically biodegradable PβAE poly (curcumin) gel microparticles, These polymer microparticles are tuned to release curcumin uniformly over 12-16 hours in order to fight and protect against oxidative stress induced OM during cancer therapies. The prolonged delivery would increase the efficacy in treating OM and improve the patient compliance in the long run, decreasing the dosage frequency to as low as once a day. To formulate the curcumin conjugated PβAE microparticles, phenolic groups of curcumin were 1^{st} functionalized into acrylates forming curcumin acrylate (CA). CA was then covalently conjugated with TTD and its co-monomer PEGDA into PβAE gel films via Michael addition reaction. The advantage of using PBAE chemistry lies behind (i) its property of getting hydrolyzed in an aqueous environment (ii) ability to tune polymer degradation based on the hydrophilic/hydrophobic nature of the monomers and (iii) protection of the active alcoholic groups of curcumin until released due to ester hydrolysis. Further synthesized gel films were cryo-ground into microparticles and suspended in a mucoadhesive solution, which served as a mouth rinse carrier to deliver the poly(curcumin) microparticles. These micron-sized particles showed tunable degradation properties by varying the molar ratios between curcumin acrylate and PEGDA. A continuous and steady release of active curcumin ranging from 12-24 hours was observed for different PBAE gel microparticle formulations. The poly(curcumin) microparticles were observed to be relatively less toxic than free curcumin towards normal human dermal fibroblasts (NHDF). Also, they did not show any negative or side

effect when administered to healthy hamsters for 10 days, implying a viable nature of the system *in vivo.* Adding to this, these microparticles showed protection against induced oxidative stress, *in vitro* for over 36 hours. Suspending the microparticles in a pre-formulated mucoadhesive solution allowed ease for local delivery of curcumin to buccal tissues of hamsters. Giving a daily rinse of this suspension over 10 days showed reduced severity of OM in chemotherapy-induced OM hamsters.

7.4 Materials

All the solvents received were ACS/HPLC grade and were used as received. Other chemicals were also used as received without any further purification. Curcumin was purchased from Chem-Impex International, Inc, Wood Dale, IL. 4,7,10-Trioxatridecane-1,13-diamine (TTD) (97% purity), poly(ethylene glycol) diacrylate (PEGDA, average molecular weight 575), acryloyl chloride (≥97%, ~400 ppm phenothiazine stabilizer), anhydrous potassium carbonate, magnesium stearate, 2,2′-azinobis-(3-ethylbenzothiazoline-6-sulfonic acid) (ABTS), Trolox, 2,7-dihydrodichlorofluorescein (H_2DCFDA), 2,4-dinitrophenylhydrazine (DNPH), trichloroacetic acid (TCA), guanidine hydrochloride, and bovine serum albumin (BSA) were bought from Sigma-Aldrich, St. Louis, MO. Sodium chloride, potassium phosphate, sodium dodecyl sulfate (SDS) and potassium thiocyanate was purchased from Fisher Scientific. Sodium hydroxide was purchased from EMD Millipore, Billerica, MA. Potassium chloride, potassium phosphate monobasic, sodium phosphate dibasic heptahydrate, calcium chloride dihydrate, and citric acid were purchased from Amresco, Solon, OH. Sodium phosphate dibasic dodecahydrate and triethylamine (TEA) (99%) was purchased from Acros Organics, NJ. Ham's F-12 media with L-glutamine and without phenol red was purchased from Caisson Laboratories Inc., Smithfield, UT. Pen/strep/fungizone as a media supplement was purchased from Lonza,

Walkersville, MD. Calcein AM red-orange was purchased from Life Technologies, Carlsbad, CA, All solvents were purchased from Pharmco-Aaper, Shelbyville, KY and were used in anhydrous form by drying over 4Å molecular sieves. Noveon AA-1 and Carbomer 971P NF were generously gifted by Lubrizol Corporation, Cleveland, OH. Eudragrit L100 was gifted by Evonik Industries, Tippecanoe, IN. Porcine buccal tissues were obtained from Animal Technologies Inc., Tyler, TX.

7.5 Methods

7.5.1 Synthesis of curcumin acrylate

Functionalization of hydroxyl (-OH) groups of curcumin into acrylate esters was done by reacting curcumin with acryloyl chloride as described in Wattamwar et al [178] with few process variations. Briefly, acryloyl chloride (19.8 ml, 0.2442 moles) was added dropwise to a solution of curcumin (30 g, 0.0814 moles) and trimethylamine (TEA, 34.1 ml, 0.2442 moles) in anhydrous tetrahydrofuran (THF), stirring continuously at 300 rpm. The reaction vessel was kept in an ice bath during the addition of acryloyl chloride in order to dissipate heat generated from the exothermic reaction of acryloyl chloride with curcumin. After purging the reaction vessel with ultrahigh purity nitrogen, the reaction was allowed to proceed for about 16-18 hours in dark at room temperature. The resultant product was vacuum filtered to remove the TEA-Hydrogen chloride salt. The THF was evaporated under vacuum to obtain a semi-dry orange to a light brown impure product. The product was re-dissolved in dichloromethane (DCM) and washed with 3x volume excess of hydrochloric acid (0.1 M in DI water) followed by potassium carbonate (0.1 M in DI water) to remove excess TEA and acryloyl chloride respectively. Residual water was removed by adding anhydrous magnesium sulfate to the DCM solution, which was removed by vacuum filtration at the end. The DCM was evaporated using vacuum for 16-18 hours to obtain dry, crystalline, orange colored microparticles

of curcumin acrylate (CA). The CA product was stored desiccated at -20°C until further use. The CA was characterized using reverse-phase HPLC (Shimadzu Prominence) with a Phenomenex Luna C18 column (4.6 x 250 mm, 5 µm particles) with 0.1% w/w phosphoric acid in DI water and acetonitrile as the mobile phase. The products (residual free curcumin, monoacrylate, diacrylate and triacrylate) were detected at 420 nm using a UV-Vis detector (SPD-20A) attached to the HPLC.

7.5.2 Synthesis of poly(curcumin) film

Crosslinked poly(curcumin) PβAE films were synthesized via a single-step Michael addition reaction between curcumin acrylate and the primary diamine crosslinker, 4, 7, 10-Trioxatridecane-1, 13-diamine (TTD). PEGDA was added as a diacrylate co-monomer to control the hydrophilicity and hence the degradation characteristics of the resulting films. Poly(curcumin) films with four different ratios of CA: PEGDA with respect to number of acrylate groups, 60:40, 70:30, 90:10 and 100:0, were synthesized. For example, in the 60:40 film, 60% of the acrylate groups were contributed by CA versus 40% by PEGDA. These films and subsequently their microparticles will be abbreviated as C60, C70, C90 and C100 respectively. The molecular weight of CA was taken as 476.47 g/mole which is the molecular weight of its diacrylate form. Finally, the amount of TTD required to synthesize the films was calculated based on three different ratios of total acrylate groups to amine protons (RTAAP) of 0.8, 1.0 and 1.2. As an example, a C60 poly(curcumin) film with RTAAP of 1.0 and target mass of 2 g was synthesized by dissolving 0.913 g of CA in 1.5 ml of anhydrous methyl ethyl ketone (MEK). PEGDA (0.735 g) and TTD (0.352 g) were reacted together for 5 minutes in 1.5 ml of MEK separately. After 5 minutes, the CA solution was quickly added to the reacting PEGDA-TTD solution while gently vortexing the PEGDA-TTD solution at low rpm. This reacting solution was quickly poured into an aluminum dish,

covered with foil and allowed to react for 1 hour at room temperature. After 1 hour, the aluminum dish was incubated at 50° C for another 23 hours, after which the crosslinked poly(curcumin) film was peeled off from the dish for further processing. A similar procedure was followed to synthesize C70, C90 and C100 PBAE films with three different RTAAP values (0.8, 1.0 and 1.2).

7.5.3 Washing and cryogenic milling of poly(curcumin) Films

7.5.3.2 Extraction of leachables

All freshly synthesized poly(curcumin) films were washed in anhydrous acetone to leach out any unreacted monomers and un-crosslinked components. Each film was placed in a 50 ml centrifuge tube, filled with 20 ml of acetone and covered with foil. The sealed tube was rotated at 25 rpm for 4 hours with the acetone replaced every hour. Every hour, an aliquot of the acetone containing the leachable from each tube was stored at -20° C for quantification of the lost curcumin using UV-Vis spectrophotometry. After washing, the films were lyophilized to remove residual solvent.

7.5.3.3 Cryogenic milling

The washed and lyophilized poly(curcumin) films were milled into microparticles under cryogenic conditions using a SPEX SamplePrep 6770 Freezer/Mill. Briefly, a film was cut into smaller pieces and loaded into the grinding vial assembly along with 1% w/w magnesium stearate (as a glidant). The loaded sample was pre-cooled under liquid nitrogen for 2 minutes followed by milling for 10 minutes with the stainless steel impactor moving at a speed of 15 cycles per second. After the milling cycle was complete, the vial assembly containing the poly(curcumin) microparticles was wrapped in paper towels and allowed to equilibrate to room temperature for about 1 hour. The

microparticle sample was then retrieved and the mass noted. The microparticle samples were stored desiccated at -20° C until further use.

7.5.4 Particle size characterization

The particle size distribution of the poly(curcumin) microparticle formulations was analyzed using a Shimadzu SALD-7101 UV particle size analyzer operated using WingSALD software (ver. 1.02, Shimadzu). The refractive index was set to 1.4. The quartz cuvette was filled with DI water and used to blank calibrate the instrument. Next, about 2-3 mg of microparticle sample was added to the cuvette, mixed with the provided L-shaped stirrer and then sonicated for 2 minutes. The sample was measured in the instrument under stirring. The instrument software automatically provided the mean particle size and the size distribution for each sample. Each sample was measured in triplicate.

7.5.5 Poly(curcumin) microparticle degradation and curcumin release

Five milligrams of the poly(curcumin) microparticle sample were suspended in 10 ml of phosphate buffered saline (PBS, pH 7.4) by bath sonication for 2 minutes. Since curcumin has poor solubility in water, 0.1% w/w sodium dodecyl sulfate (SDS) was added to the PBS to ensure complete solubility of the released curcumin. The sample suspension was incubated at 37° C in a water bath with shaking at 70 rpm. Every 2 hours, the suspension was centrifuged at 5000 rpm for 5 minutes and the supernatant was withdrawn and stored at -20° C for further analysis. The microparticle pellet was re-suspended in the same volume of fresh buffer. This step was repeated until 24 hours or until the poly(curcumin) sample had completely degraded. The collected supernatants were analyzed using a Varian Cary 50 Bio UV-Vis spectrophotometer with the absorbance measured at 420 nm (peak absorbance wavelength of curcumin). A few of the supernatant samples were also analyzed using HPLC to verify the release

of the original curcumin molecule by comparison with the chromatogram of curcumin standards.

7.5.6 Antioxidant activity of released curcumin

We utilized the trolox equivalent antioxidant capacity (TEAC) assay to quantify the antioxidant activity of the curcumin released after degradation of the poly(curcumin) microparticle formulations [273]. The TEAC assay is a colorimetric assay used to determine the antioxidant capacity of samples based on the suppression of the absorbance of 2, 2'-azinobis-(3-ethylbenzothiazoline-6-sulfonate) ($ABTS^{\bullet+}$) radical cations by antioxidants. Briefly, a 7 mM $ABTS^{\bullet+}$ radical solution was prepared by reacting equal volumes of solutions of ABTS (8 mg/ml) and potassium persulfate (1.32 mg/ml) in DI water for 16-20 hours. The $ABTS^{\bullet+}$ radical solution was diluted in PBS to obtain an absorbance not exceeding 0.4 at 734 nm for a 200 µl sample in a 96-well plate. This diluted solution was used as the working solution for the assay. For the assay, 10 µl of trolox standard solutions (concentrations ranging from 0-0.225 mM) prepared in PBS and the degradation samples were added to individual wells of a 96-well plate. To these wells, 200 µl of the $ABTS^{\bullet+}$ working solution was added and allowed to sit for 5 minutes in dark. After 5 minutes, absorbance was measured at 734 nm. The absorbance of the trolox standards was used to generate a standard calibration curve, which was used to calculate the equivalent trolox concentration for the poly(curcumin) degradation samples.

7.5.7 *In vitro* cytotoxicity assay

Primary normal adult human dermal fibroblasts (NHDF) bought from PromoCell GmbH, Heidelberg, Germany were cultured in Ham's F-12 medium supplemented with 10% v/v fetal bovine serum (FBS) and 1% v/v Pen/Strep/Fungizone at 37° C in a 5%

CO_2 incubator. NHDF that were purchased at passage 1 (P1) were grown until P4 and then used for experiments between P5 and P8.

Cells were seeded at 8000 cells/well in a 96-well plate and incubated overnight. Poly(curcumin) microparticles with equivalent curcumin concentrations ranging from 0 to 500 µg/ml were suspended in cell culture medium. Solutions of free curcumin at equivalent concentrations were also prepared in cell culture medium. 200 µl of test suspensions and solutions were pipetted onto the cells in the 96-well plates (n=5 per treatment group). After incubation for 24 hours at 37° C in a 5% CO_2 atmosphere, the cells were washed with fresh medium, followed by addition of 200 µl calcein AM red-orange cell viability dye (1 µM in Ham's F-12 medium) as a live cell tracer. Calcein AM red-orange is a mildly fluorescent molecule which upon internalization by cells is converted into the highly fluorescent calcein by cleavage of the acetoxymethyl ester group by intracellular esterases typically found only in live cells. Measurement of the fluorescence intensity can be used to quantify and compare the viability of the cells exposed to various treatments. After incubation for 1 hour, the cells were washed once more with fresh medium followed by addition of 200 µl of fresh medium for fluorescence measurements at 540/590 nm excitation/emission wavelengths using a plate reader(BioTek Synergy Mx, Gen5 2.0, Winooski, VT).

7.5.8 *In vitro* oxidative injury assay

Cells were seeded in a 96-well plate at a cell density of 8000 cells/well. Hydrogen peroxide (H_2O_2) was used as a model reagent to induce oxidative stress in NHDF. Poly(curcumin) microparticles and free curcumin suspensions in Ham's F-12 media were prepared at two concentrations: 1 and 5 µg/ml of equivalent curcumin loading. 0.5 mM of H_2O_2 was used as injury concentration. 10 mM of stock H_2O_2 was prepared

in media, 10 µL of which was added to the wells of interest to get a final concentration of 0.5 mM.

The protection offered by the antioxidant potential of the poly(curcumin) microparticles against H_2O_2 injury was assessed with three different treatment regimens: (i) Poly(curcumin) microparticles and H_2O_2 added simultaneously at t=0 and kept for 24 hours, (ii) Poly(curcumin) added at t=0 followed by H_2O_2 at t=12 hours, both kept until t=24 hours, (iii) Poly(curcumin) added at t=0 followed by H_2O_2 at t=12 hours, both kept until t=36 hours. At the end time points of each treatment regimen, cells were washed with fresh media and then incubated in 200 µl of 1 µM Calcein AM red-orange for 1 hour. Cells were washed again and incubated in fresh media for fluorescence measurement as described in section 7.3.7 to determine the cell viability and indirectly the protection potential of the poly(curcumin) microparticles. The cell viabilities for each time regimen (24 and 36 hours) were calculated with their respect no treatment control groups.

7.5.9 Pre-clinical study in a Hamster model of OM

7.5.9.1 Study protocol and sampling

All animal studies were conducted at the University of Kentucky in accordance with a protocol approved by the Institutional Animal Care and Use Committee. A total of 32 male golden Syrian hamsters (Harlan Laboratories, Indianapolis, Indiana) weighing 90 to 115 g were randomly divided into 4 groups as shown in table 7.1. Animals in the control groups (1 and 2) remained disease free. Oral mucositis was induced in animals in the OM groups (3 and 4) by administration of 5-flurouracil (5-FU, 60 mg/kg) intraperitoneally on day 0 and 2, followed by abrasion of the left cheek pouch. Treatments were administered into the left cheek pouches using needle-less syringes once daily from day 0 until euthanasia, under mild isoflurane anesthesia. The control

groups (1 and 3) received 200 µl of PBS while the treatment groups received 200 µl of 10% w/w suspension of poly(curcumin) microparticles (C70 PβAE formulation) in the mucoadhesive vehicle. C70-PβAE microparticle formulation was selected because this formulation scored highest in mucoadhesive amongst the three formulations analyzed for curcumin release, where C70 gave a uniform 12-15 hour curcumin release profile. On day 3, under ketamine (100 mg/kg) and xylazine (10 mg/kg) anesthesia, the left cheek pouches of the animals in the OM groups (3 and 4) were everted and mild erythema was created via dragging an 18 gauge needle in two 3 cm long parallel lines on the tissue surface. Once daily, all animals were weighed, their left cheek pouches were digitally photographed, and also visually scored for OM severity according to table 7.2 [274]. Animals were given 0.1-0.2 mg/kg buprenorphine once or twice daily as needed. Animals with excessive inflammation of the cheek pouches or those under significant distress (indicated by drastically reduced food intake and activity) were euthanized before the end of the study. At the end of the study on day 11, all remaining animals were euthanized by CO_2 asphyxiation. The treated (left) and control (right) cheek pouches were then excised. Half of the total number of cheek pouches were flash frozen in liquid nitrogen and immediately stored at -80°C for the tissue biomarker assays (TEAC and protein carbonyl, discussed later). The other half of the cheek pouches were processed for histological examination as described below.

Table 7.1 Pre-clinical study design and treatment plan

No.	Group	No. of Animals	Injury Day	5-FU Injection Days	Treatment (200 µl), Daily
1	No OM, Control (NOC)	5	None	None	PBS
2	No OM, Treatment (NOT)	5	None	None	10% w/w poly(curcumin) suspension
3	OM, Control (OMC)	11	3	0 & 2	PBS
4	OM, Treatment (OMT)	11	3	0 & 2	10% w/w poly(curcumin) suspension

Table 7.2 Scoring guidelines for visual observation of mucositis assessment of hamster pouch

Score	Observation
0	No erosion or vasodilation
1	Erythema but no evidence of mucosal erosion
2	Severe erythema, vasodilation and superficial erosion
3	Formation of ulcers in one or more places, not covering more than 25% of the surface area
4	Cumulative ulcer formation, about 50% of pouch surface area
5	Complete ulceration of pouch mucosa. Loss of pliability

7.5.9.2 Protein carbonyl content of cheek tissues

Oxidative stress in tissues can damage proteins by oxidation resulting in the formation of carbonyl groups in the protein chemical structure. The protein carbonyl content of the cheek tissues was quantified using the 2, 4-dinitrophenylhydrazine (DNPH) assay according to the manufacturer protocol (Cayman Chemicals). DNPH on reaction with carbonyls forms the corresponding hydrazone, which can be detected spectrophotometrically. Briefly, 200-500 mg of each tissue sample was homogenized in PBS (200 mg tissue per ml) followed by centrifugation at 3000 rpm for 10 min. 200 µl of the supernatant was mixed with 800 µl DNPH and incubated for 1 hour in dark at room temperature. An equal volume of supernatant was mixed with 800 µl of 2.5 M HCl instead of DNPH as the control group. After 1 hour, the protein was precipitated by adding 20% trichloroacetic acid (TCA) solution while incubating the samples in an ice bath. After 5 minutes, the samples were centrifuged and the supernatant discarded to remove excess DNPH. This precipitation step was repeated once more after which the protein pellets were re-suspended in 1:1 ethanol/ethyl acetate mixture. The samples were again centrifuged and the supernatant discarded. The protein pellets were re-suspended in guanidine hydrochloride and centrifuged once more. The supernatants were transferred into a 96-well plate (220 µl per sample per well) and absorbance was measured at 360 nm using a Varian Cary 50 Bio UV-Vis spectrophotometer. The protein carbonyl concentration (in nmol/ml) was calculated as follows:

$$Protein\ Carbonyl\ \left(\frac{nmol}{ml}\right) = \left(\frac{A}{0.011}\right) * 2.5$$

Where ‘A’ is the absorbance of the samples.

The protein carbonyl content was finally reported as nmol carbonyl per mg of total protein. Total protein content was quantified by treating the control (HCl) samples with

guanidine hydrochloride solution in the ratio of 1:10 v/v, and then measuring the absorbance at 280 nm. Solutions of bovine serum albumin (BSA) were used as the standards to determine the total protein concentration.

7.5.9.3 Histopathological analysis

The freshly dissected cheek tissues (described above) were spread and pinned down to Sylgard dishes and fixed in 4% paraformaldehyde solution in PBS for 24 hours. Tissues were cryoprotected in 30% sucrose solution for 24 hours followed by embedding in Tissue-Tek O.C.T. compound. Embedded tissues were then cryosectioned at 10 μm thickness, mounted on slides and stained with hematoxylin and eosin (H&E). The sections were observed and imaged using a Nikon Ti-U inverted optical microscope (Melville, NY) attached to a Nikon DS-RI1 12 MP color CCD camera at a magnification of 400x. All the section images were closely analyzed for any visible injury. Following that, ImageJ software was used to measure the thickness of the epithelial layer (outermost tissue layer) for each tissue as any disintegration and/or disruption in the epithelial layer is an important marker of inflammation. About 10-12 thickness measurements were made for each tissue and the mean thickness for each tissue was plotted against the respective OM score given during the study.

7.6 Results

7.6.1 Poly(curcumin) microparticles characterization

The curcumin conjugated PBAE gel synthesis process was optimized by Patil et. al. [275] with respect to the reaction temperature, reaction time, solvent selection and concentration to achieve a high cross-link density, uniform poly(curcumin) film. During poly(curcumin) film synthesis via reaction of CA, PEG(575)DA and TTD, the reaction mixture was kept for 1 hour at room temperature prior to incubation ay 50°C

in order to achieve an extent of reaction before the solvent evaporation process starts at higher temperature with simultaneous progression of the reaction. Solvent evaporation is an important phenomenon in this synthesis as we want to achieve a significant crosslink density which would be possible with gradual loss of reaction medium resulting in increased concentration with time giving higher probability of the intermolecular reaction. Washing of poly(curcumin) films was an important intermediate step in order to remove any unreacted monomers and other un-crosslinked chains that could unpredictably impact the physical and chemical properties of the polymers. Wash supernatants were analyzed using UV-Vis to quantify the loss of curcumin and/or its acrylates from the polymers. Measurement of mass loss of the polymer films and UV-Vis analysis of the supernatants post washing confirmed that CA, PEGDA and TTD were lost in almost the same ratio as the starting stoichiometry (data not shown).

The cryogenic milling process to obtain poly(curcumin) microparticles was also optimized with respect to milling time (10 min), sample loading (2 g), milling speed (15 cps) and magnesium stearate content (1% w/w) to obtain consistent particle size distribution irrespective of the polymer formulation. Various poly(curcumin) microparticle formulations were suspended in DI water and analyzed for their particle size using a Shimadzu SALD-7101 laser diffraction particle size analyzer with a 375 nm UV laser source. Figure 7.1 shows the particle size distribution of the C60, C70 and C90 poly(curcumin) microparticles measured after 2 minutes bath sonication. All three groups show similar particle size distributions with average particle diameters of 20.7±4.3, 20.8±2.7 and 22.7±0.28 μm respectively.

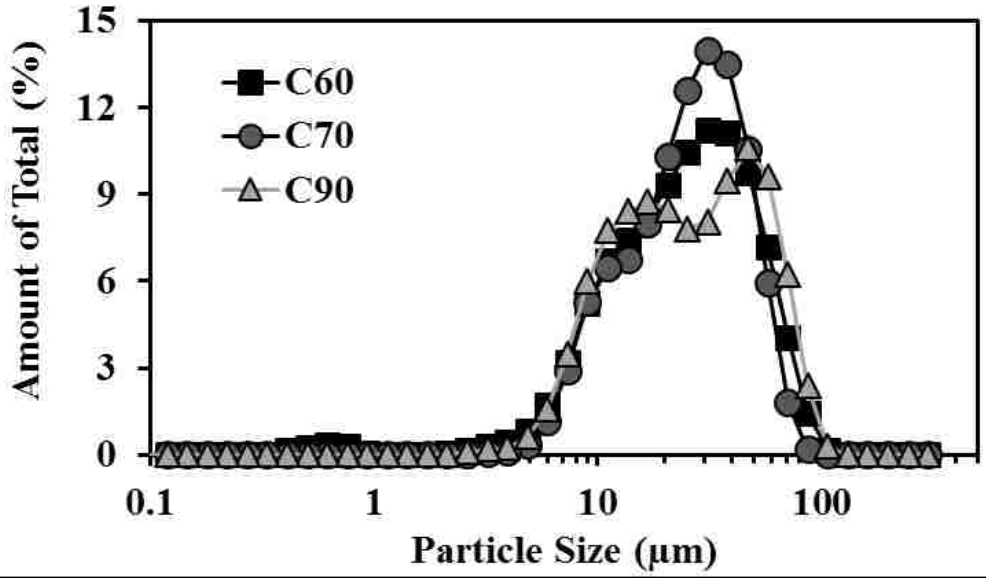

Figure 7.1 Particle size analysis of the poly(curcumin) microparticles with variable CA to PEGDA molar ratios.
For analysis, particles were suspended in DI water and ultrasonicated for 2 minutes. Variable CA to PEGDA molar ratios (60, 70 and 90%) did not affect the particle size with an average size in the range of 22.5 µm to 25.0 µm.

7.6.2 Poly(curcumin) powder hydrolytic degradation and curcumin release profile

Three poly(curcumin) microparticle formulations, C60, C70 and C90 were degraded under physiological condition to study the impact of the polymer composition (i.e. CA to PEGDA ratio) on the release profile of curcumin. The PBS was supplemented with 0.1% SDS in order to ensure the solubility of the released hydrophobic curcumin. Figure 7.2 (A) shows the cumulative curcumin release profiles versus time for the three formulations. All the formulations analyzed for curcumin release due to PβAE ester hydrolysis showed steady and uniform release. It was observed that C60 poly(curcumin) microparticles showed rapid release of curcumin within 12 hours while C70 took 15 hours and C90 took 24 hours to completely hydrolyze and release curcumin. Analysis of the degradation samples using HPLC confirmed the presence of pure curcumin post hydrolysis as shown in figure 7.3, where peaks eluting from the

microparticle degradation coincide with those of a curcumin standard at 7.3, 7.7 and 8.1 minutes.

7.6.3 Antioxidant activity of the poly (curcumin) powder released products

The TEAC assay was employed to confirm and quantify the antioxidant capacity of released curcumin for the three aforementioned formulations at every time point. As can be seen in figure 7.2(B), the cumulatively trolox concentrations over time for each formulation follow the release profiles of curcumin discussed above. A cumulative equivalent trolox concentrations of 21.2, 23.3 and 14.2 µM at 12, 15 or 24 hours for C60, C70 and C90 respectively was calculated showing the presence of active degradation products in the supernatants (Figure 7.2 (B)).

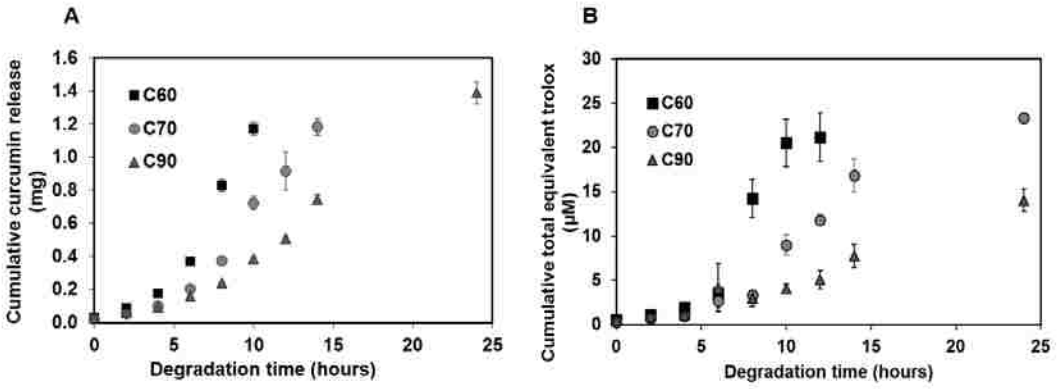

Figure 7.2 Degradation profile of poly(curcumin) microparticles
(A) Curcumin release by hydrolytic degradation of poly(curcumin) microparticles. Sustained release of curcumin over 10, 14, and 24 hours was observed for C60, C70 and C90, respectively, clearly showed a direct relationship between polymer hydrophobicity and hydrolytic degradation. (B) Anti-oxidant activity profile of released curcumin using TEAC assay. Plot represents the equivalent concentration of trolox versus time, confirming retention of the antioxidant activity of the released curcumin. (N=3, error bars are ± std. dev.)

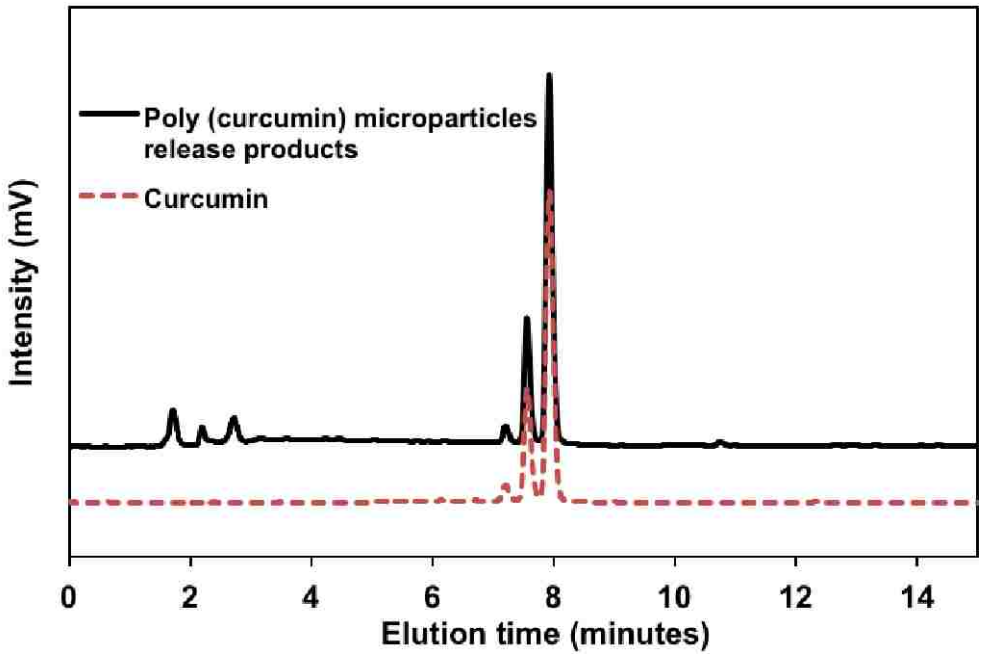

Figure 7.3 HPLC analysis of the products from degradation of poly(curcumin) microparticles collected at 26 hours.
Peaks identical to a free curcumin standard at 7.21, 7.58 and 8.00 mins were observed for degradation products as well, confirming the release of pure curcumin after polymer degradation.

7.6.4 Tissue adhesion studies with porcine buccal tissue

Poly(curcumin) microparticle adhesion properties towards porcine buccal tissue were analyzed in Bluegrass Advanced Materials LLC. laboratory in order to sort out formulation with best adhesive nature based on the CA v/s PEG(575)DA molar ratio and stoichiometric ratios (RTAAP). After analyzing the pictures post tissue-drip experiment with the help of visual ranking obtained from random subjects, it was inferred that C70 microparticles with RTAAP of 1.0 were best amongst other in adhesive properties. The methods with detailed results and discussion is not included in this document.

7.6.5 Dose dependent NHDF cytotoxicity (In vitro)

NHDF were treated with various concentrations of poly(curcumin) microparticles (C70, RTAAP 1.0) and free curcumin at equivalent curcumin concentrations for 24 hours to compare and quantify their relative cytotoxicity. Figure 7.4 shows the cytotoxicity profile of poly(curcumin) microparticles and free curcumin versus the equivalent curcumin concentrations. A sigmoidal curve fit (using SigmaPlot version 12.0) to the dose-dependent viability gave a TC_{50} value of about 12 µg/ml for curcumin and 99 µg/ml for poly(curcumin) microparticles.

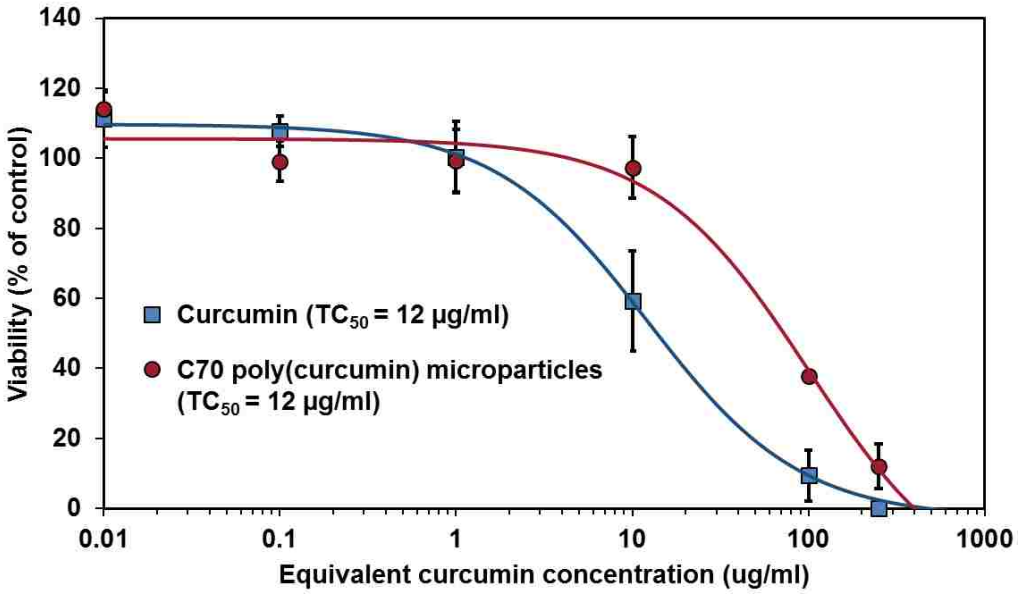

Figure 7.4 Dose dependent cytotoxicity of free curcumin and poly(curcumin) microparticles towards normal human dermal fibroblasts (NHDF) after 24 hours of exposure.
Cell viability was determined using Calcein AM red-orange cell-permeant fluorescent dye with excitation/emission wavelength of 540/590 nm. Poly(curcumin) microparticles resulted higher viability than free curcumin at corresponding same equivalent curcumin concentrations, demonstrating safer nature of the drug conjugated polymer system than free drug. N=5, error bars are ± std. dev.

7.6.6 Protection against H_2O_2 induced injury (*In vitro*)

Based on the results of the cytotoxicity assay above, non-toxic equivalent curcumin concentrations of 1 and 5 µg/ml were selected to ensure that the inherent toxicity of the

particles and free curcumin does not interfere with the oxidative injury assay. This was confirmed via lack of cytotoxicity observed in the control groups treated with only poly(curcumin) microparticles and free curcumin for 24 and 36-hour exposure but without oxidative injury (Figure 7). NHDF cells, when treated simultaneously with 0.5 mM H_2O_2 and poly(curcumin) microparticles at 1 and 5 µg/ml equivalent curcumin concentrations, showed significantly higher viability of 27.0±7.7% and 60.5±17.2% respectively versus only 1.7±0.3% and 21.5±5.9% for cells treated with free curcumin, after 24 hours of exposure (Figure 7.5). For the second regimen wherein the antioxidant treatment (poly(curcumin) and free curcumin) was started 12 hours prior to the H_2O_2 exposure for 12 hours, cell viability increased from 57.3 ± 3.6% (unprotected control group) to 97.6 ± 4.8% and 112.3 ± 4.5% for poly(curcumin) microparticles at 1 and 5 µg/ml respectively. In contrast, an insignificant increase in viability was observed with free curcumin of 59.9 ± 2.3% and 68 ± 4.0% at 1 and 5 µg/ml respectively. In the third regimen when the H_2O_2 exposure was extended to 24 hours post 12-hour pre-treatment with the antioxidants, poly(curcumin) again increased viability to 54.5 ± 9.6% and 70.6 ± 4.0% at 1 and 5 µg/ml respectively. On the other hand, curcumin at the same concentrations increased viability to a meager 10.2 ± 2.9% and 24.6 ± 3.1% respectively.

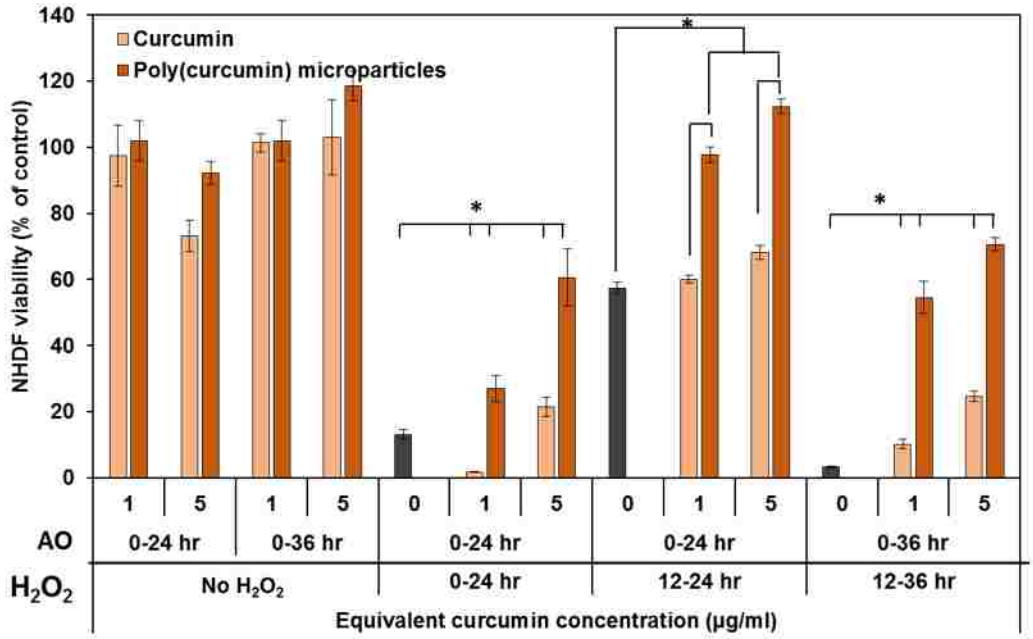

Figure 7.5 NHDF viability analyzed after exposure to poly(curcumin) microparticles/free curcumin and H_2O_2 to show protection against oxidative injury.

The x-axis from top to bottom shows 1) the equivalent curcumin concentrations (µg/ml), 2) the timescale of antioxidant (AO) (Poly(curcumin) microparticles or free curcumin) exposure, and 3) timescale of 0.5 mM H_2O_2 exposure. Poly(curcumin) controls at both the concentrations did not show any toxicity after 24 and 36-hour exposure. Similar observations were made with free curcumin except 24-hour of 5 µg/ml showed 25% cell death. 12-hour AO pre-treatment resulted in higher cell viability than AO + H_2O_2 simultaneous treatment. For all the different treatment schemes, poly(curcumin) microparticles showed superior protection than free curcumin with H_2O_2 induced OS. N=5, error bars are ±Std. dev.; **'*'** *represents statistically significant difference between the treatment groups with $p<0.050$.*

7.6.7 Pre-clinical study in a Hamster model of OM

The efficacy and safety of poly(curcumin) microparticles locally delivered to the cheek pouches was evaluated towards the prevention and treatment of OM in a hamster model. The control group without OM injury treated with DI water (NOC) or poly(curcumin) microparticles (NOT) did not show any sign of vasodilation or pouch erosion giving a score of 0 on the scale of 0-5 on day 11 (0: no injury, 5: complete ulceration of the pouch mucosa). The animal group with OM injury but without microparticle treatment (OMC) on day 11 showed erythema and swelling surrounding the scratched area giving

a score of 3.5 ± 1.8. On the contrary, the group with OM injury and treated with poly(curcumin) (OMT) scored 0.5 ± 0.5 on day 11.

7.6.7.1 Protein carbonyl content of cheek tissue

The ability of the poly(curcumin) microparticle treatment to inhibit protein oxidation in the tissues was analyzed using the DNPH based protein carbonyl assay. Protein oxidation or indirectly carbonyl content is considered to be a major marker of oxidative stress in tissues. According to the figure 7.6, tissues from the NOC and NOT groups showed total protein carbonyl content of 0.4 ± 0.3 and 1.0 ± 0.2 nM carbonyls/mg of protein. Tissues from the OMC group showed significantly higher level of protein carbonyl at 3.9 ± 2.8 nM carbonyl/mg of protein. Interestingly, the OMT tissues showed a significant decrease in the carbonyl content to 2.0 ± 0.8 nM carbonyl/mg of protein.

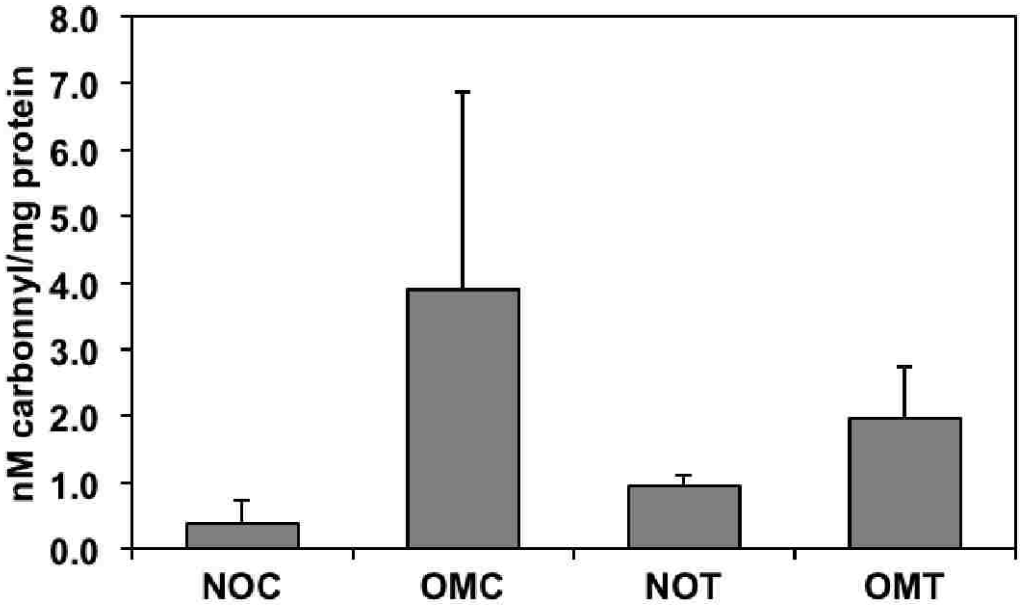

Figure 7.6 Protein carbonyl content in hamster cheek tissues.
Carbonyl content was calculated by reaction of carbonyls with DNPH followed by UV-Vis absorption analysis of reaction products at 360 nm. Carbonyl content in OMC was 8 times higher than non-treated controls (NOC) while with the injury group treated with poly(curcumin) microparticles (OMT) showed a significant decrease (half of OMC or 4 times that of NOC). NOT also showed some increase in carbonyl content probably due to metabolic signaling in tissues upon administration of a foreign substance, but was lower than both the injury groups. N=3, error bars are ± SEM.

7.6.7.2 Histopathological analysis of cheek pouch tissues and effect on epithelial layer thickness post OM injury

The epithelial layer thickness of the hamster cheek pouch was analyzed after OM induced injury (OMC) and compared with the hamsters treated with poly(curcumin) post OM injury. Figure 7.7 shows the histology images of cross-sections of cheek tissues corresponding to NOC, NOT, OMC and OMT. For the NOC and NOT groups, tissue from only one animal per group was analyzed as the remaining tissues were used for the biomarker assays. For the OMC and OMT groups, tissues from at least 2 animals per group were analyzed. ImageJ analysis determined the average epithelial layer thickness of NOC and NOT tissues to be 35.9 ± 5.3 and 45.2 ± 3.2 µm respectively. Figures 7.7 and 7.8 shows the disintegration of the epithelial layer in the OMC group tissues, with an average thickness of 16.1 ± 10.2 µm and 30.0 ± 8.6 µm for OMC I and OMC II respectively. The OMT tissues gave an average epithelial layer thickness of 35.7 ± 4.0 and 26.3 ± 6.4 µm for OMT I and OMT II respectively.

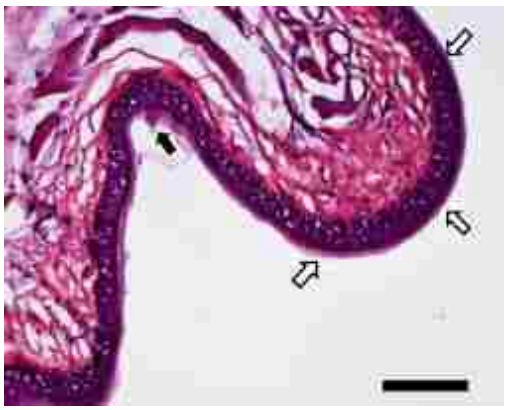

NOC

NOT

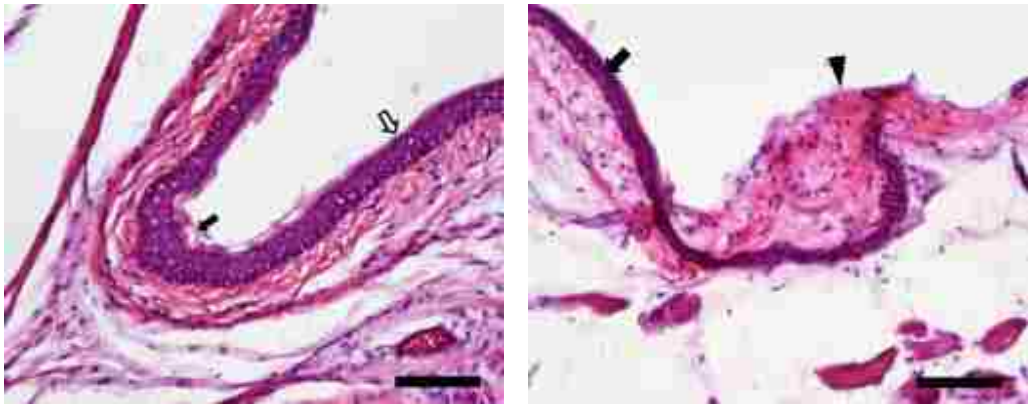

OMC I **OMC II**

OMT I **OMT II**

Figure 7.7 Histopathological sections of hamster left cheek pouches.
Optical microscopy images of cheek tissue sections stained with H&E taken at 200x magnification. NOC: No OM controls, OMC: Oral mucositis controls, NOT: No OM treatment, OMT: Oral mucositis treated with C70 microparticles. Dark arrows depict partially damaged or thinning layer with a disintegrating corneal layer of oral mucosa. NOC group shows completely intact epithelium while NOT histoimage is folded and shows very slight corneal disintegration. OMC group images shows instances of both partial disintegration and completely damaged epithelium. OMT group shows either intact or only partially disintegrated epithelium. Scale bars: 100 µm.

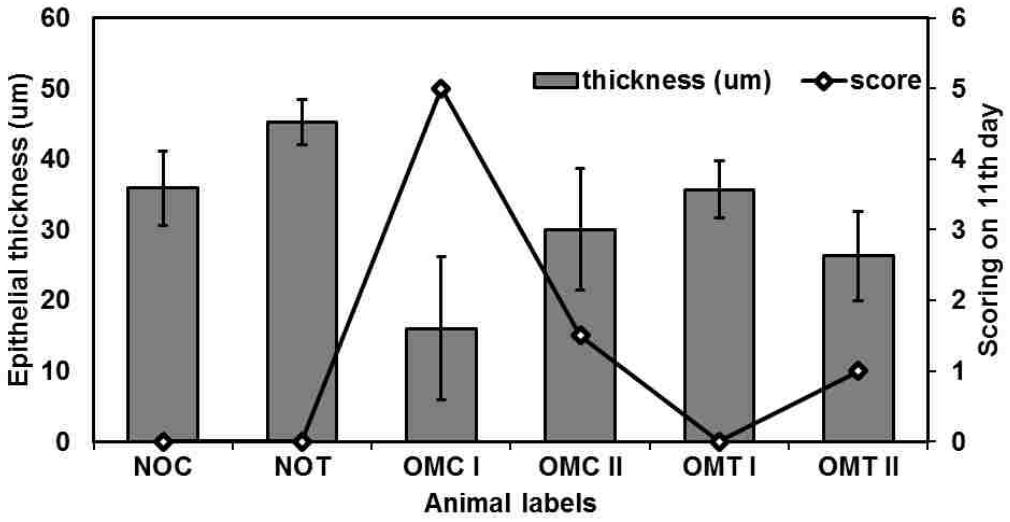

Figure 7.8 Epithelial layer thickness with corresponding animal scoring on day 11. *Poly(curcumin) treated control without injury (NOT) showed an increase in thickness as compared to NOC indicating epithelium proliferation. OMT stained tissue showed an average higher thickness as compared to OMC samples indicating protection from inflammation or healing of the inflammation. Epithelial layer thickness also complies with the visual scoring for each tissue, i.e. higher the inflammation scoring, lesser the thickness. Epithelial thickness was measured using ImageJ software. The bars represent the average thickness measurements of at least 10 different locations per stained tissue section. (Error bars: std. dev.)*

7.7 Discussion

A recent human trial showed significantly delayed the onset and reduced severity of OM after continuous turmeric (a source of curcumin) rinses without any added side effects [276]. As the development of OM has been linked to the presence of oxidative stress, the therapeutic significance of curcumin towards the treatment of this uncomfortable, painful and currently unmanageable OM condition could be clearly identified [277]. It was shown that slight increment of ROS production during cancer therapies would result in activation of NF-kB. This would lead to the release of tissue-damaging cytokines, which in turn again increase ROS production [278]. This results in a cascading cell apoptosis cycle, inhibiting oral epithelial cell proliferation, consequently resulting in the formation of ulcers. Curcumin carrying both anti-oxidant

and anti-inflammatory properties inhibits NF-kB, scavenges excess free radicals and hence overall halts the cell apoptotic process, a possible prevention to the incidence of OM. But its structural properties associated with poor bioavailability, rapid 1st pass metabolism due to its poor aqueous solubility and structural stability would require higher and frequent dosage quantities for OM treatment [279]. But increased dosage still may not be effective due to aqueous solubility limitations. Converting the polyphenolic antioxidant, curcumin into a crosslinked biodegradable PβAE polymer matrix (poly(curcumin)) via Michael addition structurally protects the curcumin from premature degradation, thus preserving its activity until released [178, 280]. Poly(curcumin) synthesized via a single-step reaction between CA, PEGDA and TTD releases curcumin in its original structural form via hydrolysis of the ester bond present in the polymer backbone. In addition to protecting a useful drug, the polymerization process also enables controlled and sustained release of curcumin for extended time. Since these polymers undergo hydrolytic degradation, it is logical that the hydrophobicity of the polymer network would govern the rate of polymer degradation, and hence the rate of drug release [281, 282]. Our goal was to identify formulations that release curcumin continuously for 12 to 24 hours in a steady and uniform fashion. This was readily achieved by varying the ratio of CA (hydrophobic) to PEGDA (hydrophilic) during polymer synthesis. Films with different ratios of CA to PEGDA with respect to a total number of acrylate groups were synthesized. For example, formulation C70 would have 70% of the acrylate groups contributed by CA, while the remaining 30% contributed by PEGDA. Cryogenic milling was chosen to micronize the poly(curcumin) films for two primary reasons: 1) to embrittle the polymer for effective micronization, and 2) to prevent heat-induced degradation of the polymer. Additionally, magnesium stearate, a widely used pharmaceutical excipient [283, 284], was added as

a dry lubricant to reduce clumping. Cryogenic milling of the C60, C70 and C90 formulations yielded microparticles with an average diameter of about 25 ± 4, 23 ± 3 and 22 ± 1 μm respectively, implying that the polymer composition had minimal, if any, effect on the milling process and particle size. Micronization of the bulk PβAE polymer films was an important step for the intended application. Formulating into microparticles followed by suspension in a mucoadhesive solution would allow ease in local delivery through oral mouth rinse. It would also allow higher mucosal surface coverage during rinses. Particulate morphology over bulk would minimize the incidence of diffusion based curcumin release but largely hydrolytic degradation based drug release.

Degrading the poly(curcumin) microparticles under simulated physiological conditions showed a CA loading dependent release profile of curcumin. The polymer formulation synthesized with the highest CA amount, C90, degraded the slowest in 24 hours, presumably because of the higher hydrophobicity from the higher curcumin content. The formulation with lower CA amount, C60, with relatively lower curcumin content, completely degraded within 12 hours due to faster hydrolysis. HPLC analysis of the degradation products detected the original curcumin confirming that the ester bond hydrolysis occurring adjacent to curcumin molecule within the polymer does release the pure polyphenol. The ability of tunable, sustained release of curcumin from the poly(curcumin) microparticles enables development of clinically relevant antioxidant delivery formulations. This is because longer release would reduce the dosage and treatment frequency thereby giving minimum possible treatment interference to the patients undergoing life-saving cancer treatments. Therapeutic application of curcumin has been limited with *in vivo* trials because of its rapid metabolism. It has been shown that increasing the amount of dosage has not improved total absorbed because of

solubility limitation. This restricts the percent bioavailability of curcumin irrespective of the dosage amounts [285]. Steady curcumin release with no major burst effect would alleviate the solubility limitation of the highly hydrophobic drug and minimize the overall systemic metabolism thereby giving an opportunity to utilize the major part of the release towards OS suppression. It was important to analyze the antioxidant activity of the poly(curcumin degradation products as that would decide the efficacy of the system towards core function of serving as an antioxidant throughout the release. Antioxidant activity was determined by analyzing the potential of degradation products to scavenge the $ABTS^{\bullet-}$ radical and reported as equivalent trolox concentration, a widely used standard for such assays [162, 286]. The continuous increase in equivalent trolox amount through the degradation time span confirmed the presence of active compounds capable of suppressing OS. This indirectly implies the release of active curcumin at all times and also proves the concept theory of preserving the structural integrity of the labile molecule in the polymer matrix and protection from premature deactivation prior to release.

The C70 poly(curcumin) microparticles showed dose dependent toxicity on human dermal fibroblast (NHDF), with a TC_{50} value of 227 µg/ml of suspended microparticles (99 µg/ml of equivalent curcumin dose) against TC_{50} of only 12 µg/ml for pure curcumin. Two key observations can be drawn from the more than 8-fold higher TC_{50} values of the poly(curcumin) microparticles compared to pure curcumin: (i) within appropriate dosage limits, the degradation products from the polymer backbone are non-toxic towards fibroblasts, and (ii) the slow release of small doses of curcumin upon degradation of the polymer is less cytotoxic than the traditional bolus delivery method of free curcumin. More importantly, sustained release of active curcumin actually improves protection of cells against oxidative injury. As shown in figure 7.5, in the case

of all three treatment regimens, cells treated with poly(curcumin) followed by H_2O_2 exposure show significantly higher viability than just those treated with free curcumin. In particular, 12-hour pretreatment with free curcumin shows minimal to no reduction in cell death after H_2O_2 injury, while pretreatment with poly(curcumin) microparticles had a significantly higher number of viable cells. Delivery of curcumin from polymer microparticles is not only effective in suppressing oxidative stress-related injury but, in fact, is more efficacious and less toxic than free curcumin. As explained earlier, one of the key causes of the onset and incidence of the OM condition arises due to the development of oxidative stress conditions, which is excess production of free radicals. The *in vitro* results if translated towards OM management would imply both (i) prophylactic action against oxidative stress during chemo and radiation therapy as well as (ii) treatment of OM by suppressing OS via simultaneous treatment during the developmental stage of the oral injury.

The viable or non-destructive nature of the poly(curcumin) microparticles were further tested *in vivo* with a hamster model. No increase in protein carbonyl content, intactness of epithelium observed with histopathological analysis for only poly(curcumin) microparticle treated control groups (NOT) demonstrated the safe nature of microparticles *in vivo* with no side effects or inflammation. Adding to this, higher epithelium thickness of NOT groups (45.2 µm) as compared to NOC (no OM, no treatment) control groups (35.87 µm) demonstrates the epithelium proliferation in the presence of curcumin (figures 7.7 and 7.8). Though NOT showed some increase in carbonyl content with reference to NOC group but this could be probably due to metabolic signaling in tissues upon administration of a foreign substance, but was significantly lower than both the injury groups. The Effect of poly(curcumin) on the hamster pouch with induced OM condition though did not show full protection from

the injury but showed a significant difference against inflammation with an average OM score of 0.5 on day 11, lower total protein carbonyl content and more intact epithelium when compared with the OM injury (OMC) control group with an average score of 3.5 (Figures 7.6, 7.7 and 7.8). The results from the preliminary *in vivo* study are not very concrete with a clear conclusion on the efficacy of the poly(curcumin) microparticles towards OM prevention and treatment. The underlying cause of variability might be arising due to the presence of human error during needle scratching of hamster pouch and high death rate due to adverse systemic effects arising from the strong 5-FU administration. In spite of these experimental irregularities, we did see results indicating the protective effect of slow and steady releasing microparticles developed in the form of oral rinse suspension for better patient compliance.

7.8 Conclusions

Curcumin conjugated PβAE gel microparticles (poly(curcumin) microparticles) were synthesized for the application of treatment and prevention of oral mucositis. These microparticles obtained by cryomilling PβAE gel films showed the uniform release of active curcumin with no burst effect. PEGDA used as a co-monomer to CA during gel film synthesis helped in tuning the curcumin release timescale ranging from 12 to 24 hours. The C70 poly(curcumin) microparticle system was selected for further *in vitro* and *in vivo* application after testing various formulations for best mucoadhesive properties. Protection against H_2O_2-induced oxidative stress was seen with both simultaneous and pre-treatment of poly(curcumin) demonstrating preventive as well as treating potential of the microparticle system. Both i*n vivo* and *in vitro* studies demonstrated the safe and viable nature of the product. *In vivo* administration of poly(curcumin) through oral rinse to OM induced hamsters showed decreased protein carbonyl content, intact epithelium and less severity of ulcers observed visually in

comparison to non-treated OM controls. The microparticle containing mouth rinse suspension would allow local and sustained delivery of antioxidant curcumin, increase overall bioavailability and reduced dosage frequency thereby minimizing the interruptions during cancer therapies. These synthesized poly(curcumin) microparticles can serve as a treatment superior to just barrier rinse or free curcumin rinse towards the management of OM.

8 SYNTHESIS AND CHARACTERIZATION OF RESVERATROL CONJUGATED PβAE GEL MICROPARTICLES FOR PROTECTION FROM UV MEDIATED OXIDATIVE STRESS

Note: The information in this chapter is the intellectual property of Bluegrass Advanced Materials LLC., not to be disclosed in public

Abstract

As induction of oxidative stress through UV radiation from sunlight is considered to be one of the reasons for skin disorders, including sunburn, skin cancer and premature skin aging, incorporation of resveratrol with its antioxidant properties could serve as a protective strategy in topical application products. In order to consider this as a viable approach for daily use, it is required for the UV-protective compound to act against radiation-induced injury for at least 12-14 hours. However, the instability of resveratrol under UV exposure results in its rapid deactivation and apparent depletion without performing the intended function. A proposed solution to overcome these limitations is to structurally protect the resveratrol via the PβAE conjugation approach and subsequently release the bioactive compound uniformly for a longer duration of time. To implement this idea, resveratrol was covalently conjugated into hydrolytically degradable PβAE gels via reaction of acrylate functionalized resveratrol (RTA) with a multifunctional amine (TTD). These gels were further cryomilled into microparticles for easier fusion into cosmetic or dermatological products. Incorporation of PEGDA as a co-monomer allowed tunable degradation of these gels (6-8 hours) and control over the fast reaction kinetics of RTA with TTD. These microparticles also showed protection against H_2O_2-induced oxidative stress in human dermal fibroblasts equivalent to free resveratrol. Therefore, these microparticle systems have the potential

to be considered for dermal application products but a more uniformly distributed and longer resveratrol release profile (10-12 hours) is desired for intended action.

8.1 Introduction

With the incidence of skin cancer, premature skin aging, and topical erythema the damaging effects of the UV part of solar radiation on skin are generally well known. [287-289]. UV radiation is broken into three distinct bands, UVA (315-400 nm), UVB (280-315 nm) and UVC (100-280 nm). While UVC is blocked by the atmospheric ozone layer, we get sunlight radiation composed of about 95% UVA and roughly 5% as UVB [290]. Both types of UV radiation serve as contributing factors to skin aging and development of skin cancers. UVA penetrates to the dermis, increases reactive oxygen species production, indirectly inducing DNA damage followed by mutagenesis [291]. On the other hand, UVB is known to be the cause of non-melanoma cancer, is absorbed at the epidermis level of the skin and results in direct DNA damage [292, 293].

While induction of oxidative stress is considered to be one of the reasons for skin damage, application of antioxidants is a well-known remedy to suppress oxidative stress and can be a possible solution to remediate UV exposed damage and prevent degenerative biochemical processes [294]. Antioxidant molecules used in cosmetic and dermatological formulations to protect skin from damage and premature aging include, but are not limited to, vitamin E, curcumin, resveratrol, quercetin, and ascorbic acid. In particular, resveratrol has gained a special interest in recent years as an antioxidant and anti-aging compound [295]. Topical application of this antibacterial compound in preventing UV-mediated oxidative and skin damage has been widely studied and has shown promising results [296]. Recent studies have also shown that it has 17 times greater antioxidant capacity than idebenone, an antioxidant widely used in anti-aging

skin products [297]. But one of the greatest technical difficulties for the use of the above antioxidant compounds is their instability under UV leading to molecular isomerization and inactivation [298]. The strong chemical activation energy derived from ultraviolet radiation induces hydrolytic reactions and degrades the antioxidant indiscriminately. This results in exponential loss of the antioxidant without performing the action it was intended to. This reduces the filtering and protection capacity of the cosmetic formulation over time. A reduction of UVB filtering capacity leads to a reduction in SPF of the formulation, and therefore to a higher burn risk. On the hand, the reduced capacity to filter UVA radiation results in a greater risk of adverse chronic effects, which might go unnoticed at initial stages.

A proposed solution to overcome these limitations is to structurally protect the resveratrol until it is made available to protect the skin from injury. This idea was implemented by converting antioxidants into biodegradable poly(beta-amino ester) (PβAE) polymers. Specifically, polyphenolic resveratrol with three alcoholic groups was first converted into its acrylate ester form **(Figure 8.1).** The phenol acrylate (resveratrol triacrylate (RTA)) was then reacted with a primary diamine crosslinker, like 4, 7, 10-Trioxa-1, 13-tridecanediamine (TTD), via the Michael addition to yield crosslinked resveratrol conjugated PβAE (R-PβAE) gels. The hydrophilicity of the polymer, and thus its degradation rate was controlled by including a diacrylate co-monomer like poly(ethylene glycol) diacrylate (PEGDA, MW 575) in desired proportions during the reaction. The gel films were further cryomilled to obtain R-PβAE microparticles. Hydrolytic degradation of these gel microparticles demonstrated resveratrol release in a sustained fashion.

By going through this route, (1) resveratrol was structurally protected from premature degradation compared to encapsulation/complexation technologies; (2) high resveratrol loadings, exceeding 20 wt. % of the polymer were obtained, (3) tunable sustained release durations ranging from 2 to 10 hours, (4) original, active resveratrol was released upon hydrolysis of the polymer.

8.2 Methods

8.2.1 Resveratrol triacrylate (RTA) synthesis (Process developed by Bluegrass Advanced Materials LLC.)

Resveratrol (20 g) dissolved in 160 ml of anhydrous THF was allowed to react with 21.36 ml of acryloyl chloride (molar ratio of 3:1 with respect to resveratrol), which was added to resveratrol-THF solution dropwise (exothermic reaction). Triethylamine (TEA) (36.64 ml) was added to the reaction mixture in the molar ratio of 3:1 w.r.t resveratrol in order to capture released HCl forming TEA-HCl salts. The reaction was allowed to proceed for 2 hours under the nitrogen purge at room temperature in the dark (aluminum foiled). During the reaction, acryloyl chloride reacts with alcoholic groups of resveratrol forming acrylate groups. Post reaction, the mixture in THF was first filtered out to remove TEA-HCl salts and then was subjected to vacuum evaporation to evaporate THF using liquid nitrogen vacuum trap. Following the complete evaporation of THF, the obtained product was re-dissolved in 40 ml of ethyl acetate (EA). As EA and water are immiscible solvents, product dissolved in EA was washed with 0.1 M HCl solution in DI water (1:3 v/v-EA/HCl solution) in order to remove any unreacted TEA in the product. After HCl wash, the product was subjected to base wash using 0.1 M K_2CO_3 solution to remove excess acrylic acid with the same EA/ K_2CO_3 ratio as for EA/HCl wash. Any residual water after the washes was removed by adding magnesium sulfate ($MgSO_4$) until the bubbling stops. The hydrated $MgSO_4$ was removed via

filtration and the EA solution containing RTA was subjected to vacuum drying with liquid nitrogen trap under stirring conditions to remove EA and get a semi-viscous RTA product. RTA was stored at -80^{o}C before further use. All solvents used were anhydrous. The final product was run through HPLC to identify the nature of the resveratrol acrylate obtained.

Figure 8.1 Reaction scheme of acrylate functionalization of resveratrol to resveratrol triacrylate (RTA) via reaction with acryloyl chloride.
There is a possibility of all three kinds of acrylate; mono, di and tri as shown in the figure. Three different forms of mono and diacrylate will exist depending upon the location of acrylation.

8.2.2 Resveratrol-PEGDA (R- PβAE) film synthesis and microparticles formulation

a. R-PβAE film synthesis (synthesized by Bluegrass Advanced Materials LLC.)

R-PβAE films were synthesized with different molar ratios of RTA (mol. wt. 390.39) v/s PEGDA (mol. wt. 575) as the acrylate monomers. The amine monomer for the Michael addition reaction used was a tetra functional amine; 4, 7, 10-Trioxa-1, 13-tridecanediamine (TTD) (mol. wt. 220 gm/mol). The total acrylate to total amine proton ratio (RTAAP) was kept at 1:1. Films with 20, 40, 60 and 80% RTA (molar ratio w.r.t. total RTA+PEGDA) were prepared. As a sample example, for 80% RTA film (R80-PβAE), 905 mg of RTA was dissolved in 1.88 ml of DCM and vortexed thoroughly.

To the RTA-DCM solution, 500 mg of PEGDA was added and again mixed thoroughly. To this mixture, 479 mg of TTD separately dissolved in 1.88 ml of DCM was added while vortexing and the reaction solution was quickly transferred to an aluminum dish and was kept in an oven for 24 hours at 50^{o} C. After the reaction was completed, a firm thin crosslinked gel film was obtained, which was peeled off the aluminum dish and subjected to acetone wash to remove any unreacted monomers or uncross-linked oligomers. The washing solvent, acetone was removed and replenished every one hour followed by mild mixing in the rotary shaker. After the 4th wash, most of the acetone was removed and the film was lyophilized using freeze-dryer overnight.

b. R-PβAE film micronization

Dry film obtained from Bluegrass Advanced Materials LLC. was weighed out and was cut into small pieces of dimensions less than 0.5x0.5 inch. The pieces were added to the cryomilling tube with 3% wt/wt of magnesium stearate and an impactor was inserted in the tube and closed. The film was subjected to cryomilling with the milling frequency of 15 cps, 2 minutes sample precool, 10 minutes of milling and 2 minutes of post cool setup. After milling, microparticles was allowed to warm up and come to room temperature after which microparticles were collected in a tube for freeze drying to remove any solvent or condensed water. Dried microparticles were stored at -20^{o}C for further characterization (Figure 8.2).

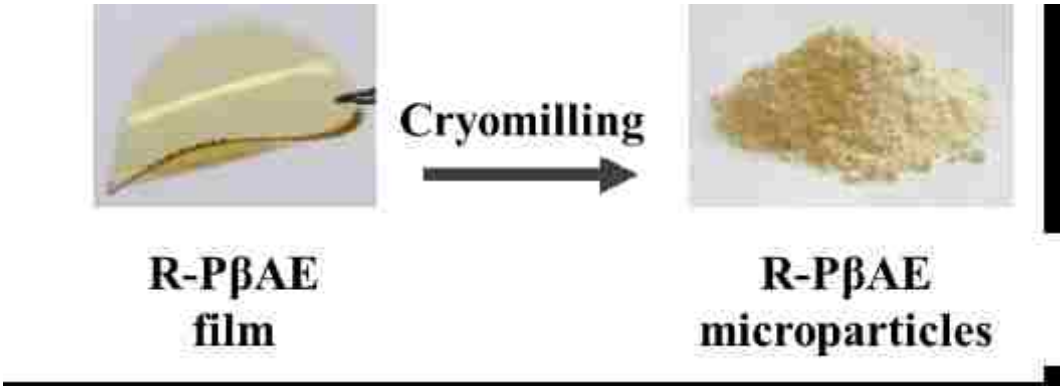

Figure 8.2 Photographic schematic of R- PβAE film to microparticle formation.

8.2.3 R-PβAE microparticle degradation

Degradation was carried out in a dissolution apparatus with a speed of 100 rpm at 37˚C in PBS buffer with 0.1% SDS. All formulations (R20, R40, R60 and R80) were subjected to degradation. The amount of microparticle powder required for degradation studies was calculated such that the final resveratrol concentration was 10 mg/L. A total of 1-liter suspension was prepared for each formulation and the study was carried out in replicates of three. Table 8.1 shows the total mass/liter required for each formulation to get 10 µg/ml of loaded resveratrol.

Table 8.1 R-PβAE microparticles composition and degradation calculations

R-PβAE formulation	% Resveratrol loading	Mass of R-PβAE microparticles/liter for 10 mg/L resveratrol (mg)
R20	4.89	204.50
R40	10.88	91.80
R60	18.40	54.36
R80	28.09	35.60

8.2.4 Dose dependent toxicity and protection against H_2O_2 induced oxidative stress towards normal human dermal fibroblasts (NHDF)

Dose dependent cell toxicity due to resveratrol and R80-PβAE exposure towards normal human dermal fibroblasts (NHDF) was analyzed after 24-hour treatment using Calcein AM red-orange live cell trace assay. Briefly, NHDF were seeded in a 96-wellplate and allowed to grow overnight. The next day, resveratrol/R80-PβAE microparticles were suspended in the Ham's-12 medium at different concentrations. The suspensions were added to the seeded well plate and allowed to incubate for 24 hours at 37º C, 5% CO_2.

Cells were then washed and incubated with 1 µM Calcein AM red-orange for an hour. All the wells were then washed, replenished with fresh medium and the fluorescence of all the groups was measured at 540/590 nm as excitation/emission wavelengths (BioTek Synergy Mx, Gen5 2.0, Winooski, VT plate reader). Fluorescence intensities were used to quantify percent viable cells and compared with different treatment groups.

Inhibition of H_2O_2 induced toxicity was also analyzed using the same live cell tracer with 0 and 12-hour antioxidant pre-exposure followed by 12 or 24 hours of 0.5 mM H_2O_2 exposure. Figure 8.3 shows the treatment sequence for three different resveratrol//R80-PβAE microparticles + H_2O_2 exposure combinations.

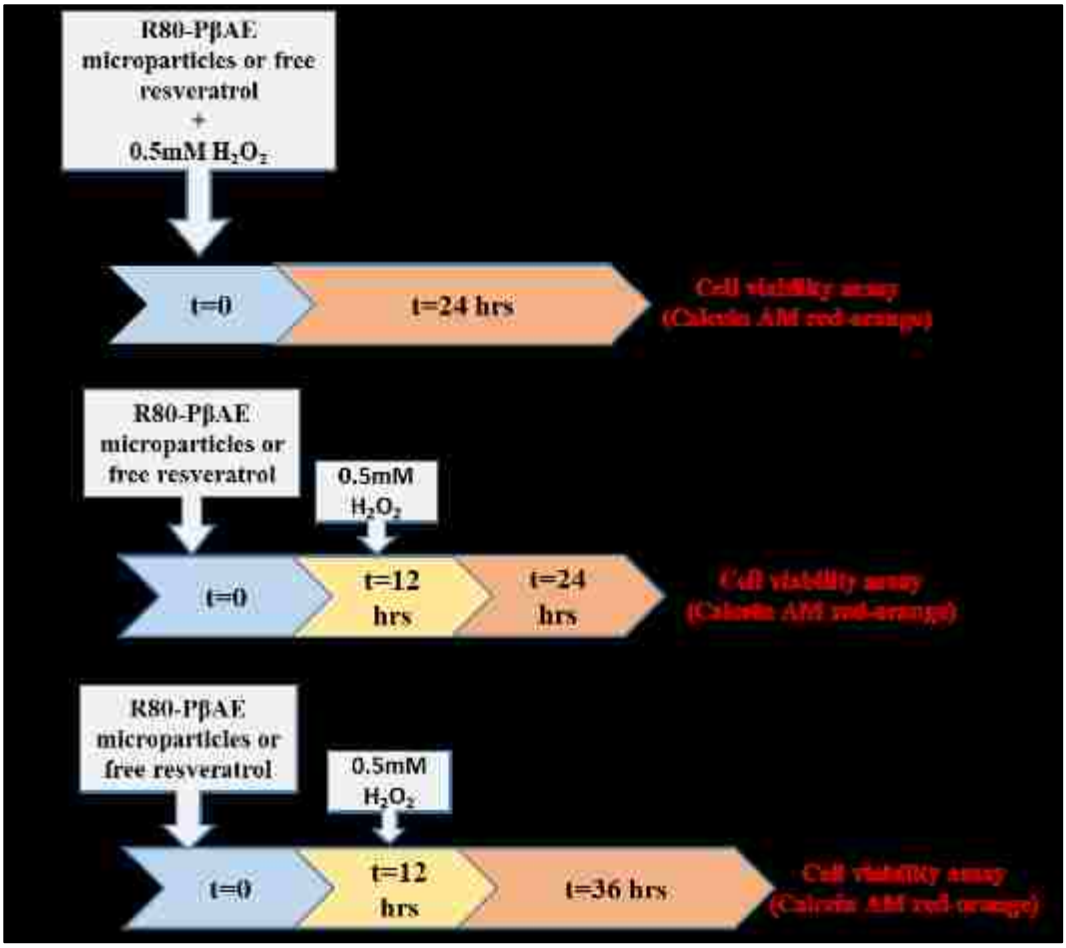

Figure 8.3 Treatment sequence timeline of resveratrol/R80-PβAE microparticles + H_2O_2 exposure to NHDF.
NHDF cells were used as the treatment substrate to analyze the protective effect against H_2O_2 induced oxidative stress.

8.3 Results

8.3.1 Analysis of RTA and R-PβAE microparticles size

HPLC elution of the acrylated product of resveratrol i.e. resveratrol triacrylate (RTA) showed no peak elution coinciding with the free resveratrol residence time (Figure 8.4). This clearly indicated that the final product did not contain any unreacted resveratrol. Three distinct peaks were observed in the elution, with the major peak eluting at 37.7 minutes corresponding to triacrylate. This peak contributed 91% of the total product based on area under the curve calculations. Other two peaks are assumed to be of mono

and diacrylate and there can be three different structural forms of mono and di acrylate depending upon the location of phenol conjugation.

Cryomilling of all different compositions of RTA-PEGDA-TTD conjugated gels gave microparticles in the range of 6-8 µm (data not shown). The amount of magnesium stearate content during cryomilling did not show any effect on the particle size.

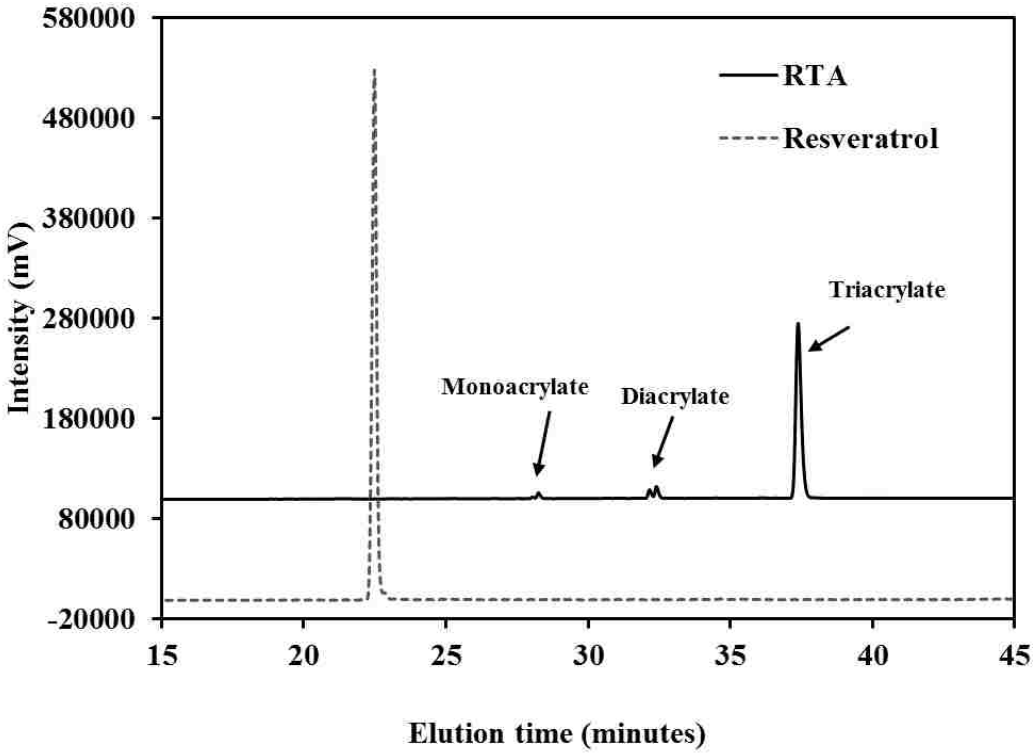

Figure 8.4 HPLC of RTA and resveratrol
Gradient method file of 70% aqueous mobile phase (DI water with 0.1% phosphoric acid) to 30% over 40 minutes against acetonitrile organic phase was used.

8.3.2 Degradation of R-PβAE microparticles and antioxidant activity of the released products

Hydrolytic degradation under physiological conditions (PBS, 37º C) showed a similar release trend with a degradation time varying from 6-8 hours for microparticles of different chemical compositions (Figure 8.5). Performing the TEAC assay on the

degradation products demonstrated sustained antioxidant potential during degradation, reported as equivalent trolox (mM) (Figure 8.6).

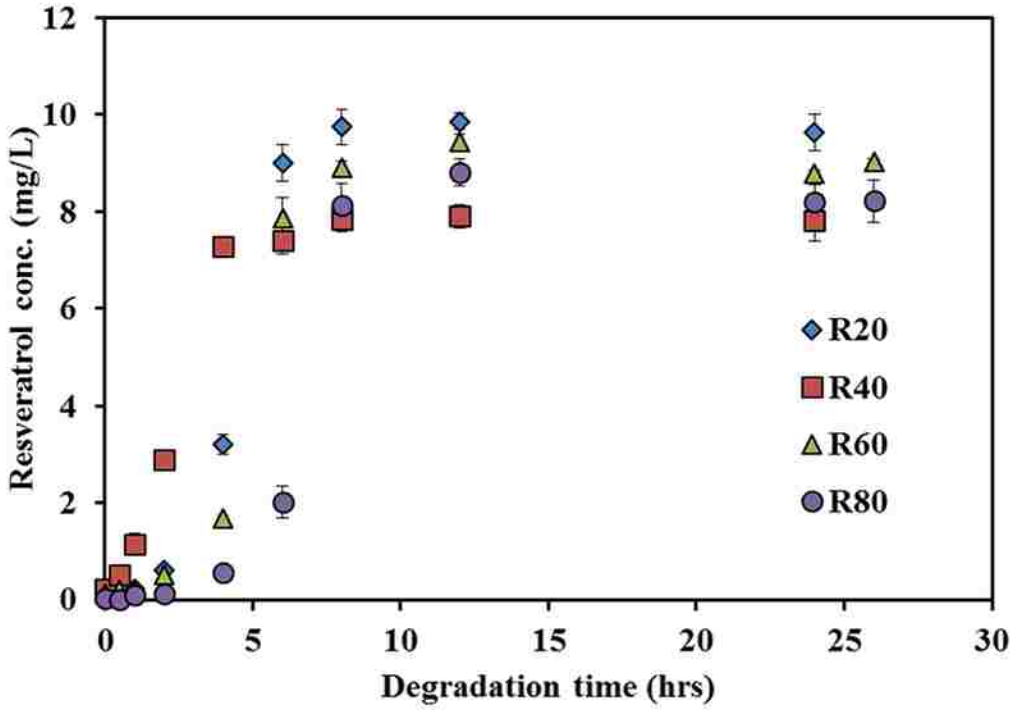

Figure 8.5 Degradation of all R-PβAE microparticles
Microparticles were suspended in PBS buffer with 0.1% SDS under physiological conditions: 37°C, in a dissolution apparatus. N=3, error bars: std. dev.

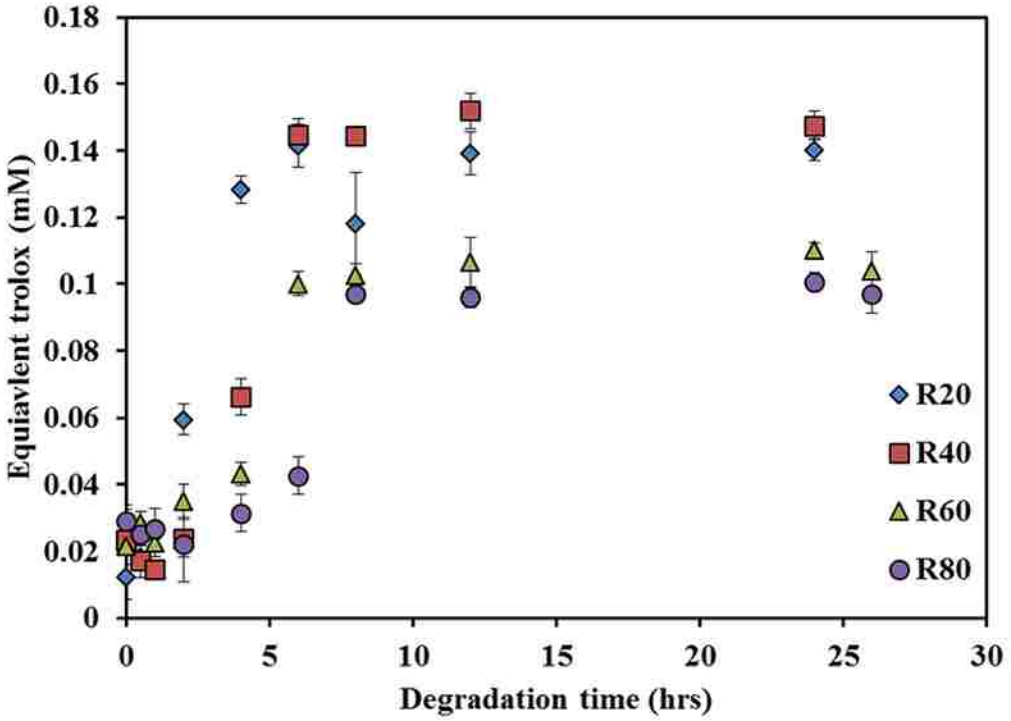

Figure 8.6 Antioxidant activity profile of R-PβAE microparticles
Antioxidant capacity was analyzed using TEAC assay and represented as trolox equivalents in mM. N=3, error bars: std. err.

8.3.3 Dose dependent toxicity and protection against H_2O_2 induced oxidative stress towards normal human dermal fibroblasts (NHDF)

Normal human dermal fibroblasts were exposed to a variable concentration of R80-PβAE microparticles and free resveratrol at similar concentrations for 24 hours. Dose dependent cell viability curve showed more viable nature of R80-PβAEs compared to free resveratrol at similar resveratrol loading (Figure 8.7). While TC_{50} value for free resveratrol exposure was calculated to be 12.3 µg/ml, R80-PβAE microparticles showed lower toxicity with TC_{50} of 52 µg/ml (resveratrol loading).

All three different sequences of resveratrol/R80-PβAE treatment did show significant protection from 0.5 mM H_2O_2 toxicity. R80-PβAE did not show any superior properties than free resveratrol in the form of cell toxicity (Figure 8.8 and 8.9).

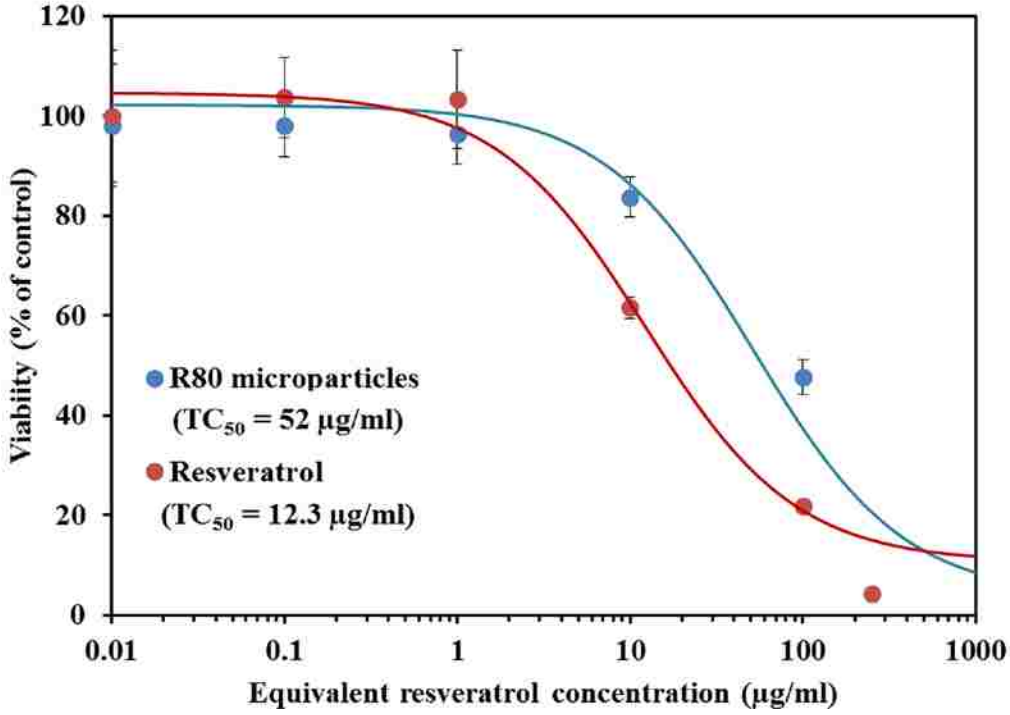

Figure 8.7 Dose dependent NHDF toxicity after 24-hour exposure to resveratrol or R80-PβAE microparticles.
Cell viability was determined using Calcein AM red-orange live cell tracer. TC_{50} values were calculated using 4-parameter sigmoidal curve model. N=5, error bars: std. dev.

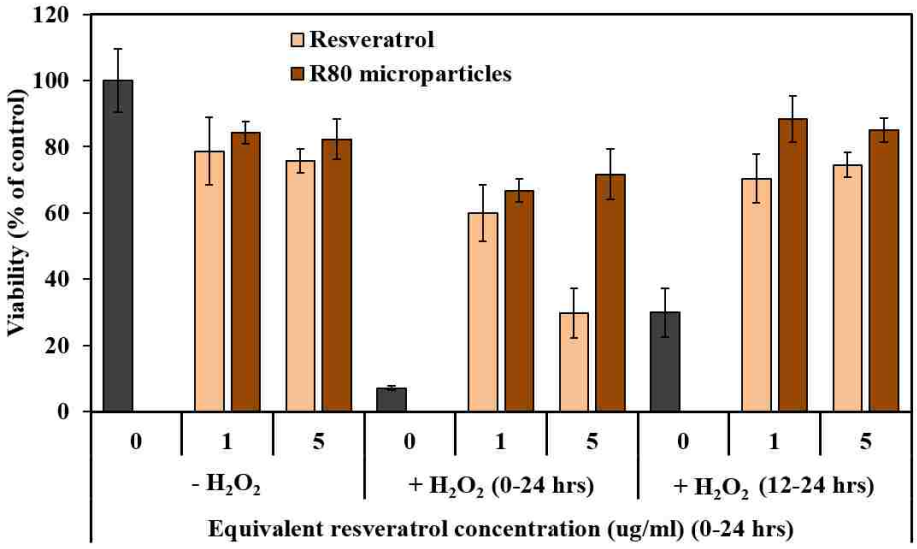

Figure 8.8 Protection against H_2O_2 induced toxicity due to R-PβAE microparticles exposure.
NHDF treated with 0 or 12-hour resveratrol/R80-PβAE pre-treatment were exposed to 0.5mM H_2O_2 for 24 or 12 hours respectively followed by Calcein AM red-orange cell viability assay. N=5, error bars: std. dev.

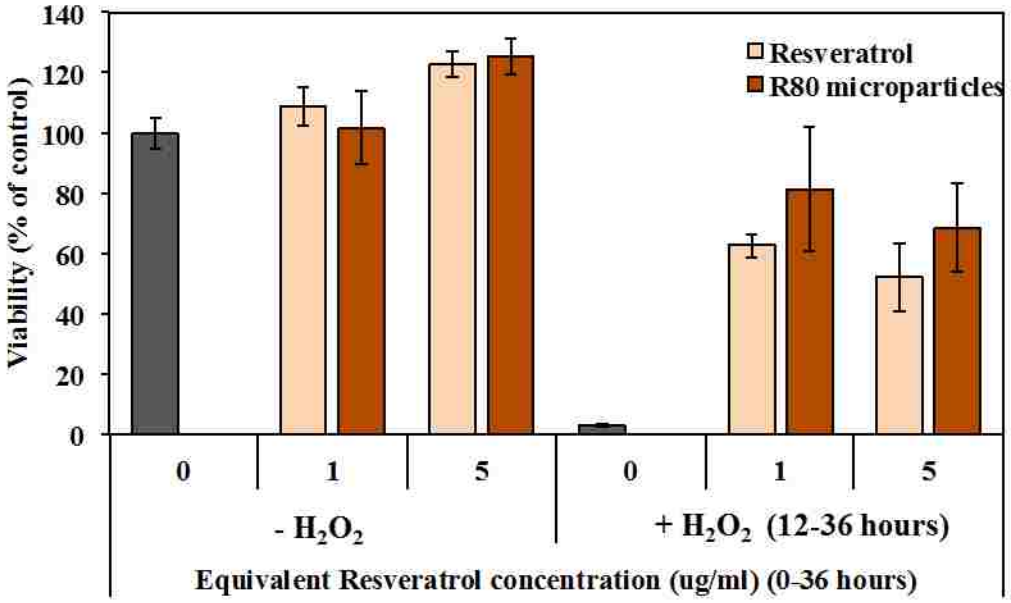

Figure 8.9 Protection against H_2O_2 induced toxicity.
NHDF pre-treated with resveratrol/R80- PβAE for 12 hours were exposed to 0.5mM H_2O_2 for 24 hours followed by Calcein AM red-orange cell viability assay. N=5, error bars: std. dev.

8.4 Comments and future directions

Utilizing the PβAE chemistry for conjugating resveratrol into the PβAE matrix, we were able to formulate prodrug gel microparticles in the range of 6-7 µm. These microparticles did show composition dependent release kinetics, where high PEG content (R20- PβAE) result in faster degradation within 5-6 hours. But resveratrol release from microparticles with the lowest PEG content i.e. R80-PβAE could only be extended to 8 hours. To be considered for a cosmetic application such as for sunblock products, a 10-12 hour release would be desired for sustained protection against UV-induced damage. Antioxidant activity of the degradation products shows the radical scavenging potential for an extended period time showing the release of active resveratrol upon ester cleavage. Also, R80-PβAEs are more viable in nature as compared to free resveratrol and show protection against H_2O_2 induced cellular oxidative stress. But, these systems did not show protective nature superior to free

resveratrol for the different treatment experiments done. This could be because resveratrol itself is a relatively stable antioxidant compared to many others in physiological environments until attacked by free radicals. Therefore, given that total resveratrol administered was same via free resveratrol and through conjugated systems, both showed similar protection against induced cellular oxidative stress. More experiments with different combinations of chemical compositions and experimental design needs to be carried out in order to better understand the protective mechanism of these gel microparticles. One proposed experimental design would be to continuously expose the system to free radicals and then analyze the scavenging potential of resveratrol conjugated PβAEs and its free form.

9 CONCLUSIONS AND FUTURE DIRECTIONS

In this work, PβAE chemistry was explored as a platform to develop antioxidant conjugated crosslinked networks for effective drug delivery. The system was developed for three different polyphenolic antioxidants, which are therapeutically significant but difficult to administer effectively due to their 1) poor aqueous solubility, 2) structurally fragile nature and hence 3) extremely low bioavailability. PβAEs are biodegradable polymer networks hydrolytically degradable through their ester linkages. This characteristic was utilized as a release mechanism for covalently conjugated antioxidants. In the current approach, direct conjugation of antioxidants into PβAE crosslinked networks through their –OH groups served as a method to structurally protect the molecule and release antioxidants in their active form upon hydrolytic degradation. Optimization of reaction and processing parameters allowed us to transform the crosslinked prodrug chemistry into micro or nanogel formulations, creating a more adaptable technology for drug delivery applications.

a. PβAE reaction chemistry under dilute conditions resulted in a self-precipitated antioxidant nanogel suspension, which was amenable to formulate antioxidants quercetin as well as curcumin conjugated system. Use of such synthesis method eliminated the requirement of a surfactant for stabilization, which otherwise becomes a controlling factor towards nanoparticle toxicity. A uniform release profile of functionally active antioxidants, with little to no burst effects further helped in apparent reduction of antioxidant toxicity. These physiochemical properties led to the demonstration of prolonged protection against induced oxidative stress in endothelial cells.

The mechanism of protective action could be through (i) cellular internalization followed by degradation of nanogels or (ii) extracellular degradation followed by diffusion of free antioxidant. The existence of the 1st case would imply high cytoplasmic concentrations of the antioxidants, which would be beneficial for the treatment of acute damage but could also be a cause of local cellular toxicity. Therefore, more insight into the working mechanism is needed to understand drug response in a better manner.

b. Aimed as a treatment solution to neurodegenerative disorders, curcumin-PβAE nanogels further demonstrated their ability to suppress mitochondrial oxidative stress without any mitochondrial specific targeting. Increased safety window of curcumin through nanogel administration was one of the critical factors towards this result, which allowed the administration of curcumin at therapeutic levels in a sustained fashion.

c. The ability of curcumin-PβAE nanogels to mitigate cellular and mitochondrial oxidative damage was further explored with the polychlorinated biphenyls (PCBs). The analysis showed that pre-treatment of endothelial cells with curcumin-PβAE nanogels helped in reducing PCB induced excess ROS production and restoration of otherwise affected mitochondrial respiration. This observation was made with the exposure of both coplanar (PCB 126) and non-coplanar (PCB 153) PCBs.

Although, curcumin-PβAE nanogels act against PCBs irrespective of the different oxidative damage through different activation paths, the mechanism of action needs to be analyzed in detail. Curcumin being a polyphenolic molecule can capture PCBs through pi-pi interaction and inhibit the damaging action or through scavenging of excess ROS/RNS.

Further, nanogel synthesis via the method used in this work can be further explored with other polyphenolic compounds with two or more –OH groups. This will create a universal synthesis approach for antioxidant delivery through nanosystems of high drug loading.

d. Apart from nanogels, the curcumin-PβAE crosslinked system was also formulated into microparticles. Being able to develop the same drug conjugated systems in different size dimensions indicates the adaptable nature of the conjugated PβAE chemistry in drug delivery. Use of PEGDA as a co-monomer in the synthesis process added the ability to control hydrophobicity/hydrophilicity of the networks and hence a degradable system with a tunable release profile. These microparticles also successfully showed *in vitro* protection against induced oxidative stress, superior to free curcumin. In an *in vivo* trial, a daily rinse of the microparticle suspension over 10 days showed indications of reduced severity of oral mucositis (OM) in chemotherapy-induced OM hamsters (5 FU/needle scratch injury induction).

This injury model incorporates a high percent of human error and administration of 5-FU drug results in systemic side effects, which indirectly interferes with OM analysis. Therefore, a better design of experiment with least human error and relatively less lethal injury model, such as γ-radiation, would allow better assessment of curcumin-PβAE microparticles as a potential solution for OM treatment.

e. The antioxidant conjugated PβAE gel microparticle synthesis process was further extended with another anti-inflammatory drug, resveratrol. Acrylate functionalized resveratrol was successfully conjugated into the backbone of the PβAE network and was further cryomilled to obtain microparticles. With the goal of

developing a slow and steady resveratrol releasing system to prevent topical UV-induced oxidative damaged, different polymer compositions were tried and analyzed for their release profile. As such, these microparticle systems showed *in vitro* protection against H_2O_2 but did not show properties superior to free resveratrol.

Although, some control over release kinetics was achieved (6-8 hours of resveratrol release), an optimization and modification in synthesis process is required for longer release profile (10-12 hours). Selection of different co-monomers or reacting amine could lead to improved physicochemical properties of the gel matrix and help attain better control over the release profile. Also, a more robust design of experiment to demonstrate the UV-protection potential is needed. A proposed idea is to continuously expose microparticle loaded systems with free radicals and study the scavenging potential of UV light and compare with free resveratrol.

APPENDIX

Based on the research article

> Prachi Gupta, Caroline Lacerda, Vinod Patil, Dipti Biswal, Paritosh Wattamwar, J. Zach Hilt and Thomas D. Dziubla, 'Degradation of poly(β-amino ester) hydrogels in alcohols through transesterification: A method to conjugate drugs to hydrogel matrices. *(to be submitted)*

Abstract

Poly(β amino ester) polymers have received growing attention in the literature, owing to their ease of synthesis, versatile co-monomer selection, and highly tunable degradation kinetics. As such, they have extensive potential in many biomedical applications. In this work, it is demonstrated for the first time that PβAE polymers containing primary and secondary amine groups can undergo degradation by primary alcohols through a transesterification process. While this work demonstrates an important aspect of solvent compatibility limitation to these networks, it also represents an interesting, simple mechanism for post synthesis drug incorporation, with riboflavin conjugation being demonstrated as a model compound.

Introduction

Poly(beta-amino ester) (PβAE) hydrogels are hydrolytically degradable systems due to the presence of β-amino ester linkages. This is one of the central features for their applicability in biomedical applications such as gene and drug delivery and tissue engineering considering it as a biodegradable system [299, 300]. Synthesized via Michael addition reaction of an acrylate molecule with a primary or secondary amine, the degradation rate of these polymers is considered to be dependent on several structural and degradation medium factors. As such they have been shown to degrade

faster in the presence of primary and secondary amines in the hydrogel matrix because of the catalyzing action of amines [301, 302]. We have previously published a single-step PβAE hydrogel synthesis reaction based upon primary diamine precursors that serve as crosslinkers during polymerization. These networks were found to hydrolyze much more rapidly than gels prepared by a two-step crosslinking system, which is straight chain polymer synthesis followed by radical catalyzed cross-linking of acrylate end-groups [303]. It was theorized that this effect was a result of unmodified amines in the network backbone catalyzing the hydrolysis reaction [304, 305].

Based upon this observation, we hypothesize that these PβAE crosslinked networks would also be sensitive to nucleophilic attack by primary alcohols and will highly depend on the nature of alcohols. Herein, we report the first demonstration of PβAE hydrogel degradation by alcohols through a transesterification mechanism, establishing the effect of acrylate to amine ratio, alcohol chain length and degree of carbon substitution on the degradation kinetics. This mechanism also permitted the post synthesis modification of the hydrogels with alcohol functionalized drug molecules, allowing for an easy approach to couple hydroxyl compounds into the backbone of the polymer. Such modifications would allow for the gels to serve as drug release vehicles for molecules having the -OH group.

Materials

Poly (ethylene glycol) 400 diacrylate (PEG400DA) was purchased from Polysciences Inc., 4, 7, 10-Trioxa-1, 13-tridecane diamine (TTD) and riboflavin were obtained from Sigma-Aldrich (St. Lois, MO). All organic solvents were either purchased from Sigma-Aldrich or Pharmco-aaper (Shelbyville, KY) and were used as received. All the other chemicals were used as received without further purification.

Methods

Poly(β-amino ester) hydrogel synthesis

A one-step Michael addition reaction between acrylates and amines was used to synthesize PβAE hydrogels, as previously described [6, 301]. Figure 1 (A) and 1 (B) depicts the reaction mechanism and the schematic of the predicted crosslinked gel structure. Diacrylate monomer (PEG(400)DA) and primary diamine (TTD) were weighed and mixed in dichloromethane (DCM) at 50% wt/wt with respect to total monomers. This solution was transferred to an aluminum dish and monomers were allowed to react for 24 hours at 50˚C in an oven. PβAE hydrogels were then washed in acetone 4 times with a cycle of 1-hour each to remove unreacted monomers followed by freeze-drying to eliminate any residual solvent. The initial ratio of total acrylate to reactive hydrogen amine groups (RTAAP) was varied from 0.6 to 1.65 to synthesize different grades of PβAE hydrogels (Table 1) Note: 1 mol of diacrylate monomer corresponds to 2 mol of reactive acrylate groups; 1 mol of primary diamine monomer corresponds to total 4 mol of primary/secondary reactive amine groups.

Table 1. Different grades of PβAE hydrogels were synthesized by varying ratio of total acrylate to amine protons (RTAAP)

Hydrogel Identification Code	Diacrylate	Diamine	RTAAP
R- 0.6	PEG(400)DA	TTD	0.6
R-1.2	PEG(400)DA	TTD	1.2
R-1.65	PEG(400)DA	TTD	1.65

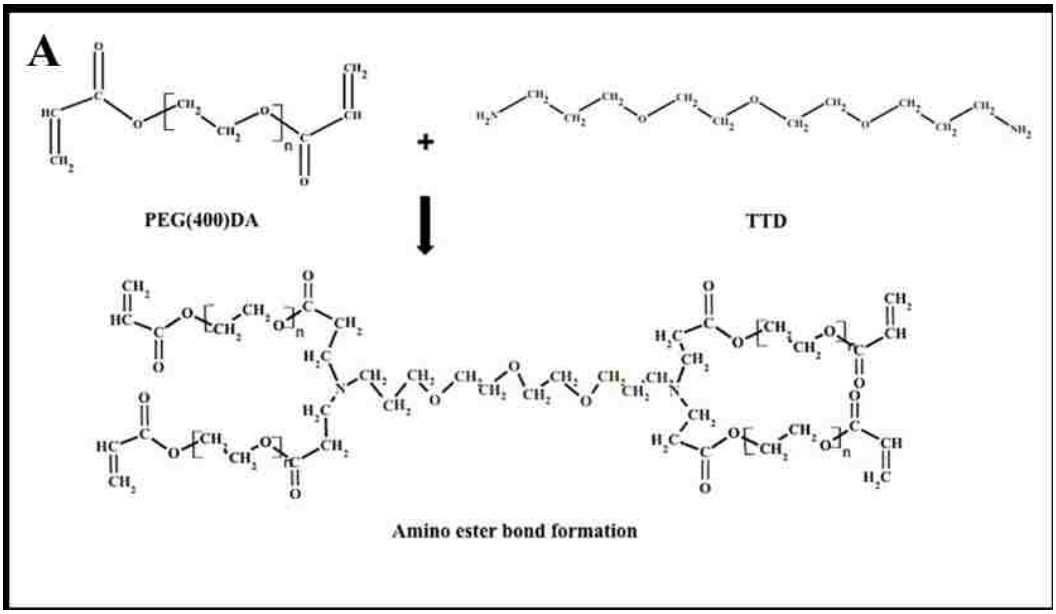

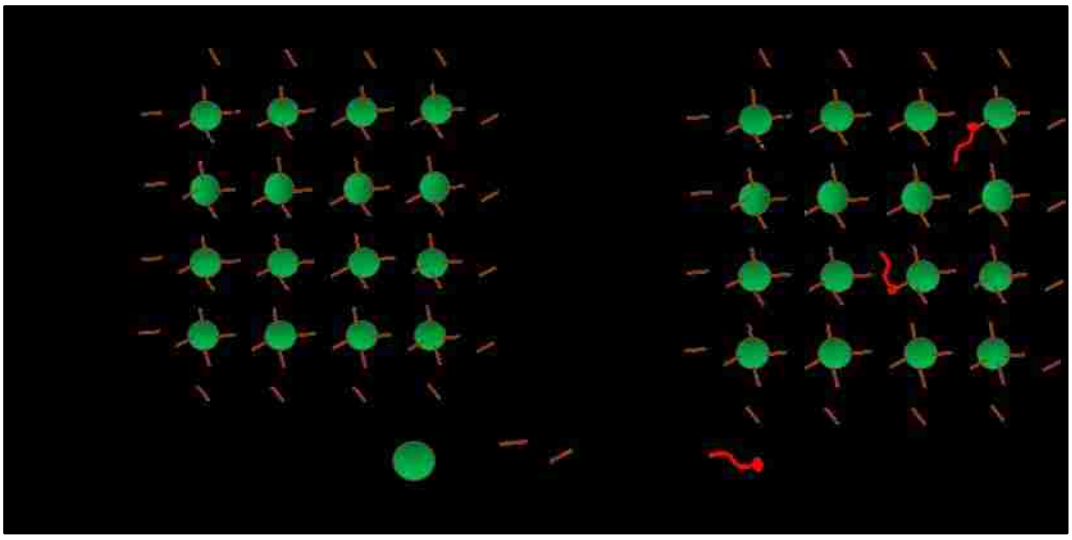

Figure 1 Synthesis of PEGDA-TTD PβAE cross-linked gels
A. Reaction scheme of PβAE hydrogel formation via reaction of PEG(400)DA and TTD in DCM solvent. B. Schematic of transesterification of PβAE hydrogels in presence of an alcohol. Ester bond of the PβAE matrix undergoes substitution with the reacting alcohol forming another ester bond.

PβAE degradation in alcohols

Degradation of PβAE hydrogels was carried out in various alcohols at 37˚C. 1 cm disc were cut from the bulk hydrogel films, weighed and were then incubated in different alcohols of interest such that discs were completely submerged. At given time points,

gels were removed from the solvent and dried under vacuum to remove residual solvent. The fraction of mass remaining was calculated from the ratio of the recorded final dry mass (W_d) and initial (W_0) mass values. The swelling ratio of the selected hydrogel-alcohol incubation system was also calculated by recording the mass of alcohol swollen hydrogels during degradation. Swelling ratio was calculated as the ratio of swollen gel mass (W_s) with initial mass (W_0).

$$\textbf{Fraction of mass remaining} = \frac{\mathbf{W_d}}{\mathbf{W_0}}$$

$$\textbf{Swelling ratio} = \frac{\mathbf{W_s}}{\mathbf{W_0}}$$

A separate set of RT-0.6 gels were degraded completely in ethanol as well as in water. Degradation products were freeze dried under vacuum and were subjected to FTIR analysis.

Conjugation of PβAE hydrogels with Riboflavin

R-0.6 and R-1.2 PβAE hydrogel discs were cut in about 1-cm discs, weighed and incubated in 1mg/ml riboflavin-DMSO solution at 37˚C and allowed to react for various durations of time up to 48 hours. After 6, 12, 24 and 48 hours, hydrogels were taken out, washed twice in DMSO to remove unreacted riboflavin followed by a single wash in acetone in order to leach out any residual DMSO. The hydrogel discs were then freeze-dried overnight to remove any residual solvents. The next day, each hydrogel disc sample was placed in separate wells of a 12-well plate and read at 444 and 600 nm using Varian Cary 50 Bio UV-Vis spectrophotometer. Absorbance at 600 nm was subtracted from absorbance value at 444 nm as a baseline correction to obtain the absorbance only due to riboflavin conjugation and not the disc thickness/optical density.

Next, the riboflavin conjugated hydrogel discs were degraded in PBS (35 mg gel/ ml of PBS) for hydrogels to undergo hydrolysis and release pure riboflavin. The degradation products in PBS were analyzed once again under UV-Vis at 444 nm and riboflavin concentrations were calculated using standard calibration curve.

Results

PβAE hydrogel synthesis

PβAE hydrogels synthesized with RTAAP of 0.6 (RT-0.6) and 1.2 (RT-1.2) resulted in uniform gels while gels synthesized with RTAAP of 1.65 (RT-1.65) resulted in partial conjugation and hence a semi-solid product. Since a properly conjugated hydrogel wasn't obtained with RT-1.65, further analysis of transesterification was limited to RT-0.6 and RT-1.2. Post synthesis, gels were washed in acetone to remove unreacted products and mass loss analysis was performed by weighing the gels before and after washing (freeze-dried). Average mass loss of 4.87 ± 0.3% for RT-0.6 and13.1 ± 0.4% for RT-1.2 was calculated.

PβAE degradation in alcohols (Mass loss and swelling ratio)

a. Effect of RTAAP on degradation and swelling ratio using ethanol as a degradation medium

RT-0.6 degraded via transesterification in 12-hours and showed a faster swelling rate, when compared to RT-1.2, with the swelling ratio of 3.5 ± 0.08 at 8 hours. After 8 hours of incubation, the gel started to lose mechanical integrity, suggesting the final stage of complete degradation, as shown in figure 2 A and 2 B. On the other hand, RT-1.2 showed very slow kinetics of transesterification derived hydrogel degradation, with no effective mass loss observed in 1st 12 hours. Even after 25 days of ethanol incubation, fraction of mass remaining was calculated to be 0.96 ± 0.01, which is 4% mass loss. RT-1.2 did show a swelling ratio of 1.46 ± 0.01 after the 1st day but only

increased to 1.65 ± 0.02 after 25 days implying extremely slow degradation kinetics in ethanol.

A similar effect of unsubstituted amines on gel degradation, with water as the degradation medium has been reported earlier. PEGDA-TTD gels synthesized with RTAAP of 0.6 degraded within 40 minutes while gels with RTAAP of 1.2 degraded completely in 130 minutes [5].

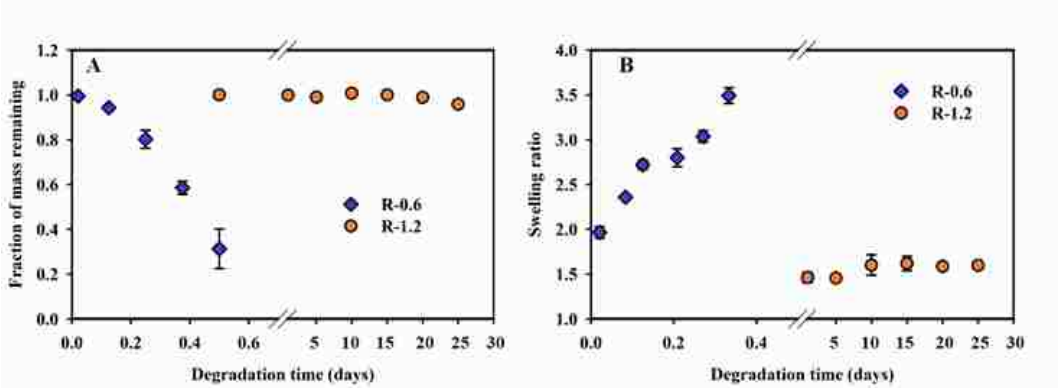

Figure 2 Effect of RTAAP on transesterification controlled degradation of PβAE gels in 200-proof ethanol at 37º C.
A.) Mass loss analysis of PβAE hydrogels (R-0.6 and R-1.2) presented as a fraction of mass remaining w.r.t. time. B.) Swelling ratio of R-0.6 and R-1.2 in ethanol w.r.t. time. Gels synthesized with RTAAP of 0.6 showed faster degradation and swelling than gels with RTAAP 1.2. N=3, error bars: std. dev.

b. Effect of primary alcohol with different chain lengths

As RT-1.2 possessed very slow degradation kinetics in ethanol, RT-0.6 PβAE gels were used to determine the impact of primary alcohols of different chain aliphatic lengths i.e. ethanol, n-propanol and n-butanol. As observed in figure 3, the degradation rate in ethanol and n-propanol was extended over 9-12 hours. However, n-butanol mediated degradation of RT-0.6 was slower extending up to 28-30 hours

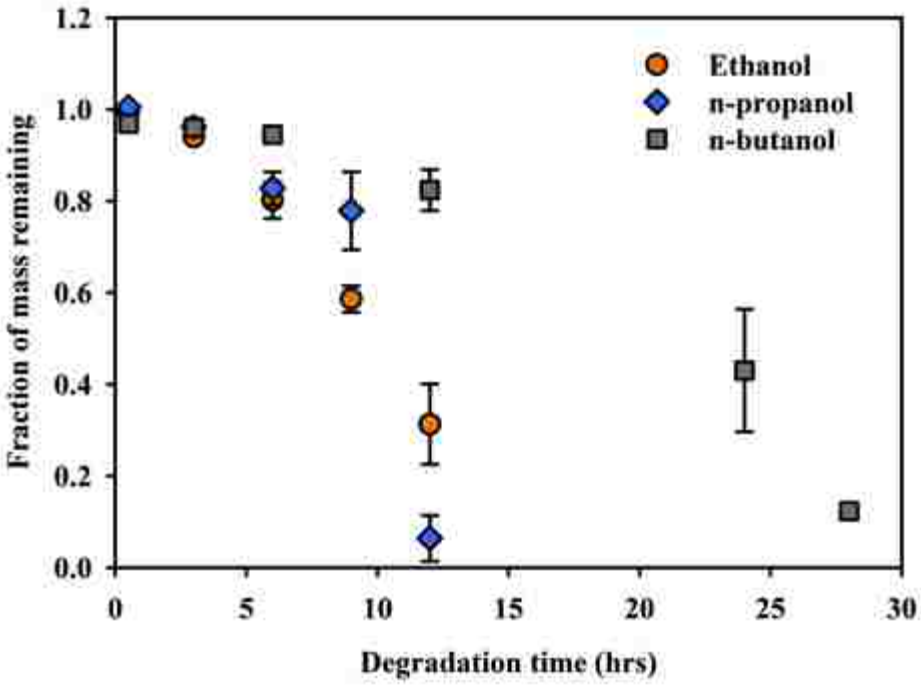

Figure 3 Degradation of PβAE hydrogels in primary alcohols of different chain lengths.
R-0.6 PβAE hydrogel was incubated in ethanol, n-propanol and n-butanol at 37° C. N=3, error bars: std. dev.

c. Effect of Alcohol Class on Degradation Kinetics

To elucidate the mechanism of gel degradation, the impact of primary, secondary, or tertiary substituted alcohol was conducted in two separate studies. First, RT-0.6 degradation was carried out with alcohols containing the same number of carbon chains but different degree of substitution i.e. n-propanol (primary, 3-carbon) and iso-propanol (secondary, 3-carbon) (figure 4 and 5). It was observed that PβAE gel incubation in primary alcohol (n-propanol) degraded within 12 hours, which is significantly faster than in secondary alcohol (iso-propanol) showing only 50% mass loss in 13 days. In the second study, RT-0.6 was incubated in primary, secondary and tertiary alcohol with different chain lengths. Ethanol (primary, 2-carbon), iso-propanol (secondary, 3-carbon) and tert-butanol (tertiary, 4-carbon) were used for transesterification. As the mass loss in tert-butanol was too slow to show significant differences over the study

time, swelling ratio for different alcohols was analyzed instead. As shown in figure 5, ethanol hydrogel incubation resulted in a swelling ratio of 3.5±0.08 within 8 hours after which it disintegrated. Iso-propanol resulted in slower kinetics giving a swelling ratio of 2.45±0.16 after 4 days and 4.61±0.6 after 9 days. Tert-butanol incubation showed even slower kinetics with swelling ratio of 1.94±0.05 after 4 days and 2.48±0.16 after 9 days. Therefore, PβAE degradation kinetics was faster in ethanol than in iso-propanol than in tert-butanol.

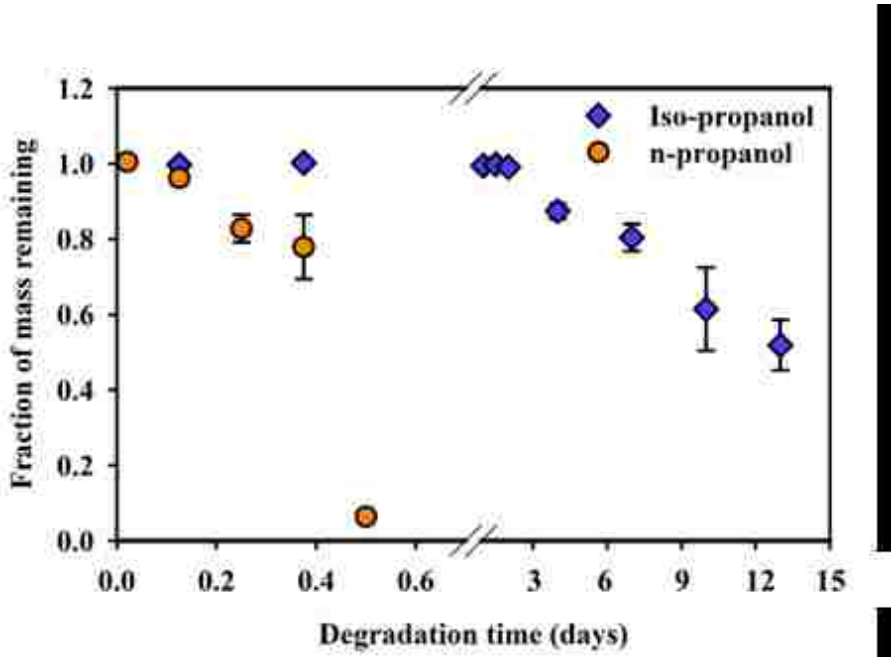

Figure 4 Effect of the degree of carbon substitution on degradation kinetics of R-0.6 PβAE hydrogels in primary and secondary alcohols.
Data presented as mass loss analysis of PβAE hydrogels degraded in n-propanol and iso-propanol at 37°C. N=3, error bars: std. dev.

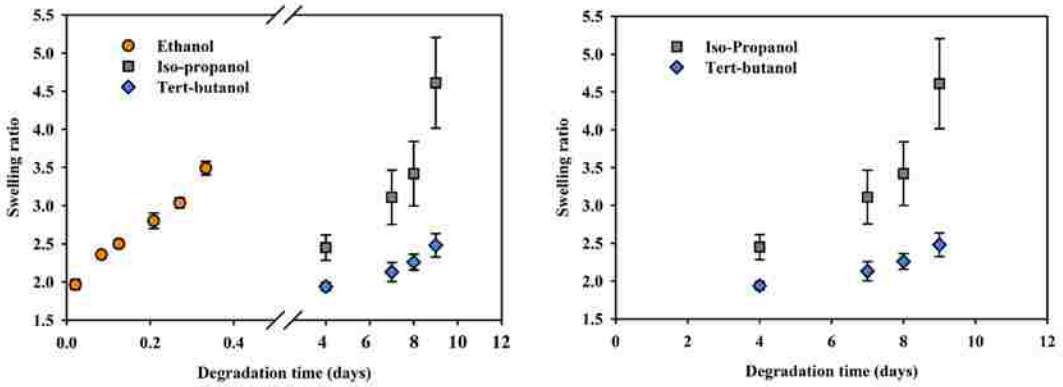

Figure 5 Swelling ratio of R-0.6 PβAE hydrogels in primary, secondary and tertiary alcohols i.e. ethanol, iso-propanol and tert-butanol respectively.
Rate of swelling and degradation decreases with increase in chain length and degree of carbon substitution. N=3, error bars: std. dev.

In a separate study, with RT-0.6 were hydrolyzed completely in ethanol and water. FTIR analysis of both the systems were compared to identify the nature of degradation products. The degradation products obtained from water showed the presence of strong acid peaks at around 1584cm^{-1} clearly indicating the hydrolysis to the corresponding acids. However, the presence of a peak near 1732cm-1 in ethanol degradation products confirmed the formation of the corresponding ester products (Figure 6).

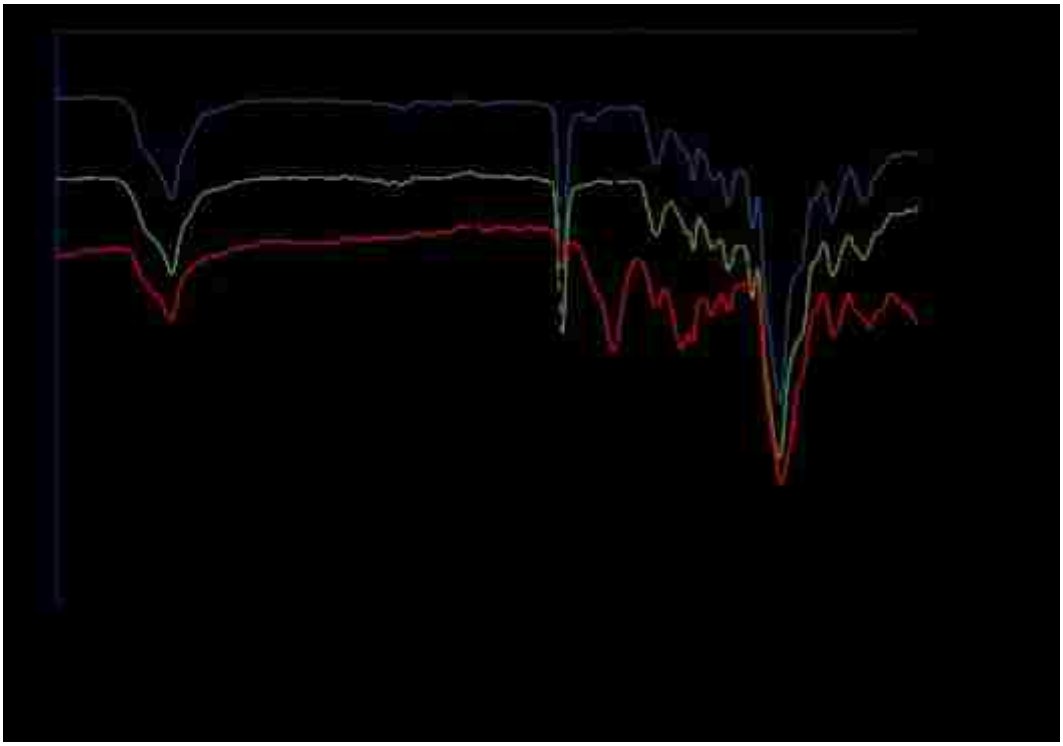

Figure 6 FTIR spectra of PβAE hydrogel RT-0.6, and the degradation products obtained by the hydrolysis of in water and ethanol.

Riboflavin conjugation to PβAE via transesterification

To study whether the transesterification mechanism can be used to link primary alcohol containing compounds to already formed PβAE gels, naturally found riboflavin (vitamin B_2) with 1-primary and 3-secondary alcohol functional group was used as a model compound to conjugate into RT-0.6 and RT-1.2 via transesterification process (figure 7 D). After incubating the gels in 1 mg/ml of riboflavin dissolved in DMSO for 6, 12, 24 and 48 hours, it was observed that RT-0.6 showed higher conjugation than RT-1.2 as seen in figure 7. When conjugated discs were observed under UV-Vis, absorbances were collected at 444 nm and 600 nm (characteristic wavelength for riboflavin). Absorbance value at 600 nm is the measure of optical density for each gel due to its thickness. Hence, to get absorbance values due to only riboflavin, absorbance at 600 nm was subtracted as a baseline from 444 nm and presented as Δabs. RT-0.6 showed Δabs of 0.22 ± 0.02, 0.28 ± 0.04, 0.5 ± 0.05 and 0.48 ± 0.06 after 6, 12, 24 and

48 hours of incubation respectively. RT-1.2 had lower Δabs values than RT-0.6 of 0.15 ± 0.5, 0.13 ± 0.01, 0.14 ± 0.5 and 0.23 ± 0.05 at the same time points (figure 7 A).

The riboflavin-conjugated gels were then subjected to hydrolytic degradation in PBS to recover the riboflavin. Degradation products were again read at 444 nm and collected absorbances gave a concentration of riboflavin in the solution using standard curve (figure 7 B and 7 C). 0.85 ± 0.03, 1 ± 0.04, 1.3 ± 0.33 and 1.86 ± 0.06 μg/ml of riboflavin was retrieved with RT-0.6 gels incubated for 6, 12, 24 and 48 hours respectively followed by PBS degradation. For RT-1.2, a lower amount of riboflavin was recovered as conjugation was less, which was 0.5 ± 0.01, 0.55 ± 0.15, 0.59 ± 0.16 and 1.1 ± 0.13 respectively under time interval degradation as for RT-0.6.

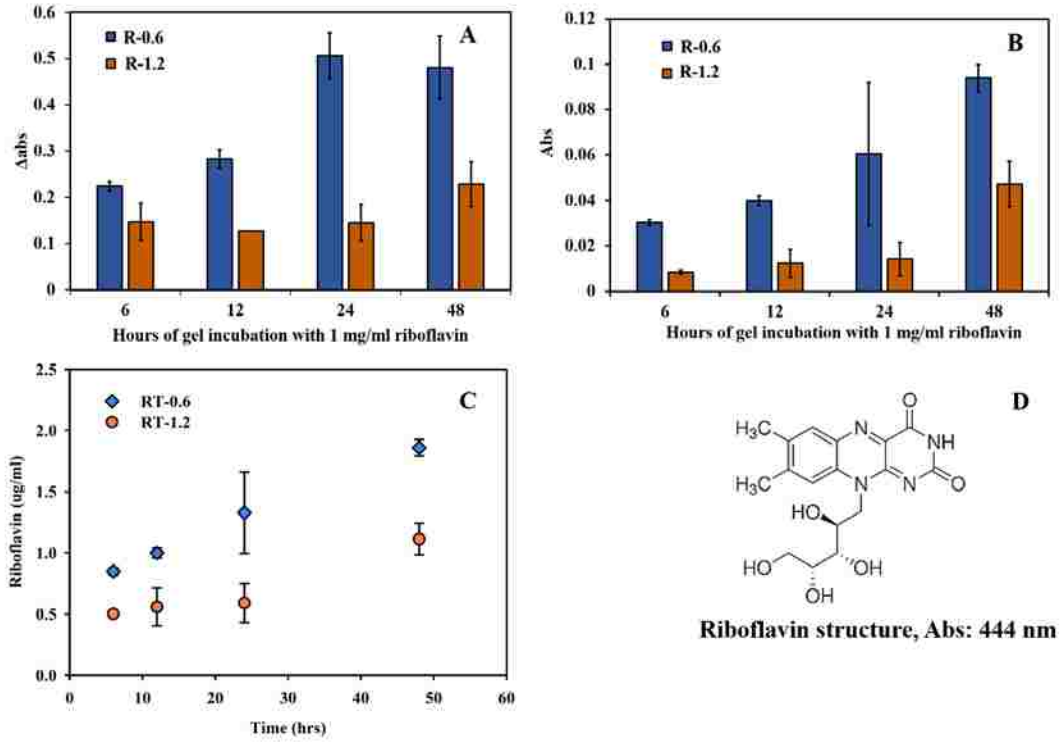

Figure 7 Conjugation of riboflavin into R-0.6 and R-1.2 PβAE hydrogels by incubation in 1 mg/ml riboflavin solution in DMSO.
A.) *Δabs of the hydrogels discs measured after different time intervals of incubation in riboflavin at 37^{o} C. Δabs = abs (444nm)-abs (600nm). Baseline subtraction at 600 nm was done for each sample separately to void the effect of optical density due to gel thickness.* ***B.)*** *Absorbance of degradation products of riboflavin conjugated PβAE hydrogels in PBS after different time intervals.* ***C.)*** *Concentration of riboflavin in PBS calculated after analyzing the degradation products under UV-Vis at 444 nm. R-0.6 gels showed the higher characteristic absorbance of riboflavin in gels discs as well as degradation products as compared to R-1.2 gels. This complies with transesterification data obtained earlier in figure 2. N=3, error bars: std. dev.*

Discussion

The degradation studies of PEG(400)DA-TTD based PβAE hydrogel synthesized at different RTAAPs were carried out in ethanol at 37^{o}C. It was initially observed that PβAEs synthesized using single step approach were unstable in ethanol. This was different from previously reported data, where ethanol was used as a stable washing solvent [306]. Originally, it was believed that degradation was due to the water content in the solvent. However, degradation still proceeded even with dried solvents.

This observation led to the theoretical conclusion that, β-amino ester bonds in the PβAE hydrogels undergo transesterification with the alcohol to form a new ester.

It was hypothesized that if transesterification was a mechanism, then the unmodified amines contained within the network could serve as a base to catalyze the transesterification process. To test this hypothesis, the levels of unmodified amine were varied by changing the total acrylate to total reactive hydrogen amine protons (RTAAP: 0.6 and 1.2). Lower RTAAP (0.6 in this case) PβAE gels with higher unreacted amine content, catalyzed the transesterification reaction via activation of surrounding alcohol into a nucleophilic entity (C_2H_5OH to $C_2H_5O^-$) [307]. The activated form, $C_2H_5O^-$ resulted in faster disintegration of PβAE matrix via substitution at the ester linkage (Figure 2).

Additionally, if the degradation of the PβAE gels is a function of transesterification, then it would be expected that the rate of degradation would be dependent upon the reactivity of the alcohol. Hence, the rate of alcohol substitution will be different for alcohols of different chain lengths or degree of carbon substitution. To verify this hypothesis, degradation properties of PβAE hydrogels were analyzed with different alcohols at 37˚C (Figures 3, 4 and 5). It was observed that the degradation of RT-0.6 PβAE hydrogel occurred fastest in ethanol followed by n-propanol and slowest with n-butanol amongst the three primary alcohols. The ethanol based transesterification reaction is typically much faster than propanol or butanol due to the high polar and acidic nature or lower carbon induced inductive effect due to shorter carbon chain length [308]. As the length of the carbon chain increases, nucleophilicity of the alkoxide anion decreases leading to a decrease in the reactivity of alkoxide anion. This causes the slower reaction rate in the order of n-butanol, n-propanol and ethanol and hence the degradation kinetics (figure 3). A similar trend was seen with the PβAE

hydrogel degradation in primary, secondary and tertiary alcohols because of the same concept of higher inductive effect with secondary as compared to primary alcohols. Therefore, iso-propanol being less acidic than n-propanol, shows slower transesterification kinetics than n-propanol (figure 4). The combined effect of chain length and degree of substitution was seen with degradation carried out in ethanol, iso-propanol and tert-butanol, where with tert-butanol, slowest degradation was observed amongst all the alcohols used because of the presence of three alkyl groups on the carbon-atom with –OH group and hence least acidic nature.

To confirm the transesterification reaction of the PβAE hydrogels, the degradation products of the RT-0.6 obtained from water and ethanol were freeze dried and analyzed with the help of an ATR-FTIR (Varian e-spectrophotometer). It has been reported previously that PβAE hydrogels degrade via hydrolysis of ester groups in the crosslinks to lower molecular weight degradation products and chains of poly(β-amino acids) and diols [300, 309]. The presence of a broad acid peak at 1584 cm^{-1} in the water degradation products of RT-0.6 with a subsequent decrease in intensity of the ester-C=O peak at 1732 cm^{-1} clearly indicates the formation of low molecular weight acids (Figure 6). The transesterification reaction of PβAE with alcohols was also confirmed by the re-formation of new ester peaks at around 1732cm^{-1} from the ethanol degradation products of RT-0.6.

Taking advantage of transesterification of PβAE network by alcohols, compounds of medicinal value containing alcohol groups (e.g. riboflavin, ascorbic acid) can be conjugated to the PβAE network without the use of additional linkers or reagents. Riboflavin is a part of the Vitamin B family (Vitamin B_2), naturally found in milk, yeast, leafy vegetables with metabolic functional significance in activating other

vitamins and reaction with flavoproteins [15, 310]. It contains one primary and three secondary alcohol groups in the molecular structure (Figure 7 D).

The extent of riboflavin conjugation into PβAE could be analyzed using UV-Vis because of its characteristic wavelength at 444 nm. As shown in Figure 7, PβAE upon incubation in riboflavin solution was able to conjugate the alcoholic molecule into its matrix and the amount of conjugation increased with time showing the progression of transesterification. Higher conjugation was seen with RT-0.6 than RT-1.2 because of the faster transesterification kinetics complying with previous studies (Figure 2). This was observed at both levels, riboflavin conjugated gel discs (figure 7 A) and released riboflavin after complete degradation of the gels (7 B).

Conclusion

It was found that PβAE synthesized by the single step non-free radical polymerization method degrades in alcohol via a transesterification mechanism. Unreacted primary/secondary amines in the PβAE network catalyze this transesterification reaction and the rate of PβAE degradation in alcohol decreases with increase in RTAAP. The degradation rate of PβAE in alcohol decreases with increasing chain length of alcohol or in order of tertiary<secondary<primary alcohols. Taking advantage of alcohol induced transesterification reaction in the PβAE network, molecules of medicinal value with alcohol groups (e.g. riboflavin) can be covalently conjugated to the PβAE network and the amount to be conjugated can be controlled with incubation time until gel disintegration while release of riboflavin via water hydrolysis can be controlled by selecting the PβAE gels of different RTAAPs.

REFERENCES

1. Federico, A., et al., *Mitochondria, oxidative stress and neurodegeneration.* J Neurol Sci, 2012. **322**(1-2): p. 254-62.
2. Pandey, K.B. and S.I. Rizvi, *Plant polyphenols as dietary antioxidants in human health and disease.* Oxidative Medicine and Cellular Longevity, 2009. **2**(5): p. 270-278.
3. Rigg, J.L., E.P. Elovic, and B.D. Greenwald, *A review of the effectiveness of antioxidant therapy to reduce neuronal damage in acute traumatic brain injury.* J Head Trauma Rehabil, 2005. **20**(4): p. 389-91.
4. Ahsan, H., et al., *Pro-oxidant, anti-oxidant and cleavage activities on DNA of curcumin and its derivatives demethoxycurcumin and bisdemethoxycurcumin.* Chem Biol Interact, 1999. **121**(2): p. 161-75.
5. Biswal, D., et al., *A single-step polymerization method for poly(β-amino ester) biodegradable hydrogels.* Polymer, 2011. **52**(26): p. 5985-5992.
6. Wattamwar, P.P., et al., *Synthesis and characterization of poly(antioxidant beta-amino esters) for controlled release of polyphenolic antioxidants.* Acta Biomaterialia, 2012. **8**(7): p. 2529-2537.
7. Gutowski, M. and S. Kowalczyk, *A study of free radical chemistry: their role and pathophysiological significance.* Acta Biochim Pol, 2013. **60**(1): p. 1-16.
8. Cameron, M.D., J.F. Poyer, and S.D. Aust, *Identification of free radicals produced during phacoemulsification.* Journal of Cataract & Refractive Surgery, 2001. **27**(3): p. 463-470.
9. Robert C. Neuman, J., *Free radical addition and substitution reactions*, in *Organic Chemistry*. 1992-2013.
10. Halliwell, B., *Oxygen and nitrogen are pro-carcinogens. Damage to DNA by reactive oxygen, chlorine and nitrogen species: measurement, mechanism and the effects of nutrition.* Mutat Res, 1999. **443**(1-2): p. 37-52.
11. Halliwell, B. and J.M. Gutteridge, *Oxygen toxicity, oxygen radicals, transition metals and disease.* Biochemical Journal, 1984. **219**(1): p. 1-14.
12. Mylonas, C. and D. Kouretas, *Lipid peroxidation and tissue damage.* In Vivo, 1999. **13**(3): p. 295-309.
13. Dröge, W., *Free Radicals in the Physiological Control of Cell Function*. Vol. 82. 2002. 47-95.
14. Trachootham, D., et al., *Redox Regulation of Cell Survival.* Antioxidants & Redox Signaling, 2008. **10**(8): p. 1343-1374.
15. Aratani, Y., et al., *Relative contributions of myeloperoxidase and NADPH-oxidase to the early host defense against pulmonary infections with Candida albicans and Aspergillus fumigatus.* Med Mycol, 2002. **40**(6): p. 557-63.
16. Babior, B.M., *NADPH oxidase.* Current Opinion in Immunology, 2004. **16**(1): p. 42-47.
17. Jacobs, J.J., Jilbert, Jeremy L., Urban, Robert M., *Current Concepts Review - Corrosion of Metal Orthopaedic Implants*. Vol. 80. 1998. 268-82.
18. Bodner, G. *Oxidation and Reduction*. [cited 2015 may 11]; Available from: http://chemed.chem.purdue.edu/genchem/topicreview/bp/ch9/redox.php.
19. Rademann, S.B.a.J., in *The Power of Functional Resins in Organic Synthesis*, J.W.a. Sons, Editor. 2008.
20. Cadet, J. and J.R. Wagner, *DNA base damage by reactive oxygen species, oxidizing agents, and UV radiation.* Cold Spring Harb Perspect Biol, 2013. **5**(2).
21. Thannickal, V.J. and B.L. Fanburg, *Reactive oxygen species in cell signaling.* American Journal of Physiology - Lung Cellular and Molecular Physiology, 2000. **279**(6): p. L1005-L1028.
22. Hœrlé, S., et al., *Advances in understanding atmospheric corrosion of iron. II. Mechanistic modelling of wet–dry cycles.* Corrosion Science, 2004. **46**(6): p. 1431-1465.
23. Rao, R.N.a.J.R., *Ferrous-ferric Oxidation in Pickle Liquor*. Journal of Scientific and Industrial Research, 2003. **62**: p. 1094-1097.
24. Rose, A.L. and T.D. Waite, *Reduction of organically complexed ferric iron by superoxide in a simulated natural water*. Environ Sci Technol, 2005. **39**(8): p. 2645-50.
25. *Wastewated Management Fact Sheet, Denitrifying Filters*, U.S.E.P. Agency, Editor.
26. Chin, D.H., et al., *Proton-induced disproportionation of superoxide ion in aprotic media.* Journal of the American Chemical Society, 1982. **104**(5): p. 1296-1299.
27. Buetyner, W.B.a.G.R., *The Vitamin C Radical and Its Reactions*, in *Vitamin C in Helath and Diseases*, L.P.a.J. Fuchs, Editor. 1997, Marcel Dekker, Inc: USA.

28. May, J.M., et al., *Reduction of the ascorbyl free radical to ascorbate by thioredoxin reductase.* J Biol Chem, 1998. **273**(36): p. 23039-45.
29. Lodish H., B.A., Zipursky SL, *Oxidation of Glucose and Fatty Acids*, in *Molecular Cell Biology*, W.H. Freeman, Editor. 2000: New York.
30. Wardman, P., *Reduction Potentials of One-Electron Couples Involving Free Radicals in Aqueous Solution.* Journal of Physical and Chemical Reference Data, 1989. **18**(4): p. 1637-1755.
31. Yang, J.J., et al., *Metal/TiO2 interfaces for memristive switches.* Applied Physics A, 2011. **102**(4): p. 785-789.
32. Desmoulins-Krawiec, S., et al., *Synthesis of nanostructured materials in supercritical ammonia: nitrides, metals and oxides.* Journal of Materials Chemistry, 2004. **14**(2): p. 228-232.
33. Pacher, P., A. Nivorozhkin, and C. SzabÓ, *Therapeutic Effects of Xanthine Oxidase Inhibitors: Renaissance Half a Century after the Discovery of Allopurinol.* Pharmacological reviews, 2006. **58**(1): p. 87-114.
34. Perez-Vizcaino, F., et al., *Antihypertensive effects of the flavonoid quercetin.* Pharmacol Rep, 2009. **61**(1): p. 67-75.
35. Starik, A.M., V.E. Kozlov, and N.S. Titova, *On the influence of singlet oxygen molecules on characteristics of HCCI combustion: A numerical study.* Combustion Theory and Modelling, 2013. **17**(4): p. 579-609.
36. Wilson, W.E., *A Critical Review of the Gas-Phase Reaction Kinetics of the Hydroxyl Radical.* Journal of Physical and Chemical Reference Data, 1972. **1**(2): p. 535-573.
37. Hawkins, C.L. and M.J. Davies, *Generation and propagation of radical reactions on proteins.* Biochimica et Biophysica Acta (BBA) - Bioenergetics, 2001. **1504**(2–3): p. 196-219.
38. Vejerno, E.W.P., *Formation and stabilization of combustion-generated environmentally persistent free radicals on transition metal oxides supported on silica*, in *Department of Chemistry*. 2011, Louisiana State University: Baton Rouge, LA.
39. Vejerano, E., S. Lomnicki, and B. Dellinger, *Lifetime of combustion-generated environmentally persistent free radicals on Zn(ii)O and other transition metal oxides.* Journal of Environmental Monitoring, 2012. **14**(10): p. 2803-2806.
40. Winterbourn, C.C., *Toxicity of iron and hydrogen peroxide: the Fenton reaction.* Toxicology Letters, 1995. **82–83**: p. 969-974.
41. Kehrer, J.P., *The Haber-Weiss reaction and mechanisms of toxicity.* Toxicology, 2000. **149**(1): p. 43-50.
42. Barbusiński, K., *Henry john horstman fenton - short biography and brief history of fenton reagent discovery.* Chemistry-Teaching-Ecology-Metrology, 2009: p. 101-105.
43. Haber, F. and J. Weiss, *The Catalytic Decomposition of Hydrogen Peroxide by Iron Salts.* Proceedings of the Royal Society of London A: Mathematical, Physical and Engineering Sciences, 1934. **147**(861): p. 332-351.
44. Bielski, B.H.J., et al., *Reactivity of HO2/O−2 Radicals in Aqueous Solution.* Journal of Physical and Chemical Reference Data, 1985. **14**(4): p. 1041-1100.
45. L. Kremer, M., *Mechanism of the Fenton reaction. Evidence for a new intermediate.* Physical Chemistry Chemical Physics, 1999. **1**(15): p. 3595-3605.
46. Friedrich, L.C., et al., *Mechanistic implications of zinc(II) ions on the degradation of phenol by the fenton reaction.* Journal of the Brazilian Chemical Society, 2012. **23**: p. 1372-1377.
47. Tavares, C.T.B.a.C.R.G., *Fenton´s Process for the Treatment of Mixed Waste Chemicals.* Organic Pollutants Ten Years After the Stockholm Convention - Environmental and Analytical Update, waste-chemicals, 2012.
48. Vile, G.F., C.C. Winterbourn, and H.C. Sutton, *Radical-driven Fenton reactions: studies with paraquat, adriamycin, and anthraquinone 6-sulfonate and citrate, ATP, ADP, and pyrophosphate iron chelates.* Arch Biochem Biophys, 1987. **259**(2): p. 616-26.
49. Fernandes, P.A. and M.J. Ramos, *Theoretical Insights into the Mechanism for Thiol/Disulfide Exchange.* Chemistry – A European Journal, 2004. **10**(1): p. 257-266.
50. Singh, R. and G.M. Whitesides, *Thiol—disulfide interchange*, in *Sulphur-Containing Functional Groups (1993)*. 2010, John Wiley & Sons, Inc. p. 633-658.
51. Gilbert, H.F., *Thiol/disulfide exchange equilibria and disulfide bond stability.* Methods Enzymol, 1995. **251**: p. 8-28.
52. Chandrasekhar, S., et al., *Thiol-Disulfide Exchange in Peptides Derived from Human Growth Hormone.* Journal of pharmaceutical sciences, 2014. **103**(4): p. 1032-1042.

53. Guo, W., J. Pleasants, and D.L. Rabenstein, *Nuclear magnetic resonance studies of thiol/disulfide chemistry. 2. Kinetics of symmetrical thiol/disulfide interchange reactions.* The Journal of Organic Chemistry, 1990. **55**(1): p. 373-376.
54. Szajewski, R.P., and Whitesides, G.M, *Rate Constants and Equilibrium Constants for Thiol-Disulfide Interchange Reactions Involving Oxidized Gluthathione.* Journal of American Chemical Society, 1980. **102**: p. 2011-2026.
55. Whitesides, G.M., Lilburn, J.E., and Szajewski, R.P, *Rates of Thiol-Disulfide Interchange Reactions between Mono- and Dithiols and Ellman's Reagent.* Journal of Oraganic Chemistry, 1977. **42**(332-338).
56. Fava, A., A. Iliceto, and E. Camera, *Kinetics of the Thiol-Disulfide Exchange.* Journal of the American Chemical Society, 1957. **79**(4): p. 833-838.
57. Hupe, D.J. and D. Wu, *Effect of charged substituents on rates of the thiol-disulfide interchange reaction.* The Journal of Organic Chemistry, 1980. **45**(15): p. 3100-3103.
58. Nagy, P., *Kinetics and Mechanisms of Thiol–Disulfide Exchange Covering Direct Substitution and Thiol Oxidation-Mediated Pathways.* Antioxidants & Redox Signaling, 2013. **18**(13): p. 1623-1641.
59. Weishaupt, K.R., C.J. Gomer, and T.J. Dougherty, *Identification of Singlet Oxygen as the Cytotoxic Agent in Photo-inactivation of a Murine Tumor.* Cancer Research, 1976. **36**(7 Part 1): p. 2326-2329.
60. McCord, J.M., *Oxygen-derived free radicals in postischemic tissue injury.* The New England journal of medicine, 1985. **312**(3): p. 159-163.
61. Gerschman, R., et al., *Oxygen poisoning and x-irradiation: a mechanism in common.* Science, 1954. **119**(3097): p. 623-6.
62. Freeman, B.A. and J.D. Crapo, *Biology of disease: free radicals and tissue injury.* Lab Invest, 1982. **47**(5): p. 412-26.
63. McCord, J.M. and I. Fridovich, *Superoxide Dismutase: An enzymatic function for erythrocuprein (hemocuprein).* Journal of Biological Chemistry, 1969. **244**(22): p. 6049-6055.
64. Klug, D., J. Rabani, and I. Fridovich, *A Direct Demonstration of the Catalytic Action of Superoxide Dismutase through the Use of Pulse Radiolysis.* Journal of Biological Chemistry, 1972. **247**(15): p. 4839-4842.
65. Chen, S.X. and P. Schopfer, *Hydroxyl-radical production in physiological reactions. A novel function of peroxidase.* Eur J Biochem, 1999. **260**(3): p. 726-35.
66. Nagy, P., A.J. Kettle, and C.C. Winterbourn, *Superoxide-mediated formation of tyrosine hydroperoxides and methionine sulfoxide in peptides through radical addition and intramolecular oxygen transfer.* J Biol Chem, 2009. **284**(22): p. 14723-33.
67. Petrat, F., et al., *Initiation of a superoxide-dependent chain oxidation of lactate dehydrogenase-bound NADH by oxidants of low and high reactivity.* Free Radic Res, 2005. **39**(10): p. 1043-57.
68. Harel, S., M.A. Salan, and J. Kanner, *Iron release from metmyoglobin, methaemoglobin and cytochrome c by a system generating hydrogen peroxide.* Free Radic Res Commun, 1988. **5**(1): p. 11-9.
69. Fessenden, R.W. and N.C. Verma, *A time-resolved electron spin resonance study of the oxidation of ascorbic acid by hydroxyl radical.* Biophys J, 1978. **24**(1): p. 93-101.
70. Wang, W., et al., *Superoxide flashes in single mitochondria.* Cell, 2008. **134**(2): p. 279-90.
71. Muller, F.L., Y. Liu, and H. Van Remmen, *Complex III releases superoxide to both sides of the inner mitochondrial membrane.* J Biol Chem, 2004. **279**(47): p. 49064-73.
72. Barja, G., *Mitochondrial Oxygen Radical Generation and Leak: Sites of Production in States 4 and 3, Organ Specificity, and Relation to Aging and Longevity.* Journal of Bioenergetics and Biomembranes, 1999. **31**(4): p. 347-366.
73. Boh, E.E., et al., *Mitochondrial chemiluminescence elicited by acetaldehyde.* J Bioenerg Biomembr, 1982. **14**(2): p. 115-33.
74. Chiueh, C.C., *Neuroprotective properties of nitric oxide.* Ann N Y Acad Sci, 1999. **890**: p. 301-11.
75. Ghafourifar, P. and E. Cadenas, *Mitochondrial nitric oxide synthase.* Trends Pharmacol Sci, 2005. **26**(4): p. 190-5.
76. Ignarro, L.J., et al., *Oxidation of nitric oxide in aqueous solution to nitrite but not nitrate: comparison with enzymatically formed nitric oxide from L-arginine.* Proceedings of the National Academy of Sciences of the United States of America, 1993. **90**(17): p. 8103-8107.
77. Kissner, R., et al., *Formation and properties of peroxynitrite as studied by laser flash photolysis, high-pressure stopped-flow technique, and pulse radiolysis.* Chem Res Toxicol, 1997. **10**(11): p. 1285-92.

78. Hsiai, T.K., et al., *Hemodynamics influences vascular peroxynitrite formation: Implication for low-density lipoprotein apo-B-100 nitration.* Free Radic Biol Med, 2007. **42**(4): p. 519-29.
79. Pacher, P., J.S. Beckman, and L. Liaudet, *Nitric oxide and peroxynitrite in health and disease.* Physiol Rev, 2007. **87**(1): p. 315-424.
80. Gow, A.J., D.G. Buerk, and H. Ischiropoulos, *A novel reaction mechanism for the formation of S-nitrosothiol in vivo.* J Biol Chem, 1997. **272**(5): p. 2841-5.
81. Ford, P.C., *Probing fundamental mechanisms of nitric oxide reactions with metal centers.* Pure and Applied Chemistry, 2004. **76**(2): p. 335-350.
82. Ballatori, N., et al., *Molecular mechanisms of reduced glutathione transport: role of the MRP/CFTR/ABCC and OATP/SLC21A families of membrane proteins.* Toxicol Appl Pharmacol, 2005. **204**(3): p. 238-55.
83. Saito, G., J.A. Swanson, and K.D. Lee, *Drug delivery strategy utilizing conjugation via reversible disulfide linkages: role and site of cellular reducing activities.* Adv Drug Deliv Rev, 2003. **55**(2): p. 199-215.
84. Ottaviano, F.G., D.E. Handy, and J. Loscalzo, *Redox regulation in the extracellular environment.* Circ J, 2008. **72**(1): p. 1-16.
85. Banerjee, R., *Redox outside the box: linking extracellular redox remodeling with intracellular redox metabolism.* J Biol Chem, 2012. **287**(7): p. 4397-402.
86. Lu, S.C., *Glutathione synthesis.* Biochim Biophys Acta, 2013. **1830**(5): p. 3143-53.
87. Eaton, D.L. and T.K. Bammler, *Concise review of the glutathione S-transferases and their significance to toxicology.* Toxicol Sci, 1999. **49**(2): p. 156-64.
88. Hu, J., L. Dong, and C.E. Outten, *The redox environment in the mitochondrial intermembrane space is maintained separately from the cytosol and matrix.* J Biol Chem, 2008. **283**(43): p. 29126-34.
89. Hwang, C., A.J. Sinskey, and H.F. Lodish, *Oxidized redox state of glutathione in the endoplasmic reticulum.* Science, 1992. **257**(5076): p. 1496-502.
90. Nohl, H., *Is redox-cycling ubiquinone involved in mitochondrial oxygen activation?* Free Radic Res Commun, 1990. **8**(4-6): p. 307-15.
91. Cuzzocrea, S., et al., *Antioxidant therapy: a new pharmacological approach in shock, inflammation, and ischemia/reperfusion injury.* Pharmacol Rev, 2001. **53**(1): p. 135-59.
92. Jones, O.T., *The regulation of superoxide production by the NADPH oxidase of neutrophils and other mammalian cells.* Bioessays, 1994. **16**(12): p. 919-23.
93. Babior, B.M., *NADPH Oxidase: An Update.* Blood 1999. **93**(5): p. 1464-1476.
94. Paravicini, T.M. and R.M. Touyz, *NADPH Oxidases, Reactive Oxygen Species, and Hypertension: Clinical implications and therapeutic possibilities.* Diabetes Care, 2008. **31**(Supplement 2): p. S170-S180.
95. Bae, Y.S., et al., *Epidermal Growth Factor (EGF)-induced Generation of Hydrogen Peroxide: Role in egf receptor-mediated tyrosine phosphorylation.* Journal of Biological Chemistry, 1997. **272**(1): p. 217-221.
96. Griendling, K.K., et al., *Angiotensin II stimulates NADH and NADPH oxidase activity in cultured vascular smooth muscle cells.* Circ Res, 1994. **74**(6): p. 1141-8.
97. MacMillan-Crow, L.A. and J.P. Crow, *Does more MnSOD mean more hydrogen peroxide?* Anticancer Agents Med Chem, 2011. **11**(2): p. 178-80.
98. Miwa, S., et al., *Superoxide and hydrogen peroxide production by Drosophila mitochondria.* Free Radical Biology and Medicine, 2003. **35**(8): p. 938-948.
99. Joy J. Goto, E.B.G., Joan Selverstone Valentine and Diane E. Cabelli, *Reactions of Hydrogen Peroxide with Familial Amyotrophic Lateral Sclerosis Mutant Human Copper-Zinc Superoxide Dismutases Studied by Pulse Radiolysis.* The Journal of Biological Chemistry, 1198. **273**(46): p. 30104-30109.
100. Haberland, A., et al., *Comparison of malondialdehyde and hydrogen peroxide modified CuZnSOD by EPR spectroscopy.* Agents and Actions, 1993. **40**(3-4): p. 166-170.
101. Goeptar, A.R., H. Scheerens, and N.P. Vermeulen, *Oxygen and xenobiotic reductase activities of cytochrome P450.* Crit Rev Toxicol, 1995. **25**(1): p. 25-65.
102. Yixin Li, J.C.T., Simon Cooper, Michelle Glenn, Howard P. Glauert and Brett T. Spear, *Expression of the Hydrogen Peroxide-Generating Enzyme Fatty Acyl CoA Oxidase Activates NF-kB.* DNA and Cell Biology, 2000. **19**(2): p. 113-120.
103. Apel, K. and H. Hirt, *Reactive Oxygen Species: Metabolism, Oxidative Stress, and Signal Transduction.* Annual Review of Plant Biology, 2004. **55**(1): p. 373-399.

104. Doroshow, J.H., G.Y. Locker, and C.E. Myers, *Enzymatic Defenses of the Mouse Heart Against Reactive Oxygen Metabolites: Alterations produced by doxorubicin.* Journal of Clinical Investigation, 1980. **65**(1): p. 128-135.
105. Puppo, A. and B. Halliwell, *Formation of hydroxyl radicals from hydrogen peroxide in the presence of iron. Is haemoglobin a biological Fenton reagent?* Biochemical Journal, 1988. **249**(1): p. 185-190.
106. Kanner, J., S. Harel, and B. Hazan, *Muscle membranal lipid peroxidation by an "iron redox cycle" system: initiation by oxy radicals and site-specific mechanism.* Journal of Agricultural and Food Chemistry, 1986. **34**(3): p. 506-510.
107. Deguillaume, L., M. Leriche, and N. Chaumerliac, *Impact of radical versus non-radical pathway in the Fenton chemistry on the iron redox cycle in clouds.* Chemosphere, 2005. **60**(5): p. 718-724.
108. Coddington, J.W., J.K. Hurst, and S.V. Lymar, *Hydroxyl Radical Formation during Peroxynitrous Acid Decomposition.* Journal of the American Chemical Society, 1999. **121**(11): p. 2438-2443.
109. Koppenol, W.H., et al., *Peroxynitrite, a cloaked oxidant formed by nitric oxide and superoxide.* Chemical Research in Toxicology, 1992. **5**(6): p. 834-842.
110. Ignarro, L.J., *Nitric oxide as a unique signaling molecule in the vascular system: a historical overview.* J Physiol Pharmacol, 2002. **53**(4 Pt 1): p. 503-14.
111. Guzik, T.J., R. Korbut, and T. Adamek-Guzik, *Nitric oxide and superoxide in inflammation and immune regulation.* J Physiol Pharmacol, 2003. **54**(4): p. 469-87.
112. Carreras, M.C., et al., *The biological significance of mtNOS modulation.* Front Biosci, 2007. **12**: p. 1041-8.
113. Powers, S.K. and M.J. Jackson, *Exercise-Induced Oxidative Stress: Cellular Mechanisms and Impact on Muscle Force Production*. Vol. 88. 2008. 1243-1276.
114. Hawkins, C.L., B.E. Brown, and M.J. Davies, *Hypochlorite- and hypobromite-mediated radical formation and its role in cell lysis.* Arch Biochem Biophys, 2001. **395**(2): p. 137-45.
115. Hawkins, C.L. and M.J. Davies, *Hypochlorite-induced damage to proteins: formation of nitrogen-centred radicals from lysine residues and their role in protein fragmentation.* Biochemical Journal, 1998. **332**(Pt 3): p. 617-625.
116. Chen, Y.R., et al., *Involvement of protein radical, protein aggregation, and effects on NO metabolism in the hypochlorite-mediated oxidation of mitochondrial cytochrome c.* Free Radic Biol Med, 2004. **37**(10): p. 1591-603.
117. Kamat, T.P.A.D.a.j.P., *Biological Significance of Singlet Oxygen.* Indian Journal of Experimental Biology, 2002. **40**: p. 680-692.
118. Miyamoto, S., et al., *Biological hydroperoxides and singlet molecular oxygen generation.* IUBMB Life, 2007. **59**(4-5): p. 322-31.
119. Beauchamp, C. and I. Fridovich, *Superoxide dismutase: Improved assays and an assay applicable to acrylamide gels.* Analytical Biochemistry, 1971. **44**(1): p. 276-287.
120. Grankvist, K., S.L. Marklund, and I.B. Taljedal, *CuZn-superoxide dismutase, Mn-superoxide dismutase, catalase and glutathione peroxidase in pancreatic islets and other tissues in the mouse.* Biochem J, 1981. **199**(2): p. 393-8.
121. Bredt, D.S., et al., *Cloned and expressed nitric oxide synthase structurally resembles cytochrome P-450 reductase.* Nature, 1991. **351**(6329): p. 714-8.
122. Bedard, K. and K.H. Krause, *The NOX family of ROS-generating NADPH oxidases: physiology and pathophysiology.* Physiol Rev, 2007. **87**(1): p. 245-313.
123. Sies, H., et al., *Glutathione Peroxidase Protects against Peroxynitrite-mediated Oxidations: A new function for selenoproteins as peroxynitrite reductase.* Journal of Biological Chemistry, 1997. **272**(44): p. 27812-27817.
124. Rotruck, J.T., et al., *Selenium: Biochemical Role as a Component of Glutathione Peroxidase.* Science, 1973. **179**(4073): p. 588-590.
125. Hampton, M.B., A.J. Kettle, and C.C. Winterbourn, *Inside the Neutrophil Phagosome: Oxidants, Myeloperoxidase, and Bacterial Killing*. Vol. 92. 1998. 3007-3017.
126. Scibior, D. and H. Czeczot, *[Catalase: structure, properties, functions]*. Postepy Hig Med Dosw (Online), 2006. **60**: p. 170-80.
127. Góth, L., *A simple method for determination of serum catalase activity and revision of reference range.* Clinica Chimica Acta, 1991. **196**(2–3): p. 143-151.
128. Rådmark, O. and B. Samuelsson, *5-Lipoxygenase: mechanisms of regulation.* Journal of Lipid Research, 2009. **50**(Suppl): p. S40-S45.

129. Cook-Moreau, J.M., et al., *Expression of 5-lipoxygenase (5-LOX) in T lymphocytes.* Immunology, 2007. **122**(2): p. 157-166.
130. Dubois, R.N., et al., *Cyclooxygenase in biology and disease.* The FASEB Journal, 1998. **12**(12): p. 1063-1073.
131. Feng, L., et al., *Involvement of reactive oxygen intermediates in cyclooxygenase-2 expression induced by interleukin-1, tumor necrosis factor-alpha, and lipopolysaccharide.* J Clin Invest, 1995. **95**(4): p. 1669-75.
132. Richardson, J.S., *On the functions of monoamine oxidase, the emotions, and adaptation to stress.* Int J Neurosci, 1993. **70**(1-2): p. 75-84.
133. Laura B Valdez, S.L.A., Juanita Bustamante, Silvia Alvarez, Lidia E Costa, Alberto Boveris, *Free radical chemistry in biological system.* Biological Research, 2000. **33**(2): p. 65-70.
134. Yan, E.B., et al., *Novel method for in vivo hydroxyl radical measurement by microdialysis in fetal sheep brain in utero.* Journal of Applied Phisiology, 2005. **98**(6): p. 2304-2310.
135. Davies, K.J., *Protein damage and degradation by oxygen radicals. I. general aspects.* J Biol Chem, 1987. **262**(20): p. 9895-901.
136. Dean, R.T., et al., *Biochemistry and pathology of radical-mediated protein oxidation.* Biochemical Journal, 1997. **324**(Pt 1): p. 1-18.
137. Davies, M., *Free Radicals, Oxidants and Protein Damage*, in *Australian Society for Biochemistry and Molecular Biology*. 2012: Sydney, Australia.
138. Goeschen, C. and U. Wille, *Damage of polyesters by the atmospheric free radical oxidant NO(3) (•): a product study involving model systems.* Beilstein Journal of Organic Chemistry, 2013. **9**: p. 1907-1916.
139. Green, K., M.D. Brand, and M.P. Murphy, *Prevention of Mitochondrial Oxidative Damage as a Therapeutic Strategy in Diabetes.* Diabetes, 2004. **53**(suppl 1): p. S110-S118.
140. Yakes, F.M. and B. Van Houten, *Mitochondrial DNA damage is more extensive and persists longer than nuclear DNA damage in human cells following oxidative stress.* Proc Natl Acad Sci U S A, 1997. **94**(2): p. 514-9.
141. Gutierrez, J., et al., *Free Radicals, Mitochondria, and Oxidized Lipids: The Emerging Role in Signal Transduction in Vascular Cells.* Circulation Research, 2006. **99**(9): p. 924-932.
142. Cadenas, E. and K.J.A. Davies, *Mitochondrial free radical generation, oxidative stress, and aging.* Free Radical Biology and Medicine, 2000. **29**(3–4): p. 222-230.
143. Crow, M.T., et al., *The Mitochondrial Death Pathway and Cardiac Myocyte Apoptosis.* Circulation Research, 2004. **95**(10): p. 957-970.
144. Ayala, A., et al., *Lipid Peroxidation: Production, Metabolism, and Signaling Mechanisms of Malondialdehyde and 4-Hydroxy-2-Nonenal.* Oxidative Medicine and Cellular Longevity, 2014. **2014**: p. 31.
145. Hogg, N. and B. Kalyanaraman, *Nitric oxide and lipid peroxidation.* Biochimica et Biophysica Acta (BBA) - Bioenergetics, 1999. **1411**(2–3): p. 378-384.
146. Goldstein, S., J. Lind, and G. Merenyi, *Reaction of Organic Peroxyl Radicals with •NO2 and •NO in Aqueous Solution: Intermediacy of Organic Peroxynitrate and Peroxynitrite Species.* The Journal of Physical Chemistry A, 2004. **108**(10): p. 1719-1725.
147. O'Donnell, V.B., et al., *Nitric oxide inhibition of lipid peroxidation: kinetics of reaction with lipid peroxyl radicals and comparison with alpha-tocopherol.* Biochemistry, 1997. **36**(49): p. 15216-23.
148. O'Donnell, V.B. and B.A. Freeman, *Interactions between nitric oxide and lipid oxidation pathways: implications for vascular disease.* Circ Res, 2001. **88**(1): p. 12-21.
149. Abuja, P.M., R. Albertini, and H. Esterbauer, *Simulation of the induction of oxidation of low-density lipoprotein by high copper concentrations: evidence for a nonconstant rate of initiation.* Chem Res Toxicol, 1997. **10**(6): p. 644-51.
150. M K Shigenaga, T.M.H., and B N Ames, *Oxidative damage and mitochondrial decay in aging.* Proceedings of the National Academy of Sciences of the United States of America, 1994. **91**(23): p. 10771-10778.
151. Richter, C., et al., *Oxidants in mitochondria: from physiology to diseases.* Biochim Biophys Acta, 1995. **1271**(1): p. 67-74.
152. Canas, P.E., *The role of xanthine oxidase and the effects of antioxidants in ischemia reperfusion cell injury.* Acta Physiol Pharmacol Ther Latinoam, 1999. **49**(1): p. 13-20.
153. Kohen, R. and A. Nyska, *Invited Review: Oxidation of Biological Systems: Oxidative Stress Phenomena, Antioxidants, Redox Reactions, and Methods for Their Quantification.* Toxicologic Pathology, 2002. **30**(6): p. 620-650.

154. Jacobs, H., et al., *An essential difference in the reactivity of the glutathione adducts of the structurally closely related flavonoids monoHER and quercetin.* Free radical biology & medicine, 2011. **51**(11): p. 2118-2123.
155. Bhalla, D.K., *Ozone-induced lung inflammation and mucosal barrier disruption: toxicology, mechanisms, and implications.* J Toxicol Environ Health B Crit Rev, 1999. **2**(1): p. 31-86.
156. Pentland, A.P., *Active oxygen mechanisms of UV inflammation.* Adv Exp Med Biol, 1994. **366**: p. 87-97.
157. Koren, H.S., *Associations between criteria air pollutants and asthma.* Environmental Health Perspective, 1995. **103**(6): p. 235-242.
158. Naito, Y., et al., *Role of oxygen radical and lipid peroxidation in indomethacin-induced gastric mucosal injury.* Dig Dis Sci, 1998. **43**(9 Suppl): p. 30s-34s.
159. Poulsen, H.E., *Oxidative DNA modifications.* Exp Toxicol Pathol, 2005. **57 Suppl 1**: p. 161-9.
160. Ghibu, S., et al., *General oxidative stress during doxorubicin-induced cardiotoxicity in rats: absence of cardioprotection and low antioxidant efficiency of alpha-lipoic acid.* Biochimie, 2012. **94**(4): p. 932-9.
161. Magalhães, L.M., et al., *Methodological aspects about in vitro evaluation of antioxidant properties.* Analytica Chimica Acta, 2008. **613**(1): p. 1-19.
162. Huang, D., B. Ou, and R.L. Prior, *The Chemistry behind Antioxidant Capacity Assays.* Journal of Agricultural and Food Chemistry, 2005. **53**(6): p. 1841-1856.
163. Halliwell, B., *The antioxidant paradox: less paradoxical now?* British Journal of Clinical Pharmacology, 2013. **75**(3): p. 637-644.
164. Galisteo, M., et al., *Effects of chronic quercetin treatment on antioxidant defence system and oxidative status of deoxycorticosterone acetate-salt-hypertensive rats.* Mol Cell Biochem, 2004. **259**(1-2): p. 91-9.
165. Bucki, R., et al., *Flavonoid inhibition of platelet procoagulant activity and phosphoinositide synthesis.* J Thromb Haemost, 2003. **1**(8): p. 1820-8.
166. Lee, E.S., et al., *The flavonoid quercetin inhibits dimethylnitrosamine-induced liver damage in rats.* J Pharm Pharmacol, 2003. **55**(8): p. 1169-74.
167. Fang, R., et al., *Design and characterization of protein-quercetin bioactive nanoparticles.* Journal of Nanobiotechnology, 2011. **9**(1): p. 19.
168. Gugler, R., M. Leschik, and H.J. Dengler, *Disposition of quercetin in man after single oral and intravenous doses.* Eur J Clin Pharmacol, 1975. **9**(2-3): p. 229-34.
169. Anand, P., et al., *Bioavailability of Curcumin: Problems and Promises.* Molecular Pharmaceutics, 2007. **4**(6): p. 807-818.
170. Lamson, D.W. and M.S. Brignall, *Antioxidants and cancer, part 3: quercetin.* Altern Med Rev, 2000. **5**(3): p. 196-208.
171. Hollman, P.C., et al., *Absorption and disposition kinetics of the dietary antioxidant quercetin in man.* Free Radic Biol Med, 1996. **21**(5): p. 703-7.
172. Wilczewska, A.Z., et al., *Nanoparticles as drug delivery systems.* Pharmacol Rep, 2012. **64**(5): p. 1020-37.
173. Jain, A.K., K. Thanki, and S. Jain, *Co-encapsulation of Tamoxifen and Quercetin in Polymeric Nanoparticles: Implications on Oral Bioavailability, Antitumor Efficacy, and Drug-Induced Toxicity.* Molecular Pharmaceutics, 2013. **10**(9): p. 3459-3474.
174. Wattamwar, P.P., et al., *Antioxidant Activity of Degradable Polymer Poly(trolox ester) to Suppress Oxidative Stress Injury in the Cells.* Advanced Functional Materials, 2010. **20**(1): p. 147-154.
175. Brey, D.M., et al., *Controlling poly(β-amino ester) network properties through macromer branching.* Acta Biomaterialia, 2008. **4**(2): p. 207-217.
176. Lynn, D.M. and R. Langer, *Degradable Poly(β-amino esters): Synthesis, Characterization, and Self-Assembly with Plasmid DNA.* Journal of the American Chemical Society, 2000. **122**(44): p. 10761-10768.
177. Bose, S. and B. Michniak-Kohn, *Preparation and characterization of lipid based nanosystems for topical delivery of quercetin.* European Journal of Pharmaceutical Sciences, 2013. **48**(3): p. 442-452.
178. Wattamwar, P.P., et al., *Synthesis and characterization of poly(antioxidant beta-amino esters) for controlled release of polyphenolic antioxidants.* Acta Biomater, 2012. **8**(7): p. 2529-37.
179. Simone, E., et al., *Synthesis and Characterization of Polymer Nanocarriers for the Targeted Delivery of Therapeutic Enzymes.* Methods in molecular biology (Clifton, N.J.), 2010. **610**: p. 145-164.

180. Ritger, P.L. and N.A. Peppas, *A simple equation for description of solute release I. Fickian and non-fickian release from non-swellable devices in the form of slabs, spheres, cylinders or discs.* Journal of Controlled Release, 1987. **5**(1): p. 23-36.
181. Lao, L.L., et al., *Modeling of drug release from bulk-degrading polymers.* International Journal of Pharmaceutics, 2011. **418**(1): p. 28-41.
182. Simone, E., et al., *Synthesis and characterization of polymer nanocarriers for the targeted delivery of therapeutic enzymes.* Methods Mol Biol, 2010. **610**: p. 145-64.
183. Steinberg, D. and J.L. Witztum, *Is the Oxidative Modification Hypothesis Relevant to Human Atherosclerosis?: Do the Antioxidant Trials Conducted to Date Refute the Hypothesis?* Circulation, 2002. **105**(17): p. 2107-2111.
184. Kerksick, C. and D. Willoughby, *The antioxidant role of glutathione and N-acetyl-cysteine supplements and exercise-induced oxidative stress.* J Int Soc Sports Nutr, 2005. **2**: p. 38-44.
185. Holdiness, M.R., *Clinical pharmacokinetics of N-acetylcysteine.* Clin Pharmacokinet, 1991. **20**(2): p. 123-34.
186. Elms, A., et al., *Fatal myocardial infarction associated with intravenous N-acetylcysteine error.* International Journal of Emergency Medicine, 2011. **4**(1): p. 54.
187. McBath, R.A. and D.A. Shipp, *Swelling and degradation of hydrogels synthesized with degradable poly([small beta]-amino ester) crosslinkers.* Polymer Chemistry, 2010. **1**(6): p. 860-865.
188. Meenach, S.A., et al., *Controlled synergistic delivery of paclitaxel and heat from poly(beta-amino ester)/iron oxide-based hydrogel nanocomposites.* Int J Pharm, 2012. **427**(2): p. 177-84.
189. Zenkevich, I., et al., *Identification of the Products of Oxidation of Quercetin by Air Oxygenat Ambient Temperature.* Molecules, 2007. **12**(3): p. 654.
190. Zhou, A. and O.A. Sadik, *Comparative analysis of quercetin oxidation by electrochemical, enzymatic, autoxidation, and free radical generation techniques: a mechanistic study.* J Agric Food Chem, 2008. **56**(24): p. 12081-91.
191. Hsieh, H.-L. and C.-M. Yang, *Role of Redox Signaling in Neuroinflammation and Neurodegenerative Diseases.* BioMed Research International, 2013. **2013**: p. 484613.
192. Maritim, A.C., R.A. Sanders, and J.B. Watkins, 3rd, *Diabetes, oxidative stress, and antioxidants: a review.* J Biochem Mol Toxicol, 2003. **17**(1): p. 24-38.
193. Reuter, S., et al., *Oxidative stress, inflammation, and cancer: How are they linked?* Free radical biology & medicine, 2010. **49**(11): p. 1603-1616.
194. Orrenius, S., V. Gogvadze, and B. Zhivotovsky, *Mitochondrial Oxidative Stress: Implications for Cell Death.* Annual Review of Pharmacology and Toxicology, 2007. **47**(1): p. 143-183.
195. Marc W. Fariss, C.B.C., Manisha Patel, Bennett Van Houten and Sten Orrenius, *Role of mitochondria in toxic oxidative stress.* Molecular interventions, 2005. **5**(2): p. 94-111.
196. Drose, S. and U. Brandt, *Molecular mechanisms of superoxide production by the mitochondrial respiratory chain.* Adv Exp Med Biol, 2012. **748**: p. 145-69.
197. Chen, Q., et al., *Production of reactive oxygen species by mitochondria: central role of complex III.* J Biol Chem, 2003. **278**(38): p. 36027-31.
198. *Mitochondria-Ros Crosstalk in the Control of Cell Death and Aging.* Journal of Signal Transduction, 2012. **2012**.
199. Madrigal, J.L., et al., *Glutathione depletion, lipid peroxidation and mitochondrial dysfunction are induced by chronic stress in rat brain.* Neuropsychopharmacology, 2001. **24**(4): p. 420-9.
200. Zhong, H. and H. Yin, *Role of lipid peroxidation derived 4-hydroxynonenal (4-HNE) in cancer: Focusing on mitochondria.* Redox Biology, 2015. **4**(0): p. 193-199.
201. Huang, S.X., et al., *Mitochondria-derived reactive intermediate species mediate asbestos-induced genotoxicity and oxidative stress-responsive signaling pathways.* Environ Health Perspect, 2012. **120**(6): p. 840-7.
202. Victor, V.M., et al., *Oxidative stress and mitochondrial dysfunction in atherosclerosis: mitochondria-targeted antioxidants as potential therapy.* Curr Med Chem, 2009. **16**(35): p. 4654-67.
203. Rolo, A.P. and C.M. Palmeira, *Diabetes and mitochondrial function: role of hyperglycemia and oxidative stress.* Toxicol Appl Pharmacol, 2006. **212**(2): p. 167-78.
204. Ichikawa, Y., et al., *Cardiotoxicity of doxorubicin is mediated through mitochondrial iron accumulation.* The Journal of Clinical Investigation, 2014. **124**(2): p. 617-630.
205. Butterfield, D.A., F. Di Domenico, and E. Barone, *Elevated risk of type 2 diabetes for development of Alzheimer disease: a key role for oxidative stress in brain.* Biochim Biophys Acta, 2014. **1842**(9): p. 1693-706.

206. Sood, P.K., U. Nahar, and B. Nehru, *Curcumin attenuates aluminum-induced oxidative stress and mitochondrial dysfunction in rat brain.* Neurotox Res, 2011. **20**(4): p. 351-61.
207. Tapia, E., et al., *Curcumin prevents maleate-induced nephrotoxicity: Relation to hemodynamic alterations, oxidative stress, mitochondrial oxygen consumption and activity of respiratory complex I.* Free Radical Research, 2014. **48**(11): p. 1342-1354.
208. Kuo, J.J., et al., *Positive effect of curcumin on inflammation and mitochondrial dysfunction in obese mice with liver steatosis.* Int J Mol Med, 2012. **30**(3): p. 673-9.
209. Ringman, J., et al., *Oral curcumin for Alzheimer's disease: tolerability and efficacy in a 24-week randomized, double blind, placebo-controlled study.* Alzheimer's Research & Therapy, 2012. **4**(5): p. 43.
210. Garcea, G., et al., *Detection of curcumin and its metabolites in hepatic tissue and portal blood of patients following oral administration.* Br J Cancer, 2004. **90**(5): p. 1011-5.
211. Anand, P., et al., *Design of curcumin-loaded PLGA nanoparticles formulation with enhanced cellular uptake, and increased bioactivity in vitro and superior bioavailability in vivo.* Biochemical Pharmacology, 2010. **79**(3): p. 330-338.
212. Zang, Q.S., et al., *Specific inhibition of mitochondrial oxidative stress suppresses inflammation and improves cardiac function in a rat pneumonia-related sepsis model.* American Journal of Physiology - Heart and Circulatory Physiology, 2012. **302**(9): p. H1847-H1859.
213. Graham, D., et al., *Mitochondria-targeted antioxidant MitoQ10 improves endothelial function and attenuates cardiac hypertrophy.* Hypertension, 2009. **54**(2): p. 322-8.
214. Robin J Smith, M.P.M., *Mitochondria-targeted Antioxidants as Therapies.* Discovery Medicine, 2011. **11**(57): p. 106-114.
215. Sheu, S.-S., D. Nauduri, and M.W. Anders, *Targeting antioxidants to mitochondria: A new therapeutic direction.* Biochimica et Biophysica Acta (BBA) - Molecular Basis of Disease, 2006. **1762**(2): p. 256-265.
216. Hirzel, E., et al., *Differential modulation of ROS signals and other mitochondrial parameters by the antioxidants MitoQ, resveratrol and curcumin in human adipocytes.* J Recept Signal Transduct Res, 2013. **33**(5): p. 304-12.
217. Reily, C., et al., *Mitochondrially targeted compounds and their impact on cellular bioenergetics.* Redox Biology, 2013. **1**(1): p. 86-93.
218. Smith, R.A., et al., *Mitochondria-targeted antioxidants in the treatment of disease.* Ann N Y Acad Sci, 2008. **1147**: p. 105-11.
219. Martinez-Morua, A., et al., *Curcumin decreases oxidative stress in mitochondria isolated from liver and kidneys of high-fat diet-induced obese mice.* J Asian Nat Prod Res, 2013. **15**(8): p. 905-15.
220. Zhu, Y.G., et al., *Curcumin protects mitochondria from oxidative damage and attenuates apoptosis in cortical neurons.* Acta Pharmacol Sin, 2004. **25**(12): p. 1606-12.
221. Mishra, S. and K. Palanivelu, *The effect of curcumin (turmeric) on Alzheimer's disease: An overview.* Annals of Indian Academy of Neurology, 2008. **11**(1): p. 13-19.
222. Zhang, L., et al., *Curcuminoids enhance amyloid-beta uptake by macrophages of Alzheimer's disease patients.* J Alzheimers Dis, 2006. **10**(1): p. 1-7.
223. Huang, H.C., K. Xu, and Z.F. Jiang, *Curcumin-mediated neuroprotection against amyloid-beta-induced mitochondrial dysfunction involves the inhibition of GSK-3beta.* J Alzheimers Dis, 2012. **32**(4): p. 981-96.
224. Swomley, A.M., et al., *Abeta, oxidative stress in Alzheimer disease: Evidence based on proteomics studies.* Biochimica et Biophysica Acta (BBA) - Molecular Basis of Disease, 2014. **1842**(8): p. 1248-1257.
225. Trujillo, J., et al., *Renoprotective effect of the antioxidant curcumin: Recent findings.* Redox Biology, 2013. **1**(1): p. 448-456.
226. *Polychlorinated Biphenyls (PCBs)*. 2013; Available from: www3.rpa.gov.
227. Charlier, C.J., et al., *Polychlorinated biphenyls contamination in women with breast cancer.* Clin Chim Acta, 2004. **347**(1-2): p. 177-81.
228. Pavuk, M., et al., *Environmental exposure to PCBs and cancer incidence in eastern Slovakia.* Chemosphere, 2004. **54**(10): p. 1509-1520.
229. Formisano, L., et al., *MS-275 inhibits aroclor 1254-induced SH-SY5Y neuronal cell toxicity by preventing the formation of the HDAC3/REST complex on the synapsin-1 promoter.* J Pharmacol Exp Ther, 2015. **352**(2): p. 236-43.
230. Ertl, H. and W. Butte, *Bioaccessibility of pesticides and polychlorinated biphenyls from house dust: in-vitro methods and human exposure assessment.* J Expo Sci Environ Epidemiol, 2012. **22**(6): p. 574-83.

231. Robinson, P.E., et al., *Trends of PCB, hexachlorobenzene, and beta-benzene hexachloride levels in the adipose tissue of the U.S. population.* Environ Res, 1990. **53**(2): p. 175-92.
232. Hennig, B., et al., *PCB-induced oxidative stress in endothelial cells: modulation by nutrients.* Int J Hyg Environ Health, 2002. **205**(1-2): p. 95-102.
233. Zhu, Y., et al., *A new player in environmentally induced oxidative stress: polychlorinated biphenyl congener, 3,3'-dichlorobiphenyl (PCB11).* Toxicol Sci, 2013. **136**(1): p. 39-50.
234. Regala, R.P., et al., *The Effects of Tributyltin (TBT) and 3,3',4,4',5-Pentachlorobiphenyl (PCB-126) Mixtures on Antibody Responses and Phagocyte Oxidative Burst Activity in Channel Catfish, Ictalurus punctatus.* Archives of Environmental Contamination and Toxicology, 2001. **40**(3): p. 386-391.
235. Kopf, P.G., et al., *Cytochrome P4501A1 is required for vascular dysfunction and hypertension induced by 2,3,7,8-tetrachlorodibenzo-p-dioxin.* Toxicol Sci, 2010. **117**(2): p. 537-46.
236. Al-Salman, F. and N. Plant, *Non-coplanar polychlorinated biphenyls (PCBs) are direct agonists for the human pregnane-X receptor and constitutive androstane receptor, and activate target gene expression in a tissue-specific manner.* Toxicology and Applied Pharmacology, 2012. **263**(1): p. 7-13.
237. Zhu, Y., et al., *Polychlorinated biphenyl (pcb)-induced oxidative stress and cytotoxicity can be mitigated by antioxidants following exposure.* Free radical biology & medicine, 2009. **47**(12): p. 1762-1771.
238. Guida, N., et al., *Resveratrol via sirtuin-1 downregulates RE1-silencing transcription factor (REST) expression preventing PCB-95-induced neuronal cell death.* Toxicology and Applied Pharmacology, 2015. **288**(3): p. 387-398.
239. Han, S.G., et al., *EGCG protects endothelial cells against PCB 126-induced inflammation through inhibition of AhR and induction of Nrf2-regulated genes.* Toxicology and Applied Pharmacology, 2012. **261**(2): p. 181-188.
240. Venkatesha, V.A., et al., *Catalase ameliorates polychlorinated biphenyl-induced cytotoxicity in nonmalignant human breast epithelial cells.* Free Radic Biol Med, 2008. **45**(8): p. 1094-102.
241. Newsome, B.J., et al., *Green tea diet decreases PCB 126-induced oxidative stress in mice by up-regulating antioxidant enzymes.* J Nutr Biochem, 2014. **25**(2): p. 126-35.
242. Danis, B., et al., *Coplanar and non-coplanar congener-specificity of PCB bioaccumulation and immunotoxicity in sea stars.* Aquatic Toxicology, 2006. **79**(2): p. 105-113.
243. Safe, S., *Molecular biology of the Ah receptor and its role in carcinogenesis.* Toxicology Letters, 2001. **120**(1–3): p. 1-7.
244. Fischer, L.J., et al., *Symposium Overview: Toxicity of Non-Coplanar PCBs.* Toxicological Sciences, 1998. **41**(1): p. 49-61.
245. Sonis, S.T. and E.G. Fey, *Oral complications of cancer therapy.* Oncology (Williston Park), 2002. **16**(5): p. 680-6; discussion 686, 691-2, 695.
246. *Oral Mucositis.* Oral Complications of Chemotherapy and Head/Neck Radiation-for health professionals (PDQ) 2015 April 23, 2014; Available from: http://www.cancer.gov/about-cancer/treatment/side-effects/mouth-throat/oral-complications-hp-pdq#cit/section_5.1.
247. Murphy, B.A., *Clinical and Economic Consequences of Mucositis Induced by Chemotherapy and/or Radiation Therapy.* The Journal of Supportive Oncology, 2007. **5**(9).
248. Rosenthal, D.I., *Consequences of mucositis-induced treatment breaks and dose reductions on head and neck cancer treatment outcomes.* J Support Oncol, 2007. **5**(9 Suppl 4): p. 23-31.
249. Posner, M.R. and R.I. Haddad, *Novel agents for the treatment of mucositis.* Journal of Supportive Oncology, 2007. **5**(9 Suppl 4): p. 33-9.
250. Mueller, B.A., et al., *Mucositis management practices for hospitalized patients: national survey results.* Journal of Pain and Symptom Management, 1995. **10**(7): p. 510-20.
251. Epstein, J.B. and M.M. Schubert, *Managing pain in mucositis.* Seminars in Oncology Nursing, 2004. **20**(1): p. 30-7.
252. Henke, M., et al., *Palifermin Decreases Severe Oral Mucositis of Patients Undergoing Postoperative Radiochemotherapy for Head and Neck Cancer: A Randomized, Placebo-Controlled Trial.* Journal of Clinical Oncology, 2011. **29**(20): p. 2815-2820.
253. Dorr, W., K. Heider, and K. Spekl, *Reduction of oral mucositis by palifermin (rHuKGF): dose-effect of rHuKGF.* Int J Radiat Biol, 2005. **81**(8): p. 557-65.
254. Finch, P.W. and J.S. Rubin, *Keratinocyte growth factor expression and activity in cancer: implications for use in patients with solid tumors.* J Natl Cancer Inst, 2006. **98**(12): p. 812-24.
255. Elting, L.S., et al., *Economic Impact of Palifermin on the Costs of Hospitalization for Autologous Hematopoietic Stem-Cell Transplant: Analysis of Phase 3 Trial Results.* Biology of Blood and Marrow Transplantation, 2007. **13**(7): p. 806-813.

256. Posner, M.R. and R.I. Haddad, *Novel agents for the treatment of mucositis.* J Support Oncol, 2007. **5**(9 Suppl 4): p. 33-9.
257. Mueller, B.A., et al., *Mucositis management practices for hospitalized patients: national survey results.* J Pain Symptom Manage, 1995. **10**(7): p. 510-20.
258. Epstein, J.B. and M.M. Schubert, *Managing pain in mucositis.* Semin Oncol Nurs, 2004. **20**(1): p. 30-7.
259. Sonis, S.T., et al., *Perspectives on cancer therapy-induced mucosal injury: pathogenesis, measurement, epidemiology, and consequences for patients.* Cancer, 2004. **100**(9 Suppl): p. 1995-2025.
260. Lionel, D.H., et al., *Oral mucositis induced by anticancer treatments: physiopathology and treatments.* Therapeutics and Clinical Risk Management, 2006. **2**(2): p. 159-168.
261. Sonis, S.T., *Pathobiology of oral mucositis: novel insights and opportunities.* J Support Oncol, 2007. **5**(9 Suppl 4): p. 3-11.
262. Dörr, W., K. Heider, and K. Spekl, *Reduction of oral mucositis by palifermin (rHuKGF): Dose-effect of rHuKGF*. International Journal of Radiation Biology, 2005. **81**(8): p. 557-565.
263. Kapoor, P., S. Sachdeva, and S. Sachdeva, *TOPICAL HYALURONIC ACID IN THE MANAGEMENT OF ORAL ULCERS.* Indian Journal of Dermatology, 2011. **56**(3): p. 300-302.
264. Rezvani, M. and G.A. Ross, *Modification of radiation-induced acute oral mucositis in the rat.* Int J Radiat Biol, 2004. **80**(2): p. 177-82.
265. van't Land, B., et al., *Role of curcumin and the inhibition of NF-kappaB in the onset of chemotherapy-induced mucosal barrier injury.* Leukemia, 2004. **18**(2): p. 276-84.
266. Rao, S., et al., *The Indian Spice Turmeric Delays and Mitigates Radiation-Induced Oral Mucositis in Patients Undergoing Treatment for Head and Neck Cancer: An Investigational Study.* Integr Cancer Ther, 2013. **13**(3): p. 201-210.
267. Wright, L.E., et al., *Bioactivity of turmeric-derived curcuminoids and related metabolites in breast cancer.* Curr Pharm Des, 2013. **19**(34): p. 6218-25.
268. Pal, A. and A.K. Pal, *Radioprotection of turmeric extracts in bacterial system.* Acta Biol Hung, 2005. **56**(3-4): p. 333-43.
269. Hatcher, H., et al., *Curcumin: from ancient medicine to current clinical trials.* Cell Mol Life Sci, 2008. **65**(11): p. 1631-52.
270. Sharma, R., W. Steward, and A. Gescher, *Pharmacokinetics and Pharmacodynamics of Curcumin*, in *The Molecular Targets and Therapeutic Uses of Curcumin in Health and Disease*, B. Aggarwal, Y.-J. Surh, and S. Shishodia, Editors. 2007, Springer US. p. 453-470.
271. Johansen, J.S., et al., *Oxidative stress and the use of antioxidants in diabetes: Linking basic science to clinical practice.* Cardiovascular Diabetology, 2005. **4**: p. 5-5.
272. Mohanty, C. and S.K. Sahoo, *The in vitro stability and in vivo pharmacokinetics of curcumin prepared as an aqueous nanoparticulate formulation.* Biomaterials, 2010. **31**(25): p. 6597-611.
273. van den Berg, R., et al., *Applicability of an improved Trolox equivalent antioxidant capacity (TEAC) assay for evaluation of antioxidant capacity measurements of mixtures.* Food Chemistry, 1999. **66**(4): p. 511-517.
274. Rios, I. and C. Tuthill, *Method of treating or preventing tissue deterioration, injury or damage due to disease of mucosa*. 2009, Google Patents.
275. Patil, V.S., T.D. Dziubla, and D.S. Kalika, *Static and dynamic properties of biodegradable poly(antioxidant β-amino ester) networks based on incorporation of curcumin multiacrylate.* Polymer, 2015. **75**: p. 88-96.
276. Elad, S., et al., *Topical curcumin for the prevention of oral mucositis in pediatric patients: case series.* Altern Ther Health Med, 2013. **19**(3): p. 21-4.
277. Rose-Ped, A.M., et al., *Complications of radiation therapy for head and neck cancers. The patient's perspective.* Cancer Nurs, 2002. **25**(6): p. 461-7; quiz 468-9.
278. Redding, S.W., *Cancer Therapy-Related Oral Mucositis.* Journal of Dental Education, 2005. **69**(8): p. 919-929.
279. Siviero, A., et al., *Curcumin, a golden spice with a low bioavailability.* Journal of Herbal Medicine, 2015. **5**(2): p. 57-70.
280. Gupta, P., et al., *Quercetin conjugated poly(β-amino esters) nanogels for the treatment of cellular oxidative stress.* Acta Biomaterialia, 2015. **27**: p. 194-204.
281. Park, T.G., *Degradation of poly(lactic-co-glycolic acid) microspheres: effect of copolymer composition.* Biomaterials, 1995. **16**(15): p. 1123-30.
282. Makadia, H.K. and S.J. Siegel, *Poly Lactic-co-Glycolic Acid (PLGA) as Biodegradable Controlled Drug Delivery Carrier.* Polymers, 2011. **3**(3): p. 1377-1397.

283. *Magnesium stearate*, in *Database of Select Committee on GRAS Substances (SCOGS) Reviews.* 1979, U.S. Food and Drug Administration.
284. Li, J. and Y. Wu, *Lubricants in Pharmaceutical Solid Dosage Forms.* Lubricants, 2014. **2**(1): p. 21.
285. Prasad, S., A.K. Tyagi, and B.B. Aggarwal, *Recent Developments in Delivery, Bioavailability, Absorption and Metabolism of Curcumin: the Golden Pigment from Golden Spice.* Cancer Research and Treatment : Official Journal of Korean Cancer Association, 2014. **46**(1): p. 2-18.
286. Prior, R.L., X. Wu, and K. Schaich, *Standardized methods for the determination of antioxidant capacity and phenolics in foods and dietary supplements.* J Agric Food Chem, 2005. **53**(10): p. 4290-302.
287. Chang, Y.M., et al., *Sun exposure and melanoma risk at different latitudes: a pooled analysis of 5700 cases and 7216 controls.* Int J Epidemiol, 2009. **38**(3): p. 814-30.
288. Hodis, E., et al., *A landscape of driver mutations in melanoma.* Cell, 2012. **150**(2): p. 251-63.
289. Bald, T., et al., *Ultraviolet-radiation-induced inflammation promotes angiotropism and metastasis in melanoma.* Nature, 2014. **507**(7490): p. 109-113.
290. *Understanding UVA and UVB.* Skin Cancer Foundation 2015; Available from: http://www.skincancer.org/prevention/uva-and-uvb/understanding-uva-and-uvb.
291. Alscher, R.G., J.L. Donahue, and C.L. Cramer, *Reactive oxygen species and antioxidants: Relationships in green cells.* Physiologia Plantarum, 1997. **100**(2): p. 224-233.
292. Peak, M.J. and J.G. Peak, *Single-strand breaks induced in Bacillus subtilis DNA by ultraviolet light: action spectrum and properties.* Photochem Photobiol, 1982. **35**(5): p. 675-80.
293. Peak, M.J., et al., *Ultraviolet action spectra for DNA dimer induction, lethality, and mutagenesis in Escherichia coli with emphasis on the UVB region.* Photochem Photobiol, 1984. **40**(5): p. 613-20.
294. Godic, A., et al., *The Role of Antioxidants in Skin Cancer Prevention and Treatment.* Oxidative Medicine and Cellular Longevity, 2014. **2014**: p. 6.
295. Ndiaye, M., et al., *The Grape Antioxidant Resveratrol for Skin Disorders: Promise, Prospects, and Challenges.* Archives of biochemistry and biophysics, 2011. **508**(2): p. 164-170.
296. Athar, M., et al., *Resveratrol: A Review of Pre-clinical Studies for Human Cancer Prevention.* Toxicology and applied pharmacology, 2007. **224**(3): p. 274-283.
297. Baxter, R.A., *Anti-aging properties of resveratrol: review and report of a potent new antioxidant skin care formulation.* J Cosmet Dermatol, 2008. **7**(1): p. 2-7.
298. Koga, C.C., et al., *Stability of Trans-Resveratrol Encapsulated in a Protein Matrix Produced Using Spray Drying to UV Light Stress and Simulated Gastro-Intestinal Digestion.* Journal of Food Science, 2015: p. n/a-n/a.
299. Anderson, D.G., D.M. Lynn, and R. Langer, *Semi-automated synthesis and screening of a large library of degradable cationic polymers for gene delivery.* Angewandte Chemie-International Edition, 2003. **42**(27): p. 3153-3158.
300. Anderson, D.G., et al., *A combinatorial library of photocrosslinkable and degradable materials.* Advanced Materials, 2006. **18**(19): p. 2614-+.
301. Biswal, D., et al., *A single-step polymerization method for poly(beta-amino ester) biodegradable hydrogels.* Polymer, 2011. **52**(26): p. 5985-5992.
302. Chen, J., et al., *Synthesis and degradation of poly(beta-aminoester) with pendant primary amine.* Polymer, 2007. **48**(3): p. 675-681.
303. Meenach, S.A., et al., *Controlled synergistic delivery of paclitaxel and heat from poly(β-amino ester)/iron oxide-based hydrogel nanocomposites.* International Journal of Pharmaceutics, 2012. **427**(2): p. 177-184.
304. Jain, S. and M.P. Sharma, *Kinetics of acid base catalyzed transesterification of Jatropha curcas oil.* Bioresource Technology, 2010. **101**(20): p. 7701-7706.
305. Singh, A.K., S.D. Fernando, and R. Hernandez, *Base-Catalyzed Fast Transesterification of Soybean Oil Using Ultrasonication.* Energy & Fuels, 2007. **21**(2): p. 1161-1164.
306. Fisher, P.D., et al., *Improved small molecule drug release from in situ forming poly(lactic-co-glycolic acid) scaffolds incorporating poly(beta-amino ester) and hydroxyapatite microparticles.* J Biomater Sci Polym Ed, 2014. **25**(11): p. 1174-93.
307. Otera, J., *Transesterification.* Chemical Reviews, 1993. **93**(4): p. 1449-1470.
308. Kim, M., et al., *Competitive transesterification of soybean oil with mixed methanol/ethanol over heterogeneous catalysts.* Bioresource Technology, 2010. **101**(12): p. 4409-4414.
309. Brey, D.M. and J.A. Burdick, *POLY 552-Biodegradable poly(beta-amino ester)s as substrates for mineralized tissue formation.* Abstracts of Papers of the American Chemical Society, 2008. **236**.

310. Powers, H.J., *Riboflavin (vitamin B-2) and health.* The American Journal of Clinical Nutrition, 2003. **77**(6): p. 1352-1360.

VITA

Prachi Gupta completed her Bachelors in Chemical Engineering with Firth Class from the Institute of Chemical Technology (formerly known as UDCT), Mumbai, India, in May 2010. She joined Department of Chemical and Material Engineering at the University of Kentucky in January 2011 to pursue Doctorate of Philosophy in Chemical Engineering.

Honors and Awards

- Pre-doctoral trainee in NIH-Superfund Research Program (2014-2016)
- 2nd position in the oral presentation at Biomaterial Day, Vanderbilt University, 2015

Publications

- **Prachi Gupta**, J. Zach Hilt, Thomas D. Dziubla. Quercetin conjugated Poly (β-Amino Esters) Nanogels for the Treatment of Cellular Oxidative Stress (Acta Biomaterialia) (Published, doi:10.1016/j.actbio.2015.08.039)
- **Prachi Gupta**, Mihail Mitov, J. Zach Hilt, Thomas D. Dziubla. Sustained Suppression of Mitochondrial Oxidative Stress using Curcumin conjugated Poly (β-Amino Esters) Nanogels (International Journal of Pharmaceutics) (Submitted)
- **Prachi Gupta**, Sandeep Ramineni, J. Zach Hilt, Thomas Dziubla, Joseph Wyse, Nihar Shah, Curcumin conjugated Poly (β- Amino Esters) gel microparticles to treat oral mucositis (to be submitted)
- **Prachi Gupta**, Andrew Lakes, Thomas Dziubla, Free Radical Chemistry Primer, Oxidative Stress and Biomaterials: The Science, Challenges, and Opportunities (Elsevier) (In process)
- **Prachi Gupta**, Caroline Lacerda, Vinod Patil, Paritosh Wattamwar, Dipti Biswal, J. Zach Hilt, Thomas Dziubla, Degradation of Poly (β- Amino Esters) in alcohols

through transesterification: A method to conjugate drugs into the hydrogel matrix, (to be submitted).

Patent

- Microparticles enabled Delivery Structures, Methods of Preparing and Using the Same, in co-authorship with Dr. Nihar Shah, Dr. Thomas D. Dziubla, Dr. J. Zach Hilt, Dr. Joseph Wyse *(U.S. Provisional Patent Application 62253827, 2015).*

Conference Presentations

Prachi has presented at papers and posters at several national, regional and local meeting including AICHE Annual Meetings (Minneapolis, MN, 2011; San Francisco, CA, 2013), SFB Annual Meeting (Charlotte, NC, 2015).